SYNTHESIS AND PROPERTIES OF INDENOFLUORENE AND DIINDENOTHIOPHENE DERIVATIVES FOR USE AS SEMICONDUCTING MATERIALS IN ORGANIC ELECTRONIC DEVICES

by

AARON GLENN FIX

A DISSERTATION

Presented to the Department of Chemistry
and the Graduate School of the University of Oregon
in partial fulfillment of the requirements
for the degree of
Doctor of Philosophy

September 2013

DISSERTATION APPROVAL PAGE

Student: Aaron Glenn Fix

Title: Synthesis and Properties of Indenofluorene and Diindenothiophene Derivatives for Use as Semiconducting Materials in Organic Electronic Devices

This dissertation has been accepted and approved in partial fulfillment of the requirements for the Doctor of Philosophy degree in the Department of Chemistry by:

David X. Tyler	Chairperson
Michael M. Haley	Advisor
Kenneth X. Doxsee	Core Member
Edward X. Olivos	Institutional Representative

and

Kimberly Andrews Espy	Vice President for Research and Innovation Dean of the Graduate School

Original approval signatures are on file with the University of Oregon Graduate School.

Degree awarded September 2013

DISSERTATION ABSTRACT

Aaron Glenn Fix

Doctor of Philosophy

Department of Chemistry

September 2013

Title: Synthesis and Properties of Indenofluorene and Diindenothiophene Derivatives for Use as Semiconducting Materials in Organic Electronic Devices

Organic electronic devices are becoming commonplace in many academic and industrial materials laboratories, and commercial application of these technologies is underway. To maximize our fundamental understanding of organic electronics, a wide array of molecular frameworks is necessary, as it allows for a variety of optical and electronic properties to be systematically investigated. With the ability to further tune each individual scaffold via derivatization, access to a broad spectrum of interesting materials is possible. Of particular interest in the search for organic semiconducting materials are the cyclopenta-fused polyaromatic hydrocarbons, including those based on the fully conjugated indenofluorene (IF) system, which comprises five structural isomers. This dissertation represents my recent contributions to this area of research.

Chapter I serves as a historical perspective on early indenofluorene research and a review of more current research on their synthesis and applications in organic electronic devices. Chapters II and III cover our early work developing the synthesis of the fully-reduced indeno[1,2-*b*]fluorene scaffold, with the latter of these chapters showing the first example of its application in an organic electronic device, a field effect transistor. Chapter IV demonstrates the first syntheses of fully-reduced indeno[2,1-*c*]fluorene

derivatives. Chapter V expands our research to encompass isoelectronic heteroatomic derivatives of that same scaffold, introducing the fully-reduced diindeno[2,1-*b*:1',2'-*d*]thiophene scaffold and showing that our synthetic methodology also can be used to produce a quinoidal thiophene core. Chapter VI concludes with a review of the similarities between the indeno[2,1-*c*]fluorene and diindeno[2,1-*b*:1',2'-*d*]thiophene molecular architectures and introduces benzo[a]indeno[2,1-*c*]fluorene derivatives, demonstrating the first example of a fully-reduced indenofluorene that possesses a non-quinoidal core and illustrating that the quinoidal core is not a prerequisite for the strong electron affinities seen across the families of fully-reduced indenofluorenes.

This dissertation encompasses previously published and unpublished co-authored material.

CURRICULUM VITAE

NAME OF AUTHOR: Aaron Glenn Fix

GRADUATE AND UNDERGRADUATE SCHOOLS ATTENDED:

University of Oregon, Eugene
University of Arizona, Tucson

DEGREES AWARDED:

Doctor of Philosophy, 2013, University of Oregon
Master of Science, Chemistry, 2008, University of Oregon
Bachelor of Science, Biochemistry and Molecular Biophysics, 2003, University of Arizona

PUBLICATIONS:

Fix, A. G.; Chase, D. T.; Haley, M. M. In *Topics in Current Chemistry*; Siegel, J. S.,Wu,Y.-T., Eds.; Springer: Berlin, Germany, 2013, in press (DOI: 10.1007/128_2012_376).

Fix, A. G.; Deal, P. E.; Vonnegut, C. L.; Rose, B. D.; Zakharov, L. N.; and Haley, M. M. *Org. Lett.*, **2013**, *15* (6), pp 1362–1365.

Chase, D. T.; Fix, A. G.; Kang, S. J.; Rose, B. D.; Weber,C. D.; Zhong, Y.; Zakharov, L. N.; Lonergan, M. C.; Nuckolls, C.; Haley, M. M. *J. Am. Chem. Soc.* **2012**, *134*, 10349–10352.

Chase, D. T.; Fix, A. G.; Rose, B. D.; Weber, C. D.; Nobusue, S.; Stockwell, C. E.; Zakharov, L. N.; Lonergan, M. C.; Haley, M. M. *Angew. Chem. Int. Ed.* **2011**, *50*, 1103–1106.

Haley, M. M.; Chase, D. T.; Rose, B. D.; Fix, A. G. "Alkynyl-Substituted Indenofluorenes Useful in Electronic and Electro-Optical Devices" U. S. PCT Patent Application No. 13/704571; Pub. No. US2013/0096336A1.

ACKNOWLEDGMENTS

I am grateful to Professor Haley for his willingness to entertain new ideas and his patience as many of my attempts at them failed to bear fruit. I am supremely grateful to Brad Rose, Matt Carnes, Rick Glover, and Doug Young for conversations about several ridiculous, and some more practical, ideas I had that touched on areas where, at the time and perhaps still, I was quite out of my depth. Their patience and insight has been a critical benefit to my development as a scientist. Sincerest thanks also must go to Profs. Dave Tyler, Ken Doxsee, and Edward Olivos for their patience with me as they performed their duties as members on my committee. I wholeheartedly thank all of the members of the Haley Lab during my tenure, as without their support and encouragement I might not have had the courage to broaden the scope of my inquiries nor accomplished half of what I was able. Dr. Lev Zakharov was a stalwart collaborator and has become a friend and without his assistance I would have been unable to prove out many of my experiments. Likewise Dr. Mike Strain, whose any-hour-of-the-day support and diligence provided instrumentation and training that I could not have done without. I would also like to acknowledge the National Science Foundation (CHE-1013032, CHE-1301485) for funding throughout my graduate studies.

On a more personal level, I'd like to thank my parents, Joan and Glenn, without whose support I never would have made it passed the second grade. More recently, my wife Danielle has shown a patience and resolve typically only heard of in mythological allegory. And lastly I thank Leola Jean.

This dissertation is dedicated to my parents, Joan and Glenn Fix, my wife, Danielle, and Leola Jean (you know who you are)

TABLE OF CONTENTS

Chapter Page

LIST OF FIGURES

Figure Page

CHAPTER II

CHAPTER III

CHAPTER IV

Figure Page

LIST OF TABLES

LIST OF SCHEMES

Scheme Page

Scheme Page

Scheme Page

CHAPTER VI

CHAPTER I

INDENOFLUORENES AND DERIVATIVES: SYNTHESES AND EMERGING MATERIALS APPLICATIONS

This chapter was co-authored with Daniel T. Chase, who had the initial vision for the review and laid the foundation, and Michael M. Haley, who provided editorial and content advice. It was originally published in the book series *Topics in Current Chemistry*. All succeeding chapters of this dissertation contain co-authored material as well.

Introduction

Polycyclic aromatic hydrocarbons (PAHs), and polyarenes (PAs) in general, have been the subject of great interest for over 150 years, and constitute a significant cornerstone of the advancement of organic chemistry in the nineteenth and twentieth centuries [1,2]. Initially discovered in the resins of fossil fuels, PAHs have been observed in a myriad of environments that range from natural mineral deposits to meteor rocks [3]. Isolation of PAH-rich tars and ashes has contributed not only to modern purification and separation techniques commonly used today but also has brought forth fundamental concepts such as aromaticity, a topic that remains a neverending source of discussion in the literature. Furthermore, efforts to elucidate the reactivity of PAHs and PAs have resulted in the discovery of many novel reaction mechanisms and catalytic pathways that represent the foundation of modern physical organic chemistry.

In the last quarter century, PAH and PA research has made a remarkable return to the literature spotlight as compound accessibility and characterization has been made easier with the advent of modern synthetic methods and instrumentation, respectively [4-

6]. One motivation for this resurgence lies with the unique optoelectronic properties that PAHs and PAs possess due to their inherently high levels of π-conjugation and delocalization. These attributes make PAHs and PAs useful for a variety of materials applications such as organic light-emitting diodes (OLEDs), field-effect transistors (OFETs), and photovoltaics (OPVs) [7,8]. Such impetus has led to the development and expansion of various PAH classes, such as higher order acenes [9,10] and condensed polycyclic aromatics [11-13]. Nontraditional structures that incorporate five-membered cyclopentyl rings (CP-PAHs) such as fullerenes [14] and buckybowls [15] have undergone rapid growth as well.

This review focuses on the pentacyclic indenofluorenes (IFs), another reemerging class of CP-PAHs, where the B and D rings are each a five-membered ring. First synthesized in the late 19th century by Gabriel [16], IF derivatives were a sporadic topic in the literature for roughly seventy years [17-24] until the pioneering work by Deuschel [25,26] and Chardonnens [27] in the 1950s devised a general strategy for their synthesis. However, at that time, modern spectroscopic and structural identification techniques were rare in the scientific community; thus, IFs were not typically characterized beyond their melting points and elemental analyses. Outside their initial syntheses, IF development languished for another forty years. A decade ago, following the realization of CP-PAHs as viable organic materials, interest in the IF scaffold resumed. Since then derivatized IFs have been recognized as potential candidates for stable emissive materials [28-34] and more recently identified as a semiconducting material in devices [35-37].

The indenofluorene family is comprised of five structural isomers which can be difficult to discern as multiple naming and numbering strategies as well as graphical

presentations have been employed over the last century to describe their shape and structure (Fig. 1). Current nomenclature uses a bracketed set of numbers and a letter to distinguish one isomer from another where the set of numbers refer to the orientation of how the indene group faces the fluorene and the letter corresponds to the edge of the indene/fluorene ring fusion. Both '1,2' isomers exhibit an *anti* relationship between the methylene bridges of the five-membered rings, while the three remaining '2,1' isomers exhibit a *syn* relationship. The IF scaffold exhibits a variety of symmetries: the [1,2-*a*] isomer is only centrosymmetric, the [1,2-*b*] isomer exhibits rotational symmetry, and the [2,1-*a*], [2,1-*b*], and [2,1-*c*] isomers possess a mirror plane. As such, each isomer has its own unique ring topology, which in turn, has pronounced structural and electronic consequences.

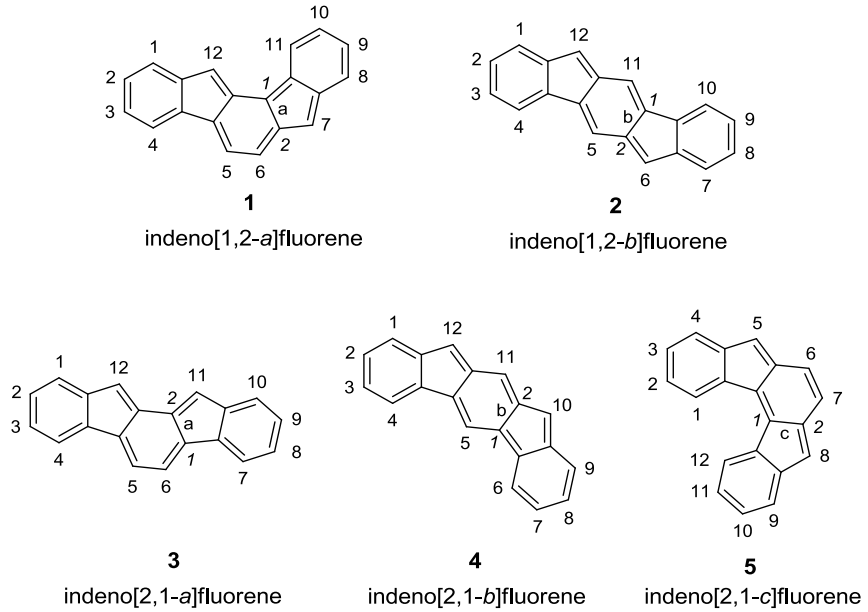

Figure 1. Nomenclature and numbering for indenofluorene isomers. Italicized numbers denote numbering for methylene bridge orientation, non-italicized numbers denote atom.

This review will cover the five IF regioisomers and describe common synthetic procedures used to obtain each form, including assorted structural, optoelectronic, and materials properties as available. IFs possessing sp^3-hybridization at the bridgehead of the

five-membered rings is a burgeoning area of research in the realm of emissive materials worthy of its own review; however, only salient examples will be described. Device information will be presented assuming the reader has a basic optical and electronic materials background. Greater detail can be found in the appropriate references.

Early Research

The first reported synthesis of an IF scaffold dates to 1884 when Gabriel condensed two equivalents of phthalic anhydride (**6**) with ethyl acetoacetonate (**7**) to form carboxylic acid **8** and later ethyl ester **9** (Scheme 1) [16].

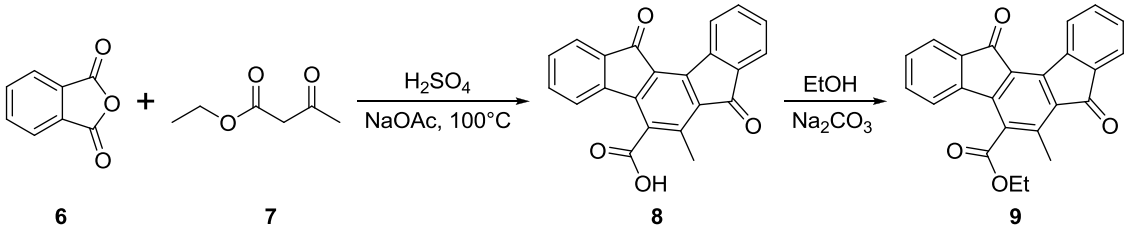

6 7 8 9

Scheme 1. Synthesis of Gabriel's [1,2-*a*] IF dione **9** [16].

In 1955, Chardonnens and Ritter isolated the parent [1,2-*a*]dione **12** through oxidative cleavage of benzo[*e*]acephenanthrylene (**10**) using sodium dichromate to generate 2-fluorenonylbenzoic acid (**11**) followed by ring closure using concentrated sulfuric acid (Scheme 2) [27].

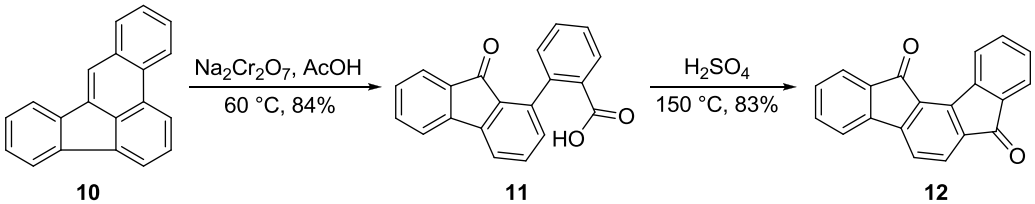

10 11 12

Scheme 2. Synthesis of parent [1,2-*a*] IF dione **12** [27].

Chardonnens and coworkers later devised a more general pathway to **12** by condensing either indenyl ketone **13a** or **13b**, respectively, with quinoline and NaOH in a

stainless steel autoclave at 250 °C to give 7-keto-12-hydroindeno[1,2-*a*]fluorenone (**14**) in 30% yield (Scheme 3) [38-40]. Incidentally, 9-keto-12-hydroindeno[2,1-*b*]fluoreneone (**15**) also formed in equal yield as addition could occur at either the 6- or 8-positions of the fluorene unit. Addition of either indenonyl ketone **16a** and **16b**, respectively, under similar conditions afforded both **12** and parent [2,1-*b*]IFdione **17** in 28% and 31% yield, respectively. Furthermore, oxidation of **14** and **15** using sodium dichromate at elevated temperatures led to the expected diones **12** and **17**. Despite the formation of two discrete condensation products, both **14** and **15** as well as **12** and **17** can be isolated separately either through soxhlet extraction or by selective crystallization. Both techniques take advantage of the key topological differences that the [1,2-*a*] and [2,1-*b*] structures possess—namely, the [2,1-*b*] isomer is more soluble than the [1,2-*a*] isomer. The greater dipole moment induced by the *syn* arrangement of the ketones makes the [2,1-*b*]IF scaffold more amenable to dissolution in polar solvents, allowing for easy separation of the isomers.

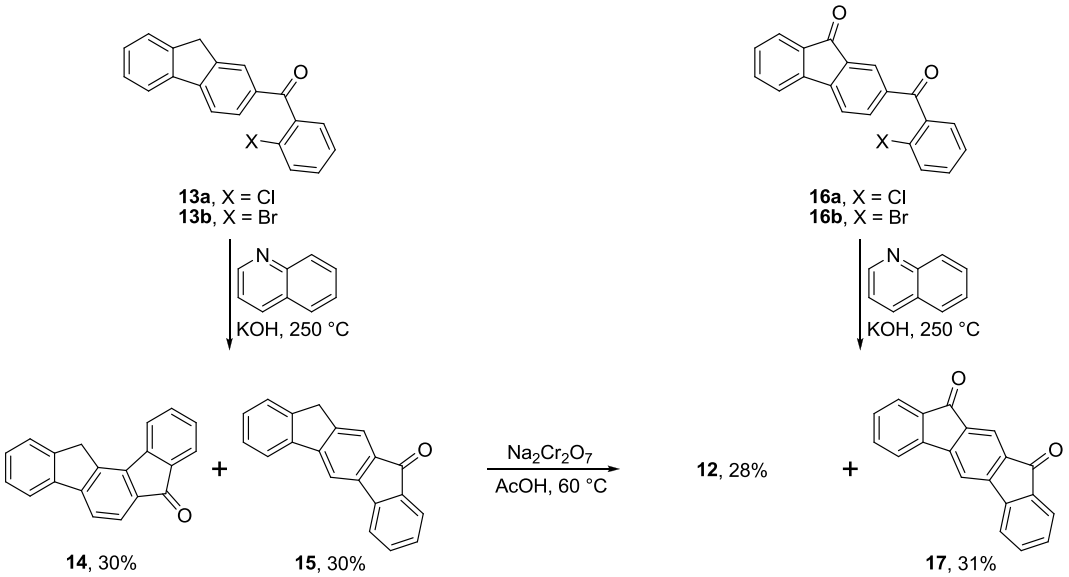

Scheme 3. Asymmetric synthesis of **12** and [2,1-*b*] IF dione **17** [38-40].

The first account of the [1,2-*b*]IF skeleton dates to 1951 when Deuschel alkylated *p*-xylene (**18**) with two equivalents of cyclohexene to give tricycle **19** (Scheme 4). Treatment with Pd/C afforded 1,4-dimethyl-2,5-diphenylbenzene (**20**). Oxidation of the methyl moieties using potassium permanganate and pyridine generated diacid **21**. Subsequent cyclization using concentrated sulfuric acid gave the parent [1,2-*b*]IF-6,12-dione **22** in 87% yield [26].

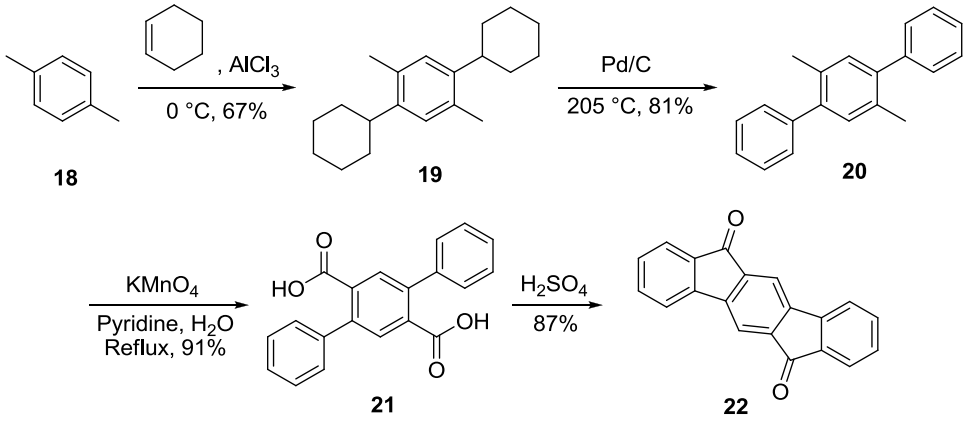

Scheme 4. Synthesis of parent [1,2-*b*]IF dione **22** [26].

Alternatively, passing a stream of chlorine gas in a neat solution of **20** at 185 °C afforded **23** in 46% yield (Scheme 5). A refluxing aqueous solution of $CuCl_2$ oxidized **23** also to dione **22**.

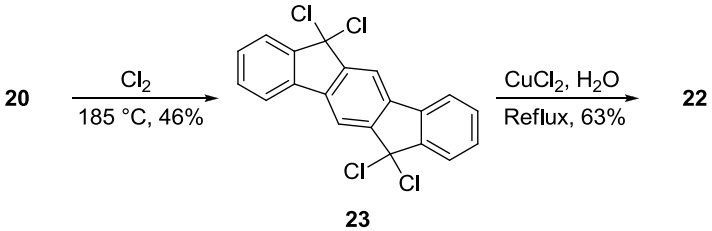

Scheme 5. Chlorination/oxidation route to **22** [26].

Access to the [1,2-*b*]IF core was also discovered through collapse of the dehydrobenzo[12]annulene scaffold. First described by Eglinton and coworkers in 1960 (Scheme 6), tetrayne **24** underwent a double transannular cyclization when reacted with

elemental Na in liquid ammonia to provide octahydroindeno[1,2-*b*]fluorene **25** as a mixture of two isomers in 69% yield [41]. Further treatment with 15% Pd/C aromatized the central ring to afford 6,12-dihydroindeno[1,2-*b*]fluorene (**26**).

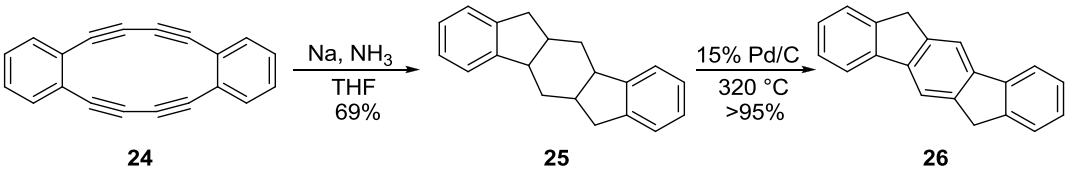

Scheme 6. Na/NH_3-induced transannular cyclization of **24** [41].

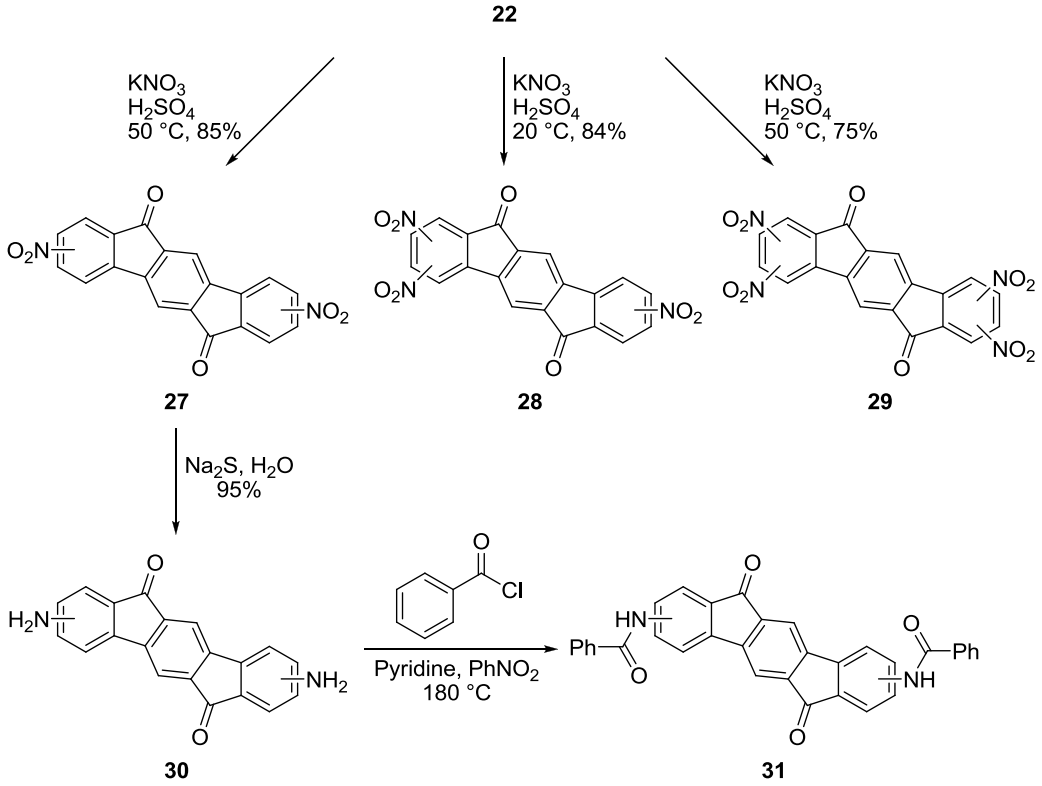

Scheme 7. Nitration, reduction, and amidation of **22** [42].

Continued work by Deuschel demonstrated that **22** was amenable to nitration using potassium nitrate in concentrated sulfuric acid at 20 °C (Scheme 7) [42]. By varying the amount of electrophile used, [1,2-*b*]IF diones could be nitrated either two (**27**), three (**28**), or four (**29**) times. Reduction of dinitro **27** with aqueous sodium sulfide afforded diaminodione **30** in 95% yield, which in turn, was amenable to amidation in a

pyridine/nitromethane solution at 180 °C to give **31**. While the sites for nitration of **22** were most likely on the peripheral rings, specific information about their exact positions remains unknown.

Chardonnens and Salamin also synthesized a number of substituted [1,2-*b*]IF diones, which were typically made in the same fashion as the [1,2-*a*]IF diones described earlier (Scheme 3) [43]. For example, treatment of 2,5-dibromoterephthalic acid (**32**) with thionyl chloride and subsequent Friedel-Crafts acylation with **33a-d** provided **34a-d** (Scheme 8). Intramolecular arylation at elevated temperatures furnished IF-diones **35a-d** in 20-28% yield. This technique has also been successfully applied to asymmetric 1,3,4-trisubstituted diones as well as 2,3,8,9-tetrasubstituted diones [42].

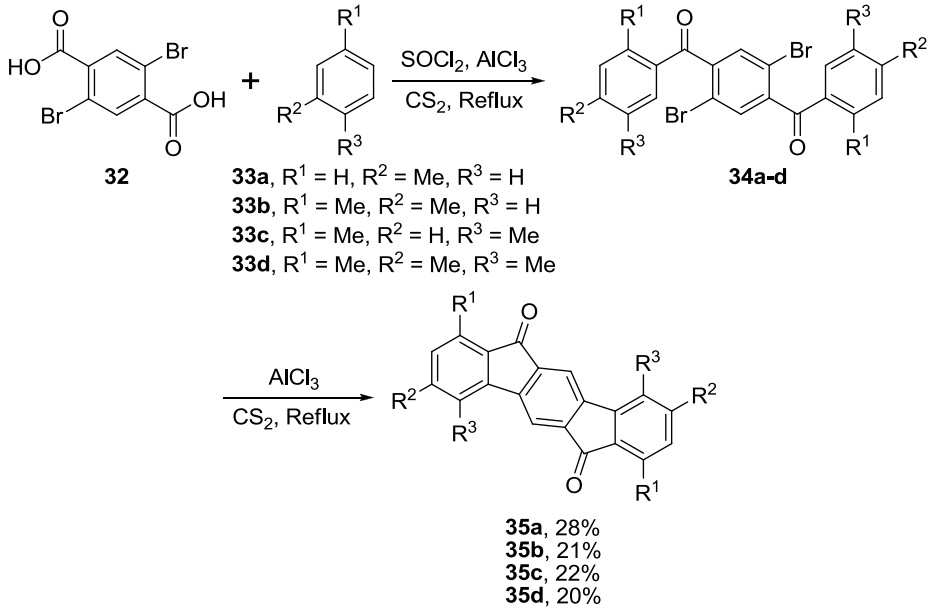

Scheme 8. Synthesis of 1,3,4,7,9,10-substituted diones **35a-d** [43].

Indeno[1,2-*a*]fluorenes

Indeno[1,2-*a*]fluorene-7,12-diones

The synthetic route utilizing Friedel-Crafts acylation via terphenyldicarboxylic acid precursors to reach the pentacyclic diketone has been applied for the assembly of a

multitude of indeno[1,2-*a*]fluorene diones [44]. In most cases, a mixture of [1,2-*a*] and [2,1-*b*] species was formed during the cyclization stage, although in some instances the [1,2-*a*] isomer was the exclusive product. One such example involves tricarboxylic acid precursor **36**, so that the acylation step forms in the correct configuration regardless of direction (Scheme 9) [45]. To achieve this, *cis*-1,3-diphenylpropene (**37**) was reacted with 3-pentanone (**38**) to yield cyclohexenone **39**. Reduction with sodium borohydride afforded cyclohexanol **40** followed by reaction with Pd/C to form 1,3,5-trimethyl-2,4-diphenylbenzene **41**. Oxidation with potassium permanganate, first using pyridine as the base yielding diacid **42**, and then using sodium carbonate provided triacid **36**. Cyclization in concentrated sulfuric acid afforded 5-carboxyindeno[1,2-*a*]fluorene dione **43** in near quantitative yield. Subsequent decarboxylation using elemental Cu at 350 °C gave **12** as the sole product.

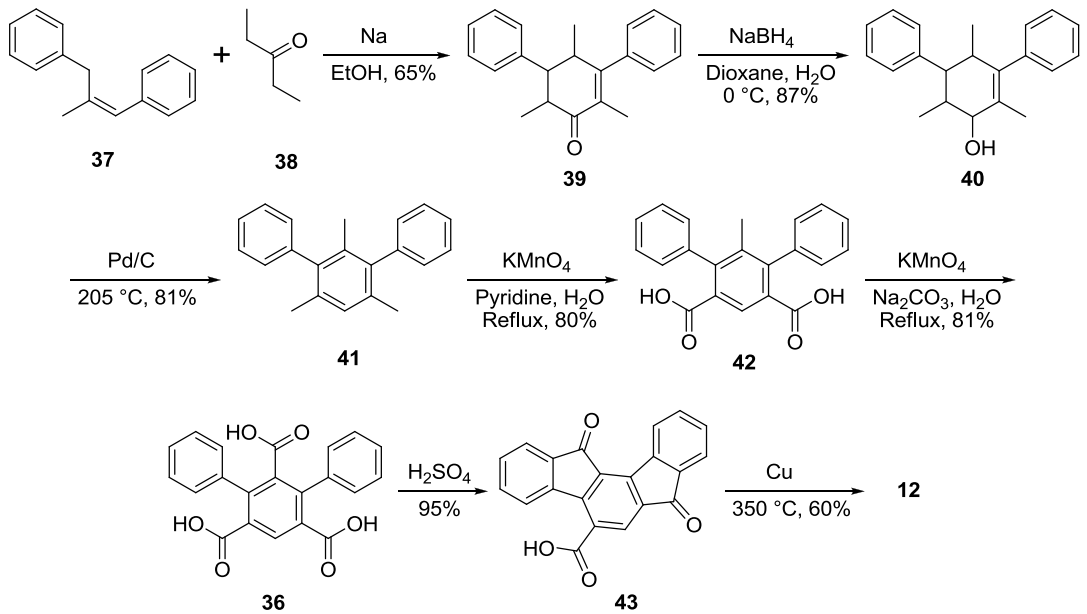

Scheme 9. Synthesis of **12** via terphenyl tricarboxylic acid precursor **42** [45].

Other indeno[1,2-*a*]fluorenes

Since the initial work of Chardonnens and others, few examples of syntheses of [1,2-*a*]IF derivatives exist outside of patent literature. Shi et al. recently reported [1,2-*a*]IFs **48a-b** and [2,1-*c*]IFs **49a-b** (Scheme 10) [46]. Diels-Alder reaction of alkynes **45a-b**, readily available from fluorenones **44a-b**, provided regioisomeric mixtures of diols **46a-b** and **47a-b**. Subsequent acid-catalyzed Friedel-Crafts condensation gives **48** and **49**. The two derivatives of both regioisomers showed quantum yields in solution of ~60% and showed good thermal stability, with decomposition occurring greater than 330 °C.

Minuti and colleagues described the syntheses of cyclophane-fused [1,2-a]IFs [47]. Reduction of **50** with sodium borohydride, followed by treatment with PBr_3 then $LiBr/LiCO_3$ gave three undetermined intermediates (Fig. 2). This mixture of molecules yielded **51** after treatment with Pd/C in triglyme at 160 °C.

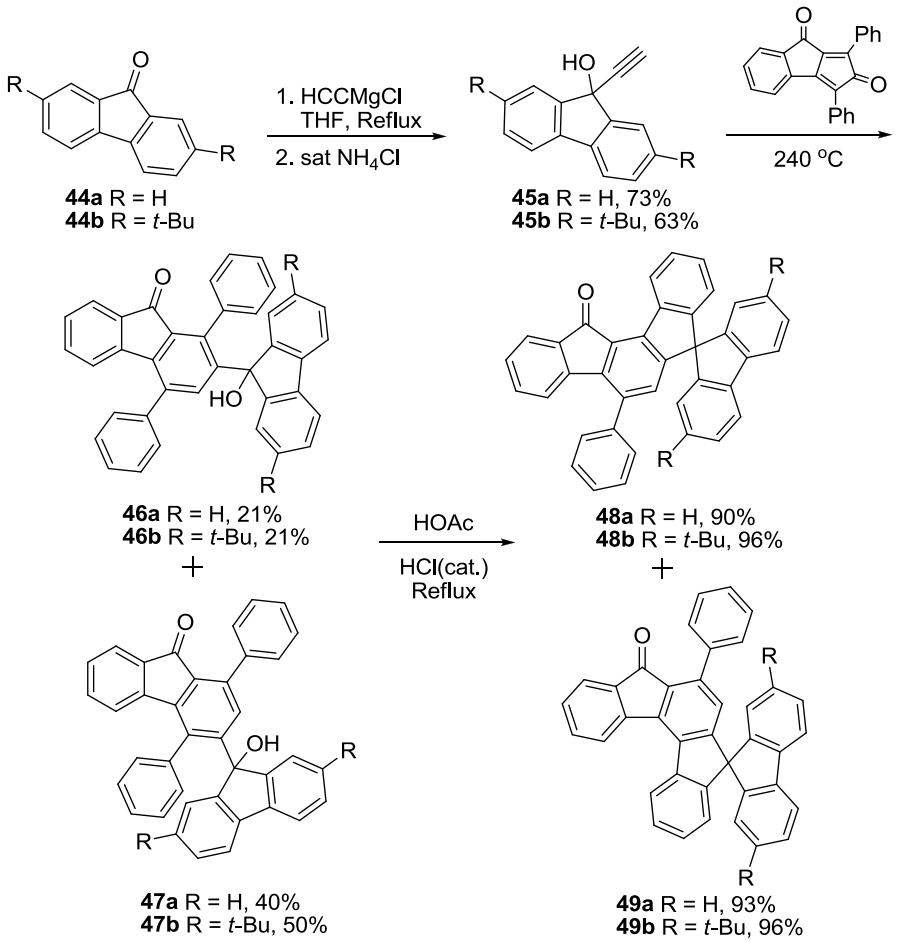

44a R = H
44b R = *t*-Bu

45a R = H, 73%
45b R = *t*-Bu, 63%

46a R = H, 21%
46b R = *t*-Bu, 21%

47a R = H, 40%
47b R = *t*-Bu, 50%

48a R = H, 90%
48b R = *t*-Bu, 96%

49a R = H, 93%
49b R = *t*-Bu, 96%

Scheme 10. Synthesis of spiro-fused [1,2-*a*]IFs **48a-b** and [2,1-*c*]IFs **49a-b** [46].

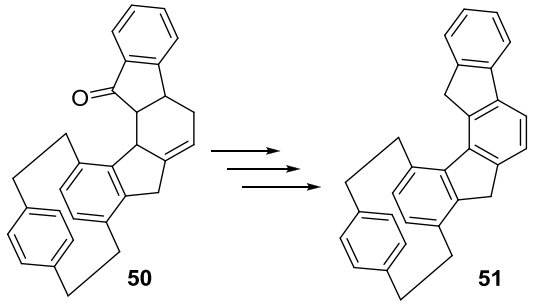

50 **51**

Figure 2. Cyclophane-functionalized precursor **50** and [1,2-*a*]IF **51** [47].

Indeno[1,2-*b*]fluorenes

Indeno[1,2-*b*]fluorene-6,12-diones

Diels-Alder methods can also be used to generate the terphenyl core that ultimately furnishes [1,2-*b*]IF diones. Wang showed that the [4+2] cycloaddition of

cyclopentadienone **52** with either diphenylacetylene (**53a**) or phenylacetylene (**53b**) followed by cheletropic elimination of CO afforded diesters **54a-b** (Scheme 11) [48]. Ester hydrolysis and subsequent Friedel-Crafts ring closure furnished 5,11-diphenyl and 5-phenyl [1,2-*b*]IF diones **55a-b** in 90% and 88% yield, respectively. A noted consequence of this alternative pathway was the suppressed formation of the corresponding [2,1-*c*]IF diones.

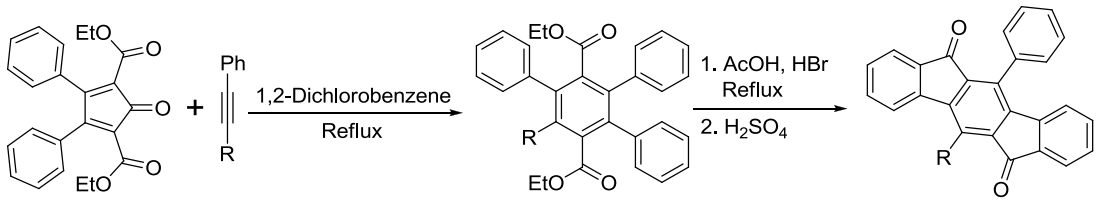

52 **53a**, R = Ph; **53b**, R = H → **54a**, 78%; **54b**, 78% → **55a**, 90%; **55b**, 88%

Scheme 11. Synthesis of IF diones **55a-b** [48].

Encouraged by the potential semiconducting properties polyacetylenes could offer, Swager reacted **24** and **56a-b** [49], and later Komatsu reacted **56c** [50,51], with iodine under aerobic conditions to give 5,11-diiodoindeno[1,2-*b*]fluorenediones **57a-d** in 33-95% yield (Scheme 12). The reactivity is reminiscent of Eglinton's earlier transannular cyclization (Scheme 6) but leading to diones in this case due to the reactive nature of the fully-reduced dibenzo-*s*-indacene intermediate (further discussed in Section 3.3).

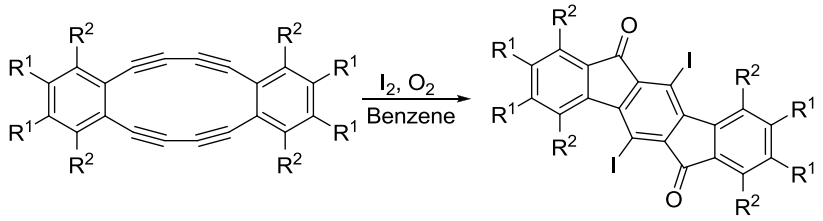

24, R^1 = H, R^2 = H
56a, R^1 = H, R^2 = $C_{10}H_{21}$
56b, R^1 = H, R^2 = $C_{12}H_{25}$
56c, R^1 = F, R^2 = F

57a, 55%
57b, 95%
57c, 54%
57d, 33%

Scheme 12. Aerobic iodine-induced transannular cyclization of **57a-d** [49,50].

Komatsu and colleagues also demonstrated n-type semiconducting behavior for **57d** in thin-film OFETs [51], a highly desirable characteristic given the relative paucity of organic n-type semiconducting scaffolds compared to p-type molecular motifs. These devices, however, possessed low electron mobilities of 2.93×10^{-5} $cm^2/V{\cdot}s$ under vacuum and 6.08×10^{-6} $cm^2/V{\cdot}s$ in air.

The most common route to IF diones is still based on Deuschels' original 1951 procedure [25]. In 2002, Wang and coworkers modified this synthesis, utilizing a Suzuki cross-coupling reaction to generate terphenyl **20**, which was then oxidized and cyclized as before to yield **22** from 2,5-dibromo-*p*-xylene **58** in 85% yield over three steps (Scheme 13) [48]. Dione **22** could subsequently be reduced to form known 6,12-dihydroindeno[1,2-*b*]fluorene (**26**).

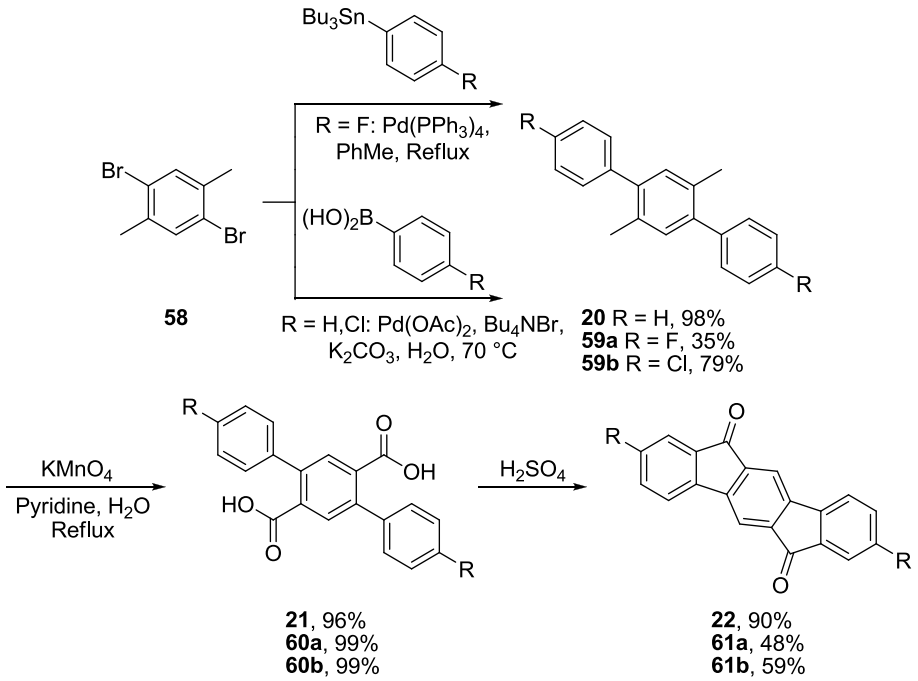

Scheme 13. Preparation of parent dione **22** and 2,8-dihalo IF diones **61a-b** [48,52].

Yamashita and colleagues synthesized **22** and **61a-c** to investigate their utility as n-type semiconducting materials in OFETs [52], inspired by the n-type behavior Komatsu had observed with **57d** [51]. Difluoro- and dichloroterphenyls **59a** and **59b** were formed via either Stille or Suzuki cross-coupling conditions from **58** (Scheme 13). Oxidation with potassium permanganate generated dihalodiacids **60a-b** and then cyclization onto the outside rings afforded dihalodiones **61a-b** in moderate yield. They assessed the performance of these substrates in HMDS-treated OFETs (vapor deposition; bottom-contact; Si/SiO_2). **61a** exhibited the best performance, with mobilities as high as 0.17 $cm^2/V{\cdot}s$ and on/off ratio greater than 10^7, while **22** exhibited no semiconducting behavior.

Marks showed that 2,8-dibromodione **61c** could be made through a slightly different manner (Scheme 14) [37]. Suzuki cross-coupling of methyl 5-bromo-2-iodobenzoate (**62**) with 1,4-dibenzenediboronic acid dipinacolate (**63**) afforded diester **64**; subsequent hydrolysis and cyclization onto the inside ring using concentrated sulfuric acid gave **61c**.

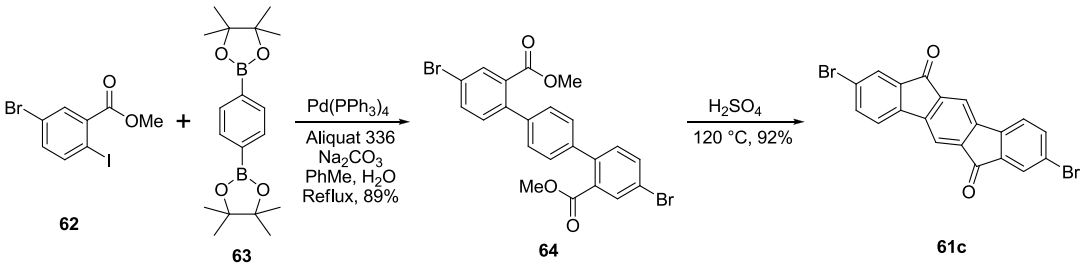

Scheme 14. Preparation of 2,8-dibromo IF dione **61c** [37].

Examination of the X-ray data for several [1,2-*b*]IF diones revealed that the extent of halogenation had a dramatic effect on the solid state ordering. For example, perfluoro **57d** exhibited one-dimensional columnar stacking while difluoro **61a** demonstrated face-

to-face π-stacking (Fig. 3) [51,52]. Despite these small structural differences, close contact distances for **57d** and **61a** were found to be 3.31 Å and 3.30 Å, respectively.

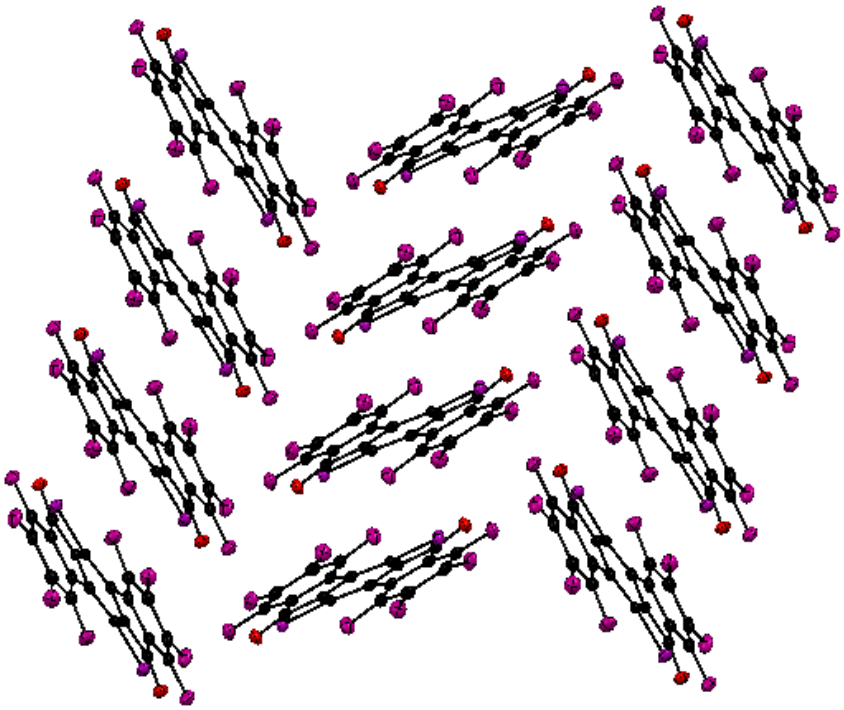

Figure 3. Solid state packing of **57d** [51].

Taking advantage of the fortuitous halogenation on the 5 and 11 positions obtained via Swager's iodine-mediated transannular cyclization route (Scheme 13), Haley and coworkers appended a variety of trialkylsilylacetylenes onto **57a**. Sonogashira cross-coupling afforded the 5,11-diethynylindeno[1,2-*b*]fluorene-6,12-diones **65a-f** in 7-61% yield (Scheme 15) [53]. Cyclic voltammetry data illustrated the ability of **65a-f** to reversibly accept two electrons. The half-wave potential for the first reduction occurs at ca. –0.80 V, which is less negative than that of parent **22** (–1.19 V) due to the electron-withdrawing acetylenes but more negative compared to halogenated IF diones **61a-c** (–0.7 V to –0.57 V) and **57d** (–0.45 V). Another advantage of silylacetylene incorporation

was a significant increase in solubility, given that minimal solubility in common organic solvents is a hallmark characteristic of nearly all [1,2-*b*]IF diones.

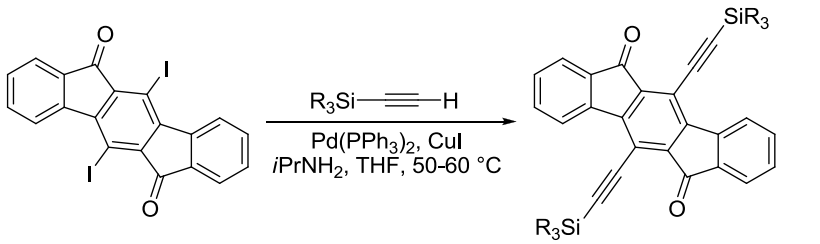

Scheme 15. 5,11-Diethynyl IF diones **65a-f** [53].

While silyl substitution on the acetylene produced little variance in the optical and electronic properties of **65a-f**, it did have a significant effect on the solid state ordering, as three separate packing motifs were observed (Fig. 4). TMS-capped acetylene **65a** possessed herringbone packing, while the larger TPS-capped acetylene **65f** displayed one-dimensional columns without π-π interactions. In accordance with Anthony's observations with 6,13-bis(triisopropylsilylethynyl)pentacene [54], TIPS-capped **65d** exhibited columnar stacking in two dimensions, also known as brick-and-mortar stacking, a packing motif often favorable for charge-transport in materials because it increases the likely hood significant intermolecular orbital overlap. This was clearly illustrated by comparison of the carbon-carbon close-contact distances of **65a**, **65d**, and **65f**, which were 3.50, 3.40, and 3.77 Å, respectively.

Despite its highly insoluble nature, 2,8-dibromodione **61c** has proven to be a useful precursor for a variety of 2,8-diarylated derivatives, as such species can further provide access to a larger variance of electron-donating/accepting substituents (Scheme

16) [37,55]. Suzuki or Stille cross-coupling of **61c** with aryls **66a-e** furnished diaryl diones **67a-e** in 43-81% yield.

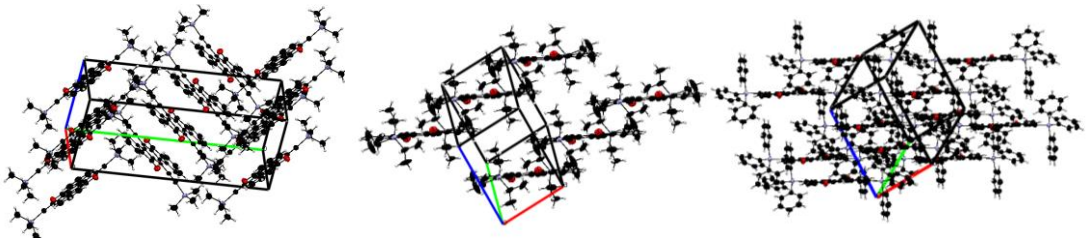

Figure 4. Solid state packing of **65a** (left), **65d**, middle, and **65f** (right) [53].

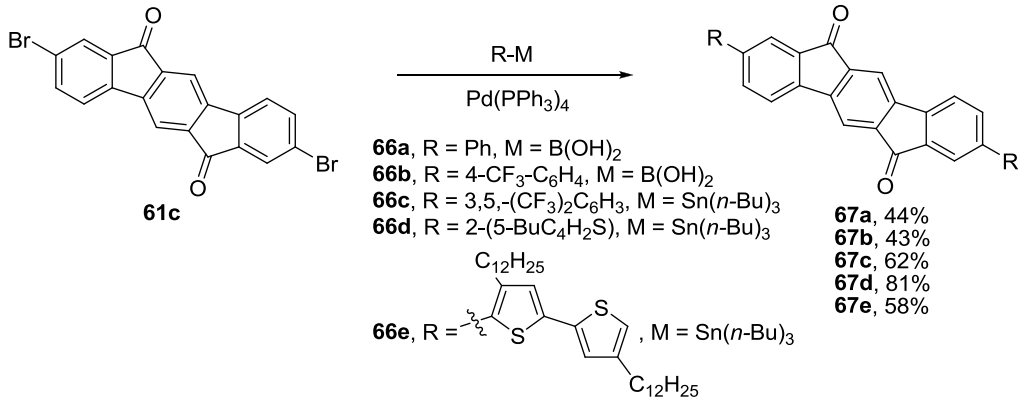

Scheme 16. Cross-coupling of 2,8-dibromo IF diones **67a-e** [37,55].

Marks installed long alkyl groups onto the IF dione core as another method to combat insolubility (Scheme 17) [37]. Kumada cross-coupling of 1,4-dichlorobenzene (**68**) with didodecylmagnesium bromide gave 1,4-didodecylbenzene (**69**). Bromination of **69** yielded 2,5-dibromo-1,4-didodecylbenzene (**70**), which was reacted with boronic acid **71** under Suzuki cross-coupling conditions to afford terphenyl **72**. Cyclization as before with concentrated sulfuric acid at elevated temperatures gave didodecyl dione **73** in 93% yield. Unlike parent **22**, **73** could be directly brominated on the 2 and 8-positions to cleanly generate **74**, which upon further cross-coupling with 2-tributylstannylthiophene (**75**) under standard Stille conditions afforded **76**.

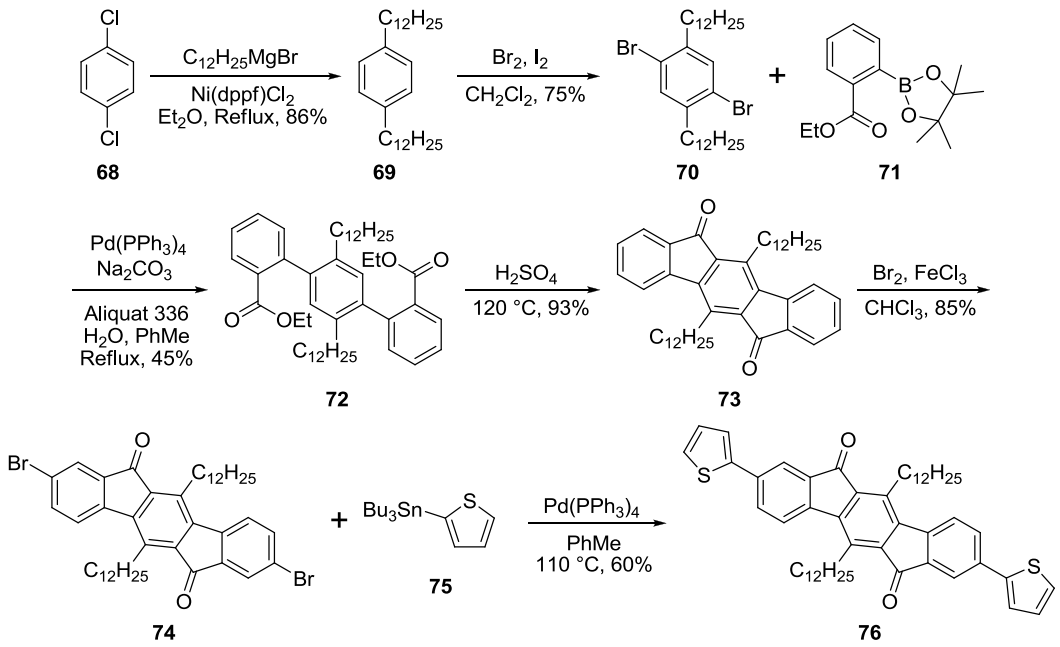

Scheme 17. Formation of 2,8-dithiophene-5,11-didodecyl IF dione **76** [37].

Like **65a-f**, cyclic voltammetry data for **67d-e**, **73**, and **76** showed that these molecules readily accept electrons at low voltages. Thiophene substitution results in a slight shift of reduction potentials to more negative values with respect to non-thiophene derivative **73**, as well as a small decrease in band gap. In addition, the authors obtained device data for these IF dione derivatives in OTFTs. For example, films of **76** showed ambipolar charge transport, having electron and hole mobilities reaching 0.01 and 6×10^{-4} $cm^2/V \cdot s$, respectively.

An alternative method to Friedel-Crafts acylation as the final step in dione synthesis involves a Pd-mediated Heck arylation to generate the indeno[1,2-*b*]fluorene skeleton. In 1989, Hellwinkel and Kistenmacher showed that parent and 2,8-di-*t*-butyl[1,2-*b*]IF diones **22** and **78**, respectively, could be isolated upon reacting precursors **77a-b** with palladium acetate in acetic acid (Scheme 18) [56,57].

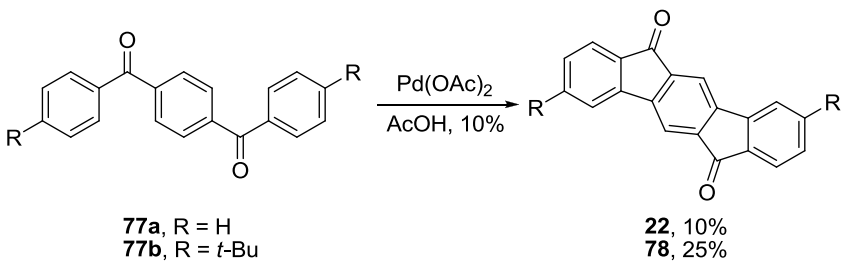

77a, R = H
77b, R = *t*-Bu

22, 10%
78, 25%

Scheme 18. $Pd(OAc)_2$-mediated cyclization of **77a-b** [56,57].

Similarly, Hu and coworkers found that the reaction of dialdehyde **79** with two equivalents phenyl and 4-*t*-butylphenyl boronic acids, **80a**, and **80b**, respectively, in the presence of a custom Pd(II) palladacycle formed diones **22** and **82** in 49% and 58% yield via a two-step, one-pot method (Scheme 19) [58]. Note that the initial step is not a Suzuki cross-coupling reaction, rather addition of the carbonyl and transmetallation of the arylboronic acid to the Pd(II) catalyst is followed by a reductive elimination to give intermediates **81a,b** and generate a Pd(0) species. Switching solvents from toluene to DMA and increasing the temperature promotes oxidative addition of the aryl halide, C-H bond activation of the central aryl ring and subsequent cross-coupling, and then oxidation of the alcohols to ketones gives [1,2-*b*]IF diones **22** and **82** in 49% and 58% yield, respectively, for this complex one-pot cascade reaction.

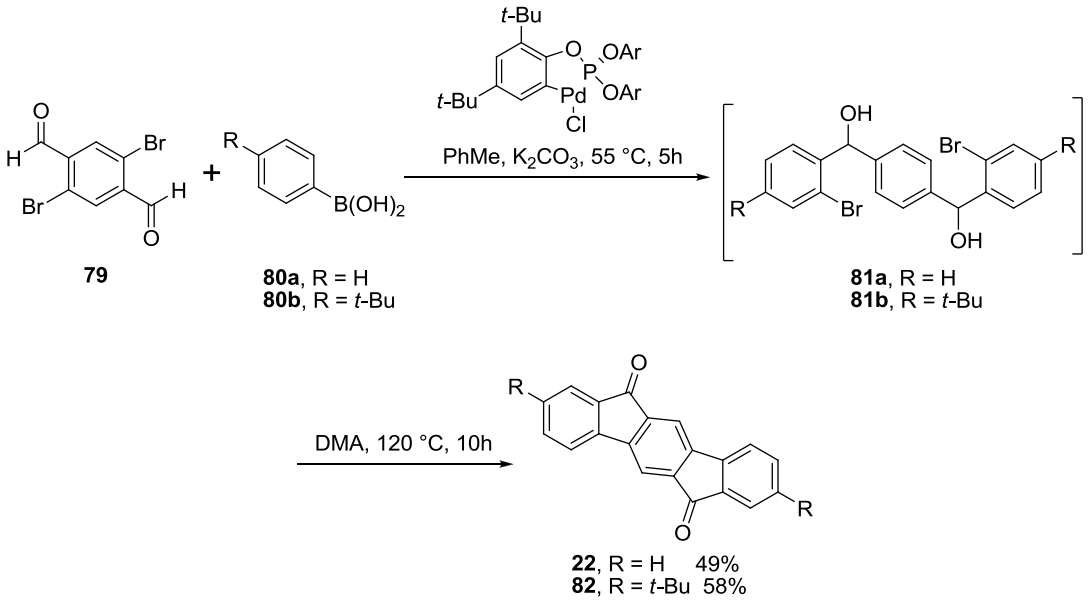

79

80a, R = H
80b, R = *t*-Bu

81a, R = H
81b, R = *t*-Bu

Scheme 19. Pd-catalyzed preparation of IF diones **22** and **82** [58].

Indeno[1,2-*b*]fluorene-6,12-olefins

While not yet as ubiquitous as the above-mentioned diones, olefination at the 6 and 12-positions on the [1,2-*b*]IF scaffold has recently gained interest because of the increased use of the electron-withdrawing dicyanovinylene moiety. This technique was initially described by Gompper in 1987 when dione **22** was reacted with two equivalents of malononitrile in the presence of $TiCl_4$ to form olefin **83a** (Scheme 20) [59], though no yield was given.

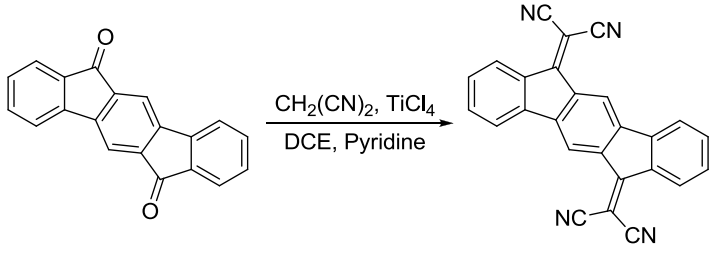

22 **83a**

Scheme 20. Preparation of [1,2-*b*]IF olefin **83a** [59].

In 2008, Marks expanded the scope of synthesizing IF olefins. Diones **67d-e** and **73** were converted to their corresponding exocyclic olefins **83b**,**c** and **84a** using the $TiCl_4$

method described above (Schemes 21-22) [37]. Olefin **84c** was synthesized through Stille cross-coupling of stannane **75** with olefin **84b** which derived from dione **74** (Scheme 22) [37].

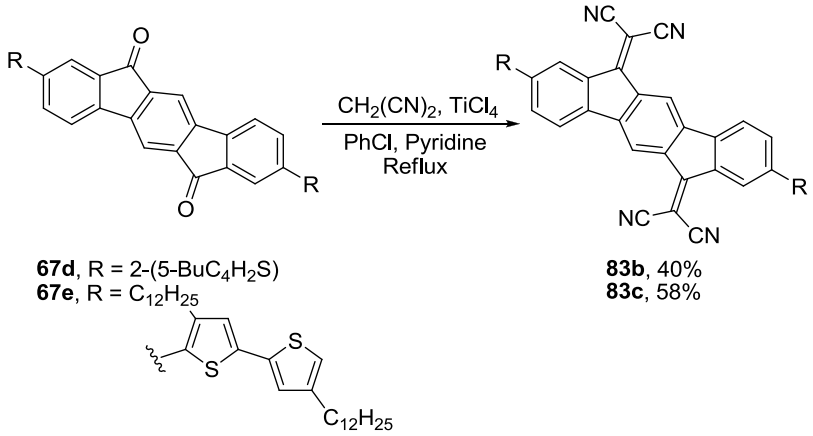

Scheme 21. Preparation of IF olefins **83b-c** [37].

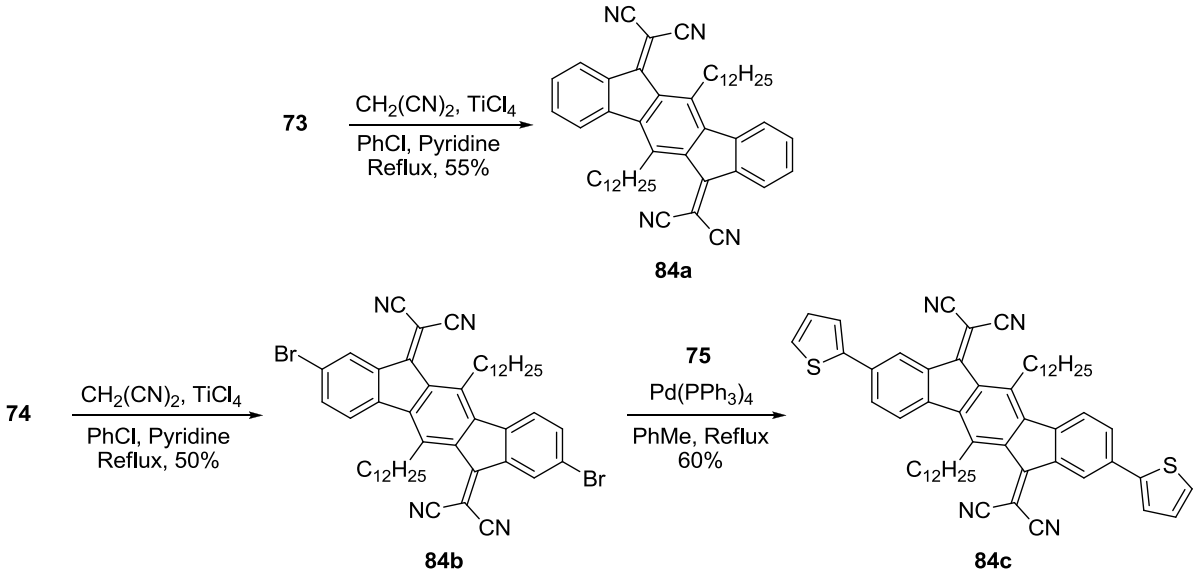

Scheme 22. Preparation of IF olefins **84a-c** [37].

Due to the highly electron deficient dicyanovinylene moiety, **83a-c** and **84b-c** showed consistent stabilization of their HOMO and LUMO levels compared to **67d-e**, **73**, and **76** by approximately 0.15 eV, and 0.6 eV, respectively, as well as a lowered energy gap of approximately 0.5 eV. Furthermore, **83b-c** and **84b-c** exhibited an approximate

+0.6 V shift with respect to **67d-e**, **73**, and **76** in reduction potentials. Solid state analysis of **84c** detailed that the IF core maintains the bond lengths of the three aromatic benzene rings found in *p*-terphenyl. Interestingly, the exocyclic dicyanovinylene groups contorted the IF core by 13° pointing opposite of the central alkyl chains. [1,2-*b*]IF dicyanovinylenes **83a-c** and **84a-c** were utilized in thin-film transistors and showed n-type and ambipolar transport. Notably, **84b** showed stable n-type transport in air with mobilities as high as 0.001 $cm^2/V \cdot s$.

Fully-conjugated Indeno[1,2-*b*]fluorene

First mentioned by Deuschel as a possible resonance structure of dione **22**, a fully conjugated indeno[1,2-*b*]fluorene (**2**, Fig. 5) might serve as a suitable small molecule analogue of fullerene due to its low-lying LUMO level, subsequently shown by Haley et al. [53,60]. Furthermore, **2** possesses no *s-cis* diene linkages in its structure, meaning that it should be less susceptible to the deleterious cycloaddition pathways that acenes and fullerenes are susceptible to. Until recently, however, there has been skepticism of the existence of fully conjugated IF species for a number of reasons: (1) the formation of **2** should be energetically costly due to the necessary disruption of the aromaticity of the central benzene ring; (2) IF **2** would possess 20 π-electrons resulting in the formation of an unfavorable antiaromatic species; and (3) the central rings of **2** would also host a *p*-xylylene (*p*-quinodimethane) core, a notoriously reactive moiety that typically cannot be isolated because of its high tendency to oligomerize/polymerize.

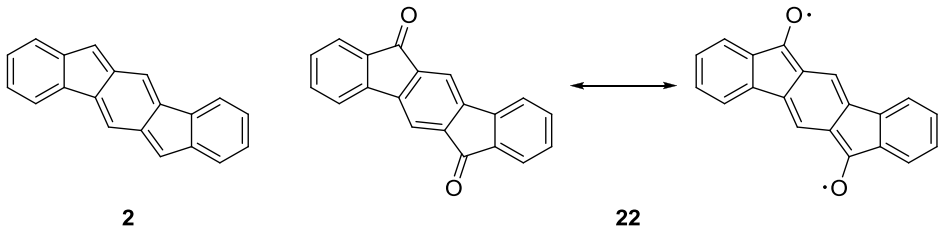

Figure 5. Fully conjugated indeno[1,2-*b*]fluorene **2** and resonance structures of **22**.

As previously mentioned, Swager and coworkers obtained diones **57a-c** through the iodine-induced transannular cyclization of **24** and **56b-c** in aerobic conditions (Scheme 12) [49]. Under anaerobic conditions, however, another class of products formed that possessed only two aromatic signals in the ^{1}H NMR spectrum that were shifted upfield from **57a-c**. Furthermore, they found that exposure to air converted these compounds into **57a-c** in near quantitative yield. Swager deduced the air-sensitive intermediates to be fully conjugated 5,6,11,12-tetraiodoindeno[1,2-*b*]fluorenes **85a-c**, given their highly reactive nature as well as the notable up-field shift of the proton resonances compared to **57a-c** due to their antiaromatic character (Scheme 23). The UV-Vis spectrum of **85a** exhibited low energy absorptions of 534 and 571 nm, nearly 250 nm bathochromically shifted from **57a**, attributable to its fully conjugated state.

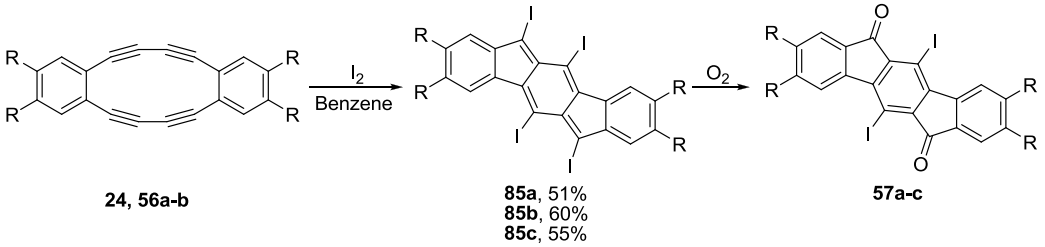

Scheme 23. Preparation of fully conjugated indeno[1,2-*b*]fluorenes **85a-c** [49].

Studies by Scherf and coworkers in 1996 on the design and structural properties of indeno[1,2-*b*]fluorene polymers (**86a**) came to a similar conclusion [61,62]. Their argument, based on structurally related 9,9'-bisfluorenes, was that in order to reduce

steric hindrance between subunits, the bridging olefinic carbons could lengthen and hence reduce the overall double bond character (**86b**, Fig. 6) [61,63]. A consequence to such a bond lengthening would be an overall decrease in band gap energy and geometric distortions. Another consequence would be an overall change of the bond structure of the subunit itself. As a model system for **86b**, IF **87a** was prepared and reported to exhibit an absorption spectrum λ_{max} of 543 nm; however, no other characterization was reported.

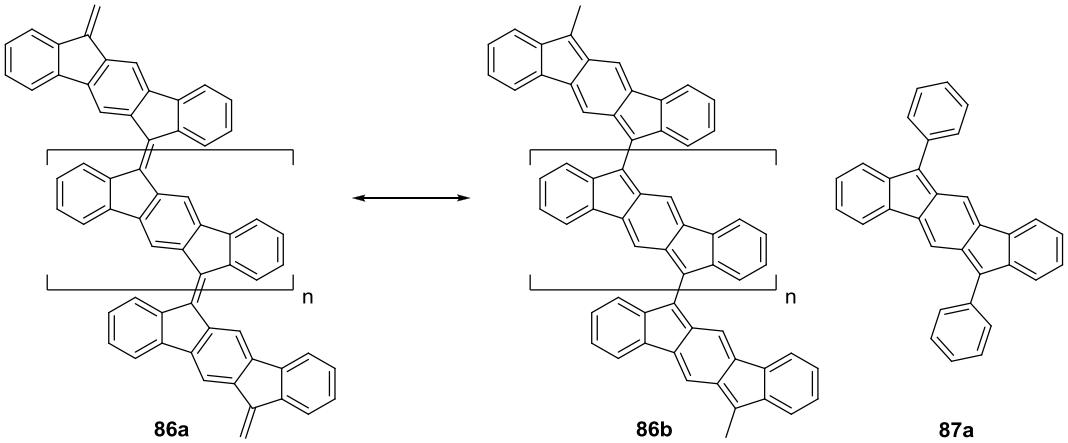

Figure 6. Resonance forms of poly(indeno[1,2-*b*]fluorene) **86a-b** and model subunit **87a** [61-63].

Works by Anthony [9,64-67] and Miller [68,69], among others [70-73], have shown that ethynylogation and/or appending heteroatoms to acenes (e.g., **88**-**89**) results in a marked increase in stability (Fig. 7).

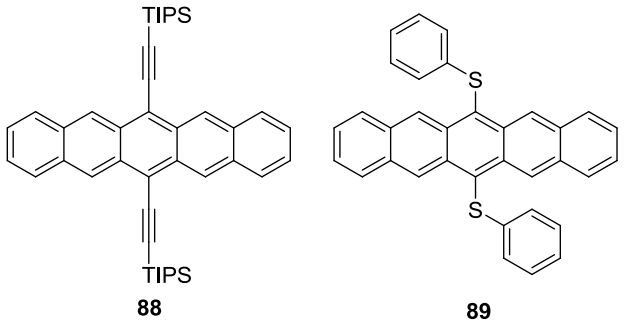

Figure 7. Examples of ethynylated (**88**) and heteroatom -substituted (**89**) pentacenes [64,68].

Applying the same rationale and synthetic methodology used to obtain diethynylated pentacenes from pentacene quinone, Haley et al. undertook the synthesis of tetraethynylindeno[1,2-*b*]fluorenes **92a-b** (Scheme 24) using the tetraiodo framework **85a-b** that Swager had already prepared [60]. Unfortunately, direct Sonogashira cross-coupling of (trimethylsilyl)acetylene (TMSA) with **85a-b** did not afford the desired product. Instead, ethynylation of diones **65d** and **90** with the anion of (triisopropylsilyl)acetylene (TIPSA) gave diols **91a-b**; subsequent reduction using anhydrous $SnCl_2$ at elevated temperatures, a common technique used in acene synthesis, afforded compounds **92a-b** in 22% and 55% yield, respectively, over two steps. As observed for **85a-c**, **92a-b** exhibit up-field aromatic chemicals shifts with respect to **65d** and **90**, an indicator of their fully conjugated, anti-aromatic state.

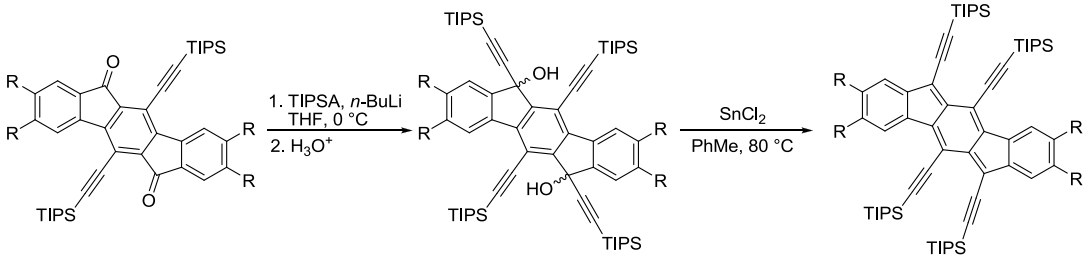

65d, R = H
90, R = $C_{10}H_{25}$

91a
91b

92a, 22%
92b, 55%

Scheme 24. Synthesis of fully conjugated 5,6,11,12-tetraethynyl IFs **92a-b** [60].

The absorption spectra of **92a-b** showed three low-energy transitions in a pattern with λ_{max} values of 594 and 614 nm, respectively, which is roughly a 25 and 45 nm bathochromic shift with respect to **85a** due to the increased conjugation and lower HOMO/LUMO gap caused by the four ethynyl groups. In comparison to **88**, whose low-energy transition λ_{max} value is 644 nm, **92a-b** were hypsochromcially shifted by 50 and

30 nm, a consequence of having two fewer π-electrons in the antiaromatic core. Unlike **88,** however, **92a-b** are non-emissive, a trait often observed for antiaromatic molecules.

As with previously mentioned IF diones **65a-f**, **67d-e**, **73** and **76**, cyclic voltammetry data of **92a** showed first and second reduction potentials of –0.62 V and –1.16 V, respectively, while decyl IF **92b** exhibited potentials of –0.73 and –1.29 V, respectively. Additionally, **92a-b** do exhibit oxidation potentials between 1.10 and 1.30 V, although this process is irreversible. Despite the lack of electron withdrawing diones, the first reduction potentials of **92a-b** meet or surpass the values of **65a-f**, **67d-e**, **73** and **76** because a two-fold reduction of the indeno[1,2-*b*]fluorene core is extremely favorable as the resultant dianion is a 22 π-electron species where each ring is fully aromatic. X-ray analysis of **92a** concluded that there was indeed long and short bond alternation throughout the central portion of the IF core (Fig. 8), which agrees with Scherf's initial hypothesis regarding the internal bond structure of polymer **86** and model compound **87a**. Interestingly, the peripheral benzene rings remain homogenized in length, suggesting that the name dibenzo-*s*-indacene is also a valid descriptor. The bond lengths in the internal

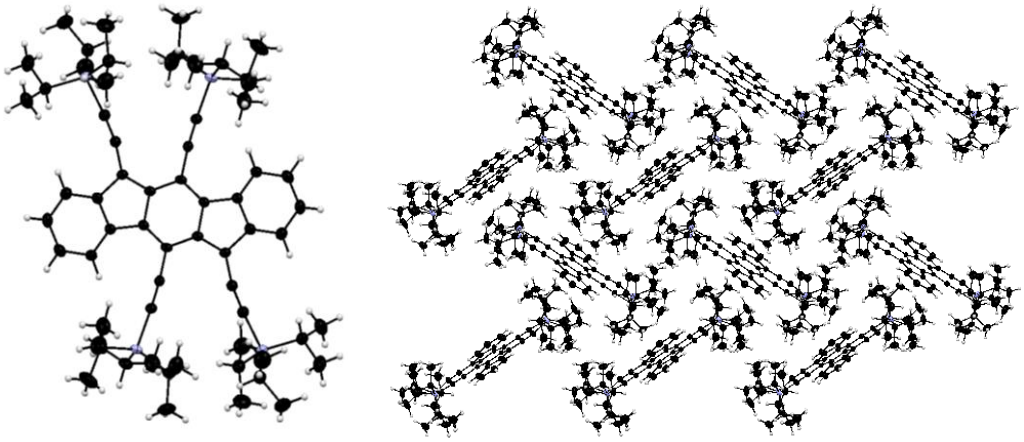

Figure 8. X-ray single crystal structure (left) and expanded herringbone crystal packing of **92a** [60].

three rings show that **92a** is indeed a stable example of a molecule containing a *p*-xylylene core, similar to what was found for Thiele's and Tschitschibabin's hydrocarbons (Fig. 9) [74]. Examination of the crystal packing indicated that **92a** exhibited an expanded herringbone pattern often found in unsubstituted acenes [75]. This undesirable packing motif is attributable to the steric bulk of the four interdigitated (triisopropylsilyl)ethynyl groups in **92a**.

93 **94**

Figure 9. Diagrams of Thiele's (**93**) and Tschitschibabin's (**94**) hydrocarbons [74].

Regarding the effect of ethynylation on the IF core, computational studies suggested that ethynyl groups on the 5- and 11-positions had only a minor influence on the overall electronics, as their removal changed the calculated HOMO and LUMO energies by +0.02 eV and –0.10 eV, respectively [55]. Functionalization of the favorable 6,12-diethynyl IF scaffold with withdrawing groups on the 2 and 8-positions further lowered the calculated HOMO and LUMO energies to levels that approach those in the fullerene PCBM [7,8,76]. Ethynylation of **22**, **61a-d**, and **67a-d** using the lithiate of TIPSA generated mixtures of diol isomers, and subsequent reduction using anhydrous $SnCl_2$ afforded fully conjugated indeno[1,2-*b*]fluorenes **96a-i** in 31-81% yield over two steps (Scheme 25).

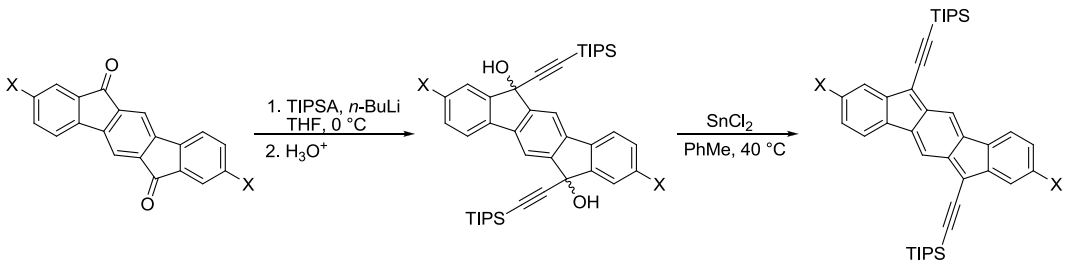

22, X = H
61a, X = F
61b, X = Cl
61c, X = Br
61d, X = Me
67a, X = Ph
67b, X = 4-$CF_3C_6H_4$
67c, X = 3,5-$(CF_3)_2C_6H_3$
67d, X = 2-(5-BuC_4H_2S)

95a-i

96a, 71%
96b, 31%
96c, 35%
96d, 47%
96e, 60%
96f, 44%
96g, 43%
96h, 62%
96i, 81%

Scheme 25. Synthesis of 6,12-diethynyl IFs **96a-i** [55].

Like **92a-b**, the absorption spectra of **96a-i** showed three low energy transitions with the λ_{max} values between 561 and 577 nm, corresponding to a band gap of 2.08−2.15 eV [55]. Cyclic voltammetry measurements exhibited first reduction potentials between –0.7 and –0.5 V and second reduction potentials between –1.2 and –1.0 V, correlating to LUMO energies that range between –4.0 and –4.1 V. Explanation for the lack of HOMO and LUMO energy level variation was due to low orbital density on the 2- and 8-positions, where only weak inductive electronic effects could be invoked.

While removal of ethynyl groups on the 5 and 11-positions did reduce steric hinderance, substitution had a significant impact on the crystal morphology of **96** [55]. Parent **96a** packed without any π-interactions (Fig. 10) where the closest intermolecular distance was an edge to face contact of 3.85 Å. Alternatively, **96h** exhibited one-dimensional columnar stacks with an intermolecular distance of 3.40 Å.

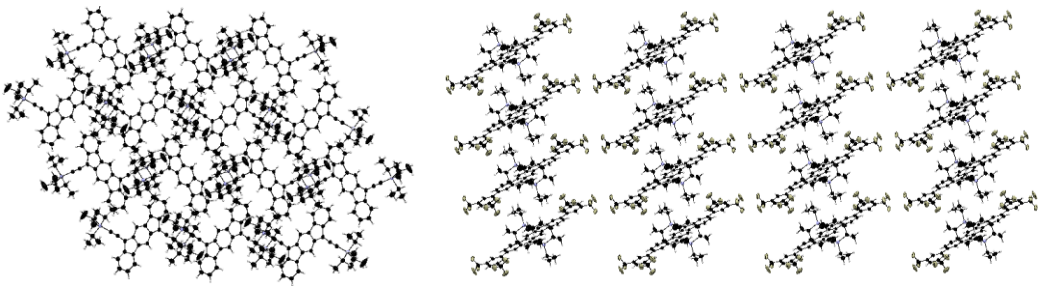

Figure 10. Solid state packing of **96a** (left) and **96h** (right) [55].

The next series of fully-conjugated indeno[1,2-*b*]fluorenes synthesized by Haley et al. was 6,12-diarylindeno[1,2-*b*]fluorenes (Scheme 26) [77]. Similar to **96a-i**, lithium-halogen exchange with the appropriate aryl halide and reaction with **22** afforded mixtures of stereoisomers **97a-i**. Reduction using anhydrous $SnCl_2$ at elevated temperatures provided **87a-j** in 36% to 59% yield. The electron withdrawing groups in **97h-j** necessitated the addition of a small amount of trifluoroacetic acid in order for the reaction to proceed in timely fashion.

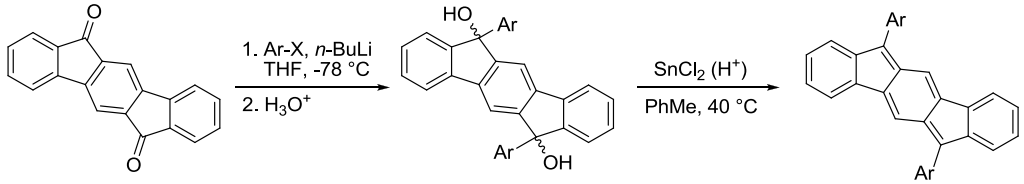

22

97a, Ar = Ph
97b, Ar = 4-$OMeC_6H_4$
97c, Ar = 2,4,6-$Me_3C_6H_2$
97d, Ar = 4-MeC_6H_4
97e, Ar = 4-FC_6H_4
97f, Ar = 4-ClC_6H_4
97g, Ar = 4-BrC_6H_4
97h, Ar = 4-$CF_3C_6H_4$
97i, Ar = 3,5-$(CF_3)_2C_6H_3$
97j, Ar = C_6F_5
97k, Ar = 2,6-$F_2C_6H_3$
97l, Ar = 9-Anthryl

87a, 55%
87b, 37%
87c, 42%
87d, 36%
87e, 50%
87f, 48%
87g, 59%
87h, 42%
87i, 39%
87j, 38%
87k, 23%
87l, 14%

Scheme 26. Synthesis of 6,12-diaryl IFs **87a-m** [77,78].

The absorption spectra for **87a-j** displayed a greater variation in λ_{max} values than **96a-i** due to the higher amount of orbital density found on the 6 and 12-positions of the IF core. Cyclic voltammetry data for **87a-j** showed that the diaryl IFs exhibit redox amphoterism, a trait not seen in the previous fully conjugated indeno[1,2-*b*]fluorenes. This is easily observed with 6,12-diphenyl [1,2-*b*]IF **87a**, as it exhibited two reduction peaks and three oxidation peaks. The reduction and oxidation values for **87a-j** corresponded to HOMO and LUMO energies that range between –5.5 to –5.8 eV and –

3.6 to –4.0 eV, respectively. Coincidentally, **87e** displayed reduction and oxidation potentials within 0.03 V that of **88**.

Single crystal OFETs were fabricated with microcrystals of **87j** as the active channel [77]. With Au source/drain contacts and Au electrodes, the OFET showed ambipolar charge transport, with saturation hole and electron mobilities of 7 x 10^{-4} and 3 x 10^{-3} $cm^2/V{\cdot}s$, respectively.

Concurrent with the Haley studies, Yamashita et al. reported the synthesis and properties of 6,12-diarylindeno[1,2-*b*]fluorenes **87k-m** as well as **87a** (Scheme 26) [78]. While their molecules exhibited redox amphoterism as well, the Japanese authors reported only a single oxidation and reduction wave for each. Vapor-deposited thin film OFETs of **87k-l** also showed ambipolar charge transport but at diminished mobilities (hole: 1.9 x 10^{-5} and 1.1 x 10^{-5} $cm^2/V{\cdot}s$, respectively; electron: 8.2 x 10^{-6} and 1.6 x 10^{-6} $cm^2/V{\cdot}s$, respectively).

Other Indeno[1,2-*b*]fluorenes

First synthesized by Deuschel in 1951 via dehalogenation of **23** (Scheme 27) [26], 6,12-dihydroindeno[1,2-b]fluorene (**26**) can be viewed as a planarized *p*-terphenyl derivative. As a result of the enforced geometry, there is greater conjugation between the phenyl rings, which imparts more desirable emissive properties; thus, this core unit has been utilized in a wide variety of molecular and polymeric systems—far too many to be reviewed herein. Rather, selected, salient examples will be presented.

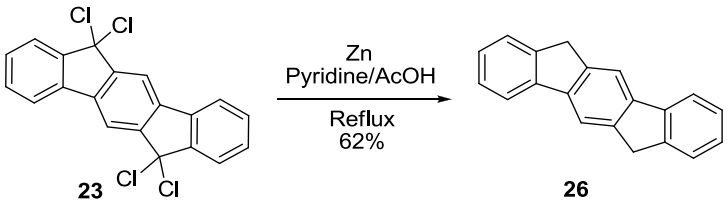

Scheme 27. Original synthesis of 6,12-dihydroindeno[1,2-*b*]fluorene (**26**) [26].

Common synthetic routes to **26** typically involve reduction of dione **22**. Another intriguing method, however, involves the use of palladium with *N*-heterocyclic carbene ligand **L** (Scheme 28) [79]. Presumably, the cascade begins with oxidative addition of the aryl halide to the catalyst. Activation of the benzylic C-H bond for insertion of the metal leads to intramolecular aryl-aryl couplings via subsequent reductivive eliminations from the palladium center. This elegant reaction can produce both 6,12-dihydro[1,2-*b*]IFs and 10,12-dihydro[2,1-*b*]IFs in greater than 90% yield from the appropriate terphenyl precursor.

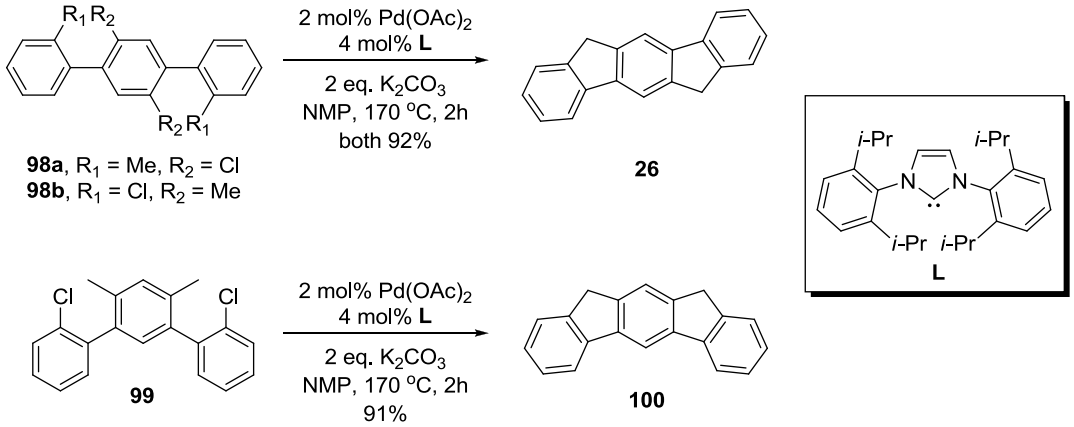

Scheme 28. Synthesis of **26** and [2,1-*b*]IF **100** [79].

Many synthetic routes are utilized to generate 6,12-functionalized dihydroindeno[1,2-b]fluorenes, typically from **22** or **26**. One direct method is base-promoted alkylation of the methylene carbons of **26**. For example, lithiation of **26** and followed by treatment with 1-bromooctane gave tetrasubstituted **101** (Scheme 29) [80].

Subsequent bromination at the 2- and 8-positions with CuBr/alumina furnished **102**, which could then be polymerized to form polyindenofluorene **103** linked at the 2- and 8-positions rather than at the 6- and 12-positions as seen in Scherf's polyindenofluorene **85**. Muellen and co-workers found that **103** showed a bathochromic shift in fluorescence compared to polyfluorene (into the visible region) and it formed a liquid crystalline phase at high temperature, possibly making a suitable LED component.

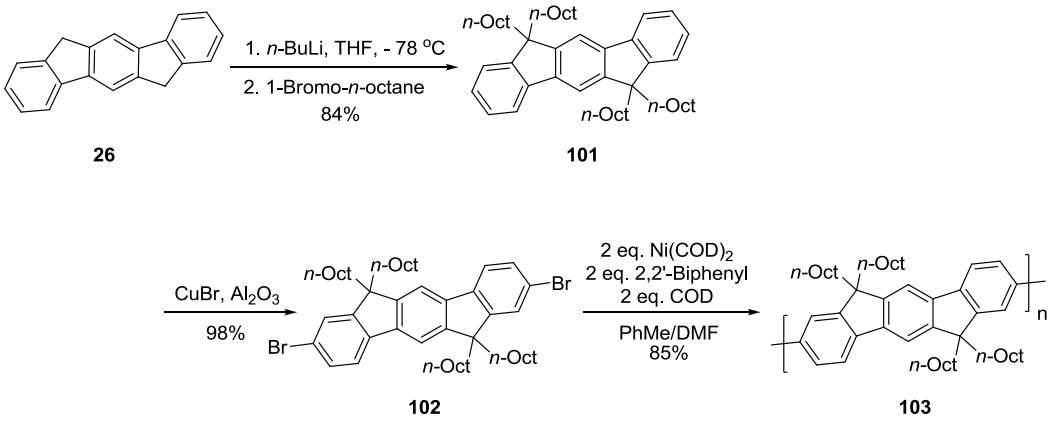

Scheme 29. Synthesis of polymer **103** starting from **26** [80].

An alternative route to functionalized dihydroindeno[1,2-*b*]fluorenes begins from fluorenone and involves intramolecular Friedel-Crafts alkylation in the final step, leading to spiro-fused derivatives—a method championed by Rault-Berthelot, Poriel, and coworkers. For instance, they prepared dispiro-fused [1,2-*b*]IF **106a** in an attempt to overcome issues in fluorene-utilizing OLEDs involving defects perturbing the color outputs of these devices (Scheme 30) [28, 81]. Beginning with 2,2"-diiodo-*p*-terphenyl (**104**), lithiation and subsequent addition of fluorenone furnished diol **105a**. Treatment with AcOH/HCl at reflux then gave **106a** in 55% yield over the two steps. Devices utilizing **110a** showed improved blue-emission without green contamination from defects [82].

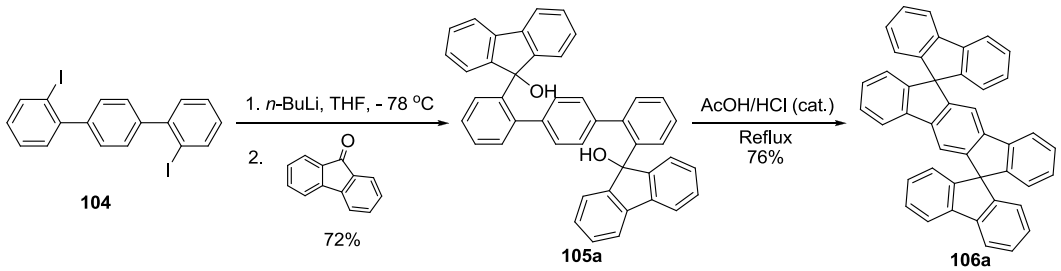

Scheme 30. Syntheses of dispiro-IF **106a** [28].

Further investigation by the same group found that, depending on the substrate and reaction conditions, two different products were often formed in this cyclization, thus limiting somewhat the scope of this synthesis to incorporate broader functionalization. When the fluorene moiety possessed steric bulk on the periphery, formation of a second product, the indeno[2,1-*a*]fluorene regioisomer, is favored. Its formation is also typically favored by use of less polar solvents and higher temperatures. In the reaction shown in Scheme 31, **106b** is formed in a ratio with **107** of roughly 3:1 when the reaction is done in DCM but the ratio shifts to 1:2 if the reaction is performed in acetonitrile, regardless of temperature. Adding even more steric bulk on the fluorene favors formation of the [2,1-*a*]IF to an even greater degree, suppressing formation of the [1,2-*b*]IF isomer completely if sufficient bulk exists [30].

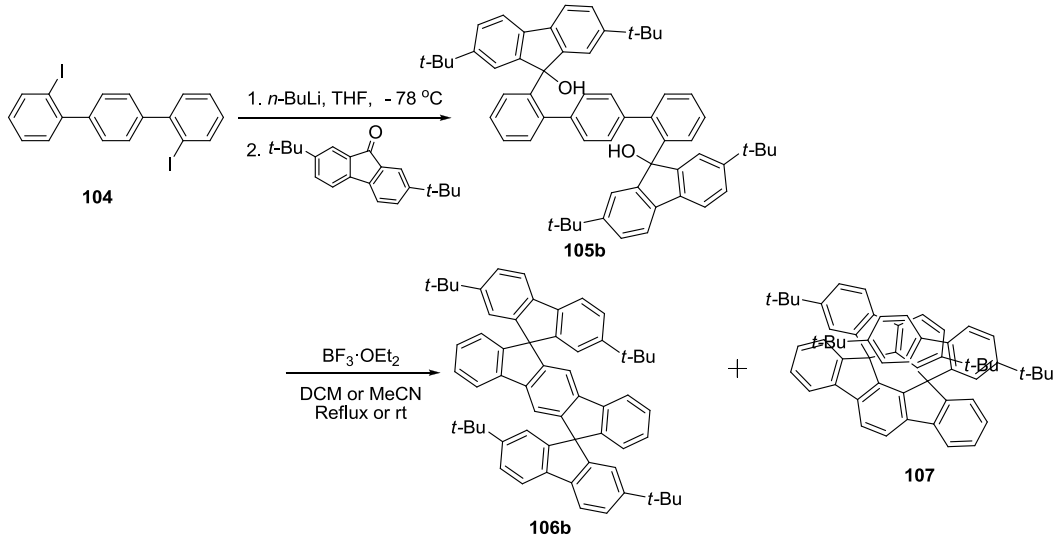

Scheme 31. Syntheses of dispiro-IFs **106b** and **107** [30].

This same group also investigated the use of dispiroxanthene-IF **108** in OLEDs, finding its properties little changed from those of the dispirofluorene-IF derivatives (Fig. 11) [83].

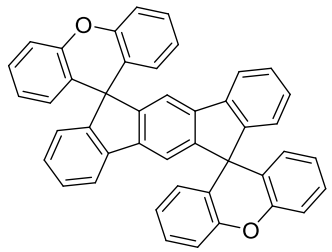

108

Figure 11. Spiroxanthene-fused [1,2-*b*]IF **108** [83].

Wong and colleagues found **109** to have a maximum power efficiency of ~4.0 lm/W and quantum external efficiencies greater than 8% when used as a red phosphorescent host with $Btp_2Ir(acac)$ in a phosphorescent OLED (PhOLED) (Fig. 12) [84]. The device also showed turn-on voltages of ~2.5-3.0 V. In addition, Wong's group has also synthesized **110** and used it as a host material for a green PhOLED with $ppy_2Ir(acac)$, achieving a hext of 14% and hp of >33 lm/W at 10000 cd/m^2 with an operating voltage of 5 V.

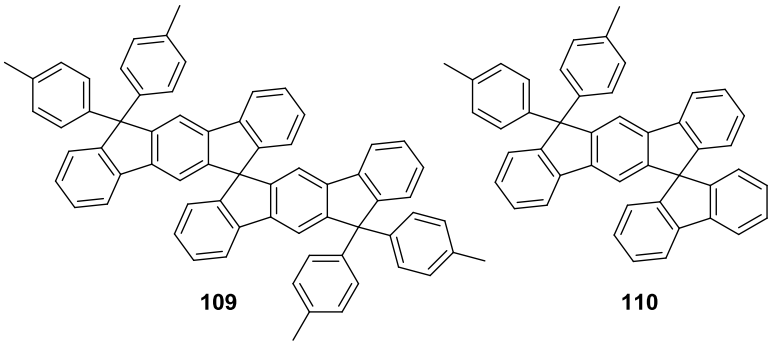

109 **110**

Figure 12. Structures of IFs **109** and **110** [84].

Lee and coworkers synthesized IF-oligomer **111** (Fig. 13) [85] and utilized it as a blue dopant in the emitting layer of a blue OLED with maximum power efficiency of 4.8 lm/W and quantum efficiency of 6.4% at 20 mA/cm^2 [86].

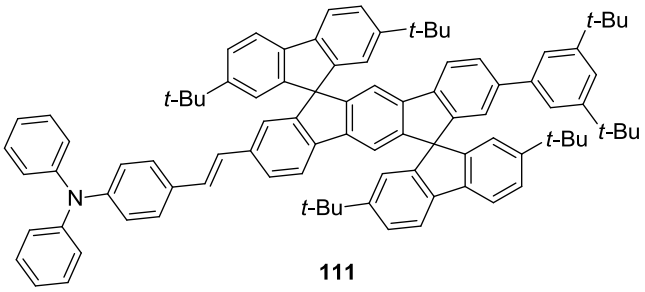

111

Figure 13. IF-oligomer **111** [85].

Ie et al. prepared fluorinated 6,12-dihydro-IF derivatives **112a-g** in an attempt to achieve large electron affinities (EAs) to facilitate n-type charge transport in OFETs (Scheme 32) [87]. With **112d**, **f**, and **g** they achieved EAs ca. –3 eV but no device attributes were discussed.

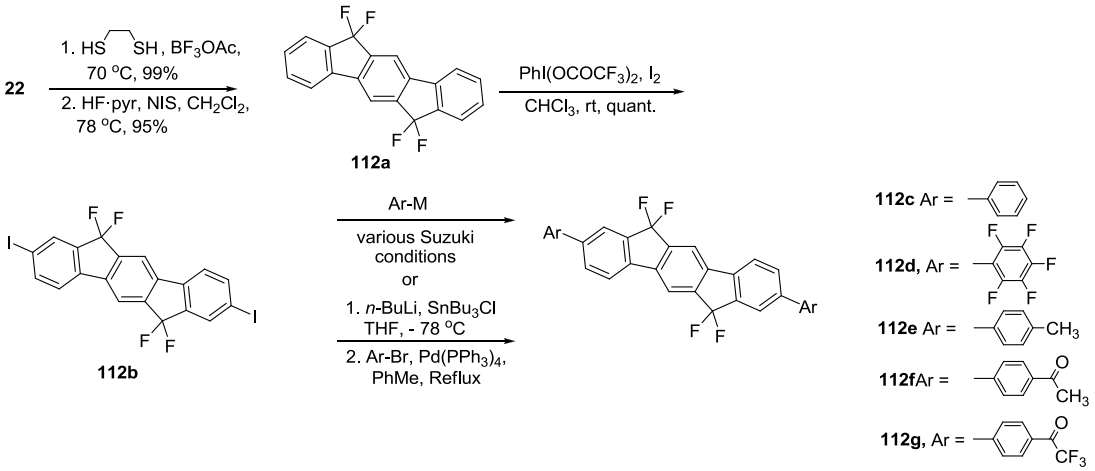

Scheme 32. Synthesis of 6,12-tetrafluoro [1,2-*b*]IFs **112a**–**g** [87].

Indeno[2,1-*a*]fluorenes

Indeno[2,1-*a*]fluorene-11,12-diones

The first account of the indeno[2,1-*a*]fluorene core in the literature dates to 1939 when Weizmann investigated polycyclic structures and their potential carcinogenic properties [23]. Intramolecular Friedel-Crafts acylation of 3,6-diphenylphthalic anhydride (**113**) in refluxing CS_2 afforded fluorenone carboxylic acid **114** (Scheme 33). Acid

chloride formation and subsequent cyclization in concentrated sulfuric acid generated the parent indeno[2,1-*a*]fluorene dione **115** in 5% yield with respect to **113**. This was reaffirmed by Deuschel in 1951 where **115** is obtained in 72% under the same conditions [26].

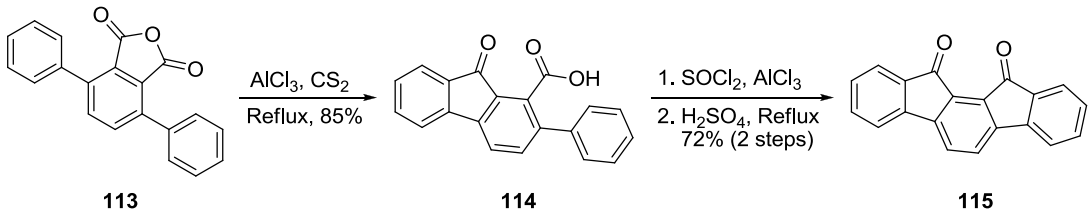

Scheme 33. Preparation of parent indeno[2,1-*a*]fluorene dione **115** [23].

Recent work by Rault-Berthelot et al. considered an alternative pathway to **115**. (Scheme 34) [33]. Diels-Alder cyclization with *trans*,*trans*-1,4-diphenyl-1,3-butadiene (**116**) and dimethyl acetylenedicarboxylate (**117**) resulted in cyclohexadiene **118** where subsequent oxidation with Pd/C afforded terphenyl **119**. Direct cyclizaton of **119** using concentrated sulfuric acid does afford **115**, but only in 12% yield. Instead, saponification of **119** to diacid **120** followed by cyclization improves the yield of **115** to 38%.

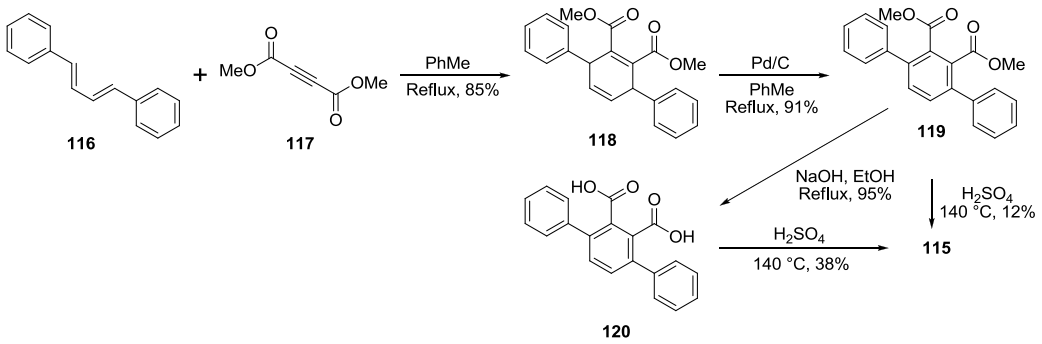

Scheme 34. Diels-Alder approach to the preparation of **115** [33].

Fully-conjugated Indeno[2,1-*a*]fluorenes

Like **2**, the indeno[2,1-*a*]fluorene isomer also supports full conjugation, illustrated by **3**, where an *o*-xylylene core (*o*-quinodimethane) is present in the structure (Fig. 14).

As such, interest in this structure lies in the potential of the *o*-xylylene core to exist as a stable open shell configuration (**3b**).

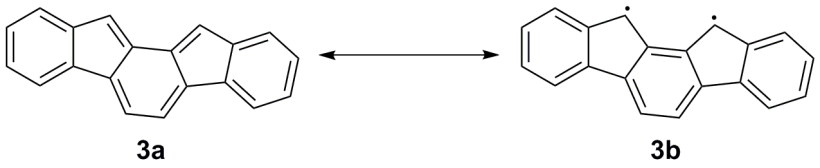

Figure 14. Resonance structures of **3**.

Work on **3** originated in 1957 when LeBerre reacted phenylmagnesium bromide with **115** to form diol **121** (Scheme 35) [88]. Refluxing in a hydrobromic acid/acetic acid solution resulted in dibromide **122**, where reduction using elemental Cu afforded diphenylindeno[2,1-*a*]fluorene **123a** in 63% yield. While **123a** readily degraded in aerobic conditions, solutions under an inert atmosphere were said to be stable but no information regarding time were given. However, due to these air-sensitivity issues as well as time limitations, no further investigation of its structural or electronic properties was explored.

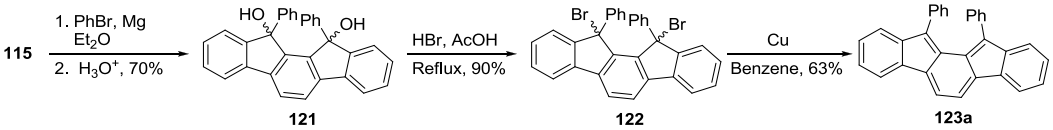

Scheme 35. Preparation of fully conjugated 11,12-diphenylindeno[2,1-*a*]fluorene **123a** [88].

Recent work by Tobe examined the synthesis of 11,12-dimesitylindeno[2,1-*a*]fluorene **123b**, which was also derived from **115** (Scheme 36) [89]. After reaction of **115** with mesitylmagnesium bromide, diol **124** was reduced with anhydrous $SnCl_2$ in the presence of trifluoroacetic acid at elevated temperatures in toluene to afford **123b** in 48% yield. Fortunately, a dichlorination **123b** was stable at least one week in light and air and

showed no reactivity with maleic anhydride. The researchers attributed this robustness to the bulky mesityl groups adequately shielding the reactive 11- and 12-positions.

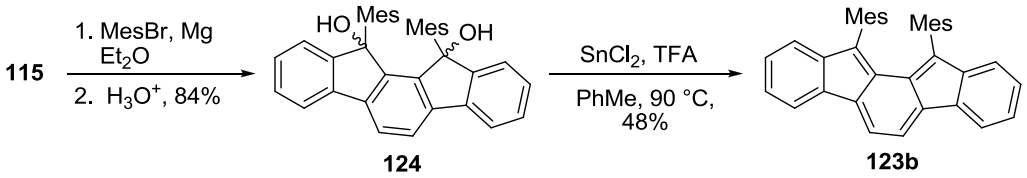

Scheme 36. Preparation of fully conjugated 11,12-dimesitylindeno[2,1-*a*]fluorene **123b** [89].

The absorption spectra of **123b** showed three distinct transitions in the 480 to 540 nm domain (λ_{max}: 537 nm) as well as a low energy tail at 730 nm, affording a 1.70 eV band gap energy. As with the previous mentioned fully conjugated [1,2-*b*] IFs, no fluorescence was observed for **123b**. Cyclic voltammetry data showed that **123b** exhibited both a reversible oxidation and reduction at –1.51 and 0.59 V, respectively.

X-ray single crystals of **123b** clearly showed the indeno[2,1-*a*]fluorene scaffold (Fig. 15). Interestingly, two independent molecules of **123b** were found where the mesityl groups are either in an eclipsed or staggered fashion (top and bottom, respectively), exhibiting a torsion angle of 1.7° and 15.2°, respectively. Examination of the internal bond lengths of **123b** revealed the expected alternating long (1.431 and 1.480 Å) and short (1.359 and 1.391 Å) motif, similar to **92a**.

Indeno[2,1-*b*]fluorenes

Indeno[2,1-*b*]fluorene-10,12-diones

The first account of 10,12-indeno[2,1-*b*]fluorene dione **17** dates to 1951 when Deuschel condensed phenylbenzoylacetylene (**125**) with ketodiester **126** to afford *m*-terphenyl diester **127** (Scheme 37) [26]. Saponification of **127** to **128** and subsequent ring

closure yielded 11-hydroxy-[2,1-*b*]IF dione **129**. Reduction using Zn metal provided 10,12-dihydro [2,1-*b*]IF **100**. A final oxidation with sodium dichromate gave dione **17**.

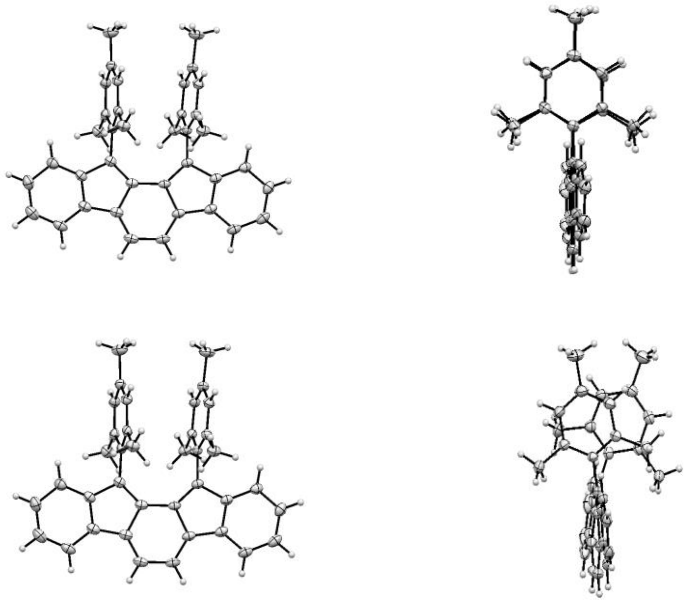

Figure 15. Eclipsed (top) and staggered (bottom) crystal morphs of **123b** [89].

Chardonnens and Ritter in 1955 reported an alternative pathway to **17** where 4,6-dibromoisophthalic acid (**130**) was converted to the acid chloride and subsequently underwent a two-fold Friedel-Crafts acylation with benzene to afford dibromodione **131** (Scheme 38) [27]. Aryl amination of **131** yielded **132** where a subsequent Sandmeyer-mediated cyclization gave **17** in 79% yield. The synthesis of substituted indeno[2,1-*b*]fluorenes has also been explored. As discussed earlier, the [2,1-*b*] isomer was often formed in equal amounts of the corresponding [1,2-*a*] isomer in a multitude of cyclizations performed by Chardonnens and coworkers (Scheme 3) [43].

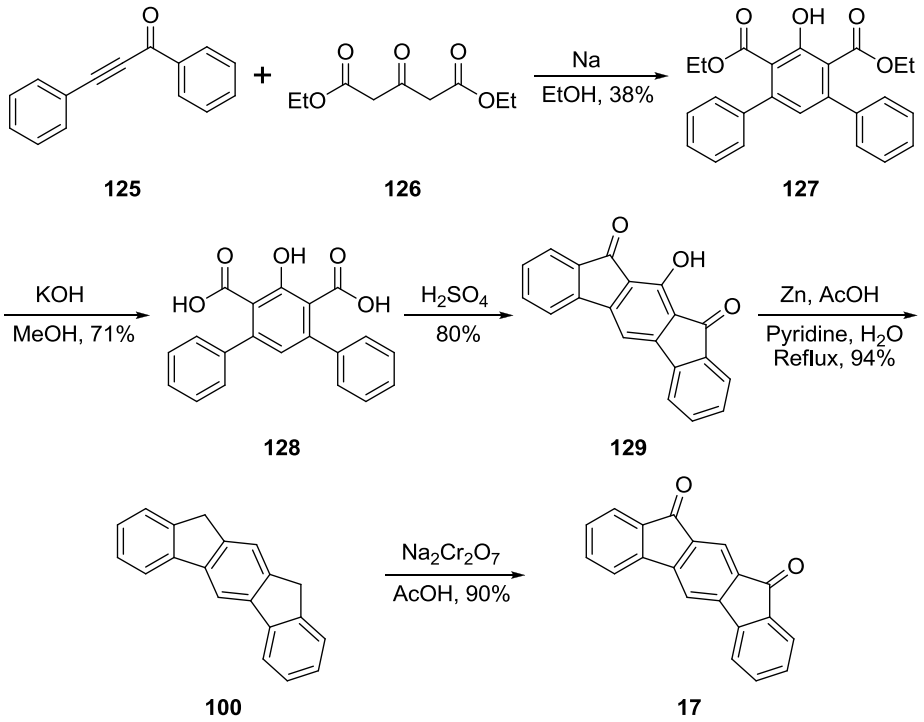

Scheme 37. Original preparation of parent indeno[2,1-*b*]fluorene dione **17** [26].

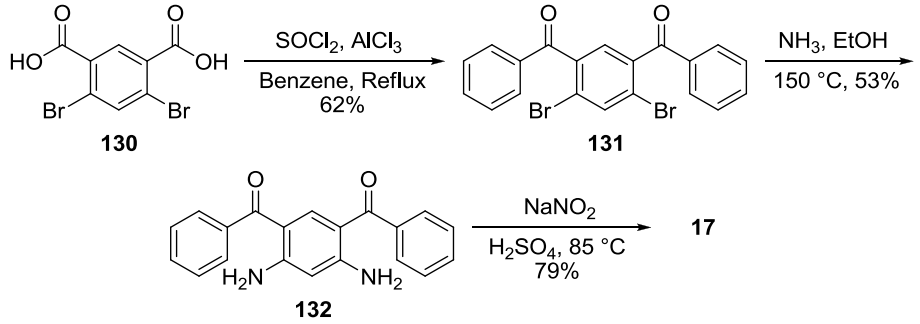

Scheme 38. Chardonnen's route to **17** [27].

Fully-conjugated Indeno[2,1-*b*]fluorenes

Full conjugation for the indeno[2,1-*b*]fluorene isomer is also possible (**4**, Fig.16). However, due to ring positioning, formation of the requisite xylylene core in **4** requires the disruption of two benzene rings rather than one needed for the [1,2-*b*] and [2,1-*a*] isomers. As such, **4** should display an asymmetrical arrangement of the π-system where the D and E-rings both possess *s-cis* diene linkages. Like the above mentioned fully conjugated [2,1-*a*] **3**, interest for **4** lies in its ground state biradical character (**4b**).

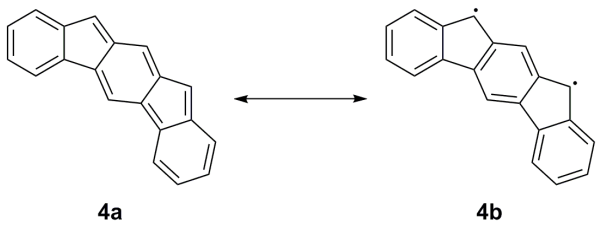

Figure 16. Resonance structures of **4**.

Currently, only one example of a fully-conjugated indeno[2,1-*b*]fluorene is known and its existence at this time remains unofficial [90]. Tobe et al. synthesized the molecule in a near identical manner in which **115** was made—IF dione **17** was reacted with two equivalents of mesitylmagnesium bromide to form diastereomeric diols **133**. Further reaction with $SnCl_2$ in the presence of trifluoroacetic acid yielded 10,12-dimesitylindeno[2,1-*b*]fluorene **134** (Scheme 39). Little is known about this molecule in terms of optoelectronic or structural properties. Due to the presence of the two *s-cis* diene linkages, however, **134** is considerably less stable than its [1,2-*b*] and [1,2-*a*] counterparts.

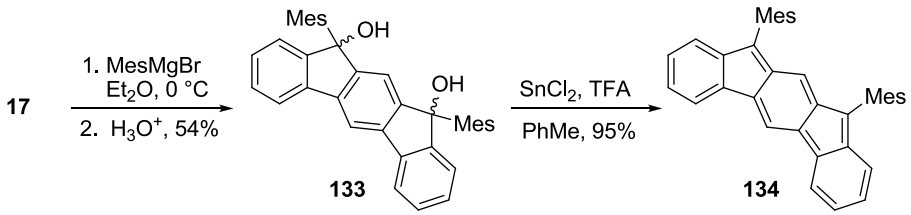

Scheme 39. Preparation of fully-conjugated 11,12-dimesitylindeno[2,1-*b*]fluorene **134** [90].

Other Indeno[2,1-*b*]fluorenes

In addition to the spiro-fused [1,2-*b*] and [2,1-*a*] IFs, Rault-Berthelot and colleagues also synthesized [2,1-*b*] derivative **137** for use in OLED devices (Scheme 40). They found that the compound had one of the highest triplet energies for a "morphologically-stable pure hydrocarbon" derivative for use in organic electronics [91].

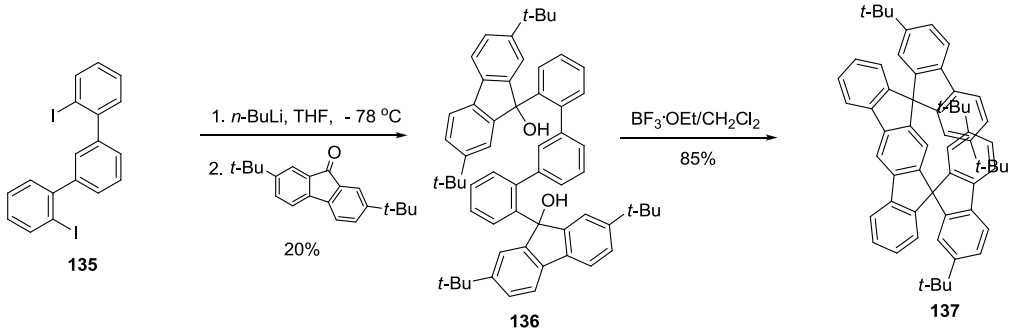

Scheme 40. Preparation of dispiro-[2,1-*b*]IF derivative **137** [91].

While pursuing their early work on [1,2-*b*] **111**, Lee and colleagues also investigated [2,1-*b*]IFs **138** and **142**. Tetraethyl IF **138** is easily synthesized by treatment of **100** with *n*-BuLi in THF and subsequent addition of 1-bromoethane (Scheme 41) [86]. Lewis acid-catalyzed bromination of **138** in chloroform gives **139**. Treatment of the dibromide with ca. 1.2 equiv. of *n*-BuLi in THF then addition of excess DMF gives the monoformylated IF **140**, followed by Suzuki cross-coupling and subsequent Horner-Wadsworth-Emmonds reaction to yield **142**.

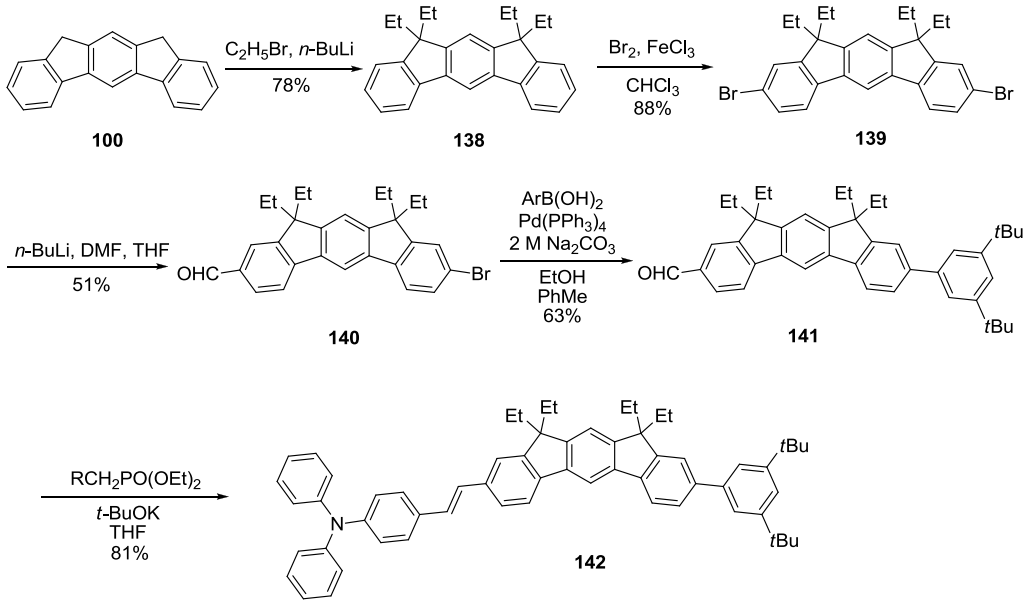

Scheme 41. Preparation of [2,1-*b*]IF derivative **142** [86].

Solid state data for **142** showed increased planarity with respect to **111**, with a bathochromic shift in fluroescence indicative of a longer conjugation pathway. The quantum yield of **142**, however, was greatly reduced compared to **111** and that, combined with poor overlap with the emission spectrum of the host compound, led to its lower device efficiencies (PE_{max} ~ 1 lm/W, EQE ~ 1.6% at 20 mA/cm^2).

Indeno[2,1-*c*]fluorenes

Indeno[2,1-*c*]fluorene-5,8-diones

The first account of the [2,1-*c*]IF dione in the literature occurred in 1961 where work by Ginsburg and Altman investigated the Diels-Alder chemistry regarding bi(cyclopentenes) and bi(cycloheptenes) (Scheme 42) [92]. They found that reaction of indanone **143** in the presence of Al amalgam resulted in pinacol **144**, which further eliminated in refluxing acetic acid and acetic anhydride to form 3,3'-biindenyl **145**. Cyclization of **145** with maleic anhydride (**146**) afforded anhydride **147**. Decarboxylation of **147** using elemental Cu, barium hydroxide, and soda glass at 400 °C generated 5,8-dihydroindeno[2,1-*c*]fluorene **148**; subsequent oxidation with sodium dichromate in refluxing acetic acid afforded dione **149**.

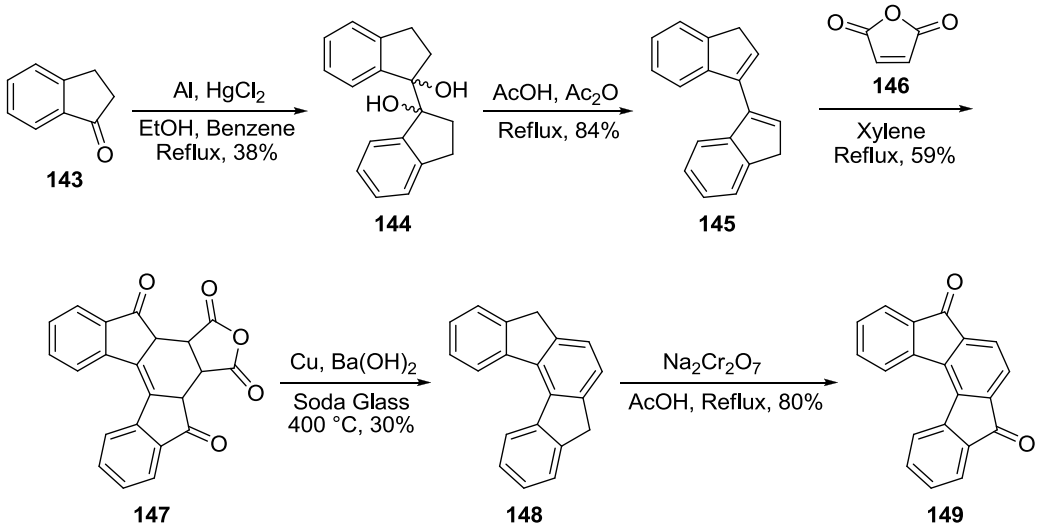

Scheme 42. Preparation of parent [2,1-*c*]IF dione **149** [92].

An alternative route to **149** was devised by Chardonnens and Chardonnens in 1966 where propiophenone (**150**) is converted to pinacol **151** through an aluminum amalgam in refluxing ethyl acetate (Scheme 43) [93]. Double elimination of **151** using acetyl chloride in refluxing acetic anhydride afforded diene **152** which is cyclized with **146** to give anhdyride **153**. Aromatization of the central ring using elemental sulfur at 280 °C formed terphenyl anhydride **154**. Saponification to **155** and subsequent decarboxylation using the Lazier catalyst at 215 °C yielded 3,6-dimethyl-1,2-diphenyl benzene (**156**). Oxidation via potassium permanganate in a refluxing solution of water and pyridine formed diacid **157** and further cyclization using concentrated sulfuric acid at elevated temperatures gave **149**.

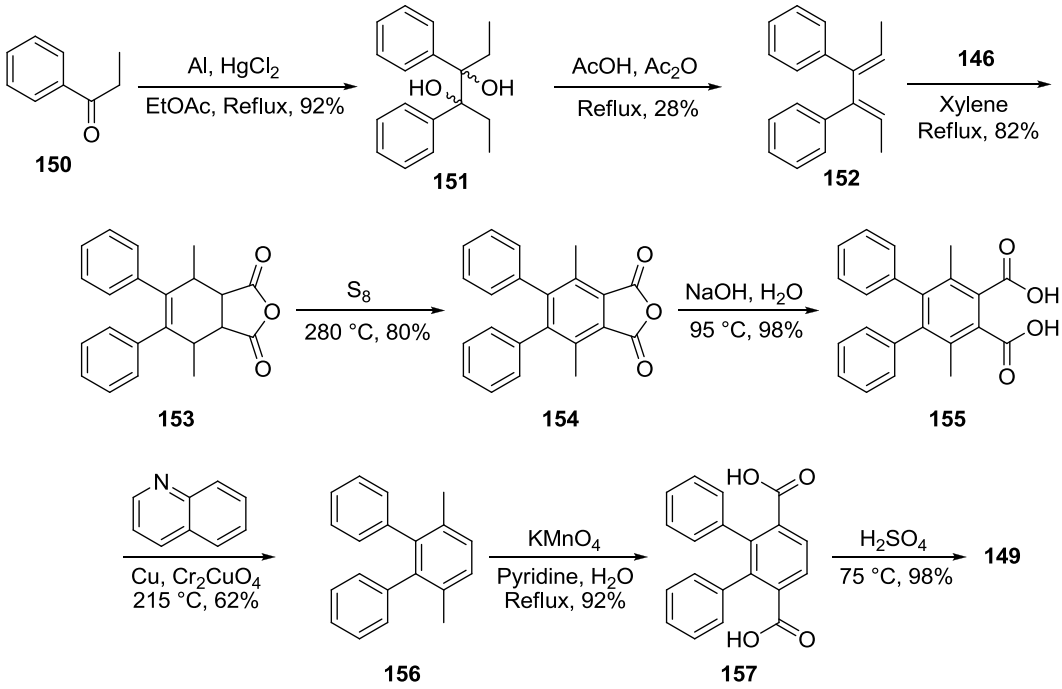

Scheme 43. Alternate synthesis to **149** [93].

The few examples of substituted [2,1-*c*]IF diones in the literature are limited to the 1, 6, 7, and 12-positions. For example, work by Wong and coworkers on the investigation of planarized cyclooctatetraenes cyclized diacid **158**, with polyphosphoric acid at elevated temperatures to form dione **159** where the 1 and 12-positions are tethered together with an ethane bridge (Scheme 44) [94]. A combination of bromination and elimination reactions on **159** resulted in an unsaturation to ethene- and ethyne-bridged IFs **160** and **161**, respectively.

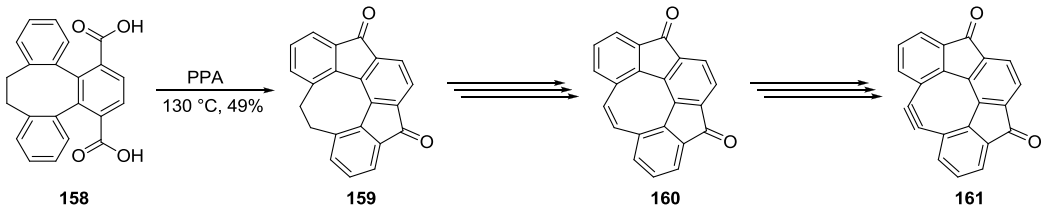

Scheme 44. Preparation of fused [2,1-*c*]IF diones **159**-**161** [94].

Wang's group achieved substitution at the 6 and 7-positions of the [2,1-*c*] core by reacting cyclopentadienone **162** with 4-octyne (**163**) in a Diels-Alder reaction to form

terphenyl diester **164** (Scheme 45) [95]. Cyclization with concentrated sulfuric acid gave 6,7-di-*n*-propyl [2,1-*c*]IF dione **165** in 79% yield. These results stand in contrast to the observations in Scheme 11 where use of either phenylacetylene or diphenylacetylene gave the corresponding [1,2-*b*] isomer in high yield.

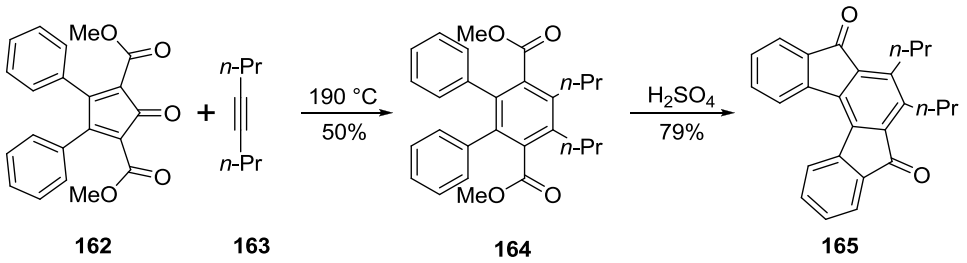

Scheme 45. Preparation of 6,7,-di-*n*-propyl [2,1-*c*]IF dione **165** [95].

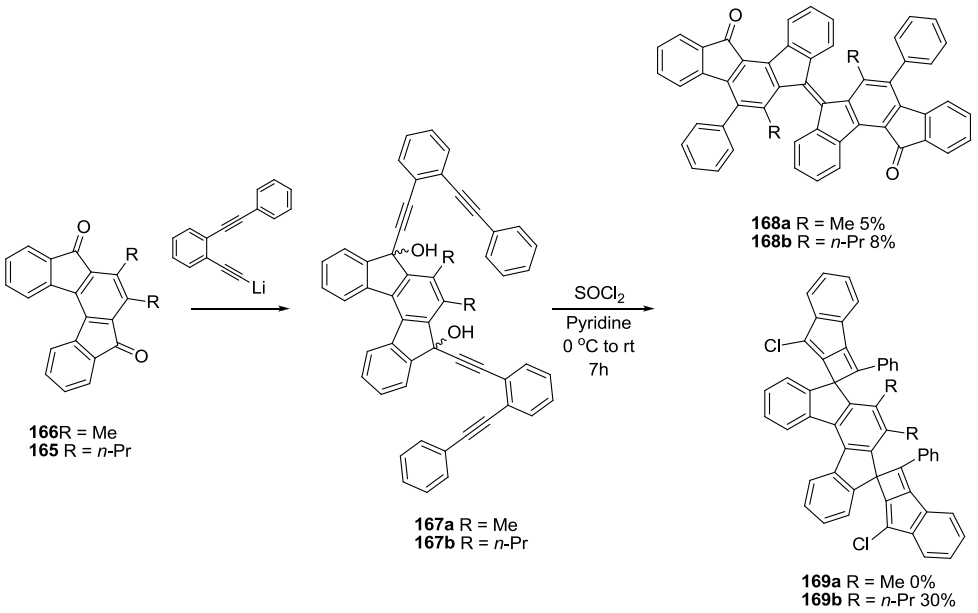

Scheme 46. Synthesis of dimerized [1,2-*a*]IFs **168a,b** and spiro-fused [2,1-*c*]IFs **169b** [95].

In addition, the same group found that reaction of [2,1-*c*]IFs **165** and **166** with an acetylide nucleophile gave diols **167a-b**; subsequent treatment with $SOCl_2$ induced a cascade cyclization forming [1,2-*a*]IF dimers **168a** and **168b** in low yield (Scheme 46) [95]. In the reaction that formed **168a**, spiro-fused [2,1-*c*]IF derivative **169a** was not detected, but in the reaction that formed **168b**, highly strained **169b** was the major product.

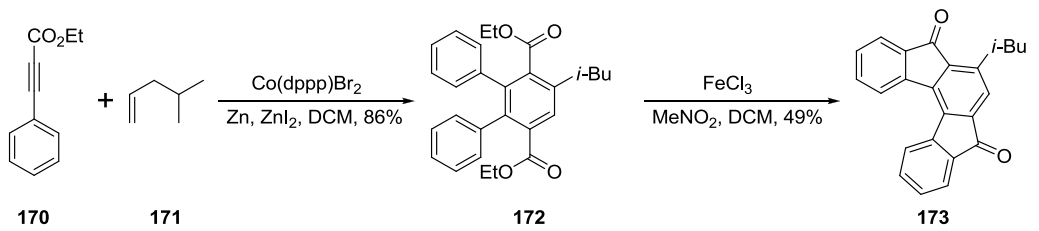

Scheme 47. Preparation of 6-isobutyl [2,1-*c*]IF dione **173** [96].

Fully-Conjugated Indeno[2,1-*c*]fluorenes

The first example of a fully-conjugated [2,1-*c*]IF (**175**) was recently realized by the Haley group [97]. Similar to earlier syntheses by Haley and Tobe, addition of mesityl anion to dione **149** gave **174** as a mixure of stereoisomers. $SnCl_2$ treatment in the succeeding step gave **175** as a green solid, as opposed to the magenta hue common to the fully-conjugated [1,2-*b*]IFs. The absorption spectrum of **175** displayed a broad region of lower energy transitions ranging from approximately 500 nm to nearly 800 nm with the local λ_{max} at 601 nm. Interestingly, and in contrast to the [1,2-*b*]IFs, cyclic voltammetry data showed that arylation/full conjugation in **175** lead to a LUMO that is destabilized with respect to that of parent [2,1-*c*]IF dione **149** (LUMO energies of 3.59 eV and 3.78 eV, respectively). Work on further derivatization of this scaffold is ongoing.

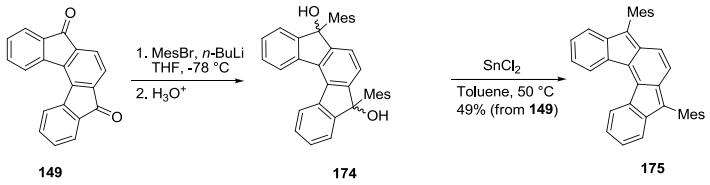

Scheme 48. Synthesis of 5,8-dimesityl [2,1-*c*]IF **175** [97].

Other Indeno[2,1-*c*]fluorenes

Youngs and Tessier synthesized one of the few [2,1-*c*]IF derivatives not already discussed [98]. Treatment of tribenzocyclotriyne **176** with four equivalents of *n*-BuLi

collapsed the annulene core to furnish the [2,1-*c*]IF dianion **177**; subsequent quenching with MeOH as the proton source affored the benzo-fused dihydroIF **178** (Scheme 49).

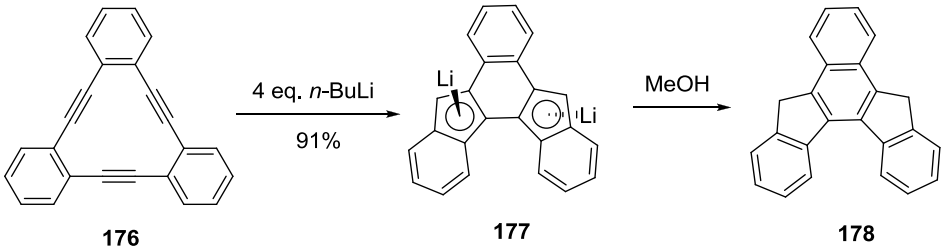

Scheme 49. Lithium-induced cyclization to form dihydro [2,1-*c*]IF **178** [98].

Conclusion

Unsurprisingly, given their interesting electronic properties, indenofluorenes, like many PAHs, are experiencing a considerable reemergence into the current literature. While recent attention has mostly pertained to the [1,2-b] isomer, it is reasonable to expect that similar studies will be performed on the remaining isomers as high-yielding synthetic routes to these core structures become increasingly available. Fully conjugated indenofluorenes, too, are of great interest both from a fundamental chemistry standpoint (paratropicity, para-quinodimethane subunit, stability, bonding) as well as potential applications as organic semiconductors (large electron affinities, charge-transport characteristics). Given the large number of indenofluorene papers generated this past decade, the future prospects for this class of molecules indeed look bright.

Bridge to Chapter II

Chapter I serves as a review of indenofluorene research through mid-2012. Chapter II serves to demonstrate our early pioneering work in the realm of fully-reduced indenofluorenes with our achievement of stable, fully-reduced ethynylated indeno[1,2-*b*]fluorenes.

CHAPTER II

SYNTHESIS, CRYSTAL STRUCTURES, AND PHOTOPHYSICAL PROPERTIES OF ELECTRON-ACCEPTING 6,12-DIETHYNYLINDENO[1,2-*b*]FLUORENES

This chapter was co-authored with Daniel T. Chase, who assisted with synthesis and wrote much of the body of the original paper, Bradley D. Rose, who performed computational studies, Christopher D. Weber, who performed electrochemical experiments, Shunpei Nobusue and Chelsea E. Stockwell, who also assisted to a lesser degree with synthetic experiments, Lev N. Zakharov, who performed single crystal X-ray analyses, as well as Mark C. Lonergan, and Michael M. Haley, who provided guidance and editorial assistance. This work was originally published in *Angewandte Chemie, International Edition*.

Introduction

Polycyclic hydrocarbons that possess extended π-conjugation are of significant interest because of their potential use as in optical and electronic device applications such as light emitting devices, field-effect transistors and solar cells.[1] While a majority of studies have focused on acenes such as pentacene and its derivatives (e.g., **1** in Figure 1),[2] these systems are susceptible to oxidative and photolytic degradation;[3] thus, there is a need for alternative, acene-like molecules. One avenue in this search has explored compounds containing five-membered rings, rather than the more traditional six-membered rings. Prime examples of such molecules are dibenzopentalene (**2**) and derivatives, where the groups of Saito, Kawase, and Tilley have recently described improved methods for their construction.[4]

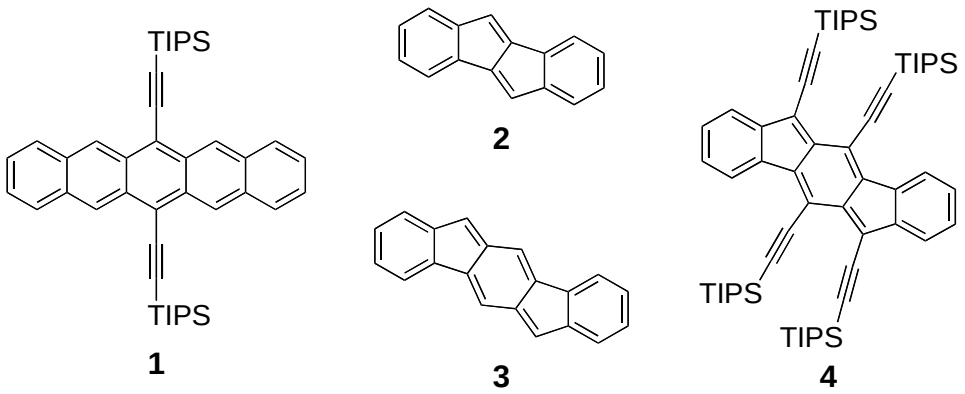

Figure 1. Polycyclic hydrocarbons **1** – **4**.

Another attractive topology is the indeno[1,2-b]fluorene (IF) skeleton (e.g., **3**), an acene analogue where the B and D rings each contain one fewer carbon atom, thus making the 20 π–electron molecule formally anti-aromatic. While the pentacyclic IF core is common in the literature, nearly all examples bear substituents on the 6 and 12 positions, resulting in either cross-conjugation (e.g., ketones, exocyclic olefins)[5] or disrupted conjugation (e.g., disubstitution, spiro-fusion).[6] Of the four fully conjugated IFs known prior to 2011, three are rapidly oxidized by trace oxygen[7] and the other is poorly characterized.[8]

Very recently we reported the synthesis of tetraalkynylated indeno[1,2-b]fluorenes (e.g., **4**).[9] The compounds exhibited similar UV-Vis absorption profiles and slightly larger HOMO/LUMO energy gaps compared to **1** while maintaining potentially superior solution stabilities; however, the packing of **4** in the solid state resembled an expanded herringbone pattern, a motif often found in unsubstituted acenes. Since the steric bulk of the four interdigitated (triisopropylsilyl)ethynyl groups was the most likely cause for inhibiting a desirable "brick and mortar" π-stacking, we sought to examine additional IF derivatives.

As a guide for experimental studies, we performed DFT calculations (B3LYP/6-311+G**)[10] on a variety of substituted IFs (Figure 2). Our initial task was to determine the effect ethynylogation of **3** has on the HOMO (–5.53 eV) and LUMO energy levels (–3.03 eV) and energy gap (2.50 eV) of the IF core (Figure 1, Table 1). Inclusion of the four ethynyl units in **5** significantly lowers the LUMO by ca. 0.5 eV while the HOMO level remains unchanged, affording a gap energy of 1.97 eV. Inclusion of only two acetylenes on positions 5 and 11 (e.g., **6**) raises both the HOMO and LUMO (–5.62 and –3.24 eV, respectively) compared to **5** (–5.53 and –3.56 eV), affording a net gap increase of 0.41 eV. If the two alkynes are located on positions 6 and 12, as in **7**, the HOMO level (–5.51 eV) is on par with **5** and the LUMO is elevated slightly (–3.46 eV), thus

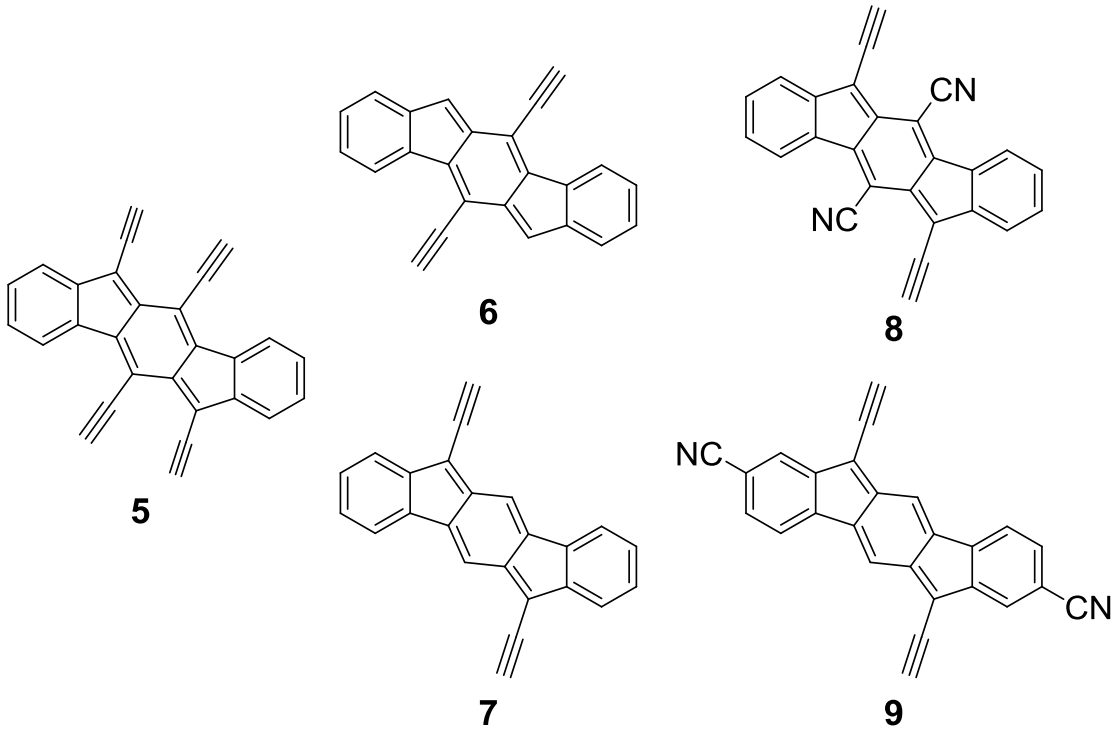

Figure 2. Calculated ethynylindenofluorene derivatives.

increasing the gap by only 0.08 eV. Similar to acenes,[2] these results illustrate that judicious positioning of the alkyne moieties will significantly affect electronic and photophysical properties.

Table 1. Computational, electrochemical, and optical data for indeno[1,2-*b*]fluorene derivatives.

	computational[a]			electrochemical[b]					optical	
compd	E_{HOMO}	E_{LUMO}	E_{Gap}	$E(A^+/A)$	$E(A/A, A/A^{2-})$	E_{HOMO}	E_{LUMO}	E_{Gap}	λ_{max}[c]	E_{Gap}[d]
3	–5.53	–3.03	2.50	—	—	—	—	—	—	—
4/5[e]	–5.53	–3.36	1.97	1.23	–0.62, –1.16	–5.92	–4.07	1.85	594	1.98
6	–5.62	–3.24	2.38	—	—	—	—	—	—	—
7	–5.51	–3.46	2.05	—	—	—	—	—	—	—
8	–6.00	–4.07	1.93	—	—	—	—	—	—	—
9	–6.19	–4.14	2.05	—	—	—	—	—	—	—
10a	–5.51	–3.46	2.05	1.20	–0.69, –1.20	–5.88	–4.00	1.88	568	2.12
10b	–5.79	–3.70	2.09	1.33	–0.60, –1.07	–6.01	–4.08	1.93	561	2.15
10c	–5.82	–3.74	2.08	1.35	–0.59, –1.07	–6.03	–4.09	1.94	567	2.13
10d	–5.83	–3.75	2.08	1.32	–0.60, –1.10	–6.01	–4.09	1.92	567	2.13
10e	–5.43	–3.36	2.07	1.16	–0.69, –1.27[f]	–5.84	–3.99	1.85	569	2.11
10f	–5.53	–3.47	2.06	1.21	–0.66, –1.20[f]	–5.90	–4.03	1.87	570	2.10
10g	–5.81	–3.75	2.06	1.25	–0.62, –1.11	–5.93	–4.06	1.87	572	2.11
10h	–5.97	–3.91	2.06	1.35	–0.52, –1.00	–6.03	–4.16	1.87	570	2.11
10i	–5.89[g]	–3.83[g]	2.06[g]	—[h]	—[h]	—[h]	—[h]	—[h]	577	2.08
PCBM[i]	—	—	—	1.54	–0.71, –1.12	–6.2	–3.95	2.35	—	—

[a] Calculations performed at the B3LYP/6-311+G** level of theory; energies in eV. For computational efficiency, the TIPS groups of **10a-i** were replaced by H atoms. [b] CV recorded using 1–5 mM of analyte in 0.1 M Bu4NOTf/CH2Cl2 using a scan rate of 50 mV/s. The working electrode was a glassy carbon electrode with a Pt coil counter electrode and Ag wire pseudo reference. Values reported as the half-wave potential (vs. SCE) using the Fc^+/Fc couple (0.46 V) as an internal standard. HOMO and LUMO energy levels were approximated using SCE = –4.2 eV vs. vacuum; see Ref. [5b]. Reduction potentials in V; energies in eV. [c] Spectra obtained in $CHCl_3$; wavelength in nm. [d] The optical HOMO–LUMO gap was determined as the intersection of the x-axis and a tangent line that passes through the inflection point of the lowest energy absorption; energies in eV. [e] Experimental data for **4**; computational data for **5**. [f] The second reduction wave was irreversible; the potential of the peak anodic current is reported. [g] Me group in place of Bu to simplify calculations. [h] Unable to obtain. [i] Converted from Ref. [12].

Functionalization of the favorable 6,12-diethynyl-IF scaffold with electron withdrawing groups further lowers the calculated HOMO and LUMO energies. For instance, dicyano-functionalized IFs **8** and **9** exhibit calculated HOMO energies of –6.00

and –6.19 eV, respectively, and LUMO energies of –4.07 and –4.14 eV, respectively. Such molecules may prove to be suitable n-type organic semiconductors, as these energy levels and gaps closely resemble those of ubiquitous electron acceptor PCBM[11] (–6.2 and –3.95 eV).[12] Encouraged by these initial computational studies, we targeted a number of 6,12-diethyn-ylindeno[1,2-b]fluorenes for synthesis and study. We disclose herein the preparation of IFs **10a**–**i** along with their respective optical, electrochemical and computa-tional data. We also report the X-ray structures of **10b** and **10h**, highlighting the effects that substit-ution on the IF core has on crystal packing.

Since the transannular cyclization route previously used to synthesize the IF core was low yielding, intolerant of facile substitution, and difficult to scale up,[7,9,13] we sought a more efficient pathway. Fortunately, dione **11a** is readily synthesized on multi-gram scale via a three-step Suzuki/Friedel-Crafts route devised by Merlet et al.[14] Addition of lithiated (triisopropylsilyl)-acetylene afforded crude diol **12a** (Scheme 1); subsequent reduction using $SnCl_2$ in toluene at 40 °C provided a deep magenta solution, from which crystalline IF **10a** was isolated in very good yield. This methodology could be extended to a number of 2,8-disubstituted IFs starting from the respective diones, either known (**11b**–**d**[15]) or easily synthesized (**11e**–**i**; see Supporting Information); thus, IFs **10b**–**i** were prepared via the same two-step process and isolated in moderate to very good yields after recrystallization (Scheme 1).

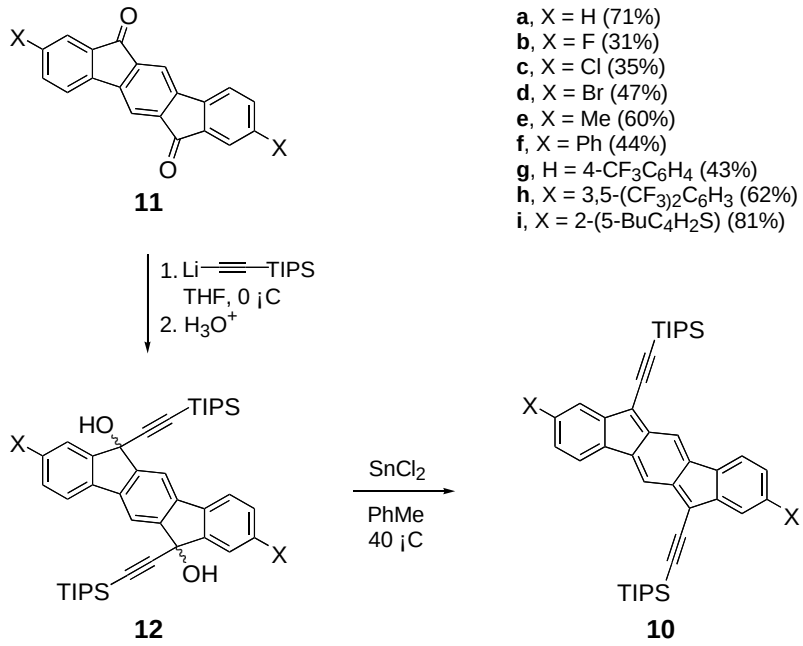

Scheme 1. Synthesis of diethynyl-IFs **10a–i**.

The absorption spectra of **4** and **10a**,**b**,**i** are shown in Figure 3 (see Supporting Information for **10c**–**h**). Similar to **4**, IF **10a** exhibits three low-energy absorptions (λ_{max} 567 nm), but these are blue-shifted ca. 25-30 nm compared to **4**. This can be attributed to removal of the two acetylenes at the 5 and 11 positions in **10a**. Interestingly, variation of the substituents bound to the IF core at the 2 and 8 positions has only modest effect on the absorption profiles: fluoro IF **10b** has the lowest λ_{max} value of 561 nm, whereas the λ_{max} of thienyl IF **10i** is at 577 nm. The optical data correspond to a relatively narrow 2.08–2.15 eV range for the HOMO-LUMO energy gaps of **10a**–**i**. As observed with **4**, **10a**–**i** are non-emissive, as is usually the case with [4*n*] π–electron systems.

Figure 4 depicts the experimental cyclic voltammetry (CV) data for **4** and **10a**,**b**,**h** (see Appendix A for **10c**–**g**). In solution, the IFdiyne scaffold shows quasi-reversible

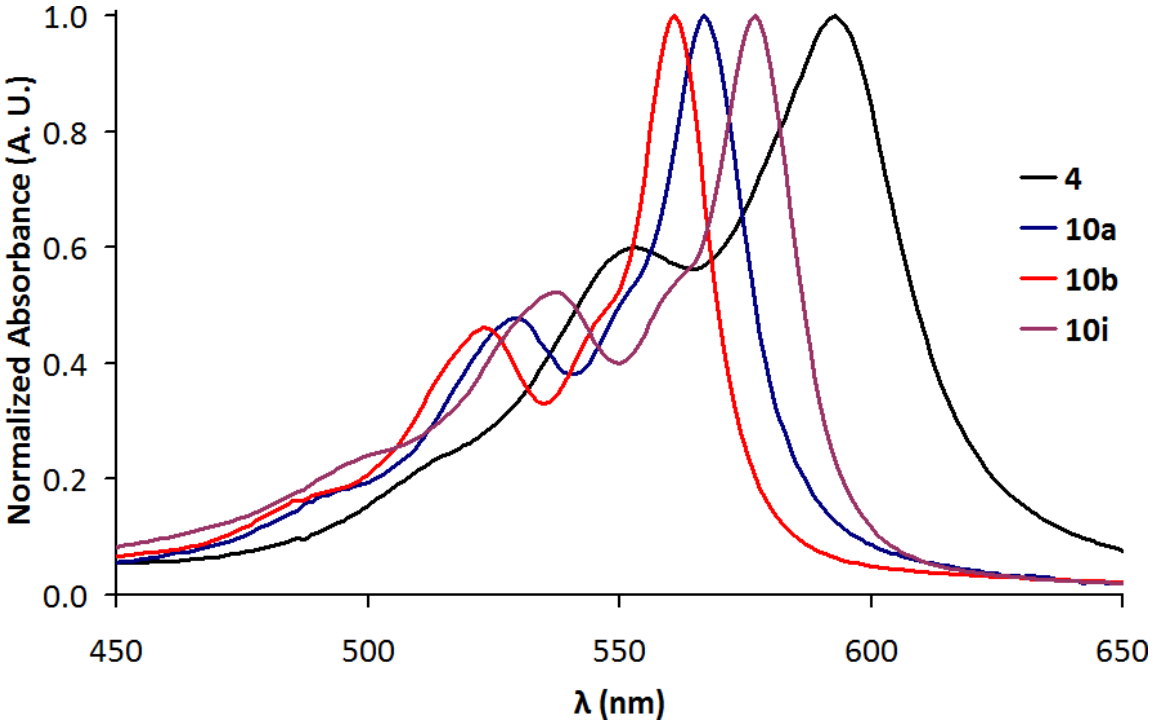

Figure 3. Electronic absorption spectra for IFs **4** and **10a**,**b**,**i**.

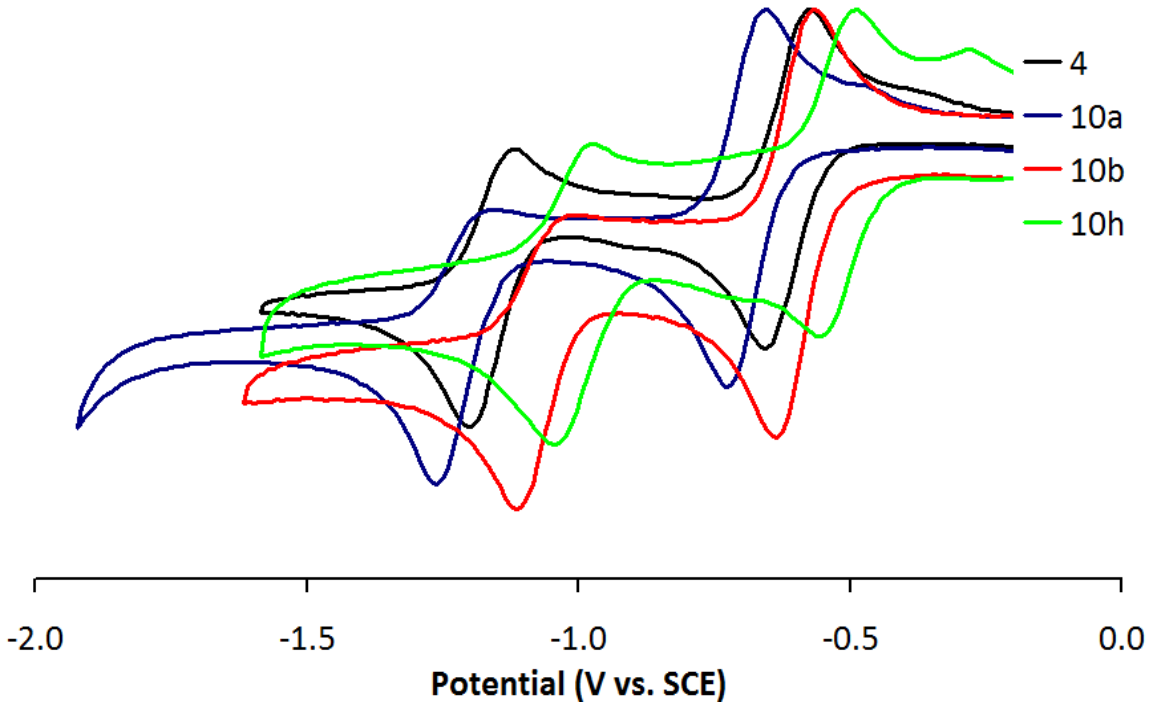

Figure 4. Cyclic voltammetry of IFs **4** and **10a**,**b**,**h**; voltammogram currents are normalized to the E_{pa} (A/A^{-}) peak.

behavior, accepting up to two electrons. The first reduction half-wave potential at ca. –0.5 to –0.7 V (vs. SCE) for **10a**–**h** is 0.2–0.3 V less negative than the recently reported diynyl IF-diones.[13] These data suggest that IFs have comparable or greater electron affinities to that of PCBM. Substitution of electron withdrawing groups on the IF core shifts the reduction half-wave potentials to less negative values. This is chiefly observed with parent **10a**, fluoro **10b**, and 3,5-$(CF_3)_2C_6H_3$ **10h**, which possess first reduction half-wave potentials of –0.69, –0.60, and –0.52 V, respectively. This trend is pronounced even further where **10a**, **10b**, and **10h** exhibit second reduction half-wave potentials of –1.20, –1.07, and –1.00 V, respectively. Unlike the IF-diones,[13] **10a**–**h** also exhibit an irreversible oxidation around 1.2–1.3 V (see Supporting Information). The above-mentioned trend also holds true for peak potentials for oxidation of the IF scaffold; substitution of increasing electron withdrawing groups shifts the potential to more positive values as demonstrated by **10a**, **10b**, and **10h**, which exhibit peak potentials of 1.20, 1.33, and 1.35 V, respectively. This behavior is justified by examining the products of reduction or oxidation: a two- electron reduction of the IF core results in a 22 π–electron species where every ring is aromatic, i.e., three benzenes and two Cp anions. Hence, an increase in electron withdrawing capability would better stabilize the dianion. Conversely, the formation of oxidative products, especially the 18 π–electron dication, would be destabilized by electron-withdrawing groups. The sole exception to the above mentioned behavior is **10i**, which exhibits an irreversible reduction and polymerizes under oxidative conditions..

Interestingly, while the electrochemically determined energy gaps are somewhat lower (1.85–1.94 eV) than the optical and computational values, all three data sets exhibit

a < 0.1 eV range of values, whether substituted with electron-rich or electron-poor groups. Examination of the calculated HOMO-LUMO plots for **10a** (Figure 5) reveals that the 2- and 8-positions possess little orbital density, and hence exhibit virtually no overlap. Therefore, perturbing the electronic nature of the IF scaffold from these positions can be performed only through weak inductive effects.

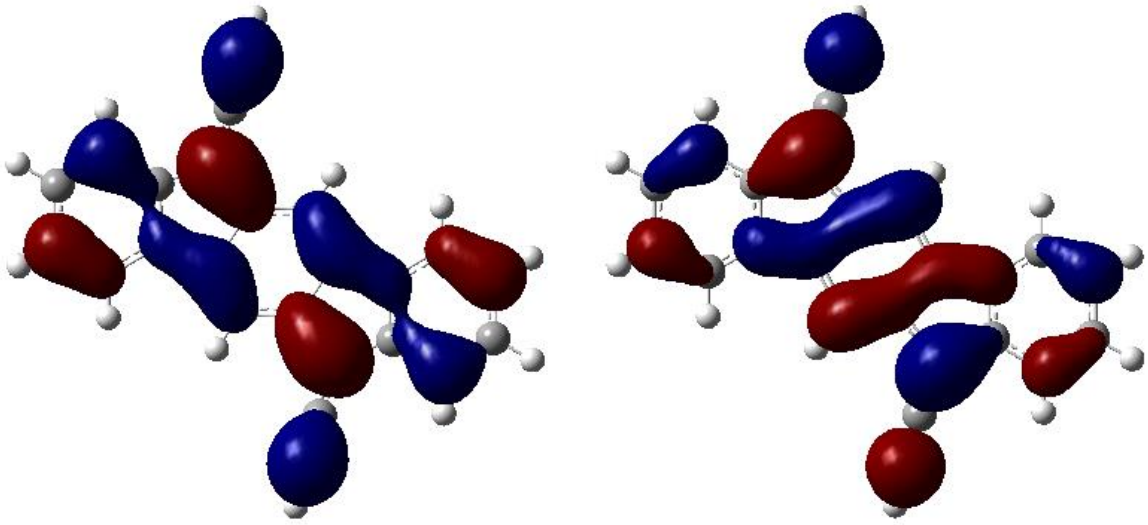

Figure 5. Calculated HOMO (left) and LUMO (right) plots of **10a**.

Single crystals of **10b** and **10h** suitable for X-ray diffraction were obtained from CH_2Cl_2/CH_3CN and $CHCl_3$, respectively (Figure 6). Similar to **4**, the molecular structures of **10b** and **10h** show that the fused ring system is essentially planar (within 0.017 and 0.042 Å, respectively); however, unlike **4**, the TIPS-capped acetylenes in both species are nearly linear (179°) and planar (0.5° deviation) with the 20-carbon-atom core, which is due to the fact that these lack the steric congestion that **4** possesses. Furthermore, the C–C bonds in the central six-membered ring are slightly compressed (0.02 Å) compared to **4**. In the crystal lattice IFs **10b** and **10h** are organized as 1-D π-stacks with close C•••C contacts of 3.43 and 3.40 Å, respectively. The 1-D π-stacks in **10b** form a layer with a

shift between two nearest π-stacks. Such an arrangement avoids strong π-interactions between the π-stacks in the layers, but some of C•••C contacts between 1-D π-stacks are in the range 3.14–3.50 Å, indicating that weak interactions between 1-D π-stacks in **10b** are possible. On the other hand, the 1-D π-stacks in the crystal of **10h** are isolated without specific interactions between them. Additionally, the peripheral 3,5-$(CF_3)_2C_6H_3$ groups for **10h** are nearly coplanar with the IF core, exhibiting a slight 5.5° twist, which is much less than the 35–45° torsion angle typically seen in most biphenyls.[16] This unexpected co-planarity is likely due to the enhanced overlap the phenyl rings provide as they lay directly above and below the central arene of the neighboring molecules as well as the interdigitation of two electron deficient $–CF_3$ groups with electron rich alkynes (3.50 Å intermolecular distance).

In summary, we have demonstrated a facile approach to a family of fully conjugated indeno[1,2-b]fluorenes. The optical and electrochemical data support the computational findings of low-lying HOMO and LUMO energy levels for **10a-i**. These values are similar to PCBM and other mainstream n-type semiconductors, suggesting that IFs could be potential compliments to the usually p-type acenes. Through X-ray crystallography, **10b** and **10h** were shown to pack in dimeric π-stacks in the solid-state, which further improves their credibility for materials applications. Future work will consist of employing **10a-i** in realistic device settings to test their performance as n-type semiconductors, as well as exploring further derivatization of the indeno[1,2-b]fluorene scaffold.

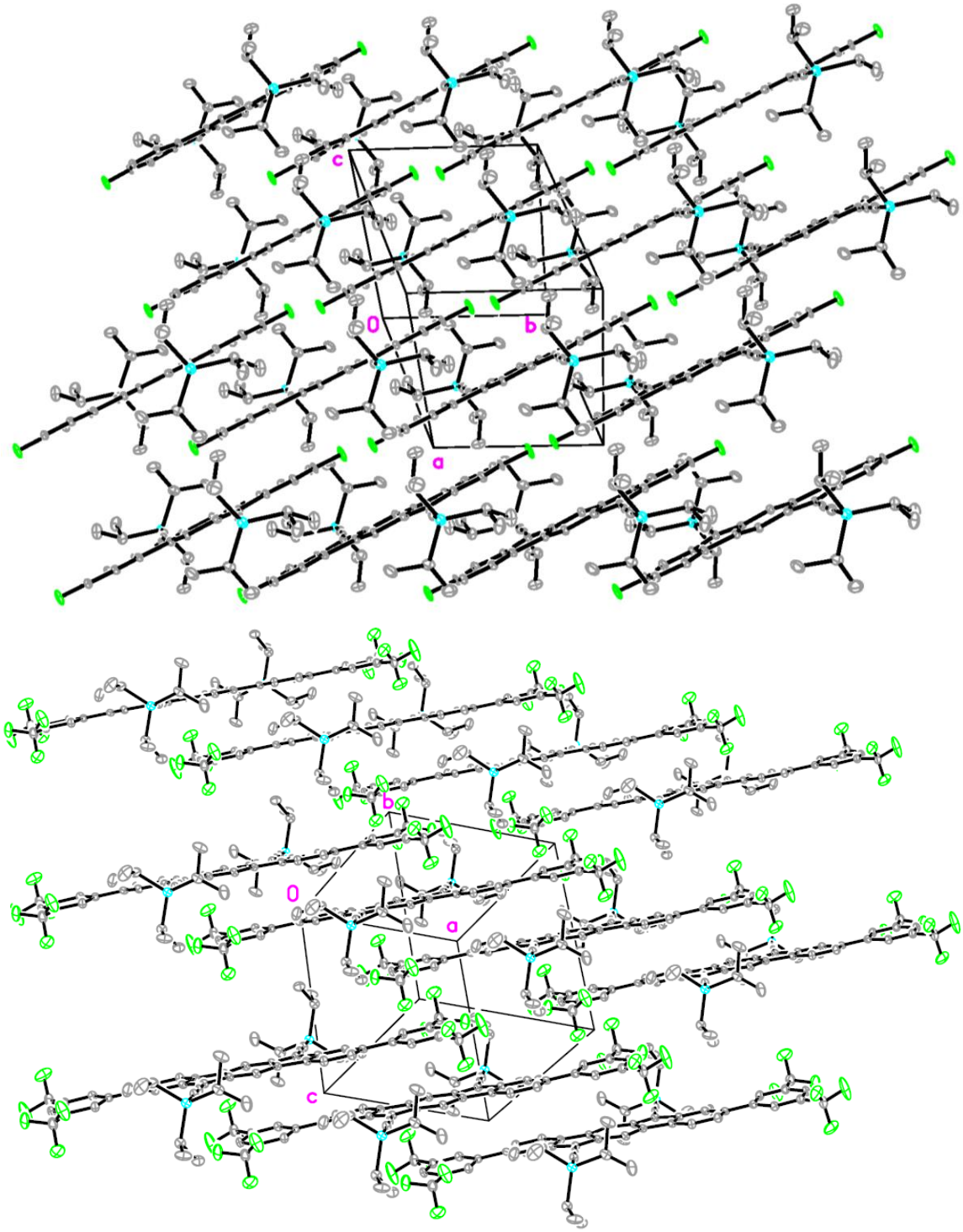

Figure 6. Crystal packing of diethynyl-IFs **10b** (top) and **10h** (bottom); ellipsoids drawn at the 30% probability level.

Experimental Section

General Comments. ^{1}H and ^{13}C NMR spectra were recorded in $CDCl_3$, CD_2Cl_2, or DMSO-d^6 using either a Varian Inova 500 (^{1}H: 500.11 MHz, ^{13}C: 125.75 MHz) or 600 (^{1}H: 599.98 MHz, ^{13}C: 150.87 MHz) NMR spectrometer. Chemical shifts (δ) are expressed in ppm relative to the residual $CHCl_3$ (^{1}H: 7.27 ppm, ^{13}C: 77.23 ppm), CH_2Cl_2 (^{1}H: 5.32 ppm, ^{13}C: 54.00 ppm), or DMSO (^{1}H: 2.50 ppm, ^{13}C: 39.51 ppm) reference. Coupling constants are expressed in hertz. UV-Vis spectra were recorded on an HP 8453 UV-Vis spectrometer. High resolution mass spectra were recorded on a JEOL MS-Route mass spectrometer. CH_2Cl_2, THF, and toluene were distilled from their appropriate drying agents under N_2. Unless otherwise stated, all reagents were purchased and used as received. Diones **11a**–**d** were synthesized according to previously described procedures.[18,19]

X-ray data for 10b: $C_{64}H_{92}Si_4$, M = 973.74, 0.26 x 0.12 x 0.05 mm, T = 173(2) K, monoclinic, space group $P2_1/c$, a = 13.579(2) Å, b = 15.042(2) Å, c = 15.054(2) Å, β = 97.502(3)°, V = 3048.6(8) Å^3, Z = 2, Z' = 0.5, D_c = 1.061 Mg/m^3, μ = 0.133 mm^{-1}, F(000) = 1064, $2\theta_{max}$ = 50.00°, 29004 reflections, 5357 independent reflections [R_{int} = 0.0554], R1 = 0.0453, wR2 = 0.1092 and GOF = 1.103 for 4217 reflections (491 parameters) with $I>2\sigma(I)$, R1 = 0.0651, wR2 = 0.1273 and GOF = 1.103 for all 5357 reflections, max/min residual electron density +0.338/–0.274 eÅ^3. X-ray data for **10h**: $C_{64}H_{92}Si_4$, M = 973.74, 0.26 x 0.12 x 0.05 mm, T = 173(2) K, monoclinic, space group $P2_1/c$, a = 13.579(2) Å, b = 15.042(2) Å, c = 15.054(2) Å, β = 97.502(3)°, V = 3048.6(8) Å^3, Z = 2, Z' = 0.5, D_c = 1.061 Mg/m^3, μ = 0.133 mm^{-1}, F(000) = 1064, $2\theta_{max}$ = 50.00°, 29004 reflections, 5357 independent reflections [R_{int} = 0.0554], R1 = 0.0453, wR2 =

0.1092 and GOF = 1.103 for 4217 reflections (491 parameters) with $I>2\sigma(I)$, R1 = 0.0651, wR2 = 0.1273 and GOF = 1.103 for all 5357 reflections, max/min residual electron density +0.338/–0.274 eÅ^3. CCDC-787154 and 787154 contain the supplementary crystallographic data for these compounds, respectively. These data can be obtained free of charge from The Cambridge Crystallographic data Centre via www.ccdc.cam.ac.uk/data_request/cif.

Diester 13. A mixture of 1,4-dibromoterephthalic acid (1.55 g, 4.08 mmol), 4-methylphenylboronic acid (2.22 g, 16.3 mmol), $Pd(OAc)_2$ (0.010 g, 0.03 mmol), and Bu_4NBr (2.63 g, 8.16 mmol) in toluene (20 mL) was degassed with Ar for 20 min. In a separate flask, a solution of K_2CO_3 (2.82 g, 20.4 mmol) in H_2O (20 mL) was also degassed with Ar for 20 min. The carbonate solution was then cannulated into the terephthalic acid solution and heated at 70 °C for 18 h. After cooling, the mixture was extracted in toluene and the organic layer was washed with H_2O until the washings were colorless. The organic layer was then dried ($MgSO_4$), filtered, and evaporated to dryness to give **13** (1.55 g, 94%) as a colorless solid. ^{1}H NMR ($CDCl_3$): δ 7.79 (s, 2H), 7.27 (d, *J* = 8.0 Hz, 2H), 7.23 (d, *J* = 8.0 Hz, 2H), 4.15 (q, *J* = 7.5 Hz, 4H), 2.42 (s, 6H), 1.07 (t, *J* = 7.5 Hz, 6H); ^{13}C NMR ($CDCl_3$): δ 168.3, 141.1, 137.6, 137.4, 133.7, 131.2, 129.1, 128.5, 61.5, 21.4, 14.0; HRMS (ESI) for $C_{26}H_{27}O_4$ [M^++1]: calcd 403.1909, found 403.1902.

Diacid 14. To a solution of **13** (0.700 g, 1.74 mmol) in anhydrous EtOH (40 mL) was added KOH (1.5 g, 37.40 mmol) dissolved in H_2O (20 mL). The resulting mixture was stirred at reflux overnight. After cooling, the EtOH was evaporated to dryness. Concentrated HCl was added until no more precipitation occurred. The precipitate was then heated to dryness at 120 °C to afford **14** (0.58 g, 95%) as a colorless solid. ^{1}H NMR

(DMSO-d_6): δ 13.06 (s, 2H), 7.63 (s, 2H), 7.30 (d, *J* = 8.0 Hz, 4H), 7.25 (d, *J* = 8.0 Hz, 4H), 2.36 (s, 6H); ^{13}C NMR (DMSO-d_6): δ 169.2, 139.2, 136.9, 136.7, 134.3, 130.8, 129.0, 128.2, 20.8; HRMS (ESI) for $C_{22}H_{18}O_4$ [M^+]: calcd 346.3759, found 346.3705.

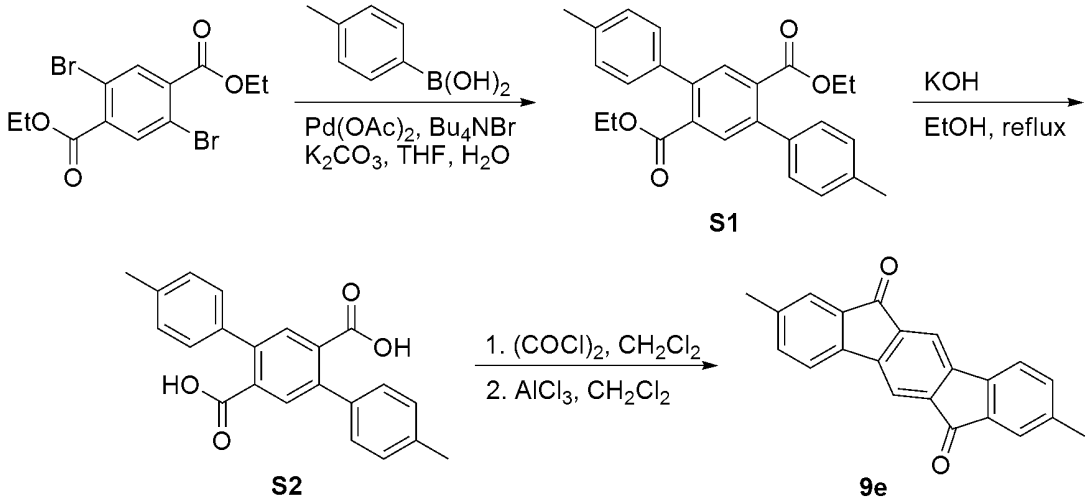

Scheme 2. Synthesis of dione **11e**.

Dione 11e. To a solution of **14** (0.58 g, 1.66 mmol) in CH_2Cl_2 (40 mL) was added oxalyl chloride (2.25 mL, 26.6 mmol) (Scheme 2). To this was added anhydrous DMF (1.0 mL) dropwise at room temperature and the resultant mixture was stirred overnight. The mixture was evaporated to dryness to yield the crude acid chloride as a yellow solid. This material was redissolved in CH_2Cl_2 (30 mL) and the solution was degassed with Ar for 20 min. The solution was cooled to 0 °C and then $AlCl_3$ (1.0 g, 7.47 mmol) was added. The mixture was stirred at 0 °C for 15 min, then warmed to room temperature for 2 h. The reaction was quenched by pouring into an ice-cold 10% HCl solution (50 mL). The resultant precipitate was collected by filtration and dried to yield **11e** (0.36 g, 68%) as a magenta solid. ^{1}H NMR ($CDCl_3$): δ 7.74 (s, 2H), 7.51 (s, 2H), 7.44 (d, *J* = 7.8 Hz, 2H), 7.35 (d, *J* = 7.8 Hz), 2.41 (s, 6H); ^{13}C NMR ($CDCl_3$): δ 193.5, 146.0, 141.3, 140.0,

139.6, 136.0, 134.5, 125.5, 120.6, 115.8, 21.6; HRMS (ESI) for $C_{22}H_{14}O_2$ [M^+]: calcd 310.0994, found 310.0986.

Dione 11f. A mixture of dione **11d** (0.25 g, 0.57 mmol), $Pd(PPh_3)_4$ (0.12 g, 0.10 mmol), phenylboronic acid (0.15 g, 1.25 mmol) and Aliquat 336 (0.1 mL) in toluene (40 mL) was degassed with Ar for 2 h. In a separate flask, a solution of K_2CO_3 (0.39 g, 2.82 mmol) in H_2O (10 mL) was also degassed with Ar for 2 h. The carbonate solution was cannulated into the bromodione solution and refluxed for 48 h. After evaporating the mixture to dryness, the crude material was placed on a fine frit and rinsed with H_2O (2 x 50 mL) and acetone (2 x 50 mL) until the washings were colorless, giving **11f** (0.20 g, 48%) as an insoluble pink solid. Mp: > 300 °C; HRMS (ESI) for $C_{32}H_{18}O_2$ [M^+]: calcd 434.1307, found 434.1314.

Dione 11g. A mixture of **11d** (0.25 g, 0.57 mmol), $Pd(PPh_3)_4$ (0.12 g, 0.10 mmol), *p*-trifluoromethylphenylboronic acid (0.24 g, 1.25 mmol) and Aliquat 336 (0.1 mL) in toluene (40 mL) was degassed with Ar for 2 h. In a separate flask, a solution of K_2CO_3 (0.39 g, 2.82 mmol) in H_2O (10 mL) was also degassed with Ar for 2 h. The carbonate solution was cannulated into the bromodione solution and refluxed for 96 h. After evaporating the mixture to dryness, the crude material was placed a fine frit and rinsed with H_2O (2 x 50 mL) and acetone (2 x 50 mL) until the washings were colorless, affording **11g** (0.165 g, 51%) as an insoluble pink solid. Mp: > 300 °C; HRMS (ESI) for $C_{34}H_{16}F_6O_2$ [M^+]: calcd 570.1054, found 570.1068.

Dione 11h. A mixture of **11d** (0.13 g, 0.30 mmol) and $Pd(PPh_3)_4$ (0.040 g, 0.04 mmol) in toluene (25 mL) was degassed with Ar for 20 min. In a separate flask, a solution of 3,5-bis(trifluoromethyl)phenyltributylstannane (0.377 g, 0.71 mmol) in

toluene (25 mL) was also degassed with Ar for 20 min. The solution containing the stannane was then transferred by cannula into the first flask and the mixture was refluxed overnight. After evaporating the mixture to dryness, the crude material was collected over a fine frit and washed with hexanes and then CH_2Cl_2 to obtain **11h** (0.168 g, 80%) as a poorly soluble red solid. ^{1}H NMR ($CDCl_3$): δ 8.05 (s, 4H), 7.96 (s, 2H), 7.94 (s, 2H), 7.91 (s, 2H), 7.85 (d, *J* = 7.2 Hz, 2H), 7.73 (d, *J* = 7.2 Hz, 2H); HRMS (ESI) $C_{36}H_{14}O_2F_{12}$ [M^+]: calcd 706.0802, found 706.0783.

Dione 11i. A mixture of **11d** (0.22 g, 0.50 mmol) and $Pd(PPh_3)_4$ (0.040 g, 0.04 mmol) in toluene (25 mL) was degassed with Ar for 20 min. In a separate flask, a solution of 2-butyl-5-tributylstannylthiophene (0.52 g, 1.2 mmol) in toluene (25 mL) was also degassed for 20 min. The solution containing the stannane was then transferred by cannula into the first flask and the mixture was refluxed overnight. After evaporating the mixture to dryness, the crude material was placed on a plug of celite and rinsed with CH_3CN until the washings were colorless, and then extracted with $CHCl_3$ and evaporated to dryness. The mixture was then suspended in pentane and the precipitate was collected to obtain **11i** (0.168 g, 60%) as a dark violet solid. ^{1}H NMR ($CDCl_3$): δ 7.87 (s, 2H), 7.78 (s, 2H), 7.72 (d, *J* = 7.5 Hz, 2H), 7.52 (d, *J* = 7.5 Hz, 2H), 7.22 (d, *J* = 3.6 Hz, 2H), 6.78 (d, *J* = 3.6 Hz, 2H), 2.85 (t, *J* = 7.2 Hz, 4H), 1.71 (m, 4H), 1.44 (m. 4H), 0.97 (t, *J* = 7.5 Hz, 6H); ^{13}C NMR ($CDCl_3$): δ 192.7, 147.0, 145.6, 141.5, 140.1, 139.6, 136.6, 134.7, 131.6, 125.4, 123.7, 121.2, 121.0, 115.9, 33.7, 30.0, 22.2, 13.8; HRMS (ESI) $C_{36}H_{30}O_2S_2$ [M^+]: calcd 558.1687, found 558.1673.

General Procedure for 10a-i. (Triisopropylsilyl)acetylene (TIPSA) was dissolved in THF (10 mL), degassed with Ar for 10 min, and cooled to 0 °C. BuLi was

added and the mixture stirred at 0 °C for 20 min. In a separate flask, **11a-i** was suspended in THF (15 mL), and also degassed with Ar for 10 min, and cooled to 0 °C. The lithiate was transferred by cannula to the cold solution containing **11a-i** and then warmed to room temperature for 2 h. The reaction was quenched with 10% HCl soln (30 mL) and extracted in Et_2O (50 mL). The organic layer was dried ($MgSO_4$), filtered, and evaporated to dryness. The crude diol was then redissolved in dry toluene (15 mL) and degassed with Ar for 10 min. $SnCl_2$ was added to the mixture and warmed to 40 °C for 2 h. The resulting magenta solution was then filtered and the filtrate was subsequently evaporated to dryness. Recrystallization of the crude material from CH_3CN/CH_2Cl_2 gave the corresponding IF derivative.

IF 10a. TIPSA (1.42 mL, 6.36 mmol), BuLi (3.3 mL, 5.30 mmol), **12a** (0.300 g, 1.06 mmol) and $SnCl_2$ (0.80 g, 4.24 mmol) were reacted according to the general procedure to afford **10a** (0.459 g, 71%) as magenta crystals. ^{1}H NMR ($CDCl_3$): δ 7.36-7.33 (m, 2H), 7.26 (s, 2H), 7.26-7.23 (m, 2H), 7.13-7.07 (m, 4H), 1.21-1.19 (br s, 42H); ^{13}C NMR ($CDCl_3$): δ 143.6, 140.9, 139.3, 137.6, 128.5, 128.2, 126.7, 122.5, 120.5, 119.1, 110.1, 102.1, 19.0, 11.6; UV-vis ($CHCl_3$) λ_{max} (log ε): 491 sh (3.89), 529 (4.37), 568 (4.70) nm; HRMS (ESI) for $C_{42}H_{52}Si_2$ [M^+]: calcd 612.3608, found 612.3623.

IF 10b. TIPSA (1.02 mL, 4.58 mmol), BuLi (2.4 mL, 3.82 mmol), **12b** (0.243 g, 0.76 mmol), and $SnCl_2$ (0.58 g, 3.06 mmol) were reacted according to the general procedure to afford **10b** (0.155 g, 31%) as magenta needles. ^{1}H NMR (CD_2Cl_2): δ 7.31 (dd, *J* = 8.4, 4.8 Hz, 2H), 7.19 (s, 2H), 6.87 (dd, *J* = 8.4, 2.4 Hz, 2H), 6.78 (ddd, *J* = 8.4, 4.8, 2.4 Hz, 2H), 1.24-1.19 (br s, 42H); ^{13}C NMR (CD_2Cl_2): δ 164.1 (d, *J* = 245.6 Hz), 145.8 (d, *J* = 8.6 Hz), 142.2, 139.1, 133.8, 126.7, 122.1 (d, *J* = 9.6 Hz), 119.2, 115.1 (d, *J*

= 24.0 Hz), 111.7, 110.0 (d, *J* = 24.0 Hz), 101.6, 19.1, 11.9; UV-vis ($CHCl_3$) λ_{max} (log ε): 485 sh (3.78), 523 (4.26), 561 (4.61) nm; HRMS (ESI) for $C_{42}H_{50}F_2Si_2$ [M^+]: calcd 648.3419, found 648.3422.

IF 10c. TIPSA (0.19 mL, 0.84 mmol), BuLi (0.44 mL, 0.70 mmol), **12c** (0.050 g, 0.14 mmol), and $SnCl_2$ (0.106 g, 0.56 mmol) were reacted according to the general procedure to afford **10c** (0.033 g, 35%) as magenta crystal. ^{1}H NMR (CD_2Cl_2): δ 7.31 (d, *J* = 8.1 Hz, 2H), 7.27 (s, 2H), 7.21 (d, *J* = 2.1 Hz, 2H), 7.10 (dd, *J* = 8.1, 2.1 Hz, 2H), 1.21-1.18 (br s, 42H); ^{13}C NMR (CD_2Cl_2): δ 145.3, 141.8, 139.0, 136.2, 134.7, 128.5, 126.8 122.9, 121.9, 119.7, 112.3, 101.5, 19.1, 11.9; UV-vis ($CHCl_3$) λ_{max} (log ε): 485 sh (3.72), 528 (4.32), 567 (4.66) nm; HRMS (ESI) for $C_{42}H_{50}Cl_2Si_2$ [M+1]: calcd 681.2906, found 681.2887.

IF 10d. TIPSA (0.43 mL, 1.16 mmol), BuLi (0.60 mL, 0.97 mmol), **12d** (0.085 g, 0.19 mmol), and $SnCl_2$ (0.15 g, 0.77 mmol) were reacted according to the general procedure to afford **10d** (0.069 g, 47%) as magenta crystals. ^{1}H NMR (CD_2Cl_2): δ 7.37 (s, 2H), 7.28 (s, 2H), 7.25 (s, 4H), 1.21-1.17 (br s, 42H); ^{13}C NMR (CD_2Cl_2): δ 145.5, 141.6, 139.1, 136.6, 131.4, 126.7, 125.8, 122.7, 122.3, 119.8, 112.4, 101.5, 19.1, 11.9; UV-vis ($CHCl_3$) λ_{max} (log ε): 486 sh (3.99), 529 (4.52), 567 (4.86) nm; HRMS (ESI) for $C_{42}H_{50}Br_2Si_2$ [M^+]: calcd 768.1818, found 768.1791.

IF 10e. TIPSA (0.17 mL, 0.76 mmol), BuLi (0.40 mL, 0.63 mmol), **12e** (0.070 g, 0.13 mmol), and $SnCl_2$ (0.096 g, 0.50 mmol) were reacted according to the general procedure to afford **10e** (0.050g, 60%) as a magenta crystals. ^{1}H NMR (CD_2Cl_2): δ 7.23 (d, *J* = 7.5 Hz, 2H), 7.18 (s, 2H), 7.04 (s, 2H), 6.90 (d, *J* = 7.5 Hz, 2H), 2.30 (s, 6H), 1.21-1.18 (br s, 42H); ^{13}C NMR (CD_2Cl_2): δ 144.1, 141.6, 139.6, 139.1, 135.3, 129.4,

126.8, 123.5, 120.7, 118.7, 110.4, 102.3, 19.1, 11.9; UV-vis ($CHCl_3$) λ_{max} (log ε): 491 sh (4.02), 531 (4.47), 569 (4.79) nm; HRMS (ESI) for $C_{44}H_{56}Si_2$ [M^+]: calcd 640.3921, found 640.3924.

IF 10f. TIPSA (0.12 mL, 0.55 mmol), BuLi (0.29 mL, 0.46 mmol), **12f** (0.040 g, 0.09 mmol), and $SnCl_2$ (0.070 g, 0.50 mmol) were reacted according to the general procedure to afford **10f** (0.030 g, 44%) as a magenta crystals. ^{1}H NMR (CD_2Cl_2): δ 7.62 (d, *J* = 7.2 Hz, 4H), 7.52 (s, 2H), 7.46 (t, *J* = 7.2 Hz, 6H), 7.37 (d, *J* = 7.2 Hz, 4H), 7.35 (s, 2H) 1.21-1.17 (br s, 42H); ^{13}C NMR (CD_2Cl_2): δ 144.7, 142.0, 141.7, 141.3, 139.4, 136.9, 129.4, 128.1, 127.6, 127.2 (2), 121.5, 121.4, 119.6, 111.4, 102.2, 19.1, 12.0; UV-vis ($CHCl_3$) λ_{max} (log ε): 484 sh (2.93), 534 (3.93), 570 (4.26) nm; HRMS (ESI) for $C_{54}H_{60}Si_2$ [M^+]: calcd 764.4234, found 764.4234.

IF 10g. TIPSA (0.15 mL, 0.68 mmol), BuLi (0.36 mL, 0.57 mmol), **12g** (0.065 g, 0.11 mmol), and $SnCl_2$ (0.087 g, 0.46 mmol) were reacted according to the general procedure to afford **10g** (0.043 g, 43%) as a magenta crystals. ^{1}H NMR (CD_2Cl_2): δ 7.73 (*AB*m, *J* = 8.4 Hz, 8H), 7.53 (s, 2H), 7.51 (d, *J* = 8.4 Hz, 2H), 7.40 (d, *J* = 8.4 Hz, 2H), 7.39 (s, 2H), 1.21-1.17 (br s, 42H); ^{13}C NMR (CD_2Cl_2): δ 145.0, 144.7, 141.6, 140.4, 139.3, 137.7, 129.8 (q, *J* = 32.4 Hz), 127.8, 127.6, 127.3, 126.3, 126.2, 121.6, 121.5, 120.0, 111.9, 102.1, 19.1, 12.0; UV-vis ($CHCl_3$) λ_{max} (log ε): 486 sh (3.95), 534 (4.47), 572 (4.80) nm; HRMS (ESI) $C_{56}H_{58}F_6Si_2$ [M^+]: calcd 900.3981, found 900.4050.

IF 10h. TIPSA (0.12 mL, 0.55 mmol), BuLi (0.29 mL, 0.46 mmol), **12h** (0.065 g, 0.09 mmol), and $SnCl_2$ (0.070 g, 0.37 mmol) were reacted according to the general procedure to afford **10h** (0.058 g, 62%) as a magenta needles. ^{1}H NMR ($CDCl_3$): δ 8.02 (s, 4H), 7.85 (s, 2H), 7.52 (d, *J* = 7.8 Hz, 2H), 7.51 (s, 2H), 7.37 (dd, *J* = 7.8, 1.2 Hz, 2H),

7.36 (s, 2H), 1.25-1.19 (br s, 42H); ^{13}C NMR ($CDCl_3$): δ 144.9. 143.0. 140.9. 132.4 (q, *J* = 33.1 Hz), 127.0, 126.8, 124.6 (q, *J* = 272.8 Hz), 121.4, 121.2, 120.0, 111.9, 101.7, 19.0. 11.6; UV-vis ($CHCl_3$) λ_{max} (log ε): 493 sh (3.79), 532 (4.08), 570 (4.35) nm; HRMS (ESI) $C_{58}H_{56}F_{12}Si_2$ [M^+]: calcd 1036.3729, found 1036.3695.

IF 10i. TIPSA (0.30 mL, 1.36 mmol), BuLi (0.87 mL, 1.13 mmol), **12i** (0.128 g, 0.23 mmol), and $SnCl_2$ (0.171 g, 0.90 mmol) were reacted according to the general procedure to afford **10i** (0.165 g, 81%) as a magenta solid. ^{1}H NMR (CD_2Cl_2): δ 7.44 (s, 2H), 7.35 (d, *J* = 7.8 Hz, 2H), 7.28 (d, *J* = 7.8 Hz, 2H), 7.13 (d, *J* = 3.3 Hz, 2H), 6.76 (d, *J* = 3.3 Hz, 2H), 2.83 (t, *J* = 7.5 Hz, 4H), 1.69 (pent, *J* = 7.5 Hz, 4H), 1.42 (sext, *J* = 7.5 Hz, 4H), 1.24-1.19 (br s, 42H), 0.96 (t, *J* = 7.5 Hz, 6H); ^{13}C NMR (CD_2Cl_2): δ 146.5, 144.7, 141.9, 141.7, 139.6, 136.2, 135.5, 126.8, 125.7, 125.4, 123.2, 121.3, 119.5, 119.2, 111.2, 102.2, 34.3, 30.4, 22.7, 19.1, 14.2, 12.0; UV-vis ($CHCl_3$) λ_{max} (log ε): 498 sh (3.95), 537 (4.24), 577 (4.47) nm; HRMS (ESI) $C_{58}H_{72}S_2Si_2$ [M^+]: calcd 888.4614, found 888.4594.

Bridge to Chapter III

Chapter II introduced the first isolated and fully-characterized indenofluorenes and hypothesized their utility as semiconducting materials in electronic devices. Chapter III serves to show that facile further derivatization of this scaffold is possible. Furthermore, it demonstrates the first examples of the use of these materials in an organic electronic device, in this case a single crystal organic field effect transistor. In addition,

we were able to demonstrate ambipolar charge transport character, an attribute that is in high demand for organic semiconducting materials.

CHAPTER III

6,12-DIARYLINDENO[1,2-*b*]FLUORENES: SYNTHESES, PHOTOPHYSICS AND AMBIPOLAR OFETS

This chapter was co-authored by Daniel T. Chase, who assisted with synthetic experiments and wrote much of the body of the original paper, Bradley D. Rose, who performed computational studies and also assisted with synthetic experiments, Shunpei Nobusue and Chelsea E. Stockwell assisted with some material synthesis, Christopher D. Weber, who performed electrochemical experiments, and Mark C. Lonergan and Michael M. Haley, who provided guidance and editorial assistance. This work was originally published in the *Journal of the American Chemical Society*.

Introduction

Conjugated polycyclic hydrocarbons have been the subject of intense research over the last two decades for their potential use in a variety of materials applications such as organic light-emitting diodes, thin film transistors, and solar cells.[1] Of particular interest is the indeno[1,2-*b*]fluorene (IF) skeleton (e.g., **1**, **2**, Figure 1), a 6-5-6-5-6 fused ring system, which in its fully conjugated state closely resembles pentacene.[2] As IFs possess two less carbon atoms, and hence two fewer π-electrons than pentacenes, they could be considered as anti-aromatic molecules. This definition, however, remains a formality as the internal core exhibits bond lengths and bond alternation resembling a dibenzo-fused *s*-indacene.[3] Furthermore, **1** and **2** are stable upon heating for prolonged periods (80 °C for **1**, 150 °C for **2**) without noticeable decomposition, a trait not typically associated with anti-aromatic compounds. These observations in stability parallel those found with structurally similar dibenzopentalene derivatives.[4]

Recently, we reported the synthesis and properties of a series of 2,8-disubstituted derivatives of **2**.[5] These compounds possessed similar UV-Vis profiles to **1** with slightly larger HOMO/LUMO gaps. As with our reported diynyl IF-diones,[6] **2** and derivatives could accept two electrons in a quasi-reversible behavior, exhibiting LUMO energy levels comparable or further from the vacuum level than that of the ubiquitous electron acceptor, PCBM.[7] Furthermore, solid-state structures of two derivatives showed one-dimensional π-stacks with intermolecular distances as little as 3.40 Å, an improvement over the expanded herringbone motif found for **1**. Functionalization on the 2 and 8-positions, however, had only a modest effect on the HOMO and LUMO energy levels as calculations revealed minimal orbital density on those positions. In addition to our studies, Tobe and Shimizu recently disclosed the synthesis of 11,12-dimesitylindeno[2,1-*a*]fluorene (**3**),[8] an isomeric IF species that possessed similar physical characteristics to **1** and **2**.

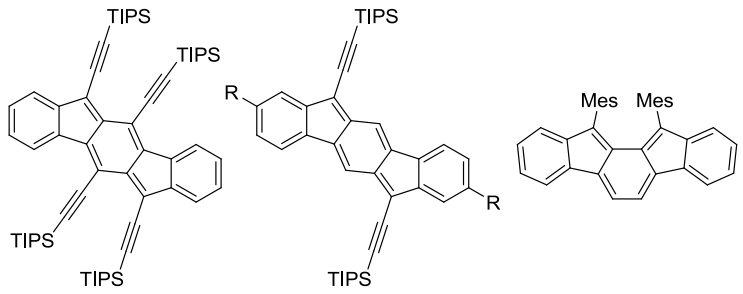

Figure 1. Fully conjugated indenofluorenes **1**–**3**.

To further expand the versatility of the IF scaffold, we considered substitution motifs beyond the previously used (triisopropylsilyl)ethynyl (TIPS) moiety. Arylation on the 6 and 12-positions represents a logical next step as arenes functionalized with either donor or acceptor groups might impart a more diverse range of IF optoelectronic properties.

This supposition is supported by the calculated HOMO/LUMO plots in Figure 2, which show considerable orbital density at those positions. The synthesis of arylated IFs also fulfills a historic purpose in that one of the original IFs exhibiting full conjugation, 6,12-diphenyl-IF **4a**, was only briefly described by Scherf.[9]

Here, we disclose the synthesis of IFs **4a**–**j** from readily available 6,12-indenofluorenedione (**5**),[10] along with the respective optical, electrochemical, and computational data. Importantly, we show that pentafluorophenyl derivative **4j** can be used to construct a field effect transistor that exhibits ambipolar behavior.

The same strategy to synthesize **2** via dione **5**[10] can be readily applied to **4a** (Scheme 1). Addition of lithiated bromobenzene gave crude diol **6a** and subsequent reduction using $SnCl_2$ in toluene at 65 °C afforded a magenta solution, from which parent **4a** was obtained in 55% yield over the two steps. This reaction scheme was then extended to a series of 6,12-diaryl-IFs (**4b**–**j**), which were isolated in good to modest yields after recrystallization. The reduction was sluggish for strongly electron deficient arenes such as **6h**–**j** and required the addition of a small amount of trifluoroacetic acid (similarly used for the synthesis of **3**)[8] for the reduction to occur smoothly.

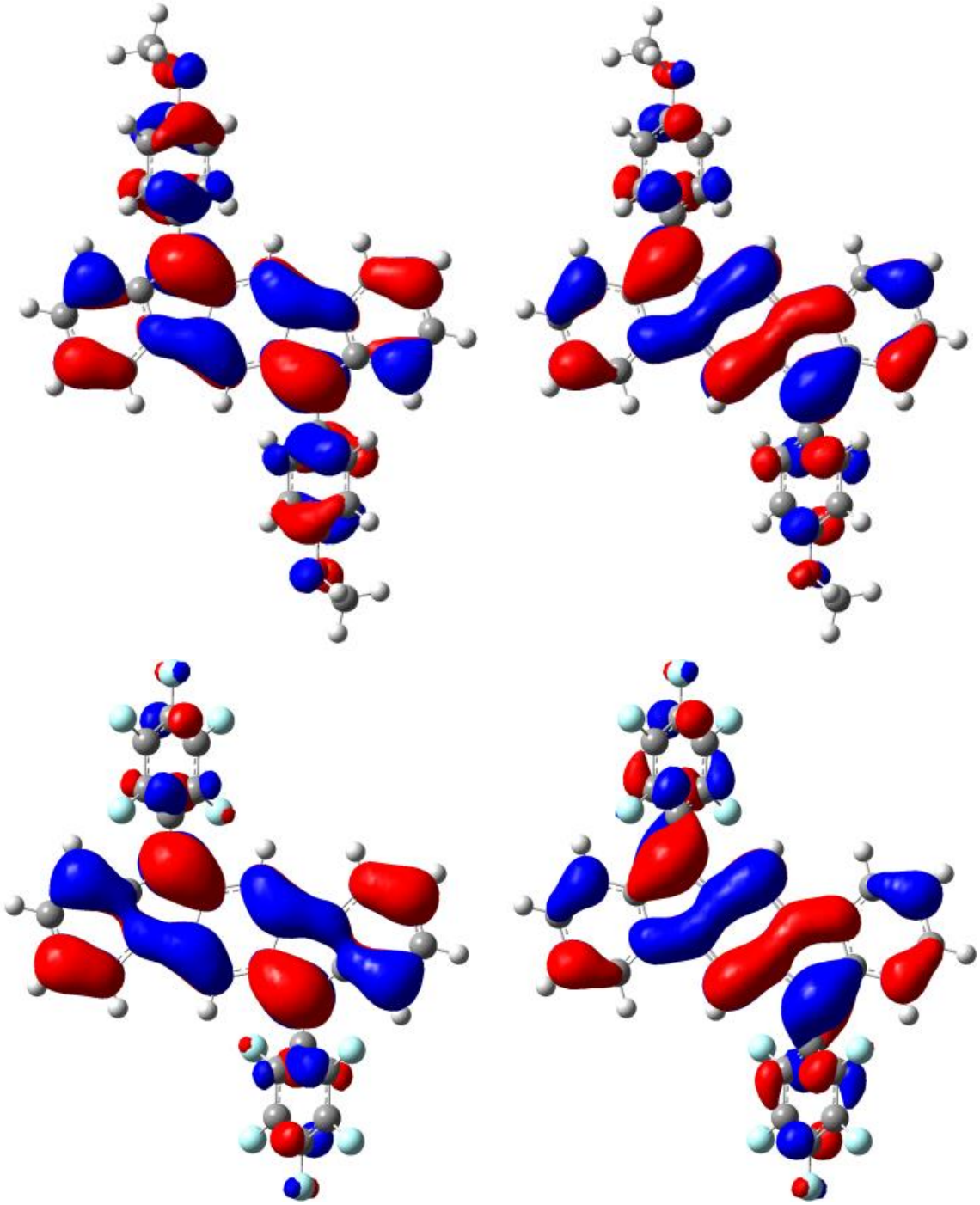

Figure 2. HOMO (left) and LUMO (right) orbital plots of IFs **4b** (top) and **4j** (bottom).

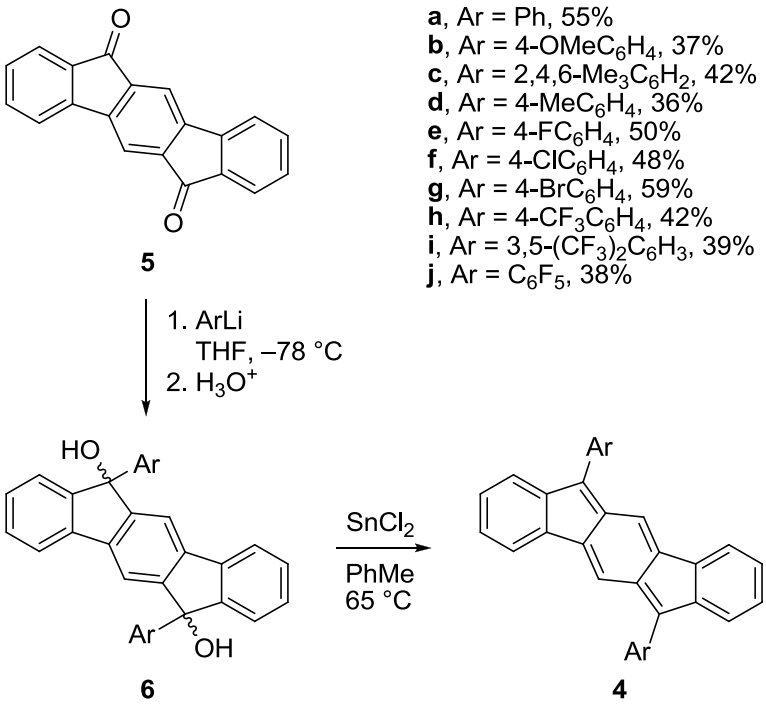

Scheme 1. Synthesis of 6,12-Diarylindeno[1,2-*b*]fluorenes.

Table 1 contains the UV-vis absorption data for all diaryl-IFs; individual spectra of **2**, **4a**–**c** and **4j** are shown in Figure 3 (see Supporting Information for **4d**–**i**). Like **2**, **4a** exhibits three low-energy absorptions (λ_{max} 544 nm) but these are hypsochromically shifted by approximately 50 and 25 nm with respect to **1** and **2**. This can be attributed to the exchange of electron-withdrawing acetylenes with aryl groups, a consequence also observed with substituted pentacenes.[11]

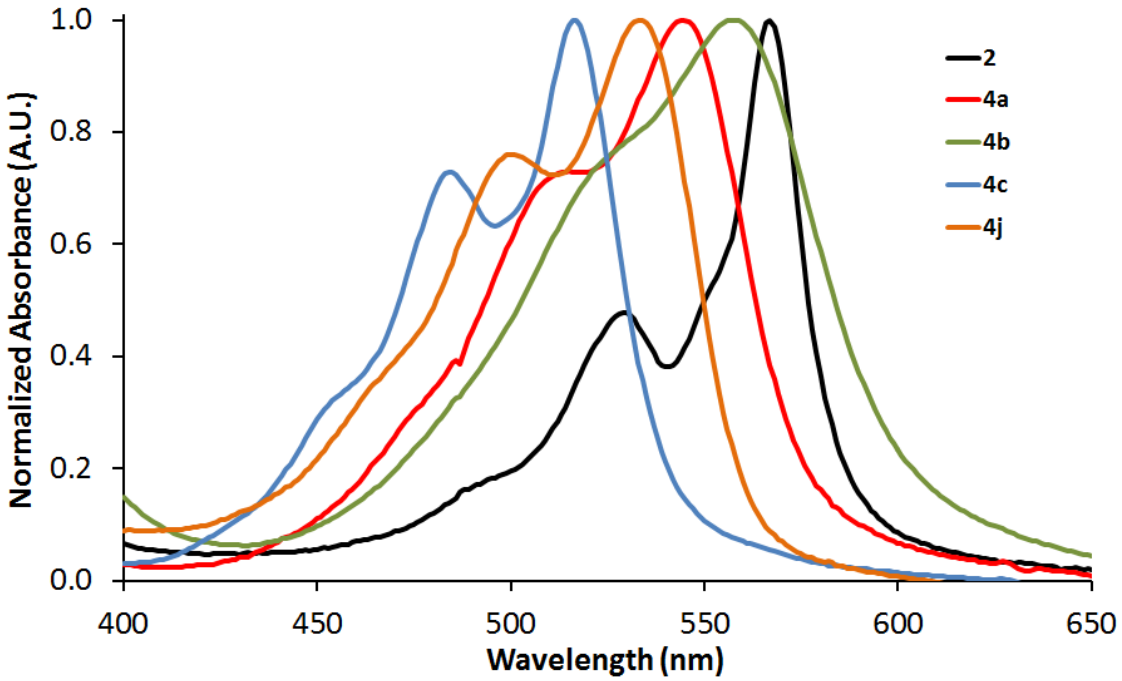

Figure 3. Electronic absorption spectra for IFs **2**, **4a**–**c**, and **4j**; all spectra recorded in $CHCl_3$ at 15–25 µM.

Variation of the aryl substituents on the 6 and 12-positions has a notable impact on the absorption profiles: methoxyphenyl **4b** exhibits a λ_{max} value of 558 nm while the λ_{max} value of pentafluorophenyl **4j** is at 533 nm. Interestingly, mesityl derivative **4c** exhibits a λ_{max} value of 516 nm, which is attributed to the *ortho*-bound methyl groups enforcing the mesityl and IF units in a nearly orthogonal relationship. The X-ray structure of **4c** (Figure 4) corroborates this hypothesis, as the dihedral angle between the mesityl and indenofluorene rings is 72° (80.6° calculated dihedral). As such, little electronic communication between the π-systems exists in this instance, which effectively reduces the conjugation path length in **4c** and thus results in the hypsochromic shift. All other arylated IFs are predicted to exhibit more typical biphenyl dihedral angles[12] (calculated 43-45° for **4a**–**i**, 50.6° for **4j**) and their spectra more strongly reflect the effects of the aryl

substituents, as noted above. As observed previously with **1** and **2**, IFs **4a**–**j** are non-emissive.

Table 1. Computational, Electrochemical, and Optical Data for Indeno[1,2-*b*]fluorenes **2** and **4a**-**4j**.

	Computational[a]			Electrochemical[b]					Optical[c]	
Compd	E_{HOMO}	E_{LUMO}	E_{Gap}	$E(A^+/A, A^{2+}/A^+, A^{3+}/A^{2+})$	$E(A/A^-, A^-/A^{2-})$	E_{HOMO}	E_{LUMO}	E_{Gap}	λ_{max}	E_{Gap}[d]
2	−5.51	−3.47	2.04	1.20	−0.69, −1.20	−5.88	−4.00	1.88	568	2.12
4a	−5.24	−3.07	2.17	1.00, 1.31[e], 1.51[e]	−0.96, −1.49[e]	−5.68	−3.72	1.96	544	2.17
4b	−5.00	−2.90	2.10	0.81, 1.07[e]	−1.01, −1.53[e]	−5.50	−3.68	1.82	558	2.05
4c	−5.34	−2.92	2.42	1.10, 1.59[e]	−1.12, −1.73[e]	−5.78	−3.56	2.22	516	2.29
4d	−5.13	−2.98	2.15	0.93, 1.21[e], 1.48[e]	−0.99, −1.50[e]	−5.61	−3.69	1.92	550	2.12
4e	−5.37	−3.20	2.17	1.03, 1.24[e], 1.52[e]	−0.93, −1.41[e]	−5.71	−3.76	1.95	543	2.16
4f	−5.42	−3.27	2.15	1.05, 1.30[e], 1.53[e]	−0.88, −1.34[e]	−5.74	−3.81	1.93	548	2.14
4g	−5.43	−3.28	2.15	1.04, 1.38[e], 1.51[e]	−0.89, −1.35[e]	−5.73	−3.80	1.93	550	2.12
4h	−5.65	−3.49	2.16	1.22, 1.41[e], 1.54[e]	−0.84, −1.12	−5.91	−3.85	2.06	545	2.16
4i	−5.89	−3.73	2.16	1.35[e], 1.67[e]	−0.73, −1.07	−6.05	−3.97	2.08	543	2.16
4j	−5.92	−3.71	2.21	1.49[e], 1.66[e]	−0.68, −1.17	−6.17	−4.00	2.17	533	2.20

[a] Calculations performed at the B3LYP/6-311+G** level of theory; energies in eV. [b] CV recorded using 1–5 mM of analyte in 0.1 M Bu_4NOTf/CH_2Cl_2 using a scan rate of 50 mV/s. The working electrode was a glassy carbon electrode with a Pt coil counter electrode and Ag wire pseudo reference. E is the half-wave potential for reversible processes and the potential of the peak anodic or cathodic current for irreversible processes. Potential values (V) are reported vs. SCE using the Fc^+/Fc couple (0.46 V) as an internal standard. HOMO and LUMO energy levels (eV) were approximated using SCE = –4.68 eV vs. vacuum; see reference 13. $E_{1/2}$ values for reversible processes and E_p values for irreversible processes. [c] Spectra obtained in $CHCl_3$; wavelength in nm. [d] The optical HOMO-LUMO gap was determined as the intersection of the x-axis and a tangent line that passes through the inflection point of the lowest energy absorption; energies in eV. [e] Irreversible wave.

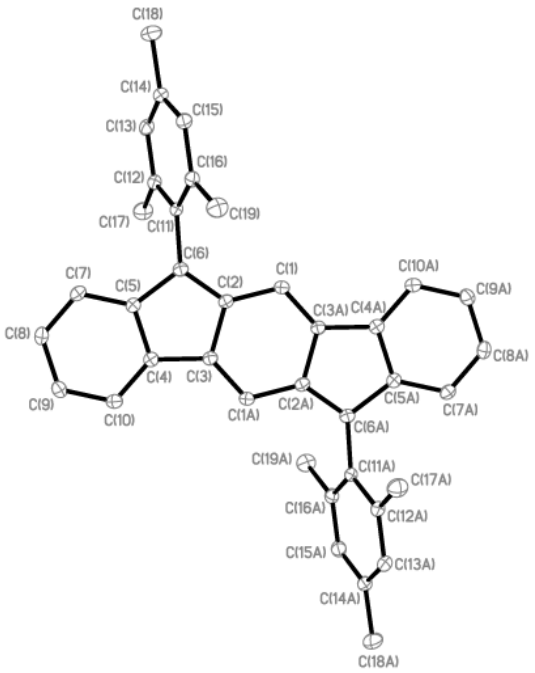

Figure 4. X-ray crystal structure of **4c**; hydrogens omitted for clarity. Ellipsoids drawn at the 30% probability level.

Cyclic voltammograms (CV) for **4b**, **4c**, and **4j** are displayed in Figure 5 (see Supporting Information for **4a**, **4d–i**). All voltammetry data are compiled in Table 1, which shows the half-wave potentials ($E_{1/2}$) for reversible waves or the potential of peak current (E_p) for irreversible waves. The $E_{1/2}$ is generally very close to the standard reduction potential. In solution, the neutral diaryl IF scaffold exhibits quasi-reversible behavior in accepting up to two electrons in separate waves (A/A^- and A^-/A^{2-}). The $E_{1/2}(A/A^-)$ for **4a–j** range from –0.68 to –1.12 V (vs. SCE), which in general are more negative than observed for **2**. Electron-withdrawing groups shift the $E_{1/2}$ to more positive values while electron-donating groups shift it to more negative values, as such groups work to respectively stabilize and destabilize the resulting anionic species. The wave for the second reduction (A^-/A^{2-}) was irreversible in most cases, although the E_p showed similar trends to $E_{1/2}(A/A^-)$. With the exception of **4i–j**, the diaryl-IFs could be reversibly

oxidized from their neutral state, an unanticipated trait based on our previous observations with **1** and **2**. The $E_{1/2}(A^+/A)$ for **4a–j** range from 0.81 to 1.49 V. Electron-withdrawing groups destabilize the resulting cationic species while electron-donating groups provide the opposite effect. A second and sometimes third anodic peak (**4a** and **4d–h**) were observed for each compound at potentials more positive of $E_{1/2}(A^+/A)$, but these processes were irreversible. The trend observed for $E_{1/2}(A^+/A)$ was also observed for $E_p(A^{2+}/A^+)$ and $E_p(A^{3+}/A^{2+})$, when observed. As a whole, the HOMO and LUMO energy levels of **4a–j** span 0.7 and 0.4 eV ranges,[13] respectively, which is far beyond the 0.15 eV range demonstrated by **2** and derivatives.[5] *p*-Anisyl-IF **4b** displays $E_{1/2}$ values for the first reduction (–1.01 V) and oxidation (0.81 V) of its neutral form, which closely mirror those found for 6,13-bis(TIPSeth-ynyl)pentacene, which are –1.10 and 0.74 V, respectively (corrected versus SCE).[11]

Micron-scale single crystals of **4j** could be prepared using a solvent exchange method.[14] Figure 6 displays the optical micrograph (OM) image of these microcrystals on a silicon wafer with 200 nm of SiO_2 on its surface. The strong and uniform birefringence of **4j** along with the reflections observed for the selective area electron diffraction (SAED) and bright field TEM images (Figure 6b) indicate that these microcrystals have a single-crystal orientation.

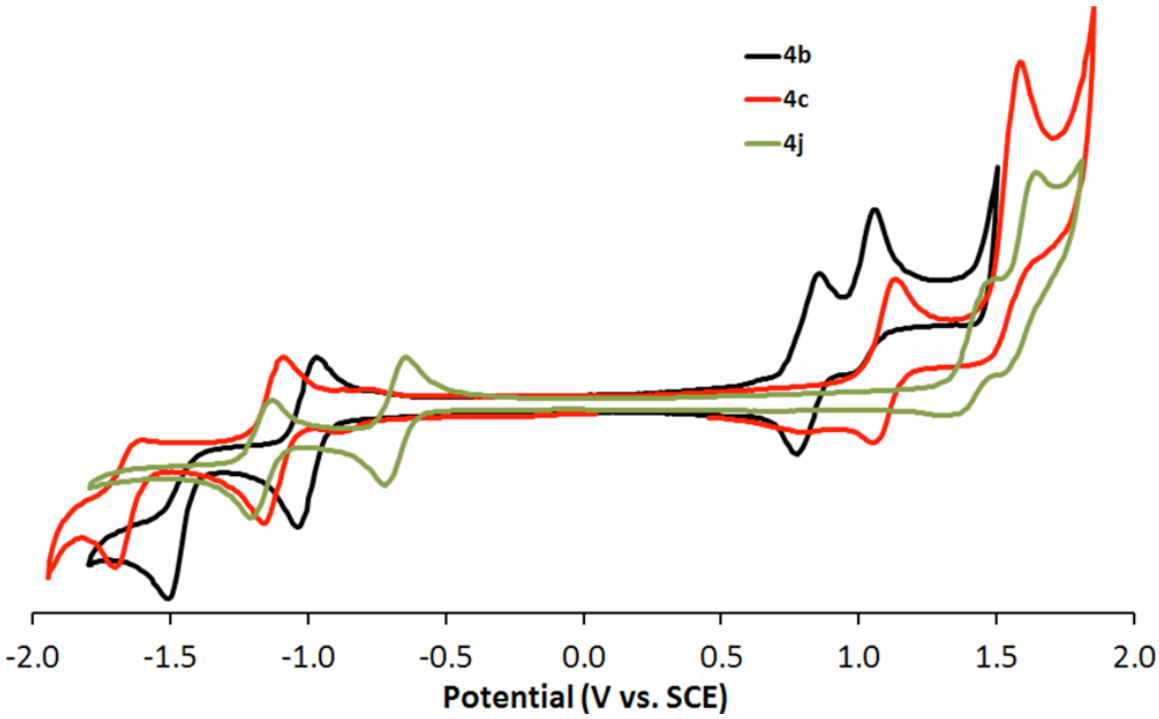

Figure 5. Cyclic voltammetry for IFs **4b**, **4c**, and **4j**.

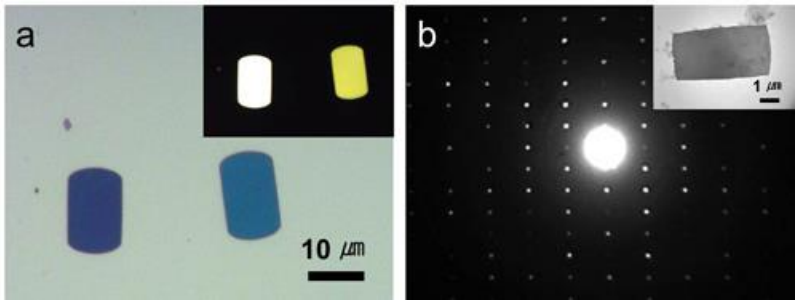

Figure 6. (a) OM image of **4j** single crystals prepared by solvent exchange method; inset shows an OM image with crossed polarizers. (b) SAED pattern of a single crystal of **4j**; inset shows bright field TEM image of a single crystal of **4j**.

After growth of the crystal on the silicon wafer, we constructed organic field effect transistors (OFETs) with the microcrystal as the active channel in the device.[15] Figure 7a is a schematic of the device, and Figure 7b is a micrograph of one of the device. To construct the device, the surface of the SiO_2 interface was passivated with a monolayer of octadecyltrichorosilane (OTS). This treatment has been shown previously

to reduce the trap sites at the dielectric/semiconductor interface.[16] The Au source/drain electrodes were thermally deposited through a TEM grid to form a top contact bottom gate transistor. The work function of Au is about 5.0 eV, meaning that both holes and electrons can be injected from Au into **4j** single crystals through the Schottky barrier at the metal–semiconductor contact.[17]

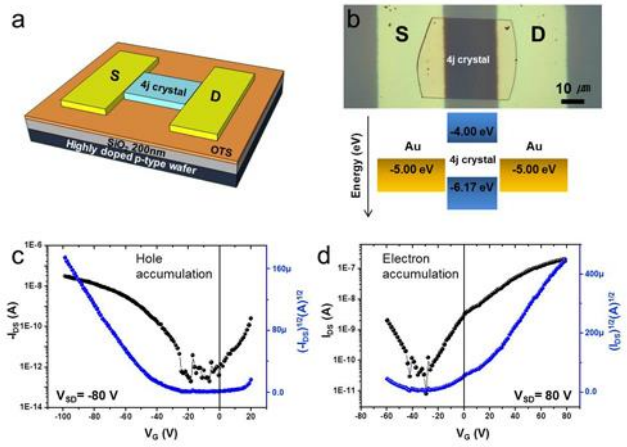

Figure 7. (a) Schematic of OFET with a **4j** single crystal active channel. (b) An OM image of top view of an OFET (top) and energy diagram of Au/**4j** crystal/Au (bottom). (c,d) *I*-*V* transfer characteristics of OFET with negative (c) and positive (d) drain voltage, respectively.

Figures 7c and 7d show the transfer characteristics of the **4j** FET device measured in an N_2-filled glove box. The transfer curves clearly exhibit ambipolar current modulation. The field-effect mobility is calculated from the slope of a plot of the square root of the drain current (I_{DS}) versus gate voltage (V_G) in the saturation regime. The field effect mobility can be calculated using $I_{DS}=(W/2L)C_i\mu(V_G-V_T)^2$, where W and L are the width and length of the channel and C_i (capacitance =17.8 nF cm^{-2}), μ and V_T correspond to the capacitance per unit area of the gate insulator, the field-effect mobility and the threshold voltage, respectively. The extracted field effect hole and electron mobilities from the

single crystal **4j** ambipolar transistor are $7x10^{-4}$ and $3x10^{-3}$ $cm^2V^{-1}s^{-1}$ in the saturation regime, respectively. The HOMO and LUMO level of diaryl-IF **4j** create well-balanced ambipolar FETs with Au electrodes because the work function of the electrodes is in the middle of the gap. Interestingly, there are very few ambipolar OFETs made from single crystals of organic semiconductors.[18] We only tested **4j** because it readily grew crystals, but the HOMO/LUMO levels of the other diaryl-IFs encourages us that these too will be active in FETs, research that is ongoing.Thin films of **4j** were inactive in FETs likely due to the morphology of the films and the dielectric interface.

In conclusion, we have prepared a family of 6,12-diaryl-indeno[1,2-*b*]fluorenes and shown that aryl substitution can significantly effect the redox properties of the molecules. In cyclic voltammetry experiments, the diaryl-IFs can either accept or donate two electrons. Pentafluorophenyl IF **4j** was utilized as the active element in a single crystal OFET and demonstrated that the device exhibits ambipolar behavior with Au source/drain contacts. Future work will focus on additional indenofluorene topologies and molecule functionalization as well as further device studies.

Experimental Procedures

General Comments. ^1H and ^{13}C NMR spectra were recorded in $CDCl_3$ using either a Varian Inova 500 (^1H: 500.11 MHz, ^{13}C: 125.75 MHz) or 600 (^1H: 599.98 MHz, ^{13}C: 150.87 MHz) spectrometer. Chemical shifts (δ) are expressed in ppm relative to the residual chloroform (^1H: 7.27 ppm, ^{13}C: 77.23 ppm) or CH_2Cl_2 (^1H: 5.32 ppm, ^{13}C: 54.00 ppm) as reference. Coupling constants are expressed in hertz. UV-Vis spectra were recorded on an HP 8453 UV-Vis spectrometer. High resolution mass spectra were recorded on a JEOL MSRoute mass spectrometer. THF, toluene, acetonitrile were

distilled from their appropriate drying agents under N_2. Unless otherwise stated, all reagents were purchased and used as received. Dione **5** was synthesized according to a previously described procedure.[1]

General Procedure for 4a-j. Haloarene was dissolved in THF (10 mL), degassed with Ar for 10 min, and cooled to –78 °C. Once cold, BuLi was added the mixture stirred at –78 °C for 20 min. In a separate flask, dione **5** was dissolved in THF (30 mL) and also degassed with Ar for 10 min, and cooled to –78 °C. Once cold, the lithiate was transferred by cannula to the solution containing **5** and warmed to room temperature for 2 h. The reaction mixture was quenched with 10% HCl solution (30 mL) and extracted in Et_2O (50 mL). The organic layer was dried over $MgSO_4$, filtered, and evaporated to dryness. The crude diol was then redissolved in 40 mL toluene and degassed with Ar for 10 min. $SnCl_2$ was added to the mixture (as was trifluoroacetic acid (TFA) in the case of **4h**–**j**) and warmed to 65 °C overnight. The solution was then filtered and the filtrate evaporated to dryness. The crude solid was redissolved in a minimal amount of acetonitrile, filtered once more, and the solid collected to afford the appropriate IF derivative **4**.

Phenyl IF 4a. Following the general procedure, iodobenzene (0.43 g, 2.12 mmol), BuLi (1.1 mL, 1.77 mmol), **5** (0.10 g, 0.35 mmol), and $SnCl_2$ (0.27 g, 1.42 mmol) were reacted to afford **4a** (0.078 g, 55%) as a magenta solid. ^{1}H NMR ($CDCl_3$): δ 7.64 (d, *J* = 7.8 Hz, 4H), 7.57 (t, *J* = 7.8 Hz, 4H), 7.48 (t, *J* = 7.2 Hz, 2H), 7.42 (d, *J* = 7.2 Hz, 2H), 7.38 (s, 2H), 7.28 (d, *J* = 7.2 Hz, 2H), 7.07 (m, 4H); ^{13}C NMR ($CDCl_3$): δ 144.5. 143.5. 139.8. 138.4. 134.4. 133.9. 129.4. 129.1. 128.7. 127.9. 127.5. 122.5. 120.6. 119.7; UV-vis ($CHCl_3$) λ_{max} (log ε): 290 (4.47), 311 (4.38), 324 (4.44), 472 (sh) (3.63), 515 (4.11), 544 (4.25) nm; HMRS (ESI) for $C_{32}H_{20}$ [M+1]: calcd 405.1643, found 405.1623.

4-MeO-Phenyl IF 4b. Following the general procedure, 4-bromoanisole (0.50 g, 2.12 mmol), BuLi (1.1 mL, 1.77 mmol), **5** (0.10 g, 0.35 mmol), and $SnCl_2$ (0.27 g, 1.42 mmol) were reacted to afford **4b** (0.060 g, 37%) as a magenta solid. ^{1}H NMR ($CDCl_3$): δ 7.60 (d, *J* = 7.8 Hz, 4H), 7.44 (m, 2H0, 7.40 (s, 2H), 7.29 (m, 2H), 7.10 (d, *J* = 7.8 Hz), 7.07 (m, 4H), 3.93 (s, 6H); ^{13}C NMR ($CDCl_3$): δ 160.1, 143.5, 139.4, 138.5, 133.4, 130.7, 127.7, 127.3, 127.1, 122.4, 120.5, 119.4, 114.6, 55.6; UV-vis ($CHCl_3$) λ_{max} (log ε): 301 (4.78), 311 (4.78), 323 (4.73), 475 (sh) (4.02), 524 (4.26), 558 (4.65) nm; HMRS (ESI) for $C_{34}H_{24}O_2$ [M+1]: calcd 465.1855, found 465.1839.

Mesityl IF 4c. Following the general procedure, 2-bromomesitylene (0.42 g, 2.12 mmol), BuLi (1.1 mL, 1.77 mmol), **5** (0.10 g, 0.35 mmol), and $SnCl_2$ (0.27 g, 1.42 mmol) were reacted to afford **4c** (0.072 g, 42%) as a red solid. ^{1}H NMR ($CDCl_3$): δ 7.31 (d, *J* = 7.2 Hz, 2H), 7.03 (s, 4H), 7.00 (t, *J* = 7.2 Hz, 2H), 6.95 (t, *J* = 7.2 Hz, 2H), 6.86 (s, 2H), 6.68 (d, 2H), 2.40 (s, 6H), 2.19 (s, 12H); ^{13}C NMR ($CDCl_3$): δ 145.5, 144.4, 139.3, 137.9, 137.7, 137.4, 135.0, 130.2, 128.4, 128.0, 127.2, 122.1, 120.5, 119.2, 21.4, 20.6; UV-vis ($CHCl_3$) λ_{max} (log ε): 306 (4.83), 319 (4.91), 455 (4.14), 484 (4.47), 517 (4.60) nm; HMRS (ESI) for $C_{38}H_{32}$ [M+1]: calcd 489.2582, found 489.2561.

4-Me-Phenyl IF 4d. Following the general procedure, 4-bromotoluene (0.36 g, 2.12 mmol), BuLi (1.1 mL, 1.77 mmol), **5** (0.10 g, 0.35 mmol), and $SnCl_2$ (0.27 g, 1.42 mmol) were reacted to afford **4d** (0.054 g, 36%) as a magenta solid. ^{1}H NMR ($CDCl_3$): δ 7.55 (d, *J* = 7.8 Hz, 4H), 7.42 (d, *J* = 6.6 Hz, 2H), 7.39 (s, 2H), 7.37 (d, *J* = 7.8 Hz, 4H), 7.28 (d, *J* = 6.6 Hz, 2H), 7.06 (m, 4H), 2.49 (s, 6H); ^{13}C NMR ($CDCl_3$): δ 144.2, 143.5, 139.5, 138.8, 138.5, 133.7, 131.6, 129.8, 129.3, 127.8, 127.4, 122.5, 120.5, 119.6, 21.7; UV-vis ($CHCl_3$) λ_{max} (log ε): 298 (4.64), 312 (4.59), 325 (4.59), 475 (sh) (3.95), 515 (4.34), 550 (4.48) nm; HMRS (ESI) for $C_{34}H_{25}$ [M+1]: calcd 433.1956, found 433.1948.

4-F-Phenyl IF 4e. Following the general procedure, 1-bromo-4-fluorobenzene (0.37 g, 2.12 mmol), BuLi (1.1 mL, 1.77 mmol), **5** (0.10 g, 0.35 mmol), and $SnCl_2$ (0.27 g, 1.42 mmol) were reacted to afford **4e** (0.077 g, 50%) as a magenta solid. ^{1}H NMR ($CDCl_3$): δ 7.60 (dd, *J* = 8.4, 2.8 Hz, 4H), 7.42 (d, *J* = 7.2 Hz, 2H), 7.32 (s, 2H), 7.26 (d, 8.4 Hz, 4H), 7.22 (d, *J* = 7.2 Hz, 2H), 7.08 (m, 4H); ^{13}C NMR ($CDCl_3$): δ 163.0 (d, *J* = 249.1 Hz), 143.4 (d, *J* = 9.8 Hz), 139.7, 138.3, 133.9, 131.0 (d, *J* = 8.1 Hz), 130.3 (d, *J* = 3.5 Hz), 128.0, 127.7, 122.3, 120.7, 119.4, 116.3 (d, *J* = 21.4 Hz); UV-vis ($CHCl_3$) λ_{max} (log ε): 296 (4.52), 311 (4.54), 323 (4.56), 471 (sh) (3.88), 508 (4.26), 545 (4.40) nm; HMRS (ESI) for $C_{32}H_{19}F_2$ [M+1]: calcd 441.1455, found 441.1435.

4-Cl-Phenyl IF 4f. Following the general procedure, 1-bromo-4-chlorobenzene (0.41 g, 2.12 mmol), BuLi (1.1 mL, 1.77 mmol), **5** (0.10 g, 0.35 mmol), and $SnCl_2$ (0.27 g, 1.42 mmol) were reacted to afford **4f** (0.080 g, 48%) as a magenta solid. ^{1}H NMR ($CDCl_3$): δ 7.55 (dd, *J* = 11.4, 2.4 Hz, 8H), 7.41 (d, *J* = 7.2 Hz, 2H), 7.31 (s, 2H), 7.22 (d, *J* = 7.2 Hz, 2H), 7.08 (m, 4H); ^{13}C NMR ($CDCl_3$): δ 143.5, 143.2, 139.9, 138.3, 134.7, 134.0, 132.7, 130.6, 129.4, 128.2, 127.8, 122.3, 120.7, 119.4; UV-vis ($CHCl_3$) λ_{max}: 298 (4.63), 312 (4.56), 325 (4.56), 473 (sh, 3.86), 512 (4.27), 548 (5.41) nm; HMRS (ESI) for $C_{32}H_{19}Cl_2$ [M+1]: calcd 473.0864, found 473.0877.

4-Br-Phenyl IF 4g. Following the general procedure, 1,4-dibromobenzene (0.50 g, 2.12 mmol), BuLi (1.1 mL, 1.77 mmol), **5** (0.10 g, 0.35 mmol), and $SnCl_2$ (0.27 g, 1.42 mmol) were reacted to afford **4g** (0.116 g, 59%) as a magenta solid. ^{1}H NMR ($CDCl_3$): δ 7.69 (d, *J* = 6.0 Hz, 4H), 7.49 (d, *J* = 6.6 Hz, 4H), 7.41 (m, *J* = 6.6 Hz, 2H), 7.30 (s, 2H), 7.21 (d, *J* = 5.4 Hz, 2H), 7.10 (m, 4H); ^{13}C NMR ($CDCl_3$): 143.5, 143.1, 140.0, 138.3 134.1, 133.2, 132.3, 128.2, 127.9 122.9, 122.3, 120.8, 119.4; UV-vis ($CHCl_3$) λ_{max}: 298

(4.63), 312 (4.56), 325 (4.54), 472 (sh, 3.82), 513 (4.24), 550 (4.38) nm; HMRS (ESI) for $C_{32}H_{19}Br_2$ [M+1]: calcd 560.9854, found 560.9832.

4-CF_3-Phenyl IF 4h. Following the general procedure, 4-bromobenzyltrifluoride (0.48 g, 2.12 mmol), BuLi (1.1 mL, 1.77 mmol), **5** (0.10 g, 0.35 mmol), and $SnCl_2$ (0.27 g, 1.42 mmol) were reacted. TFA (0.30 mL) was also added. Reaction work-up afforded **4h** (0.080 g, 42%) as a magenta solid. ^{1}H NMR ($CDCl_3$): δ 7.82 (d, *J* = 7.8 Hz, 4H), 7.73 (d, *J* = 7.8 Hz, 4H), 7.44-7.41 (m, 2H), 7.30 (s, 2H), 7.22-7.19 (m, 2H), 7.12-7.08 (m, 4H); ^{13}CNMR ($CDCl_3$): δ 143.6, 143.0, 140.3, 138.2, 137.8, 134.6, 130.5 (t, *J* = 16.1 Hz), 129.6, 128.4, 128.1, 126.1, 126.0 (t, *J* = 4.5 Hz), 123.4, 122.4, 120.9, 119.6; UV-vis ($CHCl_3$) λ_{max}: 298 (5.02), 314 (4.97), 326 (5.00), 473 (sh, 3.85), 512 (4.01), 545 (4.09) nm; HMRS (ESI) for $C_{34}H_{18}F_6$ [M+1]: calcd 541.1391, found 541.1388.

3,5-Bis(CF_3)$_2$-phenyl IF 4i. Following the general procedure, 3,5-bis(trifluoromethyl)-bromobenzene (0.62 g, 2.12 mmol), BuLi (1.1 mL, 1.77 mmol), **5** (0.10 g, 0.35 mmol), and $SnCl_2$ (0.27 g, 1.42 mmol) were reacted. TFA (0.30 mL) was also added. Reaction work-up afforded **4e** (0.088 g, 39%) as a red solid. ^{1}H NMR ($CDCl_3$): δ 8.04 (s, 4H), 7.99 (s, 2H), 7.40 (d, *J* = 7.2 Hz, 2H), 7.29 (s, 2H), 7.11-7.15 (m, 6H); ^{13}C NMR ($CDCl_3$): δ 142.6, 142.4, 140.7, 137.9, 136.1, 134.9, 132.7 (q, *J* = 100 Hz), 129.2, 128.6 (d, *J* = 22.5 Hz), 123.4 (q, *J* = 818 Hz), 122.3 (t, *J* = 6.9 Hz), 122.0, 121.2, 119.2; UV-vis ($CHCl_3$) λ_{max} (log ε): 292 (4.41), 312 (4.38), 324 (4.37), 472 (sh, 3.63), 513 (3.96), 543 (4.08) nm; HMRS (ESI) for $C_{36}H_{16}F_{12}$ [M+1]: calcd 677.1139, found 677.1127.

1,2,3,4,5-Pentafluorophenyl IF 4j. Following the general procedure, pentafluoro-iodobenzene (0.36 g, 2.12 mmol), BuLi (1.1 mL, 1.77 mmol), **5** (0.10 g, 0.35 mmol), and $SnCl_2$ (0.27 g, 1.42 mmol) were reacted. TFA (0.30 mL) was also added.

Reaction work-up afforded **4j** (0.078 g, 38%) as a red solid. ^{1}H NMR ($CDCl_3$): δ 7.35 (d, *J* = 7.2 Hz, 2H), 7.09 (t, *J* = 7.2 Hz, 2H), 7.05 (t, *J* = 7.2 Hz, 2H), 6.90 (s, 2H), 6.85 (d, *J* = 7.2 Hz); ^{13}C NMR ($CDCl_3$): δ 145.5, 143.5, 142.5, 140.7, 139.3, 137.4, 137.2, 131.3, 129.3, 128.9, 128.6, 128.4, 125.5, 122.6, 121.2, 119.6; UV-vis ($CHCl_3$) λ_{max} (log ε): 288 (4.35), 304 (4.42), 317 (4.48), 464 (sh) (3.84), 500 (4.11), 533 (4.21) nm; HMRS (ESI) for $C_{32}H_{10}F_{10}$ [M+1]: calcd 585.0701, found 585.0674.

X-ray Crystallography. Diffraction intensities for **4c** were collected at 173(2) K on a Bruker Apex CCD diffractometer using MoKα radiation λ = 0.71073 Å. Space group was determined based on systematic absences. Absorption corrections were applied by SADABS.[2] The structure was solved by direct methods and Fourier techniques and refined on F^2 using full matrix least-squares procedures. All non-H atoms were refined with anisotropic thermal parameters. All H atoms were refined in calculated positions in a rigid group model. In the crystal structure the main molecule is located on an inversion center. All calculations were performed by the Bruker SHELXTL (v. 6.10) package.[3] **4c**: $C_{38}H_{32}$, M = 488.64, 0.38 x 0.20 x 0.03 mm, T = 173 K, monoclinic, space group $P2_1/c$, a = 14.517(5) Å, b = 7.166(3) Å, c = 13.861(5) Å, β = 109.016(6)°, V = 1363.4(9) Å^3, Z = 2, Z'=0.5, D_c = 1.190 Mg m^{-3}, μ = 0.067 mm^{-1}, F(000) = 520, $2\theta_{max}$ = 50.00°, 12613 reflections, 2406 independent reflections [R_{int} = 0.0447], R1 = 0.0456, wR2 = 0.1095 ($I>2\sigma(I)$), R1 = 0.0617, wR2 = 0.1189 (all data), GOF = 1.065, max/min residual electron density +0.248/–0.189 eÅ^{-3}.

Structure Characterization of 4j. The single microcrystals of **4j** were examined in the TEM (JEOL 100CX-II) under bright field and selected area electron diffraction at 100 kV.

Fabrication of FET devices. The 200 nm SiO_2 substrates were coated with the monolayers of octadecyltrichorosilane (OTS) by immersion in toluene solution (1 mM) for 12 h at room temperature, rinsed with chloroform, IPA and DI water. The single crystal **4j** active channel was deposited on SAMs treated substrate by solvent exchange method. The source and drain Au electrodes were thermally evaporated through a TEM grid under a pressure of 10^{-6} mbar. Measurements were collected in an N_2-filled glove box (<0.1 ppm O_2 and H_2O).

Bridge to Chapter IV

With proof that fully-conjugated indeno[1,2-*b*]fluorene derivatives are organic semiconductors I turned my sights toward the development of another indenofluorene framework, namely indeno[2,1-*c*]fluorene. This molecular scaffold was the only one that, in generating the *para*-quinoidal core, showed no non-benzenoid *s*-cis diene linkages, so decreasing the potential for a range of deleterious decomposition pathways. Chapter IV shows the first synthesis and characterization of this class of compounds and shows these molecules also possess electronic characteristics known to be favorable for electron and ambipolar charge transport in organic electronic materials.

CHAPTER IV

INDENO[2,1-*c*]FLUORENE: A NEW ELECTRON-ACCEPTING SCAFFOLD FOR ORGANIC ELECTRONICS

This chapter was co-authored with Parker E. Deal, who provided synthetic support under my supervision, Bradley D. Rose, who performed the computational experiments, Chris L. Vonnegut, who performed the Cyclic Voltammetry, and Michael Haley, who provided editorial and material support. This work was originally published in *Organic Letters*.

Introduction

Organic electronic devices are becoming commonplace in many academic and industrial materials laboratories, and commercial application of these technologies is underway.[1] To maximize our understanding of organic electronics, a wide array of molecular frameworks is necessary, as it allows for a variety of optical and electronic properties to be systematically investigated.[2] With the ability to further tune each individual scaffold via derivatization, access to a broad spectrum of interesting materials is possible.[2,3] Of particular interest in the search for organic electronic materials are the cyclopenta-fused polyaromatic hydrocarbons (CP-PAHs, e.g., fullerenes,[4] buckybowls[5]).[6] The cyclopentadiene rings within these compounds impart a higher electron affinity because of the driving force to aromatize the cyclopentadiene by accepting an electron. Another family of cyclopenta-fused molecules under investigation is based on the fully conjugated indenofluorene (IF) system,[7] which is comprised of five structural isomers (e.g., **1** - **5**, Figure 1).

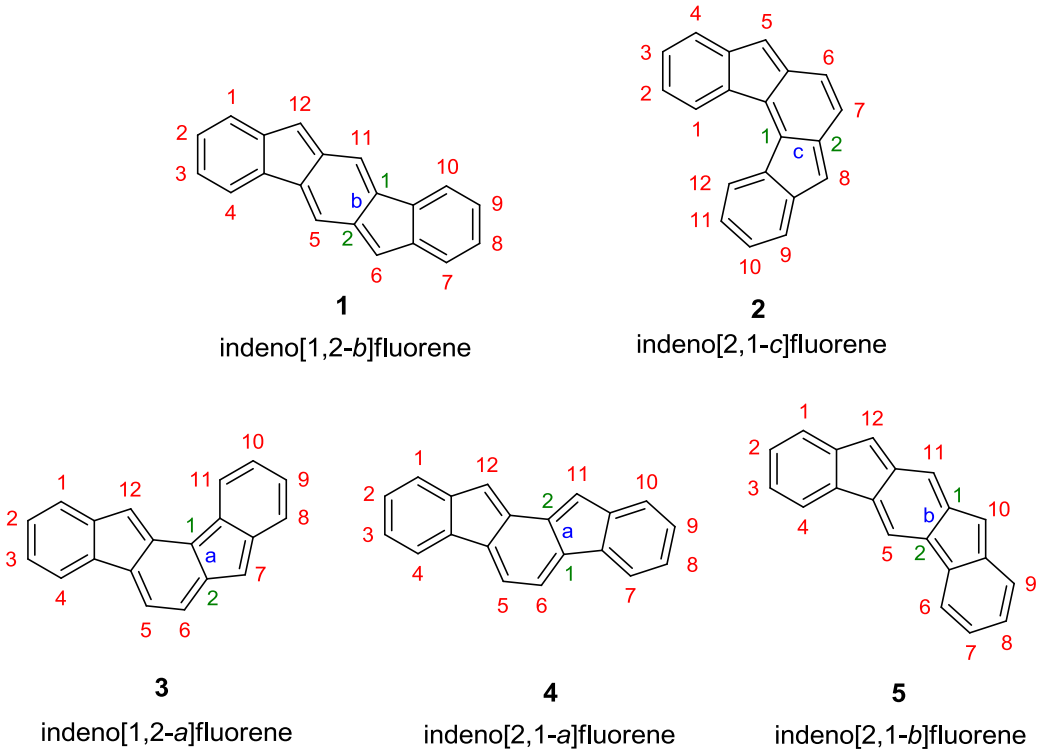

Figure 1. The five major indenofluorene regioisomers.

To date nearly all reported studies have focused on derivatives of **1** (25 examples),[8,9] as well as derivatives of **4** (2 examples).[10] Importantly, the [1,2-*b*]IF scaffold can serve as an electron-accepting or ambipolar material for organic electronics, with derivatives of **1** showing ambipolar transport in both a single crystal OFET[8c] and thin-film OFETs.[9c] Of the remaining unknown regioisomers, formation of IFs **3** and **5** will dearomatize an internal and a peripheral benzene to achieve closed-shell structures; thus, we anticipate the resultant molecules would be considerably less stable than **1**. Like **1**, the formation of **2** requires dearomatization of only one internal benzene ring, and the immediate IF-dione precursor is easily accessible in multigram quantities in four steps from cheap, commercially available precursors.[11] Reported herein are the synthesis and

charcterization of three derivatives of the fully conjugated indeno[2,1-*c*]fluorene scaffold ([2,1-*c*]IF, **2**).

Results and Discussion

Synthesis. Realization of target molecules **2a-c** occurs by nucleophilic attack on dione **6** with either an aryl or ethynyl lithiate and subsequent reductive dearomatization with anhydrous $SnCl_2$ (Scheme 1), producing the desired compounds in moderate yields after purification. Unlike the [1,2-*b*]IFs and [2,1-*a*]IFs, which are blue/purple in solution, [2,1-*c*]IFs **2a-c** are green in solution and green/black in the solid state.

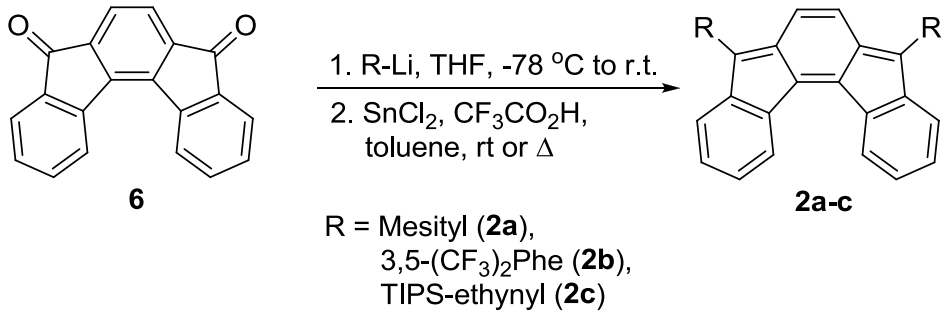

Scheme 1. Synthesis of Indeno[2,1-*c*]fluorenes

Electronic Absorption Spectra. The UV-vis spectra of **2a-c** (Figure 2) display strong absorbances in the higher energy range, with a broad, low energy absorbance that extends into the near-IR region. Interestingly, these broad low-energy bands (550-800 nm) are similarly observed in the spectrum of 11,12-dimesityl[2,1-*a*]IF (**4a**),[10b] which also possesses the *as*-indacene core. This is in contrast to the spectra of [1,2-*b*]IFs, which are based on the *sym*-indacene skeleton, as the lowest energy peak of the derivatives of **1** to date has been less than 615 nm.[8,9] Similar to other fully conjugated IFs, **2a-c** are nonemissive.

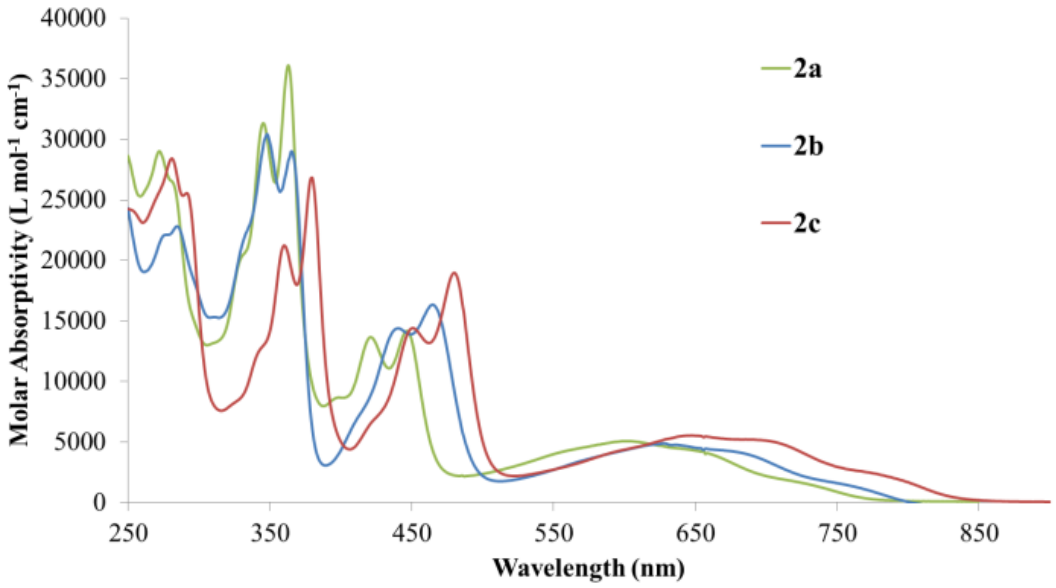

Figure 2. Overlaid UV/Vis spectra of [2,1-*c*]IFs **2a-c**.

Solid State Studies. Single crystals of **2a** suitable for X-ray diffraction were obtained via slow crystallization from toluene. The resultant structure solution (Figure 3) shows that the molecule packs in two symmetrically independent arrangements, with each molecule bent slightly out of plane. The two independent molecules possess helicene-like axial chirality, but the barrier to inversion is extremely small, calculated to be 0.02 kcal mol^{-1}.[12,13] Dihedral angles between the average planes of the central six-membered ring, the bridging five-membered ring, and the terminal six-membered ring of the *P*-isomer of **2a** are 2.26(5), 4.32(5) and 1.98(5), 2.40(6), respectively; the corresponding angles in the *M*-isomer are 4.78(7), 6.63(6) and 4.67(8), 3.66(8). There is no cofacial packing within the crystal lattice, and the closest interplanar contact distance (C90-C20) is 3.47 Å.

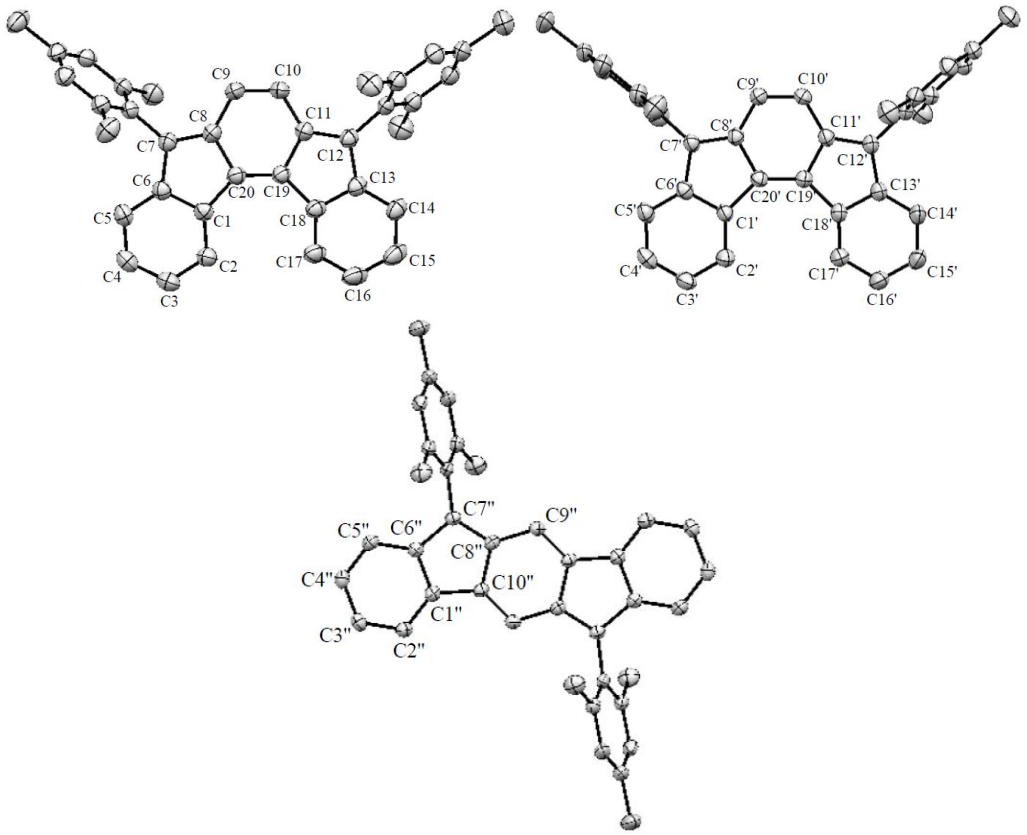

Figure 3. Crystal structure of **2a** with bond lengths for the two crystallographically independent molecules within the packing structure. Orbitals drawn at the 30% and hydrogens omitted for clarity. The crystal structure of 6,12-dimesityl[1,2-*b*]IF (**1a**) is shown on the right for comparison.

While both the [2,1-*a*]IFs and [2,1-*c*]IFs contain the *as*-indacene core, the [2,1-*a*]IF possesses the reactive *o*-quinodimethane motif. For structural comparison, we chose the two independent molecules of **2a** and 6,12-dimesityl[1,2-*b*]IF **1a**[8c] as both incorporate a central p-quinodimethane unit. As can be seen in Table 1, there is very little difference in the quinoidal bond lengths between molecules. For example, C1-C11 in **2a** (1.359/ 1.355 Å) is essentially identical to C1-C3A in **1a** (1.356 Å), whereas C3-C13 (1.367/ 1.364 Å) is marginally longer. The quinoidal "double bonds" in the five-membered ring of **2a** (C2-C6, avg. 1.371 Å; C12-C16, avg. 1.374 Å) are slightly shorter than those found in **1a** (C2-C6, 1.380 Å). The structural similarity of the two IF skeletons extends

to the bonds in the peripheral arene rings, where the homogeneous bond lengths (avg. 1.387 Å for **2a**, 1.389 Å for **1a**) clearly suggest retention of their aromatic character. Only the bond shared with the five-membered ring (C4-C5) shows a slight elongation from that of a typical aryl subunit. Despite the presence of the *p*-quino-dimethane moiety, calculations reveal that the scaffold exists as a closed shell ground state and has little biradical character as determined utilizing broken symmetry UB3LYP/6-311*G(2df,2pd) (see Supporting Information).

Table 1. Bond Lengths in angstroms.

	2a-*P* (left)	**2a-*M*** (right)	**1a** (bottom)
C1 – C2	1.380(2)	1.384(2)	1.382(3)
C1 – C6	1.415(2)	1.415(2)	1.413(2)
C1 – C20	1.482(2)	1.475(2)	1.469(2)
C2 – C3	1.401(2)	1.393(3)	1.394(2)
C3 – C4	1.383(2)	1.387(3)	1.390(3)
C4 – C5	1.396(2)	1.382(3)	1.388(3)
C5 – C6	1.384(2)	1.389(2)	1.391(2)
C6 – C7	1.467(2)	1.462(2)	1.471(3)
C7 – C8	1.370(2)	1.370(2)	1.380(2)
C8 – C9	1.429(2)	1.436(2)	1.433(3)
C8 – 20	1.473(2)	1.473(2)	1.467(3)
C9 – C10	1.359(2)	1.352(2)	1.356(2)
C10 – C11	1.432(2)	1.435(2)	
C11 – C12	1.371(2)	1.375(2)	
C11 – C19	1.471(2)	1.470(2)	
C12 – C13	1.466(2)	1.461(2)	
C13 – C14	1.382(2)	1.384(2)	
C13 – C18	1.414(2)	1.421(2)	
C14 – C15	1.389(2)	1.389(2)	
C15 – C16	1.388(3)	1.383(2)	
C16 – C17	1.395(2)	1.397(2)	
C17 – C18	1.385(2)	1.383(2)	
C18 – C19	1.479(2)	1.472(2)	
C19 – C20	1.367(2)	1.364(2)	

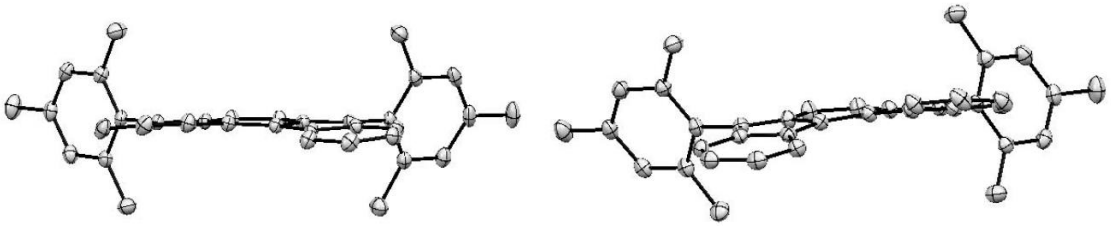

Figure 4. Side-on view of the *P*- and *M*- helicenes (left and right, respectively) found within the single crystal of **2a**. The barrier to inversion is calculated at 0.02 kcal/mol.

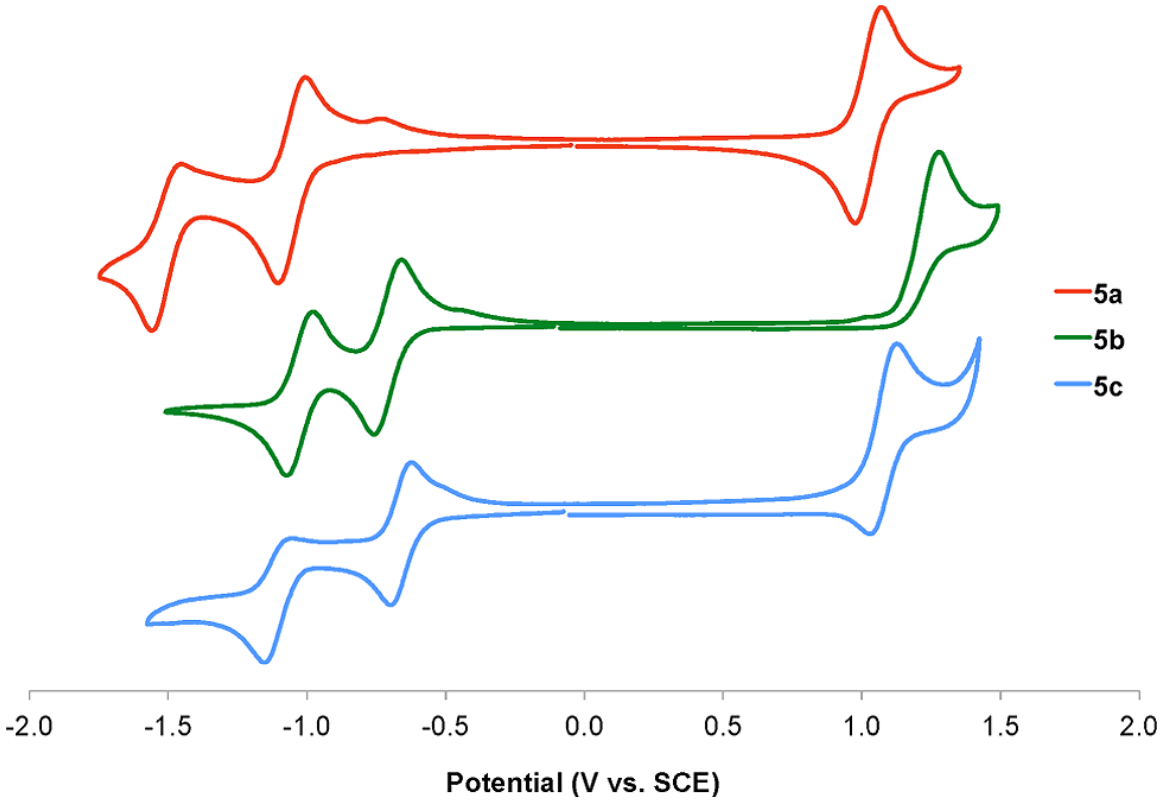

Figure 5. Cyclic voltammetry of [2,1-*c*]IFs **2a-c**; voltammogram currents are normalized to the E_{anodic}^{1} peak.

Electrochemical Studies. Cyclic voltametry (CV) data indicate that **2a-c**, like the [1,2-*b*]IFs and [2,1-*a*]IFs, are electron deficient (Figure 5, Table 2). The molecules can reversibly accept up to two electrons and possess LUMO energies estimated at 3.6 to 4.0 eV, analogous to those found in derivatives of **1**;[8b,c] however, the HOMO energies of **2a-c** are roughly 0.15 eV higher, thus leading to reduced gap energies compared to their

identically substituted analogs of **1** (e.g., 1.89 eV for **1c** vs. 1.73 eV for **2c**).[8b,c] These results suggest that **2a-c** could be good candidates for use as n-type organic semiconducting materials with low threshold voltages.[3,14]

Table 2. Optical and Electrochemical Data.

	electrochemical						**optical**		
cmpd	E_{red}^1 (V)[a]	E_{red}^2 (V)[a]	E_{ox} (V)[a]	E_{LUMO} (eV)[b]	E_{HOMO} (eV)[b]	E_{gap} (eV)	λ_{max} (nm)	ε ($\times 10^4$ L M^{-1} cm^{-1})	E_{gap} (eV)[c]
2a	-1.05	-1.51	1.02	-3.59	-5.66	2.08	345, 363, 421, 447, 603	3.13, 3.61, 1.37, 1.42, 0.51	1.60
2b	-0.71	-1.02	-[d]	-3.93	-[d]	-[d]	348, 365, 441, 465, 627	3.04, 2.90, 1.44, 1.64, 0.49	1.54
2c	-0.66	-1.11	1.07	-3.98	-5.71	1.73	360, 380, 451, 480, 647	2.12, 2.68, 1.44, 1.90, 0.55	1.48

[a] CV recorded using 1-5 mM of analyte in 0.1 M tetrabutylammonium trifluoromethane-sulfonate/CH_2Cl_2 using a scan rate of 50 mV/s. The working electrode was a glassy carbon electrode with a platinum coil counter electrode and silver wire pseudoreference. Values reported as the half-wave potential (vs SCE) using the Fc/Fc^+ couple (0.46 V) as an internal standard; see ref 15. [b] Determined by $E_{LUMO} = -(4.44 + E_{red}^1)$; see ref 16. [c] Determined using the wavelength at the maximum absorption of the lowest energy $\pi \rightarrow \pi^*$ transition from the UV vis spectrum. [d] Reversible oxidation of **2b** was not achieved.

In conclusion, we have synthesized and characterized a short series of [2,1-*c*]IF derivatives. The ease of manufacture, high electron affinities, and small HOMO-LUMO energy gaps of these new molecules should make this class of cyclopenta-fused hydro-carbons attractive candidates for application in a variety of organic electronic devices. We are currently exploring the preparation of additional fully conjugated indeno[2,1-*c*]-fluorenes as well as device studies with these new electron-accepting materials.

Experimental Details

General Comments. ^{1}H and ^{13}C NMR spectra were recorded in $CDCl_3$ using either a Varian Mercury 300 MHz (1H: 300.09 MHz) or Bruker Avance III HD 600 MHz (1H: 600.02 MHz, 13C: 150.89 MHz) NMR spectrometer with Prodigy multinuclear broadband cryoprobe. Chemical shifts (δ) are expressed in ppm relative to the residual CHCl3 (1H: 7.27 ppm, 13C: 77.23 ppm. UV-Vis spectra were recorded on an HP 8453 UV-Vis spectrometer. High resolution mass spectra were recorded on a JEOL MS-Route mass spectrometer. Melting points were determined on a Meltemp II apparatus and are uncorrected. THF was distilled from potassium under N2. Unless otherwise stated, all solvents and reagents were purchased and used as received. Dione **6** was synthesized according to a previously described procedure.[17]

5,8-Dimesitylindeno[2,1-c]fluorene (2a). A solution of bromomesitylene (0.76 g, 3.83 mmol) in THF (10 mL) was degassed with Ar for 10 min and then cooled to –78 °C. n-BuLi(1.42 mL, 3.45 mmol, 2.5 M) was added and the mixture stirred at –78 °C for 20 min. In aseparate flask, dione **6** (0.20 g, 0.71 mmol) in THF (30 mL) was degassed with Ar for 10 min and also cooled to –78 °C. The lithiate solution was cannulated into the cold dione solution, and the reaction warmed to rt over 2 h. The reaction was quenched by addition of aq. 10% HCl soln (30 mL) and extracted with Et_2O. The organic layer was dried over $MgSO_4$, filtered, and evaporated to dryness. The crude diol was then re-dissolved in toluene (40 mL) and degassed with Ar for 10 min. $SnCl_2$ (0.5 g, 2.64 mmol) and trifluoroacetic acid (~ 0.1 mL) were added, and the reaction stirred overnight at 50 °C. The solution was filtered and the filtrate subsequently evaporated to dryness. Flash chromatography (hexanes) and vacuum distillation at 200 °C to remove residual

bromomesitylene gave **2a** (0.17 g, 49%) as a green solid. Mp 182-183 °C; ^{1}H NMR (600 MHz, $CDCl_3$) δ 8.11 (d, J = 7.2 Hz, 2H), 7.16 (t, J = 7.1 Hz, 2H), 7.12 (t, J = 7.0 Hz, 2H), 6.98 (s, 2H), 6.71 (d, J = 6.6 Hz, 2H), 6.13 (s, 2H), 2.37 (s, 6H), 2.16 (s, 12H); ^{13}C NMR (151 MHz, $CDCl_3$) δ 146.11, 143.35, 138.83, 137.38, 137.03, 136.33, 136.28, 129.92, 129.09, 128.13, 126.45, 125.38, 121.67, 120.89, 21.15, 20.27; UV-Vis (CH_2Cl_2) λ_{max} (ε) 345 (31,300), 363 (36,100), 421 (13,700), 447 (14,200), 603 (5,100) nm; HRMS (ESI) for C38H33 [M+]: calcd 489.2558, found 489.2567.

5,8-Bis(3,5-bis(trifluoromethyl)phenyl)indeno[2,1-c]fluorene (2b). A solution of 1-bromo-3,5-bis(trifluoromethyl)benzene (1.4 g, 4.79 mmol) in THF (10 mL) was degassed with Ar for 10 min and then cooled to –78 °C. n-BuLi (1.77 mL, 4.42 mmol, 2.5 M) was added and the mixture stirred at –78 °C for 20 min. In a separate flask, dione **6** (0.25 g, 0.89 mmol) in THF (30 mL) was degassed with Ar for 10 min and also cooled to –78 °C. The lithiate solution was cannulated into the cold dione solution, and the reaction warmed to rt over 2 h. The reaction was quenched by addition of aq. 10% HCl soln (30 mL) and extracted with Et_2O. The organic layer was dried over $MgSO_4$, filtered, and evaporated to dryness. The crude diol was then re-dissolved in toluene (40 mL) and degassed with Ar for 10 min. $SnCl_2$ (0.5 g, 2.64 mmol) and trifluoroacetic acid (~ 0.1 mL) were added, and the reaction stirred overnight at 50 °C. The solution was filtered and the filtrate subsequently evaporated to dryness. Recrystallization from Ar-saturated MeOH gave **2b** (0.23 g, 39%) as a dark green solid. Mp 240 °C (dec); ^{1}H NMR (600 MHz, $CDCl_3$) δ 8.14 (d, J = 7.0 Hz, 2H), 7.99 (s, 4H), 7.95 (s, 2H), 7.25 (td, J = 7.5, 1.2 Hz, 2H), 7.22 (td, J = 7.5, 1.1 Hz, 2H), 7.14 (d, J = 7.0 Hz, 2H), 6.64 (s, 2H); ^{13}C NMR (151 MHz, $CDCl_3$) δ 144.31, 140.16, 139.96, 136.58, 136.21, 135.82, 132.30 (q, J = 33.6

Hz), 129.78, 129.14 (d, J = 3.6 Hz), 127.83, 126.17, 123.19 (q, J = 273 Hz), 121.99 (sept, J = 3.1 Hz), 121.66, 121.42; UV-Vis (CH_2Cl_2) λ_{max} (ε) 348 (30,400), 365 (29,000), 441 (14,400), 465 (16,400), 627 (4,900) nm; HRMS (ESI) for C36H17F12 [M+]: calcd 677.1130, found 677.1139.

5,8-Bis(triisopropylsilylethynyl)indeno[2,1-c]fluorene (2c). Triisopropylsilyl)acetylene (0.67 mL, 2.87 mmol) in THF (10 mL) was degassed with Ar for 10 min, and then cooled to 0 °C. n-BuLi (1.06 mL, 2.66 mmol, 2.5 M) was added and the mixture stirred at 0 °C for 20 min. In a separate flask, dione **6** (0.15 g, 0.53 mmol) in THF (15 mL) was degassed with Ar for 10 min and then cooled to 0 °C. The lithiate solution was cannulated into the cold dione solution and the reaction warmed to rt over 2 h. The reaction was quenched by addition of aq. 10% HCl soln (30 mL) and extracted with Et_2O. The organic layer was dried over $MgSO_4$, filtered, and evaporated to dryness. The crude diol was then re-dissolved in dry toluene (15 mL), degassed with Ar for 10 min, $SnCl_2$ (0.5 g, 2.64 mmol) was added, and the mixture stirred overnight at room temperature. The resultant green solution was filtered and the filtrate evaporated to dryness. Recrystallization from MeOH gave **2c** (0.15 g, 46%) as a dark green solid. Mp 152-153 °C; ^{1}H NMR (600 MHz, $CDCl_3$) δ 7.93 (d, J = 7.4 Hz, 2H), 7.28 (d, J = 7.3 Hz, 2H), 7.21 (t, J = 7.3 Hz, 2H), 7.16 (t, J = 7.4 Hz, 2H), 6.87 (s, 2H), 1.21 (br s, 42H); ^{13}C NMR (151 MHz, $CDCl_3$) δ 144.71, 142.70, 139.06, 135.77, 129.56, 127.50, 125.28, 125.15, 122.12, 121.65, 109.46, 101.67, 18.78, 11.34; UV-Vis (CH_2Cl_2) λ_{max} (ε) 360 (21,200), 380 (26,800), 451 S4 (14,400), 480 (19,000), 647 (5,500) nm; HRMS (ESI) for C42H52Si2 [M+]: calcd 613.3686, found 613.3666.

Bridge to Chapter V

Though demonstrating favorable electronic character, the indeno[2,1-*c*]fluorene derivatives introduced in Chapter IV possessed what is often seen to be a fatal flaw in organic semiiiconductors, a morphology that deviated from planarity and showed flexibility that disrupts the crystal lattice in the solid state, thus significantly diminishing their likelihood to show reproducilble charge transport characteristics in devices.

I hypothesized that substituting a thiophene ring in the center of the compound would lead to a planarized solid state morphology. Initial calculations suggested this to be the case as well and the results of these calculations led to the synthesis and characterization of a new class of quinoidal thiophene derivatives based on the diindeno[2,1-*b*:1',2'-*d*]thiophene scaffold demonstrated in Chapter V. This chapter also shows the first crystal structure of diindeno[2,1-*b*:1',2'-*d*]thiophene-5,7-dione and demonstrates that it possesses electronic and solid state characteristics that make it a candidate for use as an electron-transport semiconducting material in devices.

CHAPTER V

FULLY-CONJUGATED DIINDENO[2,1-*b*:1',2'-*d*]THIOPHENES AND DIINDENO-[2,1-*b*:1',2'-*d*]THIOPHENE-5,7-DIONE: SYNTHESES AND OPTOELECTRONIC PROPERTIES

This chapter was co-authored with Parker E. Deal, who provided synthetic support under my supervision, Chris L. Vonnegut, who performed the cyclic voltammetry, and Michael Haley, who provided editorial and material support. This work is being prepared for publication in *Organic Letters*.

Introduction

The search continues for a diverse array of solution processable compounds for use as electron-transport and ambipolar materials with the goal of cheap, facile implementation in organic electronic devices such as organic field effect transistors (OFETs) and organic photovoltaics (OPVs).[1,2] Oligothiophenes, quinoidal thiophenes, and various thiophene-fused PAHs have been shown to have amphoteric redox properties and many have shown good charge transport performances, some as high as 30 cm^2/Vs (holes).[2,3] Good ambipolar transport characteristics are also seen, with some compounds showing balanced hole and electron mobilities on the order of 0.5 – 1 cm^2/Vs.[2] In fact, the first single conjugated organic semiconducting material to show ambipolar charge transport characteristics in a thin-film OFET (OTFT) was a quinoidal thiophene, DCMT, though the mobilities for both holes and electrons were less than 10^{-4} cm^2/Vs (Figure 1).[4a] Typically, however, the quinoidal thiophenes need to be appended with strongly electron-withdrawing substiuents such as dicyanomethylene to observe higher electron affinities

(lower LUMO energies) and electron transport character and these compounds often do not display ambipolar charge transport.[4]

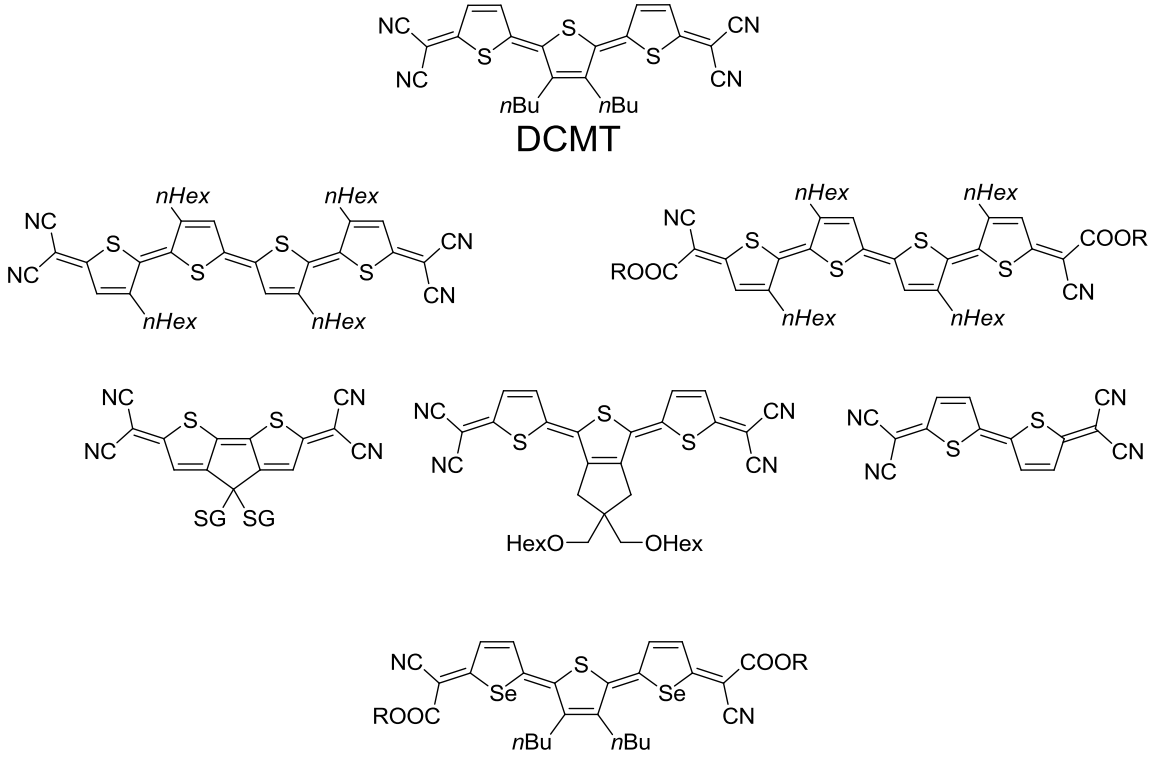

Figure 1. DCMT and other more recent examples of quinoidal thiophenes (SG is a solubilizing group).[4]

Recently, our lab and others have been investigating compounds containing cyclopenta-fused polyaromatic hydrocarbons (CP-PAHs) for use as electron or ambipolar charge-transport materials, including those containing thiophenes.[5,6] To install the obtain the desired compounds we typically dearomatize a central benzene ring in an indenofluorene molecule to generate a quinoidal antiaromatic indacene core. We recently reported the synthesis of indeno[2,1-*c*]fluorene ([2,1-*c*]IF, **1**) derivatives which showed redox properties favorable for organic semiconducting materials but possessed a slight

deviation from planarity in the solid state due to the steric interaction between the hydrogen atoms in the bay region (Figure 2a).[7]

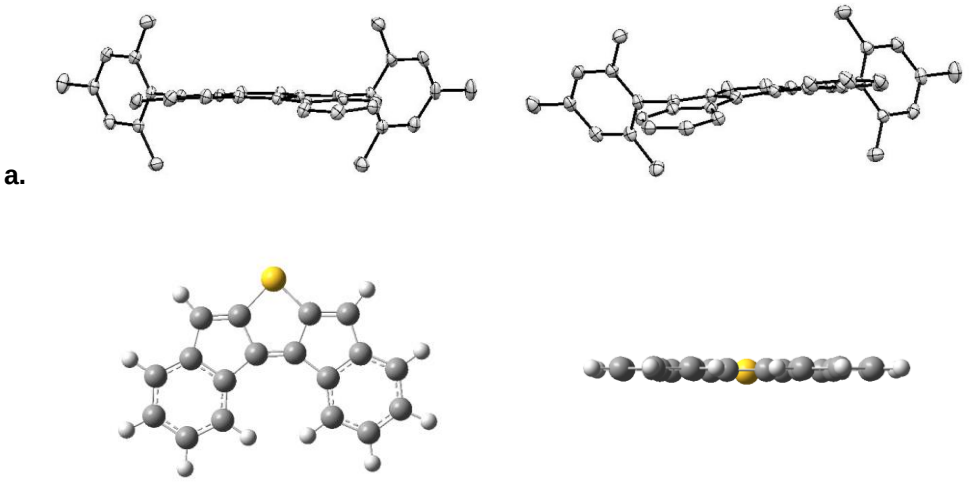

Figure 2. a. The two helicene diastereomers within the crystal structure of dimesitylindeno[2,1-*c*]fluorene (**1a**). **b.** The calculated minimized molecular geometry of parent diindeno[2,1-*b*:1',2'-*d*]thiophene scaffold (**2**).[9]

We hypothesized that one solution to overcome this deficiency in optimal solid-state morphology, while maintaining the favorable redox character, was to replace the central benzene ring with the isoelectronic thiophene ring, thereby widening the bay region and separating the hydrogen atoms enough to eliminate the steric interaction and planarize the scaffold. Evidence of this was seen in a topologically similar 6-5-5-5-6 fused-ring molecule, bis(benzo[4,5]-thieno)[2,3-*b*:3',2'-*d*]thiophene (BBTT, Figure 3), that had a planar morphology in the solid state.[8] Additionally, the introduction of a thiophene ring should impart an improvement to charge-transport character given the greater polarizability and generally lower reorganization energies of sulfur-containing molecules.[2,3] Calculations of the minimized molecular geometry of the unsubstituted diindeno[2,1-*b*:1',2'-*d*]thiophene scaffold (DIT, **2**) corroborate the general hypothesis (Figure 2b).[9] Also, the calculated HOMO and LUMO levels suggested that the orbital

energies are only slightly altered when compared to the calculated values for **1** (Figure 4).[9]

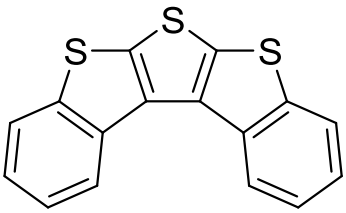

Figure 3. Structure of BBTT.

Of fundamental interest to us as well is how different aromatic motifs respond to dearomatization, e.g., how this alters their optoelectronic properties, stability, etc. Quinoidal thiophenes have been seen to have good stability (with some demonstrating operational stablility in air)and several have shown promise as ambipolar or electron-transport semiconducting materials.[4] Our thought was that this inherent property combined with the electron-accepting nature of the cyclopentadiene-like moiety should give this material an ambipolar or electron-accepting character without the need to append strongly electron-withdrawing substituents like dicyanomethylene.

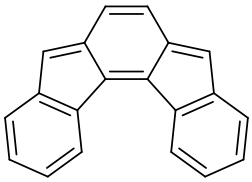

1
HOMO (eV): -5.32
LUMO (eV): -2.99
Gap (eV): 2.33

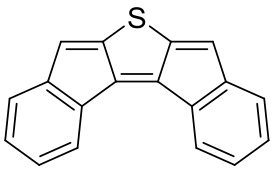

2
HOMO (eV): -5.46
LUMO (eV): -2.93
Gap (eV): 2.53

Figure 4. Calculated HOMO/LUMO energies for the parent scaffolds of [2,1-*c*]IF, **1**, and DIT, **2.** Geometries were minimized using broken symmetry UB3LYP/cc-pVTZ. Energies were detrmined from this geometry and it was then used to generate the HOMO/LUMO maps using Avogadro.[9]

Additionally, to our knowledge, the optoelectronic properties of the desired known molecular precursor, diindeno[2,1-*b*:1',2'-*d*]thiophene-5,7-dione (DITDO, **6**), have yet to be investigated.[10] Given the performance and stability seen in indeno[1,2-*b*]fluorene-6,12-diones, we hypothesized that this compound could be of interest for organic electronic materials also.[11]

Results and Discussion

Synthesis of the known dione **6** was achieved via an alternate route to that used previously.[10] Suzuki cross-coupling of the commercially available compounds **3** and **4** followed by saponification and ring closing via Friedel Crafts conditions gives **5** in 55% overall yield on a multi-gram scale (Scheme 1). Use of anhydrous DMF was critical to obtaining high yields for this Suzuki reaction.

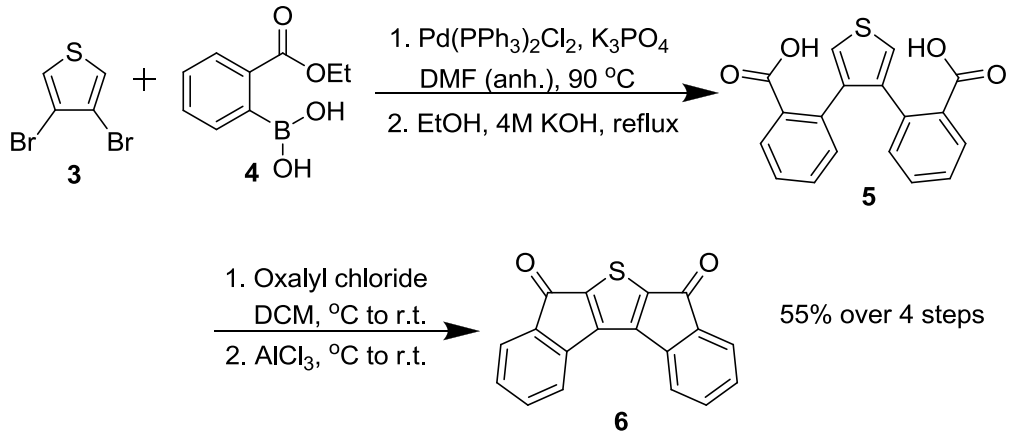

Scheme 1. New synthesis of DITDO **6**.

Analogous to the IFs, manufacture of the target DIT molecules occurs by nucleophilic attack on the diones with an aryl or ethynyl lithiate and subsequent reductive dearomatization with anhydrous $SnCl_2$ (Scheme 2). The desired compounds are obtained in modest yields after purification. Like the [2,1-*c*]IFs, the DITs are green of hue.[7]

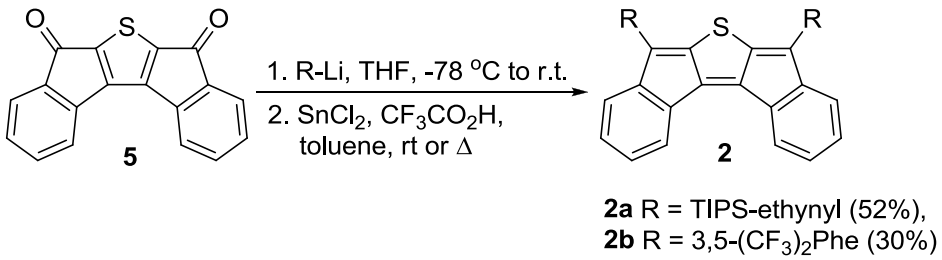

Scheme 2. Synthesis of diindeno[2,1-*b*:1',2'-*d*]thiophenes **2a,b**.

The spectra show strong similarities to the [2,1-*c*]IFs, with strong absorbances in the higher energy range of the spectrum and a broad lower energy absorbance region that extends to the near IR (Figure 5, Table 1). Also like the fully-conjugated IFs, DITs **2a,b** are non-emissive.

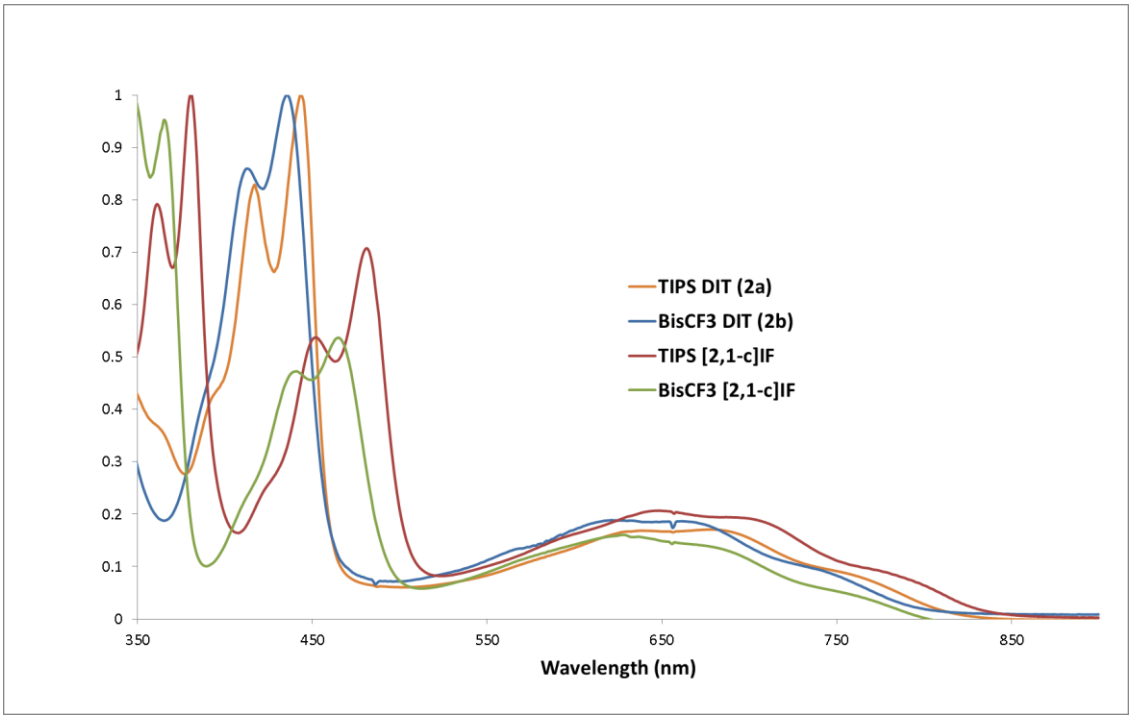

Figure 5. Normalized UV/Vis absorption spectra of DITs **2a**,**b** and the related [2,1-*c*]IF derivatives.

Single crystals of **2a** were grown via slow crystallization from chlorobenzene and the structures determined using x-ray diffraction (Figure 6). The crystal structure shows

that the molecule packs in centrosymmetric dimers that stack alternately, one on top of another. The packing within each dimer is tighter (C-C close contact 3.34 Å) than that between adjacent dimers (C-C close contact 3.38 Å). There is significant cofacial overlap (π- stacking) at the contact points and the overall packing motif is a 1-D chain. In addition, it still appears that the DITs may deviate slightly from planarity, though too a much less significant degree than that seen in the [2,1-*c*]IFs.

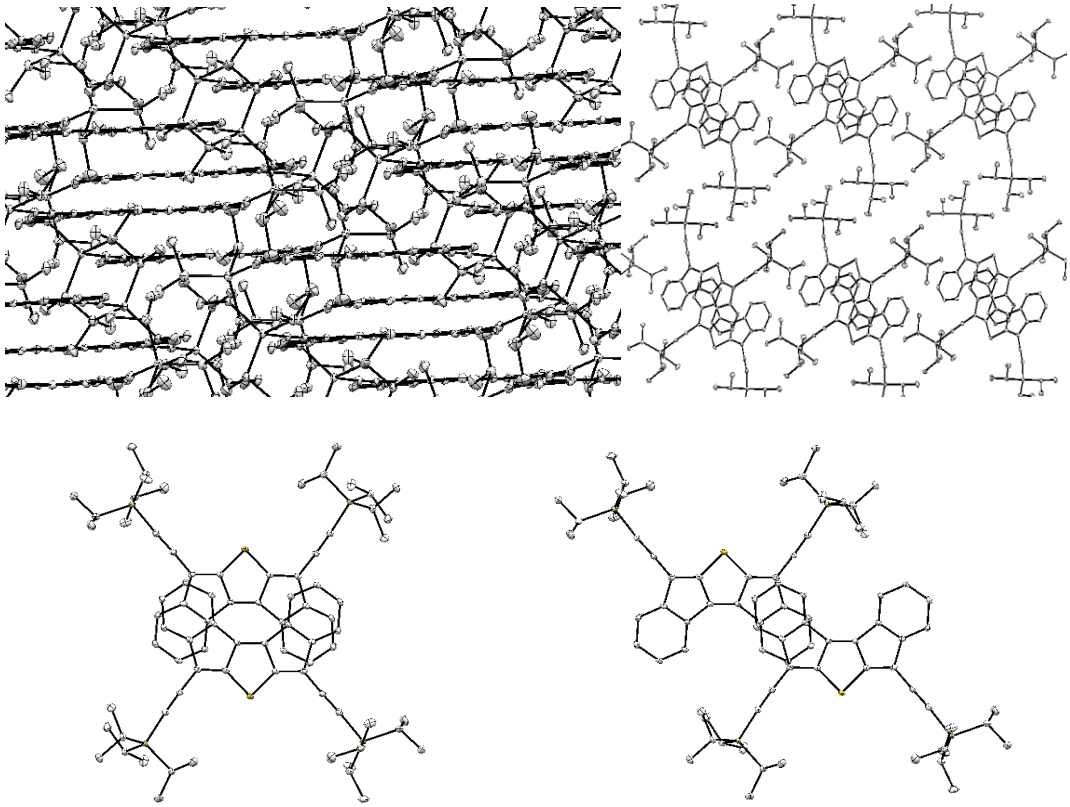

Figure 6. Solid state data for **2a**. View of crystal packing side-on (top left) and top-down (top right); top-down view of the two dimeric cofacial motifs found within the crystal (bottom). Ellipsoids drawn at the 30% probability level and hydrogens omitted for clarity.

Single crystals of **6** were grown via solvent exchange from chloroform with cyclohexane countersolvent and the structures determined using x-ray diffraction (Figure 7). The crystal structure shows that the molecule packs in 1-D columns, with molecules

alternating between two different orientations within each stack. The packing shows a C-C close contact distance of 3.39 Å, and a C-S close contact distance of 3.41 Å, both less than the Van der Waals radii of the respective atoms. The molecules are bowed in the center, though only slightly. Interestingly, oxygen atoms in a molecule in one stack show a strong association with the bay hydrogens in the molecule in the adjacent stack and this motif persists throughout the crystal structure.

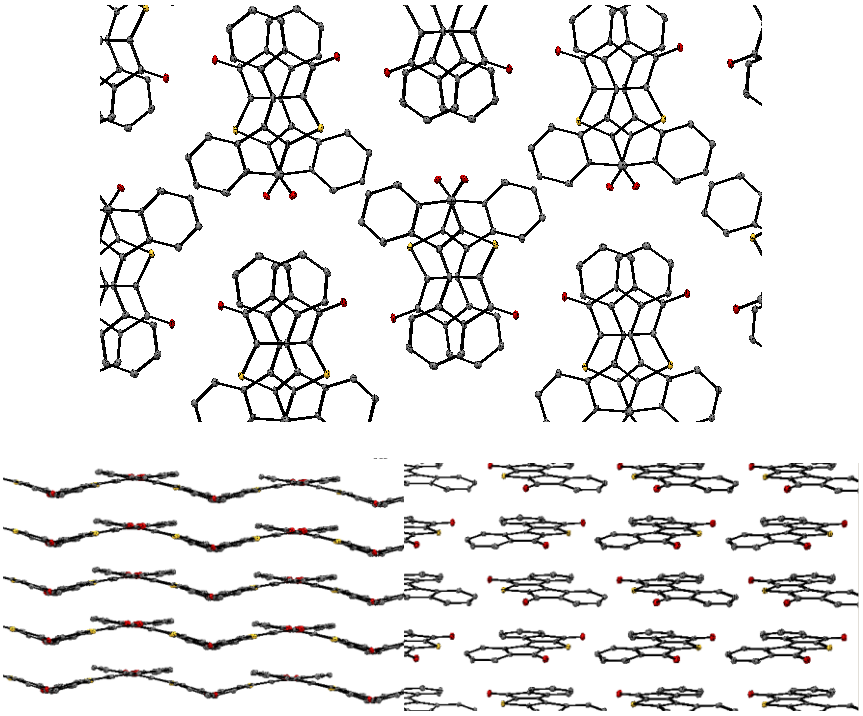

Figure 7. Top-down (top) and side-on (bottom) views of the packing within the crystal structure of **6**. Ellipsoids drawn at 30% probablity and hydrogens omitted for clarity.

HOMO/LUMO maps were also calculated for unsubstituted **2** and **6** (Figure 8).[9] It can be seen from these maps that the orbital rdensity of the two compounds is located in somewhat disimilar regions. The presence of LUMO density on the sulfur atom of **5** is is not seen on the corresponding sulfur atom in **2**, which shows HOMO density there but no LUMO density.

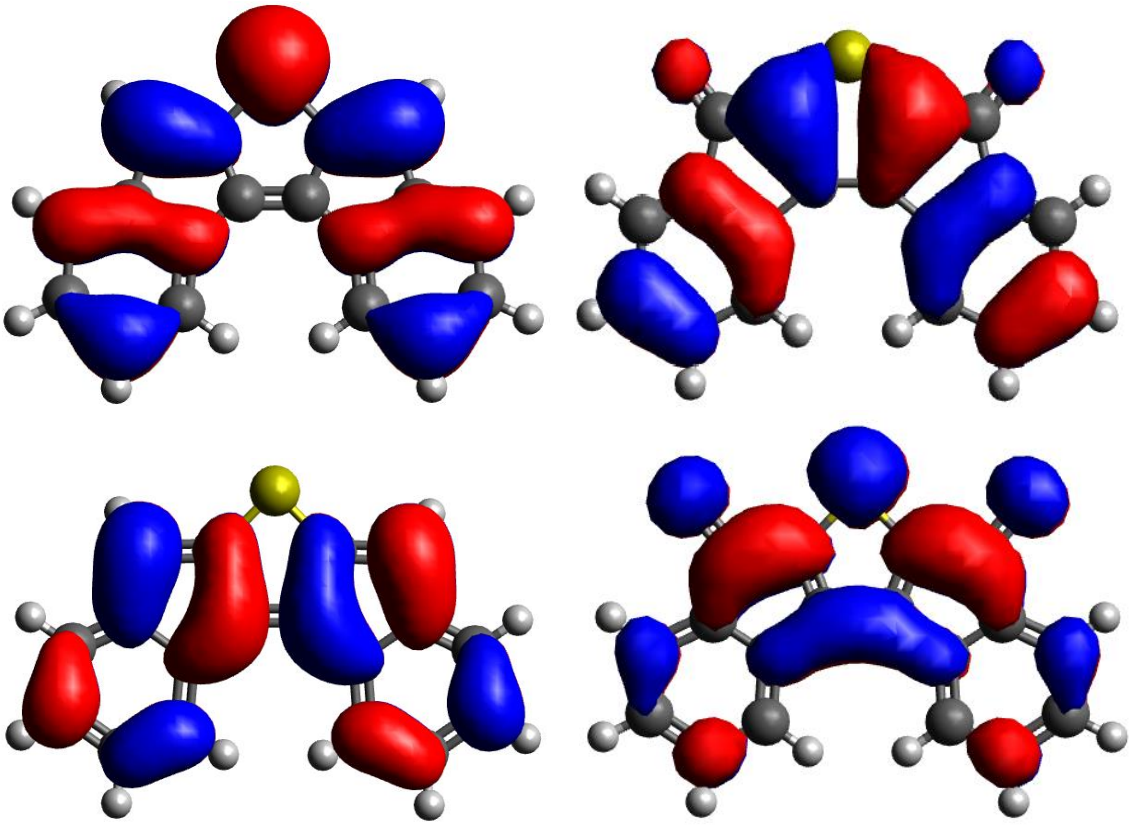

Figure 8. HOMO (top) and LUMO (bottom) maps of **2** (left) and **6** (right).[9]

Of particular interest are the results of the cyclic voltammetry (Figure 9, Table 1). Like previous derivatives of **1**, derivatives of **2** show two fully-reversible reductions. DIT **2b** also showed a reversible oxidation, something not seen in the corresponding derivative of **1**. The synthesized derivatives of **2** show LUMO energies of less than -3.8 eV, within the range believed to confer operational stability in air to organic semi-conductors.[12] In contrast to **2a** and **b**, **6** could not be oxidized though it did show two reversible reductions and a LUMO energy of -3.92 eV.

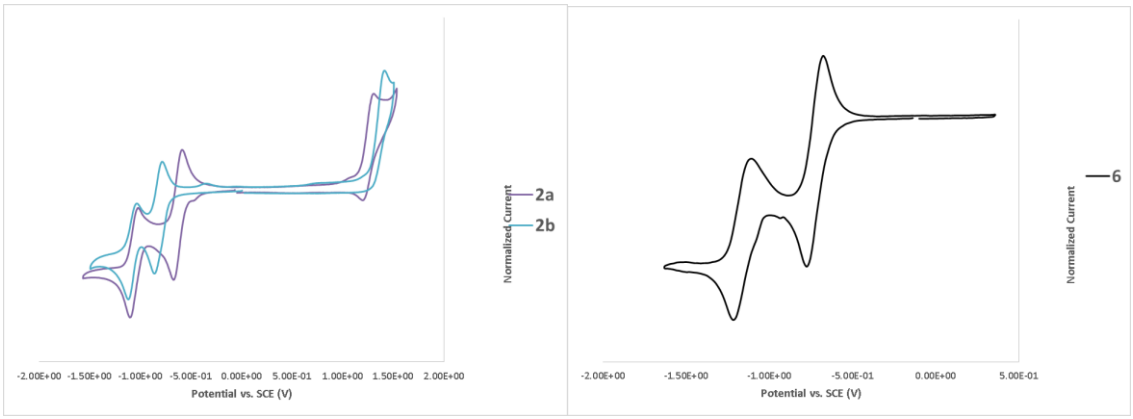

Figure 9. Cyclic voltamograms of **2a**,**b** (left), and **6** (right).

Table 1. Tabulated optoelectronic data for **2a**,**b** and **6**.

	electrochemical						**optical**	
cmpd	E_{red}^1 (V)[a]	E_{red}^2 (V)[a]	E_{ox} (V)[a]	E_{LUMO} (eV)[b]	E_{HOMO} (eV)[b]	E_{gap} (eV)	λ_{max} (nm)	E_{gap} (eV)[c]
2a	-0.800	-1.22	1.13	-3.84	-5.77	1.93	315, 417, 443, 638, 642, 652, 676, 679	1.83
2b	-0.707	-0.976	1.35	-3.93	-5.99	2.06	320, 413, 435, 489, 584, 592, 621, 640, 647, 654, 660	1.88
6	-0.725	-1.16	-[d]	-3.92	-[d]		245, 262, 314, 447[e]	2.76

[a] CV recorded using 1-5 mM of analyte in 0.1 M tetrabutylammonium trifluoromethanesulfonate/CH_2Cl_2 using a scan rate of 50 mV/s. The working electrode was a glassy carbon electrode with a platinum coil counter electrode and silver wire pseudoreference. Values reported as the half-wave potential (vs SCE) using the Fc/Fc^+ couple (0.46 V) as an internal standard; see ref 13. [b] HOMO and LUMO energy levels in eV were approximated using SCE= -4.68 eV vs vacuum; see ref 14. [c] Determined using the wavelength at the maximum absorption of the lowest energy transition from the UV-vis spectrum. [d] Reversible oxidation of **6** was not achieved. [e]Absorption spectrum for **6** can be found in Appendix E.

Conclusion

We have manufactured and begun characterization of a new class of redox amphoteric molecules based on the diindeno[2,1-*b*:1',2'-*d*]thiophene (DIT) molecular

scaffold. In addition, we have developed an alternate synthetic route to the known dione **6** and began characterization of its optical and electronic properties for the first time, showing that it possesses a high electron affinity. Work on these materials and related derivatives is ongoing, with implementation in OFET and OPV devices underway.

Experimental Details

General Comments. ^{1}H and ^{13}C NMR spectra were recorded in $CDCl_3$ using either a Varian Mercury 300 MHz (^{1}H: 300.09 MHz) or Bruker Avance III HD 600 MHz (^{1}H: 600.02 MHz, ^{13}C: 150.89 MHz) NMR spectrometer with Prodigy multinuclear broadband cryoprobe. Chemical shifts (δ) are expressed in ppm relative to the residual $CHCl_3$ (^{1}H: 7.27 ppm, ^{13}C: 77.23 ppm. UV-Vis spectra were recorded on an HP 8453 UV-Vis spectrometer. High resolution mass spectra were recorded on a JEOL MS-Route mass spectrometer. Melting points were determined on a Meltemp II apparatus and are uncorrected. THF was distilled from potassium under N_2. Unless otherwise stated, all solvents and reagents were purchased and used as received.

5,8-Bis(triisopropylsilylethynyl)diindeno[2,1-*b*:1',2'-*d*]thiophene (2a). Triisopropylsilylacetylene (0.66 mL, 2.8 mmol) in THF (50 mL) was degassed with Ar for 10 min, and then cooled to 0 °C. n-BuLi (1.04 mL, 2.60 mmol, 2.5 M) was added and the mixture stirred at 0 °C for 20 min. In a separate flask, dione **6** (0.15 g, 0.52 mmol) in THF (50 mL) was degassed with Ar for 10 min and then cooled to 0 °C. The lithiate solution was cannulated into the cold dione solution and the reaction warmed to rt over 2 h. The reaction was quenched by addition of aq. 10% HCl soln (30 mL) and extracted with Et_2O. The organic layer was dried over $MgSO_4$, filtered, and evaporated to dryness. The crude diol was then re-dissolved in dry toluene (15 mL), degassed with Ar for 10

min, $SnCl_2$ (0.50 g, 2.6 mmol) was added, and the mixture stirred overnight at room temperature. The resultant green solution was filtered and the filtrate evaporated to dryness. Trituration with MeOH gave **2a** (0.15 g, 52 %) as a dark green solid. Mp xxx-xxx °C; ^{1}H NMR (600 MHz, $CDCl_3$) δ 7.55 (d, J = 7.3 Hz, 2H), 7.22 (t, J = 7.5 Hz, 2H), 7.16 (d, J = 7.3 Hz, 2H), 7.09 (t, J = 7.4 Hz, 2H), 1.19 (br s, 42H); ^{13}C NMR (151 MHz, $CDCl_3$) δ 153.78, 148.91, 143.96, 130.79, 130.21, 125.79, 124.38, 120.70, 116.33, 105.94, 99.69, 18.73, 11.27; UV-Vis (CH_2Cl_2) λ_{max} (ε) 315 (x), 417 (x), 443 (x), 638 (x), 679 (x) nm; HRMS (ESI) for C40H50SSi2 [M+]: calcd 618.3172, found x.

5,7-Bis(3,5-bis(trifluoromethyl)diindeno[2,1-*b*:1',2'-*d*]thiophene (2b). A solution of 1-bromo-3,5-bis(trifluoromethyl)benzene (1.4 g, 4.7 mmol) in THF (50 mL) was degassed with Ar for 10 min and then cooled to –78 °C. n-BuLi (1.7 mL, 4.3 mmol, 2.5 M) was added and the mixture stirred at –78 °C for 20 min. In a separate flask, dione **6** (0.25 g, 0.87 mmol) in THF (50 mL) was degassed with Ar for 10 min and also cooled to –78 °C. The lithiate solution was cannulated into the cold dione solution, and the reaction warmed to rt over 2 h. The reaction was quenched by addition of aq. 10% HCl soln (30 mL) and extracted with Et_2O. The organic layer was dried over $MgSO_4$, filtered, and evaporated to dryness. The crude diol was then redissolved in toluene (40 mL) and degassed with Ar for 10 min. $SnCl_2$ (0.82 g, 4.3 mmol) and trifluoroacetic acid (~ 0.1 mL) were added, and the reaction stirred overnight at 50 °C. The solution was filtered and the filtrate subsequently evaporated to dryness. Trituration with MeOH gave **2b** (0.18 g, 30%) as a dark green solid. Mp xx-xx °C; ^{1}H NMR (600 MHz, $CDCl_3$) δ 8.05 (s, 4H), 7.90 (s, 2H), 7.77 (d, J = 7.2 Hz, 2H), 7.30 (d, J = 7.x? Hz, 2H), 7.27 (d, J = 7.6 Hz, 2H), 7.21 (t, J = 7.1 Hz, 2H); ^{13}C NMR (151 MHz, $CDCl_3$) δ 149.10, 147.45, 143.80, 135.66, 132.60 (dd,

J = 67.1, 33.5 Hz), 131.99, 131.75, 130.35, 127.66 (m), 126.22, 125.82, 124.04, 122.24, 121.74 (dd, J = 7.8, 4.3 Hz), 120.35; UV-Vis (CH_2Cl_2) λ_{max} (ε) 320 (x), 413 (x), 489 (x), 621 (x), 660 (x) nm; HRMS (ESI) for C36H16F12S [M+]: calcd 686.0625, found x.

5,7-Diindeno[2,1-*b*:1',2'-*d*]thiophenedione (6). To a stirbar-equipped round bottom flask containing 3,4-dibromothiophene (5.0 g, 21 mmol), ethyl benzeneboronic acid-2-carboxylate (10.0 g, 51.7 mmol), and $PdCl_2(PPh_3)_2$ (1.5 g, 10 mol%) was added approx. 100 mL anhydrous DMF. The flask was evacuated and backfilled 3 times with argon and then K_3PO_4 (17.5 g, 83 mmol) was added and the flask was again evacuated and backfilled with agron 3 times. The reaction was heated to 110 °C and stirred overnight. The reaction mixture was subjected to aqueous workup and multiple extractions with DCM. The organic layers were combined and the solvent removed by rotovap. The resultant crude product was added to a 100 mL round-bottom flask and 40 mL of methanol and 40 mL of 4M KOH (aq) was added. The reaction mixture was heated to reflux and stirred overnight. The reaction mixture was filtered over celite and stripped by rotovap to approx. half the original volume. Acidification with conc. HCl and collection by vacuum filtration yielded the crude diacid. This was suspended in 120 mL DCM (anh.) in a 250 mL flask and the flask was evacuated and backfilled three times with Ar. The reaction mixture was cooled to 0 °C, and oxalyl chloride (4.25 mL, 50 mmol) was added via syringe. DMF (anh.) (1.93 mL, 25 mmol) was then added via syringe and the reaction mixture was stirred at 0 °C for one hour and then allowed to warm to room temperature overnight. The solvent was then stripped via rotovap, more DCM (anh.) (120mL) was added, $AlCl_3$ (7.8g, 58 mmol) was added, and the flask was evacuated and backfilled with Ar three times. The reaction was heated to 45 °C in a sandbath and stirred

overnight. The reaction mixture was then poured over approx. 100mL con HCl on ice. The crude orange solid was collected by vacuum filtration and washed with $NaHCO_3$ and water. Recrystallization from chloroform gave **6** (2.1 g, 55% over 4 steps) as orange needles. Mp xx-xx °C; UV-Vis (CH_2Cl_2) λ_{max} (ε) 262 (x), 314 (x), 447 (x) nm. HRMS (ESI) for C18H8O2S [M+]: calcd 288.0245, found x.

Bridge to Chapter VI

Chapter VI serves to show a more complete picture of the relationship between that indeno[2,1-*c*]fluorene and diindeno[2,1-*b*:1',2'-*d*]thiophene scaffolds. Additionally, benzo[*a*]indeno[2,1-*c*]fluorene derivatives are introduced for the first time. This new derivatization of the indenofluorene scaffold led to the first example of fully-conjugated indenoflourenes that do not possess a quinoidal core. To our knowledge, this chapter also demonstrates for the first time optoelectronic characterization of the respective indenofluorenedione precursors that we use to then synthesize the fully-conjugated systems.

CHAPTER VI

DERIVATIVES OF INDENO[2,1-*c*]FLUORENE AND ITS ISOELECTRONIC CONGENER DIINDENO[2,1-*b*:1',2'-*d*]THIOPHENE: ELECTRON-ACCEPTING AND AMPHOTERIC REDOX SCAFFOLDS FOR CHARGE-TRANSPORT IN ORGANIC ELECTRONICS

This chapter was co-authored with Parker E. Deal, who provided synthetic support under my supervision, Bradley D. Rose, who performed the diradical computational experiments, Chris L. Vonnegut, who performed the Cyclic Voltammetry, and Michael Haley, who provided editorial and material support. This work is being prepared for publication in the *Journal of Organic Chemistry*.

Introduction

With a drive to develop new energy sources and to make devices that we utilize every day more energy-efficient, there has been a massive research effort focused on developing organic electronic materials for niche uses in these areas.[1] From OPVs to flexible display technologies that use a fraction of the energy of those in ubiquitous use today, organic electronic devices are begininning to move from the research laboratory to commercial application.[2]

To make this possible, one of the directives of this research has been to develop new organic semiconducting materials in the hope of discovering compounds that are solution-processible, possess robust operational stability to common environmental contaminants/doping, are relatively cheap and easy to manufacture, are easily functionalized/tuned in the final synthetic step(s), etc.[2,3] Of particular interest in the search for organic electronic materials are the cyclopenta-fused polyaromatic hydrocarb-

ons (CP-PAHs, e.g., fullerenes,[4] buckybowls[5]).[6] The five-membered rings within these compounds are theorized to impart a higher electron affinity because of the driving force to aromatize to cyclopentadienyl anions by accepting an electron.

Our work with this class of molecules has focused mainly on a subset of the fully conjugated indenofluorene (IF) system (Figure 1),[7] a family of cyclopenta-fused molecules comprised of five structural isomers (e.g., **1** - **5**, Figure 1). Until very recently, nearly all reported studies have focused on derivatives of **2** (at least 25 examples)[8,9] and **3** (2 examples).[10] Importantly from an applied standpoint, our lab and others have shown that the [1,2-*b*]IF scaffold can serve as an electron-accepting or ambipolar material for organic electronics, with derivatives of **2** showing ambipolar transport in both a single crystal OFET[8c] and thin-film OFETs.[9c] Of the remaining regioisomers, formation of IFs **1** and **4** will dearomatize an internal and a peripheral benzene to achieve closed-shell structures, likely making these molecules markedly less stable than **5**. The Tobe group recently showed this to indeed be the case with their synthesis and character-ization of a derivative of **4** showing an open-shell ground state.[11] Like **2**, formation of **5** requires dearomatization of only one internal benzene ring, and the immediate IF-dione precursor is accessible in multigram quantities in four steps from inexpensive, commercially available precursors.[12] We recently reported the synthesis and charcterization of three derivatives of this fully-conjugated indeno[2,1-*c*]fluorene scaffold (TIF, **5**).[13]

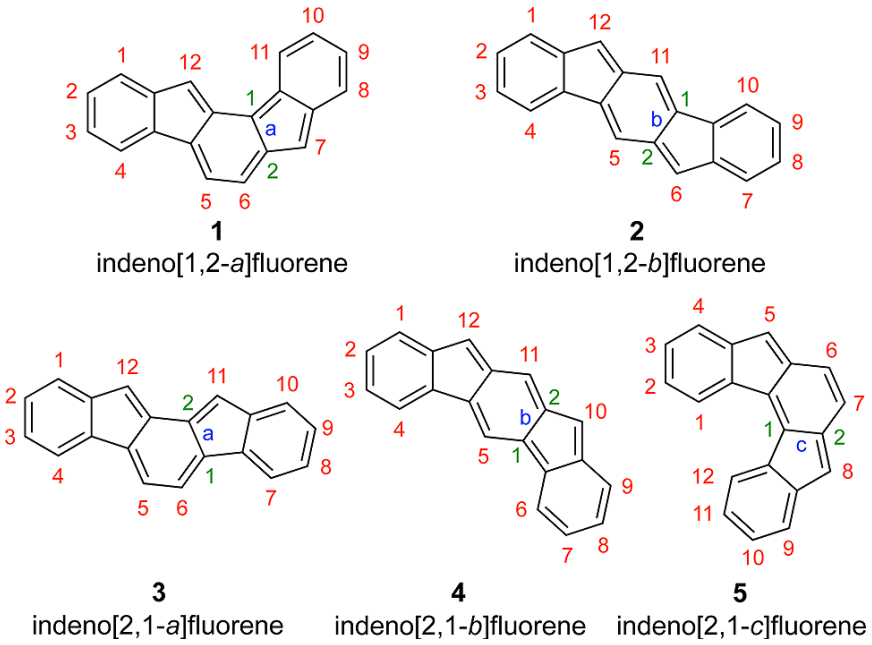

Figure 1. The five major indenofluorene regioisomers.

Our recent work has also examined a related molecular architecture, diindeno[2,1-*b*:1',2'-*d*]thiophene (DIT, **7**), that is isoelectronic with **5** (see Chapter V of this dissertation). It was seen that these compounds have very similar absorption and redox profiles to those of **5**, with the major difference being seen in the molecular topology.

In this work we will review this previous research as well as expand upon it, disclosing new TIF derivatives based on benzo[a]indeno[2,1-c]fluorene (BTIF, **6**), and reporting for the first time the optoelectronic properties of the TIF dione (**8**) and BTIF dione (**9**), with their comparison to the previously reported DIT dione **10**.[13,14]

Results and Discussion

Dione-functionalized TIF, BTIF and DIT. The diones **8**, **9**, and **10** have been known for years.[12-14] Until recently when we reported results for **10**, however, no optoelectronic data for these compounds had been reported in the literature (see Chapter V of this dissertation). Manufacture of these molecules is easily accomplished via multiple

synthetic routes, providing facile derivatization opportunities and enabling route selection by choice of the most inexpen-sive substrates to reach the desired functionalized target compound. Utilization of an aldol condensation/Diels-Alder sequence or cross-coupling reactions followed by ring closure via Friedel Crafts conditions are the routes typically employed (Schemes 1 and 2).

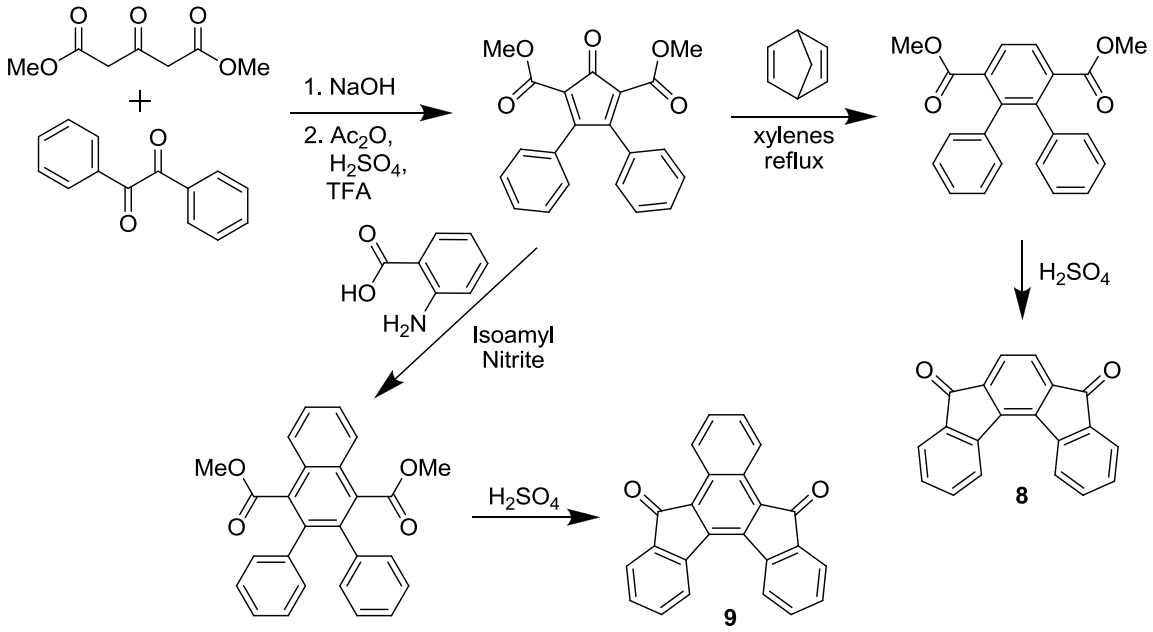

Scheme 1. Synthesis of diones **8** and **9**.[12, 14]

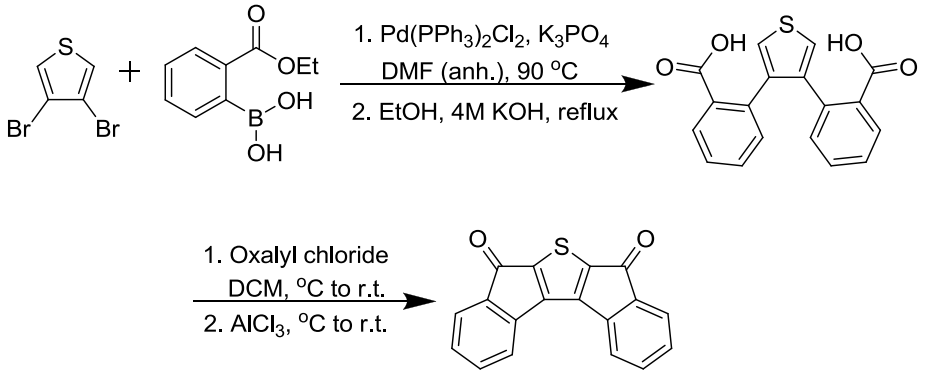

Scheme 2. Synthesis of DIT dione **10** (see Chapter V of this dissertation).

The absorption spectra of the three diones are displayed in Figure 2. All three diones show nearly identical absorption energies just beyond 300 nm (λ_{max} for: **8** – 311nm; **9** – 315 nm; **10** – 314 nm). There is also a remarkable similarity in the spectra of **9** and **10** in the 400 nm to 500 nm range, while the spectrum of TIF dione **8** is relatively featureless in this region.

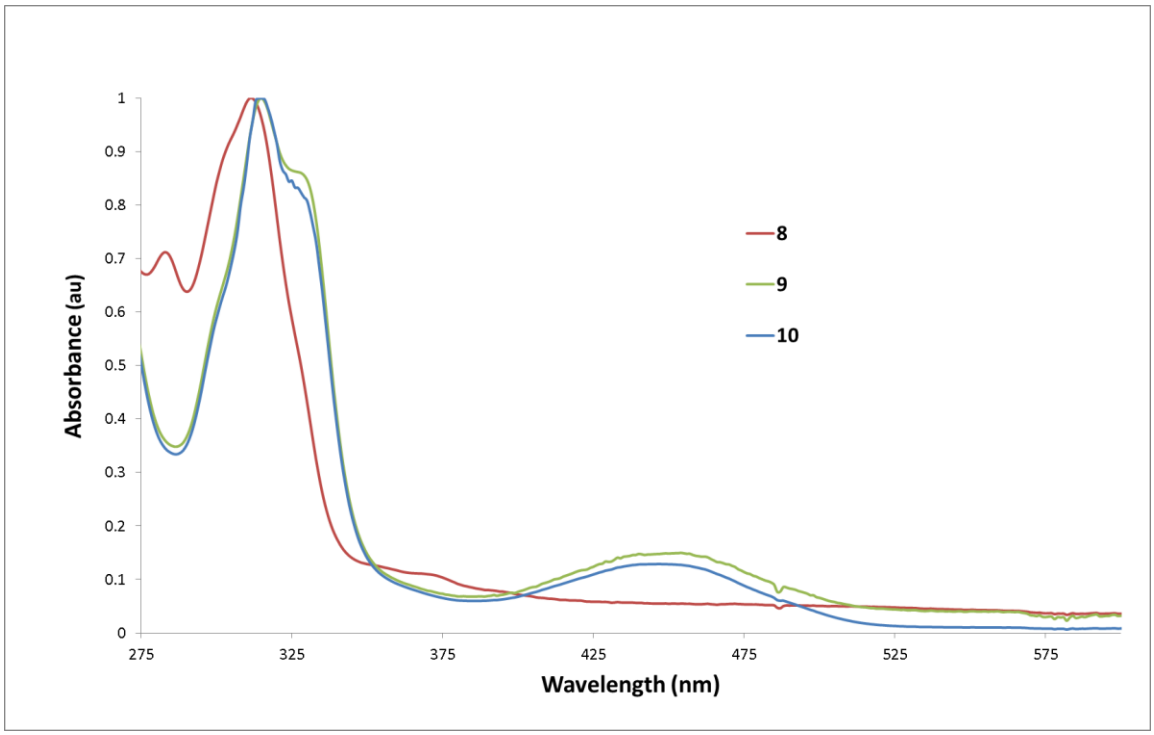

Figure 2. Overlaid UV/Vis spectra of diones **8**, **9**, and **10**.

Single crystals of **10** were grown via solvent exchange from chloroform with cyclohexane countersolvent and the structures determined using x-ray diffraction (Figure 3). The crystal structure shows the molecule alternating between two different orientations within each of the 1-D columns, with molecules alternating between two different orientations within each stack. The packing shows a C-C close contact distance of 3.39 Å, and a C-S close contact distance of 3.41 Å, both less than the Van der Waals radii of the respe]'ctive atoms. The molecules are bowed in the center, though only

slightly. Interestingly, oxygen atoms in a molecule in one stack show a strong association with the bay hydrogens in the molecule in the adjacent stack due to a significant dipole along the short central axis of the molecule.

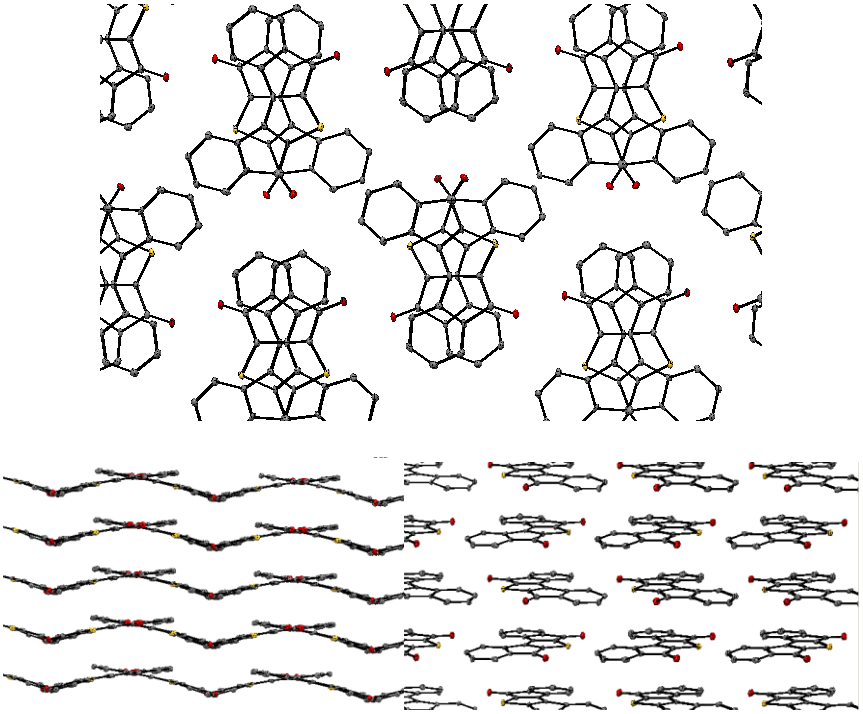

Figure 3. Top-down (top) and side-on (bottom) views of the packing within the crystal structure of **10**. Ellipsoids drawn at 30% probablity and hydrogens omitted for clarity.

Results of the cyclic voltammetry performed on **8** – **10** show that all three diones accept two electrons and show no oxidation under the experimental conditions (Figure 4, Table 1; voltammogram currents are normalized to the E_{anodic}^{1} peak). While **8** is just on the threshold of the -3.80 eV – 4.60 eV energy range for the LUMO believed to be where compounds show air stablility in devices,[15] clearly both **9** and **10** have LUMO en-ergies well within that range, having LUMO energies of -4.01eV and -3.92 eV, respect-ively.

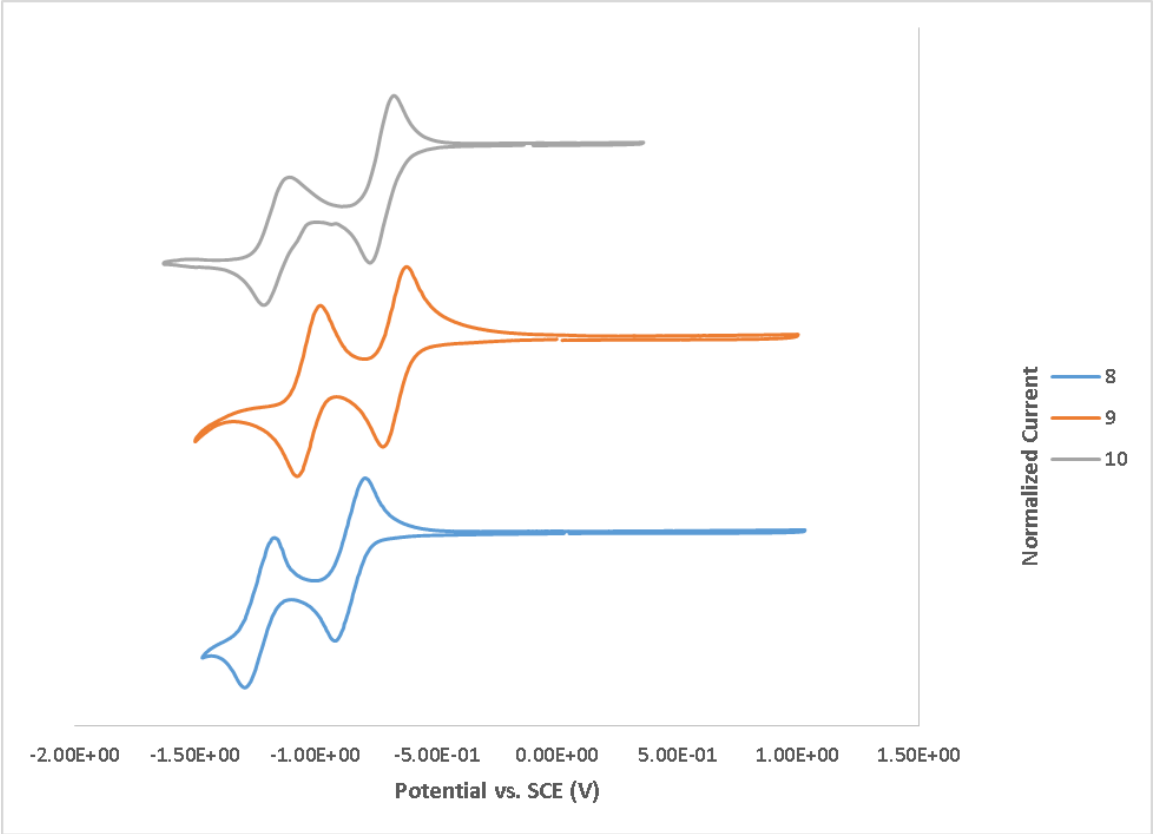

Figure 4. Cyclic voltammograms of diones **8**, **9**, and **10**.

Fully-reduced TIFs, BTIFs, and DITs. Realization of target molecules **5a-c** occurs by nucleophilic attack on dione **8** with either an aryl or ethynyl lithiate and subsequent reductive dearomatization with $SnCl_2$ (Scheme 3), producing the desired compounds in moderate yields after purification. **6a,b** and **7a**,**b** are synthesized in the same fashion from diones **9** and **10** respectively. As previously discussed, the [1,2-*b*]IFs and [2,1-*a*]IFs, which are blue/purple in solution, while the [2,1-*c*]IFs **5a-c**, BIFs **6a**,**b** and DITs **7a**,**b** are green in solution and green/black in the solid state (see Ref. 13 and Chapter V of this dissertation).

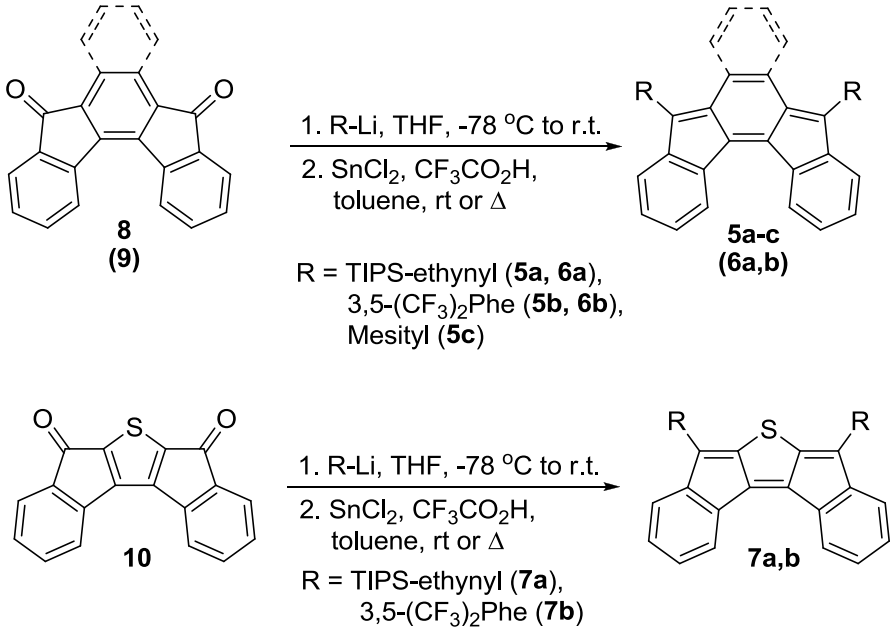

Scheme 3. Synthesis of [2,1-*c*]IFs **5a-c**, DITs **6a**,**b** and BIFs **7a**,**b**.

The absorption spectra of **5a-c**, **7a**, **b**, and **6a**,**b** (Figure 5) display strong absorbances in the higher energy range, with a broad, low energy absorbance that extends into the near-IR region. Interestingly, these broad low-energy bands (550-800 nm) are similarly observed in the spectrum of 11,12-dimesityl[2,1-*a*]IF (**3a**),[10b] which, like the TIFs, possesses the *as*-indacene core. This is in contrast to the spectra of [1,2-*b*]IFs, which are based on the *sym*-indacene skeleton, as the lowest energy peak of the derivatives of **2** to date has been less than 615 nm.[8,9] Similar to other fully conjugated TIFs, **5a-c**, BTIFs **6a**,**b**, and DITs **7a**,**b** are nonemissive.

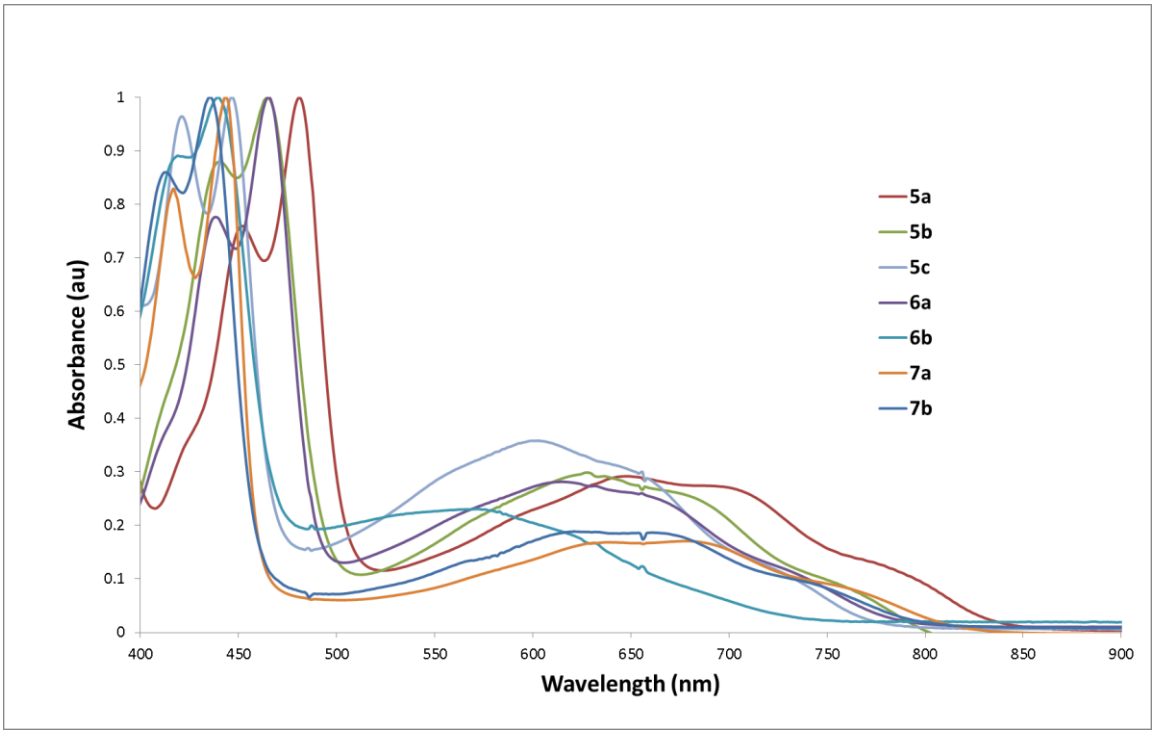

Figure 5. Overlaid UV/Vis spectra of TIFs **5a-c**, BTIFs **10a**,**b** and DITs **6a**,**b**.

Single crystals of **5c** suitable for X-ray diffraction were obtained via slow crystallization from toluene (Figures 6 and 7). The resultant determined structure (Figure 8) shows that the molecule packs in two symmetrically independent arrangements, with each molecule bent slightly out of plane. The two independent molecules possess helicene-like axial chirality, but the barrier to inversion is extremely small, calculated to be 0.02 kcal mol^{-1}.[16,17] Dihedral angles between the average planes of the central six-membered ring, the bridging five-membered ring, and the terminal six-membered ring of the *P*-isomer of **5c** are 2.26(5), 4.32(5) and 1.98(5), 2.40(6), respectively; the corresponding angles in the *M*-isomer are 4.78(7), 6.63(6) and 4.67(8), 3.66(8).

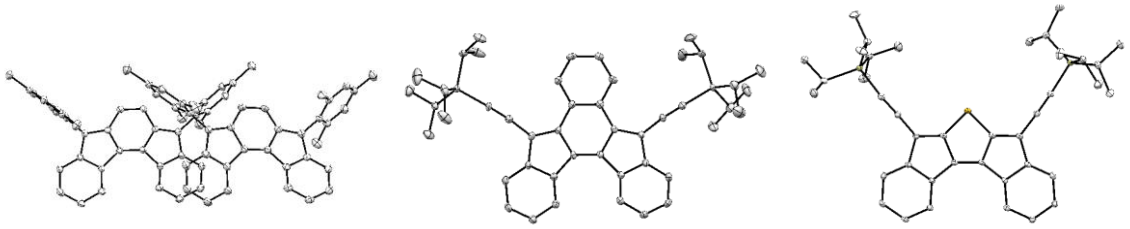

Figure 6. Crystal structure of **5c** (two crystallographically independent conformers in unit cell), **6a**, and **7a**. Ellipsoids drawn at the 30% probability level.

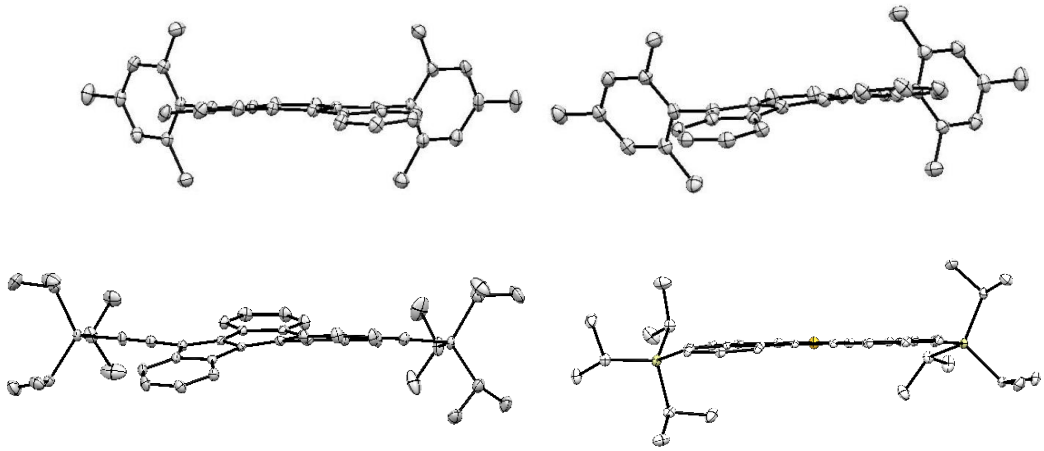

Figure 7. Side-on view of the bay regions of *P*- and *M*- helicene-like conformers (top left and right, respectively) found within the single crystal of **5c**, **6a** (bottom left), and **7a** (bottom right).[13,14] Ellipsoids drawn at the 30% probability level and hydrogens omitted for clarity.

A similar distortion from planarity for **6a** is easily seen in Figure 7. More difficult to see is the very slight non-planarity of **7a**. The lesser deviation has a drastic impact on the packing, with far better overlap seen in the packing of DIT **7a** compared to the TIF and BIF structures. Individual molecules within the crystal lattice of **5c** show no significant cofacial overlap, though this may also be due to the bulkier mesityl substituents, and a close C-C contact distance of 3.47 Å, while those of **6a** show some cofacial overlap and close contacts of 3.42 Å. The more appreciable cofacial overlap of

molecules of **7a** is seen in C-C close contact distances of 3.34 Å within each dimer and 3.38 Å between adjacent dimers which then arrange in 1-D chains.

As we have previously noted, both the [2,1-*a*]IFs and TIFs contain the *as*-indacene core, but the [2,1-*a*]IF possesses the more reactive *o*-quinodimethane motif. The DITs can, analogous to the TIFs, be considered to be *p*-quinoidal in character. Interestingly, the BIF scaffold can be considered to be the first non-quinoidal IF synthesized, as one of the previously-quinoidal bonds is isolated within a fully aromatic benzene ring. This is illustrated in the elongated bond length of 1.42 Å vs. a 1.36 Å bond length in the analogous bonds in the core structures of the TIF crystal and that of the [1,2-*b*]IF. The remaining non-benzenoid double bond has a bond length of 1.36 Å, similar to that seen in the analogous bond of the TIF core.

Cyclic voltammograms of compounds **5**-**7** are arrayed below (Figure 8; voltammogram currents are normalized to the E_{anodic}^{1} peak) and results compiled in Table 1. Like many of the other IFs, these compounds reversibly accept up to two electrons and many of the deriviatives are also oxidizable, giving the possibility for ambipolar transport in organic electronic devices.

Table 2. Summary of optical and electrochemical data of compounds **5** - **10**.

	electrochemical						optical	
cmpd	E_{red}^1 (V)[a]	E_{red}^2 (V)[a]	E_{ox} (V)[a]	E_{LUMO} (eV)[b]	E_{HOMO} (eV)[b]	E_{gap} (eV)	λ_{max} (nm)	E_{gap} (eV)[c]
5a	-0.661	-1.11	1.07	-3.98	-5.71	1.73	360, 380, 451, 480, 647	1.48
5b	-0.707	-1.02	-[d]	-3.93	-[d]	-[d]	348, 365, 441, 465, 627	1.54
5c	-1.05	-1.51	1.02	-3.59	-5.66	2.08	345, 363, 421, 447, 603	1.60
6a	-0.629	-1.06	1.25	-4.01	-5.89	1.87	347, 364, 438, 465, 615	1.89
6b	-0.822	-1.08	-[d]	-3.82	-[d]	-[d]	328, 419, 440, 571	2.12
7a	-0.800	-1.22	1.13	-3.84	-5.77	1.93	315, 417, 443, 638, 679	1.83
7b	-0.707	-0.976	1.35	-3.93	-5.99	2.06	320, 413, 435, 489, 621, 660	1.88
8	-0.856	-1.23	-[d]	-3.78	-[d]	-[d]	283, 311, 429	
9	-0.673	-1.03	-[d]	-3.97	-[d]	-[d]	261, 315, 455	
10	-0.725	-1.163	-[d]	-3.92	-[d]	-[d]	262, 314, 447	2.76

[a] CV recorded using 1-5 mM of analyte in 0.1 M tetrabutylammonium trifluoromethane-sulfonate/CH_2Cl_2 using a scan rate of 50 mV/s. The working electrode was a glassy carbon electrode with a platinum coil counter electrode and silver wire pseudoreference. Values reported as the half-wave potential (vs SCE) using the Fc/Fc^+ couple (0.46 V) as an internal standard; see ref 18. [b] Determined by $E_{LUMO} = -(4.44 + E_{red}^1)$; see ref 19. [c] Determined using the wavelength at the maximum absorption of the lowest energy transition from the UV vis spectrum. [d] Reversible oxidation of these compounds was not achieved.

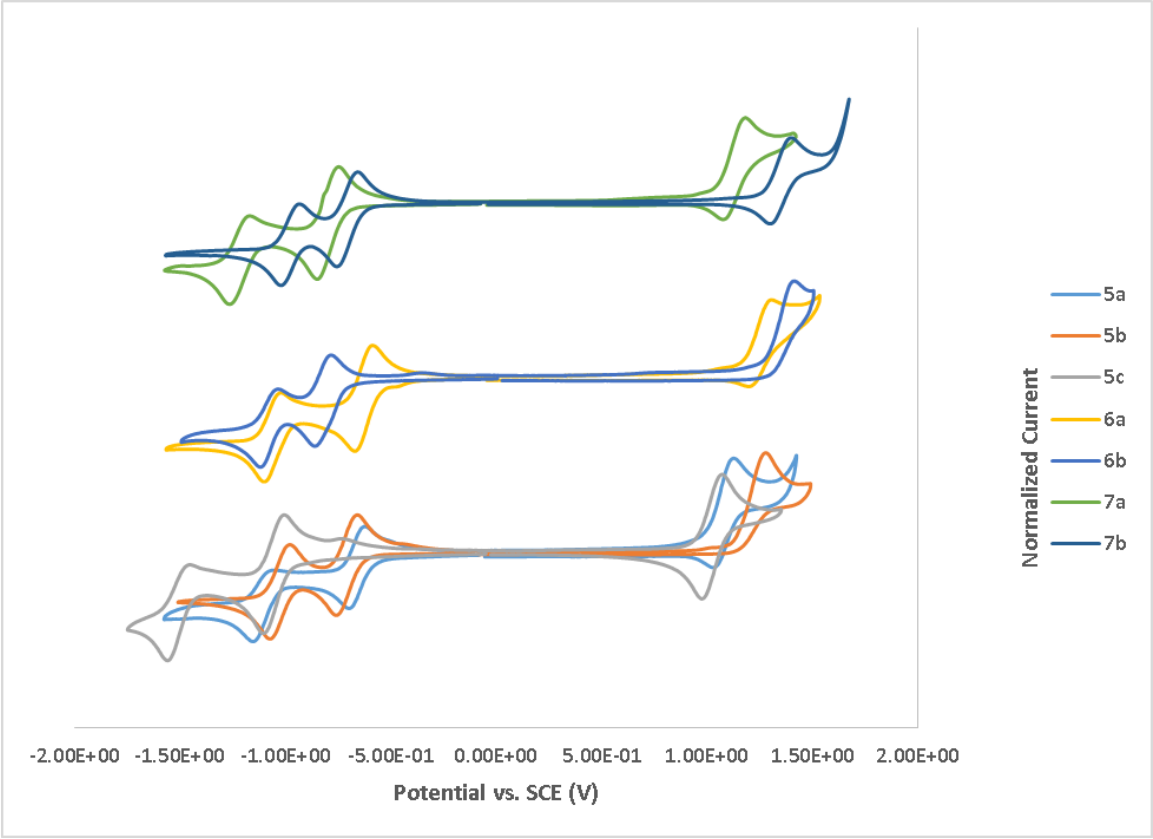

Figure 8. Cyclic voltammograms of **5a-c**, **6a**,**b** and **7a**,**b**.

Conclusion

Expansion of the fully-reduced indenofluorene family continues and we have clearly shown that our synthetic methodology can be expanded to include isoelectronic heteroatomic derivatives. The interesting properties of these compounds, e.g., long wavelength absorption, non-emissiveness, low-lying LUMO energies, etc., make them fertile ground for study, both from a theoretical and an applied standpoint. Investigation of these materials in OPV and OFET devices is ongoing and derivatization to further alter the morphology, crystal packing, and optoelectronic characteristics of these compounds continues.

Experimental Details

General Comments. ^{1}H and ^{13}C NMR spectra were recorded in $CDCl_3$ using either a Varian Mercury 300 MHz (^{1}H: 300.09 MHz), Varian Inova 500 MHz (^{1}H: 500.11 MHz, ^{13}C: 125.75 MHz) or Bruker Avance III HD 600 MHz (^{1}H: 600.02 MHz, ^{13}C: 150.89 MHz) NMR spectrometer with Prodigy multinuclear broadband cryoprobe. Chemical shifts (δ) are expressed in ppm relative to the residual $CHCl_3$ (^{1}H: 7.27 ppm, ^{13}C: 77.23 ppm. UV-Vis spectra were recorded on an HP 8453 UV-Vis spectrometer. High resolution mass spectra were recorded on a JEOL MS-Route mass spectrometer. Melting points were determined on a Meltemp II apparatus and are uncorrected. THF was distilled from potassium under N_2. Unless otherwise stated, all solvents and reagents were purchased and used as received. Diones **8** and **9** were synthesized according to previously described procedures.[12,14]

5,8-Bis(triisopropylsilylethynyl)indeno[2,1-c]fluorene (5a). Triisopropylsilyl)acetylene (0.67 mL, 2.87 mmol) in THF (10 mL) was degassed with Ar for 10 min, and then cooled to 0 °C. n-BuLi (1.06 mL, 2.66 mmol, 2.5 M) was added and the mixture stirred at 0 °C for 20 min. In a separate flask, dione **8** (0.15 g, 0.53 mmol) in THF (15 mL) was degassed with Ar for 10 min and then cooled to 0 °C. The lithiate solution was cannulated into the cold dione solution and the reaction warmed to rt over 2 h. The reaction was quenched by addition of aq. 10% HCl soln (30 mL) and extracted with Et_2O. The organic layer was dried over $MgSO_4$, filtered, and evaporated to dryness. The crude diol was then re-dissolved in dry toluene (15 mL), degassed with Ar for 10 min, $SnCl_2$ (0.5 g, 2.64 mmol) was added, and the mixture stirred overnight at room temperature. The resultant green solution was filtered and the filtrate evaporated to

dryness. Recrystallization from MeOH gave **5a** (0.15 g, 46%) as a dark green solid. Mp 152-153 °C; ^{1}H NMR (600 MHz, $CDCl_3$) δ 7.93 (d, J = 7.4 Hz, 2H), 7.28 (d, J = 7.3 Hz, 2H), 7.21 (t, J = 7.3 Hz, 2H), 7.16 (t, J = 7.4 Hz, 2H), 6.87 (s, 2H), 1.21 (br s, 42H); ^{13}C NMR (151 MHz, $CDCl_3$) δ 144.71, 142.70, 139.06, 135.77, 129.56, 127.50, 125.28, 125.15, 122.12, 121.65, 109.46, 101.67, 18.78, 11.34; UV-Vis (CH2Cl2) λmax (ε) 360 (21,200), 380 (26,800), 451 S4 (14,400), 480 (19,000), 647 (5,500) nm; HRMS (ESI) for C42H52Si2 [M+]: calcd 613.3686, found 613.3666.

5,8-Bis(3,5-bis(trifluoromethyl)phenyl)indeno[2,1-c]fluorene (5b). A solution of 1-bromo-3,5-bis(trifluoromethyl)benzene (1.4 g, 4.79 mmol) in THF (10 mL) was degassed with Ar for 10 min and then cooled to –78 °C. n-BuLi (1.77 mL, 4.42 mmol, 2.5 M) was added and the mixture stirred at –78 °C for 20 min. In a separate flask, dione **8** (0.25 g, 0.89 mmol) in THF (30 mL) was degassed with Ar for 10 min and also cooled to –78 °C. The lithiate solution was cannulated into the cold dione solution, and the reaction warmed to rt over 2 h. The reaction was quenched by addition of aq. 10% HCl soln (30 mL) and extracted with Et_2O. The organic layer was dried over $MgSO_4$, filtered, and evaporated to dryness. The crude diol was then re-dissolved in toluene (40 mL) and degassed with Ar for 10 min. $SnCl_2$ (0.5 g, 2.64 mmol) and trifluoroacetic acid (~ 0.1 mL) were added, and the reaction stirred overnight at 50 °C. The solution was filtered and the filtrate subsequently evaporated to dryness. Recrystallization from Ar-saturated MeOH gave **5b** (0.23 g, 39%) as a dark green solid. Mp 240 °C (dec); ^{1}H NMR (600 MHz, $CDCl_3$) δ 8.14 (d, J = 7.0 Hz, 2H), 7.99 (s, 4H), 7.95 (s, 2H), 7.25 (td, J = 7.5, 1.2 Hz, 2H), 7.22 (td, J = 7.5, 1.1 Hz, 2H), 7.14 (d, J = 7.0 Hz, 2H), 6.64 (s, 2H); ^{13}C NMR (151 MHz, $CDCl_3$) δ 144.31, 140.16, 139.96, 136.58, 136.21, 135.82, 132.30 (q, J = 33.6

Hz), 129.78, 129.14 (d, J = 3.6 Hz), 127.83, 126.17, 123.19 (q, J = 273 Hz), 121.99 (sept, J = 3.1 Hz), 121.66, 121.42; UV-Vis (CH_2Cl_2) λ_{max} (ε) 348 (30,400), 365 (29,000), 441 (14,400), 465 (16,400), 627 (4,900) nm; HRMS (ESI) for C36H17F12 [M+]: calcd 677.1130, found 677.1139.

5,8-Dimesitylindeno[2,1-c]fluorene (5c). A solution of bromomesitylene (0.76 g, 3.83 mmol) in THF (10 mL) was degassed with Ar for 10 min and then cooled to –78 °C. n-BuLi(1.42 mL, 3.45 mmol, 2.5 M) was added and the mixture stirred at –78 °C for 20 min. In aseparate flask, dione **8** (0.20 g, 0.71 mmol) in THF (30 mL) was degassed with Ar for 10 min and also cooled to –78 °C. The lithiate solution was cannulated into the cold dione solution, and the reaction warmed to rt over 2 h. The reaction was quenched by addition of aq. 10% HCl soln (30 mL) and extracted with Et_2O. The organic layer was dried over $MgSO_4$, filtered, and evaporated to dryness. The crude diol was then re-dissolved in toluene (40 mL) and degassed with Ar for 10 min. $SnCl_2$ (0.5 g, 2.64 mmol) and trifluoroacetic acid (~ 0.1 mL) were added, and the reaction stirred overnight at 50 °C. The solution was filtered and the filtrate subsequently evaporated to dryness. Flash chromatography (hexanes) and vacuum distillation at 200 °C to remove residual bromomesitylene gave **5c** (0.17 g, 49%) as a green solid. Mp 182-183 °C; ^{1}H NMR (600 MHz, $CDCl_3$) δ 8.11 (d, J = 7.2 Hz, 2H), 7.16 (t, J = 7.1 Hz, 2H), 7.12 (t, J = 7.0 Hz, 2H), 6.98 (s, 2H), 6.71 (d, J = 6.6 Hz, 2H), 6.13 (s, 2H), 2.37 (s, 6H), 2.16 (s, 12H); ^{13}C NMR (151 MHz, $CDCl_3$) δ 146.11, 143.35, 138.83, 137.38, 137.03, 136.33, 136.28, 129.92, 129.09, 128.13, 126.45, 125.38, 121.67, 120.89, 21.15, 20.27; UV-Vis (CH_2Cl_2) λ_{max} (ε) 345 (31,300), 363 (36,100), 421 (13,700), 447 (14,200), 603 (5,100) nm; HRMS (ESI) for C38H33 [M+]: calcd 489.2558, found 489.2567.

5,8-Bis(triisopropylsilylethynyl)benzo[*a*]indeno[2,1-c]fluorene (6a). Triiso-propylsilylacetylene (0.98 mL, 4.35 mmol) in THF (10 mL) was degassed with Ar for 10 min, and then cooled to 0 °C. n-BuLi (1.61 mL, 4.03 mmol, 2.5 M) was added and the mixture stirred at 0 °C for 20 min. In a separate flask, dione **9** (0.25 g, 0.81 mmol) in THF (15 mL) was degassed with Ar for 10 min and then cooled to 0 °C. The lithiate solution was cannulated into the cold dione solution and the reaction warmed to rt over 2 h. The reaction was quenched by addition of aq. 10% HCl soln (30 mL) and extracted with Et_2O. The organic layer was dried over $MgSO_4$, filtered, and evaporated to dryness. The crude diol was then re-dissolved in dry toluene (15 mL), degassed with Ar for 10 min, $SnCl_2$ (0.60 g, 3.2 mmol) was added, and the mixture stirred overnight at room temperature. The resultant green solution was filtered over celite and the filtrate evaporated to dryness. Recrystallization from MeOH gave **6a** (0.32 g, 60%) as a dark green solid. Mp 152-153 °C; ^{1}H NMR (600 MHz, $CDCl_3$) δ 7.93 (d, J = 7.4 Hz, 2H), 7.28 (d, J = 7.3 Hz, 2H), 7.21 (t, J = 7.3 Hz, 2H), 7.16 (t, J = 7.4 Hz, 2H), 6.87 (s, 2H), 1.21 (br s, 42H); ^{13}C NMR (151 MHz, $CDCl_3$) δ 145.50, 139.65, 138.16, 134.56, 129.73, 128.90, 127.85, 126.95, 125.71, 125.02, 122.11, 121.49, 110.74, 103.63, 77.25, 77.04, 76.83, 18.81, 11.47; UV-Vis (CH_2Cl_2) λ_{max} (ε) 360 (21,200), 380 (26,800), 451 S4 (14,400), 480 (19,000), 647 (5,500) nm; HRMS (ESI) for C46H54Si2 [M+]: calcd 662.3764, found x.

5,8-Bis(3,5-bis(trifluoromethyl)phenyl)benzo[*a*]indeno[2,1-c]fluorene (6b). A solution of 1-bromo-3,5-bis(trifluoromethyl)benzene (0.92 g, 3.1 mmol) in THF (10 mL) was degassed with Ar for 10 min and then cooled to –78 °C. n-BuLi (1.2 mL, 3.0mmol, 2.5 M) was added and the mixture stirred at –78 °C for 20 min. In a separate flask, dione

9 (0.20 g, 0.60 mmol) in THF (30 mL) was degassed with Ar for 10 min and also cooled to –78 °C. The lithiate solution was cannulated into the cold dione solution, and the reaction warmed to rt over 2 h. The reaction was quenched by addition of aq. 10% HCl soln (30 mL) and extracted with Et_2O. The organic layer was dried over $MgSO_4$, filtered, and evaporated to dryness. The crude diol was then re-dissolved in toluene (40 mL) and degassed with Ar for 10 min. $SnCl_2$ (0.2 g, 1.1 mmol) and trifluoroacetic acid (~ 0.1 mL) were added, and the reaction stirred overnight at 80 °C. The solution was filtered over celite and the filtrate subsequently evaporated to dryness. Recrystallization from Ar-saturated MeOH gave **6b** (0.098 g, 22%) as a dark green solid. Mp °C (dec); ^{1}H NMR (600 MHz, $CDCl_3$) δ 8.34 (d, *J* = 6.8 Hz, 2H), 8.05 (s, 2H), 8.00 (s, 4H), 7.29 (t, *J* = 9.3 Hz, 4H), 6.99 (d, *J* = 80.5 Hz, 4H), 6.87 (d, *J* = 6.8 Hz, 2H); ^{13}C NMR (126 MHz, $CDCl_3$) δ 146.23, 140.05, 138.73, 138.24, 134.66, 133.93, 132.81 (q, *J* = 33.6 Hz), 129.86, 129.56, 128.83, 127.50, 127.19, 126.09, 125.78, 124.25, 122.20 (m), 122.08, 121.06; UV-Vis (CH_2Cl_2) λ_{max} (ε) 348 (30,400), 365 (29,000), 441 (14,400), 465 (16,400), 627 (4,900) nm; HRMS (ESI) for C40H19F12 [M+]: calcd 726.1217, found x.

5,8-Bis(triisopropylsilylethynyl)diindeno[2,1-*b*:1',2'-*d*]thiophene (7a). Triiso-propylsilylacetylene (0.66 mL, 2.8 mmol) in THF (50 mL) was degassed with Ar for 10 min, and then cooled to 0 °C. n-BuLi (1.04 mL, 2.60 mmol, 2.5 M) was added and the mixture stirred at 0 °C for 20 min. In a separate flask, dione **10** (0.15 g, 0.52 mmol) in THF (50 mL) was degassed with Ar for 10 min and then cooled to 0 °C. The lithiate solution was cannulated into the cold dione solution and the reaction warmed to rt over 2 h. The reaction was quenched by addition of aq. 10% HCl soln (30 mL) and extracted with Et_2O. The organic layer was dried over $MgSO_4$, filtered, and evaporated to dryness.

The crude diol was then re-dissolved in dry toluene (15 mL), degassed with Ar for 10 min, $SnCl_2$ (0.50 g, 2.6 mmol) was added, and the mixture stirred overnight at room temperature. The resultant green solution was filtered and the filtrate evaporated to dryness. Trituration with MeOH gave **7a** (0.15 g, 52 %) as a dark green solid. Mp xxx-xxx °C; ^{1}H NMR (600 MHz, $CDCl_3$) δ 7.55 (d, J = 7.3 Hz, 2H), 7.22 (t, J = 7.5 Hz, 2H), 7.16 (d, J = 7.3 Hz, 2H), 7.09 (t, J = 7.4 Hz, 2H), 1.19 (br s, 42H); ^{13}C NMR (151 MHz, $CDCl_3$) δ 153.78, 148.91, 143.96, 130.79, 130.21, 125.79, 124.38, 120.70, 116.33, 105.94, 99.69, 18.73, 11.27; UV-Vis (CH_2Cl_2) λ_{max} (ε) 315 (x), 417 (x), 443 (x), 638 (x), 679 (x) nm; HRMS (ESI) for C40H50SSi2 [M]: calcd 618.3172, found x.

5,7-Bis(3,5-bis(trifluoromethyl)diindeno[2,1-*b*:1',2'-*d*]thiophene (7b). A solution of 1-bromo-3,5-bis(trifluoromethyl)benzene (1.4 g, 4.7 mmol) in THF (50 mL) was degassed with Ar for 10 min and then cooled to –78 °C. n-BuLi (1.7 mL, 4.3 mmol, 2.5 M) was added and the mixture stirred at –78 °C for 20 min. In a separate flask, dione **10** (0.25 g, 0.87 mmol) in THF (50 mL) was degassed with Ar for 10 min and also cooled to –78 °C. The lithiate solution was cannulated into the cold dione solution, and the reaction warmed to rt over 2 h. The reaction was quenched by addition of aq. 10% HCl soln (30 mL) and extracted with Et_2O. The organic layer was dried over $MgSO_4$, filtered, and evaporated to dryness. The crude diol was then redissolved in toluene (40 mL) and degassed with Ar for 10 min. $SnCl_2$ (0.82 g, 4.3 mmol) and trifluoroacetic acid (~ 0.1 mL) were added, and the reaction stirred overnight at 50 °C. The solution was filtered and the filtrate subsequently evaporated to dryness. Trituration with MeOH gave **7b** (0.18 g, 30%) as a dark green solid. Mp xx-xx °C; ^{1}H NMR (600 MHz, $CDCl_3$) δ 8.05 (s, 4H), 7.90 (s, 2H), 7.77 (d, J = 7.2 Hz, 2H), 7.30 (d, J = 7.x? Hz, 2H), 7.27 (d, J = 7.6 Hz, 2H),

7.21 (t, J = 7.1 Hz, 2H); ^{13}C NMR (151 MHz, $CDCl_3$) δ 149.10, 147.45, 143.80, 135.66, 132.60 (dd, J = 67.1, 33.5 Hz), 131.99, 131.75, 130.35, 127.66 (m), 126.22, 125.82, 124.04, 122.24, 121.74 (dd, J = 7.8, 4.3 Hz), 120.35; UV-Vis (CH_2Cl_2) λ_{max} (ε) 320 (x), 413 (x), 489 (x), 621 (x), 660 (x) nm; HRMS (ESI) for C34H14F12S [M]: calcd 686.0625, found x.

5,7-Diindeno[2,1-*b*:1',2'-*d*]thiophenedione (10). To a stirbar-equipped round bottom flask containing 3,4-dibromothiophene (5.0 g, 21 mmol), ethyl benzeneboronic acid-2-carboxylate (10.0 g, 51.7 mmol), and bis(triphenylphosphino)palladium dichloride (1.5 g, 10 mol%) was added approx. 100 mL anhydrous DMF. The flask was evacuated and backfilled 3 times with argon and then pottassium phosphate (17.5 g, 83 mmol) was added and the flask was again evacuated and backfilled with agron 3 times. The reaction was heated to 110 °C and stirred overnight. The reaction mixture was subjected to aqueous workup and multiple extractions with dichloromethane. The organic layers were combined and the solvent stripped by rotovap. The resultant crude product was added to a 100 mL round-bottom flask and 40 mL of methanol and 40 mL of 4M KOH (aq) was added. The reaction mixture was heated to reflux and stirred overnight. The reaction mixture was filtered over celite and stripped by rotovap to approx. half the original volume. Acidification with conc. HCl and collection by vacuum filtration yielded the crude diacid. This was suspended in 120 mL DCM (anh.) in a 250 mL flask and the flask was evacuated and backfilled three times with Ar. The reaction mixture was cooled to 0 °C, and oxalyl chloride (4.25 mL, 50 mmol) was added via syringe. DMF (anh.) (1.93 mL, 25 mmol) was then added via syringe and the reaction mixture was stirred at 0 °C for one hour and then allowed to warm to room temperature overnight. The solvent was then

stripped via rotovap, more DCM (anh.) (120mL) was added, $AlCl_3$ (7.8g, 58 mmol) was added, and the flask was evacuated and backfilled with Ar three times. The reaction was heated to 45 °C in a sandbath and stirred overnight. The reaction mixture was then poured over approx. 100mL con HCl on ice. The crude orange solid was collected by vacuum filtration and washed with $NaHCO_3$ and water. Recrystallization from chloroform gave **10** (2.1 g, 55% over 4 steps) as orange needles. Mp xx-xx °C; UV-Vis (CH_2Cl_2) λ_{max} (ε) 262 (x), 314 (x), 447 (x) nm. HRMS (ESI) for C18HO2S [M]: calcd 288.0245, found x.

APPENDIX A

EXPERIMENTAL DETAILS FOR CHAPTER II

X-ray crystallography. X-ray diffraction data were collected at 173 K on a Bruker Apex diffractometer using MoKα-radiation (λ=0.71073 Å). Absorption corrections were applied by SADABS.[3] Both structures were determined by direct methods and refined on F^2 by a full-matrix least-squares procedure. All non-H atoms were refined with anisotropic thermal parameters. All H atoms were refined in calculated positions in a rigid group model. All calculations were performed by the Bruker SHELXTL 6.10 package.[4]

Crystal data for 8b. $C_{42}H_{50}F_2Si_2$, M_r = 649.00, 0.23 x 0.19 x 0.03 mm, triclinic, *P*-1 (N 2), *a* = 7.585(3) Å, *b* = 7.910(3) Å, *c* = 16.802(6) Å, α = 86.918(5) °, β = 84.113(6) °, γ = 68.699(5)°,*V* = 934.2(5) $Å^3$, *Z* = 1, ρ_{calcd} = 1.154 g sm^{-1}, μ = 0.132 mm^{-1}, $2\theta_{max}$ = 50.00°, *T* = 173(2) K, 8788 measured reflections, 3278 independent reflections [R_{int}=0.0669], 208 independent refined parameters, *R*1 = 0.0714, *wR*2 = 0.1545 (with $I > 2\sigma(I)$), *R*1 = 0.1165, *wR*2 = 0.1818 (all data), GOF = 1.067, max/min residual electron density +0.539/-0.319 e $Å^{-3}$.

Crystal data for 8h. $C_{58}H_{56}F_{12}Si_2$, M_r = 1037.21, 0.37 x 0.05 x 0.02 mm, triclinic, *P*-1 (N 2), *a* = 9.268(2) Å, *b* = 11.807(3) Å, *c* = 12.531(3) Å, α = 80.996(4) °, β = 79.842(4) °, γ = 76.792(4)°,*V* = 1304.4(5) $Å^3$, *Z* = 1, ρ_{calcd} = 1.320 g sm^{-1}, μ = 0.149 mm^{-1}, $2\theta_{max}$ = 50.00°, *T* = 173(2) K, 12578 measured reflections, 4559 independent reflections [R_{int}=0.0558], 437 independent refined parameters, *R*1 = 0.0591, *wR*2 = 0.1127 (with $I > 2\sigma(I)$), *R*1 = 0.1017, *wR*2 = 0.1311 (all data), GOF = 1.053, max/min residual electron density +0.330/-0.263 e $Å^{-3}$.

Computational Details

Structures were minimized using the B3LYP[5] method and 6-311+G(d,p) basis set. All energies are given in Hartrees.

3

Energy = –769.528249572

Sum of electronic and zero-point Energies = –769.277775

Imaginary Frequencies = 0

Atom	X	Y	Z
H	2.181891	1.289451	0
H	-2.181891	-1.289451	0
H	0.425262	3.55209	0
H	-0.425262	-3.55209	0
H	-4.200917	0.5303	0
H	-2.072045	5.053146	0
H	4.200917	-0.5303	0
H	2.072045	-5.053146	0
H	5.59089	-2.581651	0
H	4.544081	-4.815931	0
H	-4.544081	4.815931	0
H	-5.59089	2.581651	0
C	1.259317	-0.642113	0
C	1.259317	0.717324	0

C	-0.002672	1.401403	0
C	-1.259317	0.642113	0
C	-1.259317	-0.717324	0
C	0.002672	-1.401403	0
C	-0.295674	2.744374	0
C	-1.738469	2.918433	0
C	-2.344143	1.629758	0
C	2.344143	-1.629758	0
C	0.295674	-2.744374	0
C	1.738469	-2.918433	0
C	-3.726144	1.505681	0
C	-2.526665	4.068259	0
C	3.726144	-1.505681	0
C	2.526665	-4.068259	0
C	4.510081	-2.666166	0
C	3.9172	-3.931429	0
C	-3.9172	3.931429	0
C	-4.510081	2.666166	0

5

Energy = -1074.19271902

Sum of electronic and zero-point Energies = -1073.907008

Imaginary Frequencies = 0

Atom	X	Y	Z
H	-4.202974	0.581467	0
H	-2.021759	5.072534	0
H	4.202974	-0.581467	0
H	2.021759	-5.072534	0
H	5.571087	-2.640605	0
H	4.506448	-4.868681	0
H	-4.506448	4.868681	0
H	-5.571087	2.640605	0
H	-1.835944	-5.779304	0
H	-4.438881	-2.603592	0
H	1.835944	5.779304	0
H	4.438881	2.603592	0
C	1.247161	-0.669074	0
C	1.273555	0.709847	0
C	0.008943	1.408401	0
C	-1.247161	0.669074	0
C	-1.273555	-0.709847	0
C	-0.008943	-1.408401	0
C	-0.275981	2.773752	0
C	-1.730487	2.938476	0
C	-2.332621	1.655624	0

C	2.332621	-1.655624	0
C	0.275981	-2.773752	0
C	1.730487	-2.938476	0
C	-3.720537	1.548184	0
C	-2.497613	4.098669	0
C	3.720537	-1.548184	0
C	2.497613	-4.098669	0
C	4.489658	-2.717594	0
C	3.888671	-3.977904	0
C	-3.888671	3.977904	0
C	-4.489658	2.717594	0
C	-2.497613	-1.432916	0
C	-0.590897	-3.88138	0
C	-1.235455	-4.902729	0
C	-3.533923	-2.046689	0
C	2.497613	1.432916	0
C	0.590897	3.88138	0
C	1.235455	4.902729	0
C	3.533923	2.046689	0

6

Energy = -921.859763721

Sum of electronic and zero-point Energies = -921.591516

Imaginary Frequencies = 0

Atom	X	Y	Z
H	-6.578808	0.819374	-0.000001
H	-5.970475	-1.572034	-0.000004
H	-3.595483	-2.277072	0.000004
H	-4.813278	2.569182	0.000009
H	4.813278	-2.569182	-0.000009
H	6.578808	-0.819374	0.000001
H	5.970475	1.572034	0.000004
H	3.595483	2.277072	-0.000004
H	-1.93789	2.992592	0.000025
H	1.93789	-2.992592	-0.000025
H	1.488085	4.930577	-0.000027
H	-1.488085	-4.930577	0.000027
C	-5.533486	0.531895	0.000001
C	-5.188905	-0.820756	-0.000001
C	-3.847086	-1.224814	0.000002
C	-2.854447	-0.252793	0.000011
C	-3.206957	1.12734	0.000013
C	-4.543283	1.518677	0.000006
C	-1.38854	-0.320221	0.000028
C	-0.908264	1.063888	-0.000011

C	-1.986604	1.912195	0.000025
C	-0.508296	-1.372688	0.000044
C	0.908264	-1.063888	0.000011
C	1.38854	0.320221	-0.000028
C	0.508296	1.372688	-0.000044
C	1.986604	-1.912195	-0.000025
C	3.206957	-1.12734	-0.000013
C	2.854447	0.252793	-0.000011
C	4.543283	-1.518677	-0.000006
C	5.533486	-0.531895	-0.000001
C	5.188905	0.820756	0.000001
C	3.847086	1.224814	-0.000002
C	0.914712	2.735879	-0.000039
C	1.211913	3.904222	-0.000032
C	-0.914712	-2.735879	0.000039
C	-1.211913	-3.904222	0.000032

7

Energy = -921.872407785

Sum of electronic and zero-point Energies = -921.603982

Imaginary Frequencies = 0

Atom	X	Y	Z

H	6.571293	0.808761	0.000422
H	5.38569	2.972957	0.000201
H	2.909182	3.06209	-0.00017
H	5.296895	-1.329567	0.000247
H	-5.296895	1.329567	-0.000103
H	-6.571293	-0.808761	-0.000201
H	-5.38569	-2.972957	-0.000054
H	-2.909182	-3.06209	0.000181
H	0.252987	2.517719	-0.00061
H	-0.252987	-2.517719	0.000592
H	-3.205586	4.989652	0.00007
H	3.205585	-4.989652	-0.000211
C	5.487407	0.825258	0.000271
C	4.815855	2.050716	0.000128
C	3.417164	2.103829	-0.000094
C	2.701518	0.913953	-0.000219
C	3.386542	-0.328912	-0.000094
C	4.77736	-0.378016	0.000199
C	1.264361	0.624338	-0.000393
C	1.122619	-0.826684	0.000077
C	2.389884	-1.40382	-0.000489
C	0.16846	1.436277	-0.000543
C	-1.122619	0.826684	-0.000125

C	-1.264361	-0.624338	0.000359
C	-0.16846	-1.436277	0.000522
C	-2.389884	1.40382	0.000368
C	-3.386542	0.328912	0.000122
C	-2.701518	-0.913953	0.0002
C	-4.77736	0.378016	-0.000069
C	-5.487407	-0.825258	-0.00011
C	-4.815855	-2.050717	-0.000019
C	-3.417164	-2.103829	0.000116
C	-2.688968	2.778149	0.000258
C	-2.965413	3.954418	0.000158
C	2.688968	-2.778149	-0.000389
C	2.965413	-3.954418	-0.000294

8a

Energy = -921.872420748

Sum of electronic and zero-point Energies = -921.603989

Imaginary Frequencies = 0

Atom	X	Y	Z
H	-4.192255	0.515122	0
H	-2.084404	5.04783	0
H	4.192255	-0.515122	0

H	2.084404	-5.04783	0
H	5.59458	-2.558419	0
H	4.561168	-4.799134	0
H	-4.561168	4.799134	0
H	-5.59458	2.558419	0
H	-2.101898	-5.545057	0
H	2.101898	5.545057	0
H	2.173507	1.295606	0
H	-2.173507	-1.295606	0
C	1.254331	-0.644265	0
C	1.254331	0.719632	0
C	-0.004007	1.394037	0
C	-1.254331	0.644265	0
C	-1.254331	-0.719632	0
C	0.004007	-1.394037	0
C	-0.294604	2.755886	0
C	-1.751476	2.916996	0
C	-2.342534	1.626732	0
C	2.342534	-1.626732	0
C	0.294604	-2.755886	0
C	1.751476	-2.916996	0
C	-3.724622	1.493666	0
C	-2.53977	4.063972	0

C	3.724622	-1.493666	0
C	2.53977	-4.063972	0
C	4.514328	-2.649329	0
C	3.929236	-3.91837	0
C	-3.929236	3.91837	0
C	-4.514328	2.649329	0
C	-0.631871	-3.814097	0
C	-1.412508	-4.736311	0
C	0.631871	3.814097	0
C	1.412508	4.736311	0

8b

Energy = -1120.40853210

Sum of electronic and zero-point Energies = -1120.156787

Imaginary Frequencies = 0

Atom	X	Y	Z
H	2.096755	5.062687	0
H	5.600235	2.591346	0
H	4.197307	0.522337	0
H	-4.197307	-0.522337	0
H	-5.600235	-2.591346	0
H	-2.096755	-5.062687	0

H	-2.094448	5.552014	0
H	2.094448	-5.552014	0
H	2.173767	-1.296117	0
H	-2.173767	1.296117	0
C	2.527595	4.069201	0
C	3.72494	1.498099	0
C	1.749513	2.915967	0
C	3.906134	3.896482	0
C	4.519195	2.649819	0
C	2.342608	1.627355	0
C	0.291772	2.754502	0
C	1.25541	0.644006	0
C	0.004017	1.393338	0
C	-1.25541	0.719	0
C	-1.25541	-0.644006	0
C	1.25541	-0.719	0
C	-0.004017	-1.393338	0
C	-0.291772	-2.754502	0
C	-2.342608	-1.627355	0
C	-1.749513	-2.915967	0
C	-3.72494	-1.498099	0
C	-4.519195	-2.649819	0
C	-3.906134	-3.896482	0

C	-2.527595	-4.069201	0
C	-0.632425	3.814234	0
C	-1.40884	4.739779	0
C	0.632425	-3.814234	0
C	1.40884	-4.739779	0
F	-4.693172	-5.001001	0
F	4.693172	5.001001	0

8c

Energy = -1841.11692468

Sum of electronic and zero-point Energies = -1840.867873

Imaginary Frequencies = 0

Atom	X	Y	Z
H	2.084134	5.052748	0
H	5.597259	2.572514	0
H	4.199006	0.522895	0
H	-4.199006	-0.522895	0
H	-5.597259	-2.572514	0
H	-2.084134	-5.052748	0
H	-2.091562	5.55384	0
H	2.091562	-5.55384	0
H	2.173275	-1.297314	0

H	-2.173275	1.297314	0
C	2.530299	4.066365	0
C	3.724202	1.497613	0
C	1.751158	2.914374	0
C	3.915673	3.907475	0
C	4.517705	2.649271	0
C	2.342087	1.625226	0
C	0.293319	2.755302	0
C	1.25487	0.643262	0
C	0.004385	1.393764	0
C	-1.25487	0.720316	0
C	-1.25487	-0.643262	0
C	1.25487	-0.720316	0
C	-0.004385	-1.393764	0
C	-0.293319	-2.755302	0
C	-2.342087	-1.625226	0
C	-1.751158	-2.914374	0
C	-3.724202	-1.497613	0
C	-4.517705	-2.649271	0
C	-3.915673	-3.907475	0
C	-2.530299	-4.066365	0
C	-0.630096	3.8155	0
C	-1.406482	4.741116	0

C	0.630096	-3.8155	0
C	1.406482	-4.741116	0
Cl	4.935899	5.34058	0
Cl	-4.935899	-5.34058	0

8d

Energy = -6068.95626833

Sum of electronic and zero-point Energies = -6068.708503

Imaginary Frequencies = 0

Atom	X	Y	Z
H	2.079626	5.050856	0
H	5.597059	2.56746	0
H	4.19918	0.522823	0
H	-4.19918	-0.522823	0
H	-5.597059	-2.56746	0
H	-2.079626	-5.050856	0
H	-2.091741	5.553639	0
H	2.091741	-5.553639	0
H	2.173185	-1.29726	0
H	-2.173185	1.29726	0
C	2.530247	4.066672	0
C	3.724003	1.497402	0

C	1.751127	2.914136	0
C	3.915888	3.907696	0
C	4.518071	2.649337	0
C	2.341976	1.624987	0
C	0.293258	2.755249	0
C	1.254739	0.643209	0
C	0.004388	1.393746	0
C	-1.254739	0.720394	0
C	-1.254739	-0.643209	0
C	1.254739	-0.720394	0
C	-0.004388	-1.393746	0
C	-0.293258	-2.755249	0
C	-2.341976	-1.624987	0
C	-1.751127	-2.914136	0
C	-3.724003	-1.497402	0
C	-4.518071	-2.649337	0
C	-3.915888	-3.907696	0
C	-2.530247	-4.066672	0
C	-0.630245	3.815353	0
C	-1.406746	4.740845	0
C	0.630245	-3.815353	0
C	1.406746	-4.740845	0
Br	5.027271	5.469575	0

Br	-5.027271	-5.469575	0

8e

Energy = -1000.52708199

Sum of electronic and zero-point Energies = -1000.204539

Imaginary Frequencies = 0

Atom	X	Y	Z
H	-2.989045	5.120655	-0.001399
H	2.989045	-5.120654	-0.001751
H	3.055748	2.932933	-0.011872
H	5.225229	-1.559968	-0.004473
H	-3.055744	-2.932931	-0.012986
H	-5.225229	1.559968	-0.005191
H	5.514361	2.728025	-0.015975
H	-5.514357	-2.728023	-0.017524
H	0.358223	2.505209	-0.001403
H	-0.358223	-2.505209	-0.001921
H	-7.411021	-0.253172	1.030203
H	-7.407233	0.315509	-0.637945
H	-7.516844	-1.415409	-0.293225
H	7.410821	0.253124	1.031718
H	7.407357	-0.315482	-0.636457

H	7.516901	1.41542	-0.291637
C	5.543039	0.58013	-0.003875
C	4.907323	1.828695	-0.008529
C	3.512596	1.949161	-0.00618
C	2.738144	0.798793	-0.000753
C	3.370497	-0.470616	0.000186
C	4.75564	-0.581432	-0.002241
C	2.328185	-1.502938	-0.000988
C	1.086858	-0.872952	-0.001412
C	-0.228991	-1.428196	-0.001757
C	-1.290167	-0.571775	-0.001834
C	-1.086858	0.872953	-0.001463
C	1.290168	0.571776	-0.001484
C	0.228991	1.428197	-0.001456
C	-2.738144	-0.798793	-0.001421
C	-2.328185	1.502938	-0.001163
C	-3.370497	0.470616	-0.000374
C	-3.512594	-1.94916	-0.007204
C	-4.75564	0.581432	-0.003047
C	-5.543038	-0.580131	-0.005043
C	-4.90732	-1.828694	-0.009799
C	-2.568271	2.888896	-0.001207
C	-2.794449	4.075952	-0.001321

C	2.568271	-2.888896	-0.001236
C	2.794449	-4.075951	-0.001522
C	-7.049486	-0.4799	0.021155
C	7.049481	0.479897	0.022609

8f

Energy = -1384.09525467

Sum of electronic and zero-point Energies = -1383.666212

Imaginary Frequencies = 0

Atom	X	Y	Z
H	-0.432628	2.493809	-0.024294
H	0.432663	-2.493665	-0.024967
H	5.172533	1.714943	0.015412
H	3.138836	-2.841587	-0.021635
H	5.586314	-2.567583	-0.021422
H	-5.172349	-1.714938	0.014127
H	-3.138954	2.841705	-0.021181
H	-5.586291	2.567634	-0.021657
H	7.355897	-1.870021	1.433046
H	7.086707	1.346834	-1.396789
H	9.809836	-1.650948	1.448349
H	9.538499	1.586372	-1.357119

H	10.919102	0.084282	0.059744
H	-7.356732	1.870589	1.430929
H	-7.086167	-1.34757	-1.397356
H	-9.810551	1.651382	1.445284
H	-9.537834	-1.587362	-1.358418
H	-10.919174	-0.084674	0.057134
H	2.839169	5.207001	-0.014104
H	-2.838895	-5.20691	-0.016668
C	-1.060252	-0.90539	-0.024501
C	-1.306098	0.53277	-0.024653
C	-0.271025	1.421216	-0.024864
C	1.060286	0.905532	-0.024131
C	0.271062	-1.421072	-0.025237
C	1.306131	-0.532626	-0.024662
C	2.282452	1.572064	-0.020823
C	3.353994	0.570271	-0.02127
C	2.75884	-0.716758	-0.020884
C	4.734268	0.723867	-0.010705
C	5.557188	-0.416164	-0.000066
C	3.567112	-1.845169	-0.012409
C	4.95522	-1.686737	-0.002564
C	-2.282411	-1.571933	-0.021593
C	-3.353956	-0.570141	-0.021902

C	-2.7588	0.716892	-0.021017
C	-4.734213	-0.723797	-0.011675
C	-5.557233	0.416175	-0.000891
C	-4.95525	1.686754	-0.002868
C	-3.567148	1.845248	-0.012357
C	7.035697	-0.279586	0.015213
C	7.830369	-1.123515	0.806096
C	7.677431	0.698962	-0.759111
C	9.2165	-0.993899	0.822041
C	9.063565	0.828835	-0.743477
C	9.839829	-0.016983	0.047261
C	-7.035711	0.279514	0.013953
C	-7.830817	1.12375	0.804091
C	-7.677115	-0.699458	-0.760132
C	-9.216942	0.994035	0.819546
C	-9.063234	-0.829462	-0.744964
C	-9.839906	0.016677	0.04503
C	2.48225	2.96416	-0.01877
C	2.674098	4.157147	-0.016916
C	-2.482199	-2.964031	-0.019983
C	-2.673978	-4.15703	-0.018873

8g

Energy = -2058.39491825

Sum of electronic and zero-point Energies = -2057.957187

Imaginary Frequencies = 0

Atom	X	Y	Z
H	0.406681	2.488799	0.218366
H	-0.406681	-2.488797	-0.218366
H	-5.188517	1.655029	0.143422
H	-3.106751	-2.862479	-0.264868
H	-5.555983	-2.615149	-0.2622
H	5.188517	-1.655027	-0.14342
H	3.106752	2.862481	0.264866
H	5.555983	2.615151	0.262197
H	7.357407	2.067646	-1.210001
H	7.077259	-1.396618	1.311658
H	9.810468	1.870521	-1.206046
H	9.528379	-1.610559	1.288722
H	-7.357407	-2.067648	1.209996
H	-7.07726	1.396623	-1.311654
H	-9.810467	-1.870526	1.20604
H	-9.52838	1.610561	-1.288718
H	-2.898514	5.157388	0.446677
H	2.898514	-5.157386	-0.446675

C	1.06949	-0.891595	-0.072635
C	1.299873	0.543336	0.05366
C	0.256111	1.418731	0.124676
C	-1.069489	0.891597	0.072635
C	-0.25611	-1.418728	-0.124676
C	-1.299872	-0.543333	-0.05366
C	-2.298261	1.543881	0.124501
C	-3.358382	0.53521	0.028717
C	-2.750262	-0.741656	-0.076811
C	-4.739942	0.673935	0.037426
C	-5.548836	-0.47184	-0.057414
C	-3.545843	-1.875179	-0.172984
C	-4.935314	-1.732523	-0.161437
C	2.298261	-1.543879	-0.124501
C	3.358382	-0.535208	-0.028717
C	2.750263	0.741659	0.076811
C	4.739942	-0.673933	-0.037426
C	5.548837	0.471842	0.057413
C	4.935315	1.732526	0.161435
C	3.545844	1.875182	0.172982
C	7.027595	0.349848	0.049229
C	7.826138	1.268364	-0.64837
C	7.668027	-0.68971	0.741353

C	9.21139	1.15427	-0.657773
C	9.052103	-0.809868	0.736437
C	9.828939	0.114581	0.037206
C	-7.027595	-0.349847	-0.049229
C	-7.826138	-1.268365	0.648367
C	-7.668027	0.689712	-0.741351
C	-9.211389	-1.154272	0.657769
C	-9.052104	0.80987	-0.736435
C	-9.828939	-0.114582	-0.037208
C	-11.321916	0.047313	0.013015
C	11.321915	-0.047317	-0.013015
C	-2.514074	2.927974	0.246844
C	-2.720749	4.113688	0.352247
C	2.514074	-2.927972	-0.246843
C	2.720749	-4.113686	-0.352245
F	-11.819131	0.574221	-1.129912
F	-11.960801	-1.126209	0.221422
F	-11.707646	0.878751	1.016965
F	11.960803	1.126197	-0.221458
F	11.819132	-0.574192	1.129928
F	11.707642	-0.878787	-1.01694

8h

Energy = -2732.68844834

Sum of electronic and zero-point Energies = -2732.29452301

Imaginary Frequencies = 0

Atom	X	Y	Z
H	0.441286	-2.492662	-0.017095
H	-0.441285	2.492627	-0.016423
H	-5.162991	-1.7334	0.012613
H	-3.143983	2.831951	-0.020178
H	-5.588106	2.553582	-0.028677
H	5.162985	1.733365	0.013431
H	3.143993	-2.831982	-0.020788
H	5.588114	-2.553605	-0.029062
H	-7.366231	1.87702	1.384686
H	-7.070502	-1.39329	-1.378114
H	-10.916596	-0.099356	0.011172
H	7.366195	-1.877436	1.384576
H	7.070541	1.393674	-1.377287
H	10.916591	0.099399	0.011802
H	-2.835118	-5.215356	-0.010768
H	2.835112	5.215321	-0.009094
C	1.056962	0.909529	-0.015694

C	1.30666	-0.527458	-0.01682
C	0.275709	-1.420763	-0.016884
C	-1.056962	-0.909565	-0.016019
C	-0.275708	1.420727	-0.016501
C	-1.306659	0.527423	-0.016754
C	-2.276513	-1.581095	-0.014407
C	-3.349825	-0.582254	-0.01714
C	-2.759345	0.70738	-0.015842
C	-4.729357	-0.740147	-0.012772
C	-5.551395	0.399539	-0.005973
C	-3.569411	1.834668	-0.011243
C	-4.956488	1.673197	-0.005734
C	2.276511	1.58106	-0.013812
C	3.349824	0.582222	-0.016759
C	2.759347	-0.707414	-0.015866
C	4.729355	0.740117	-0.012262
C	5.551397	-0.399568	-0.005741
C	4.956493	-1.673227	-0.005901
C	3.569416	-1.8347	-0.01154
C	-7.028899	0.260523	0.000346
C	-7.829572	1.116905	0.768895
C	-7.662419	-0.729611	-0.760332
C	-9.215168	0.987976	0.767982

C	-9.049917	-0.857363	-0.750844
C	-9.839759	-0.000139	0.009388
C	7.028899	-0.26054	0.000691
C	7.829551	-1.117134	0.769027
C	7.662439	0.729824	-0.75967
C	9.215145	-0.988183	0.768214
C	9.049934	0.857598	-0.750078
C	9.839755	0.000165	0.009939
C	-2.475	-2.972925	-0.012717
C	-2.668404	-4.165429	-0.011855
C	2.474997	2.97289	-0.01171
C	2.668399	4.165394	-0.010494
C	-10.047906	1.881432	1.651047
C	-9.697204	-1.897203	-1.629213
C	10.047863	-1.881881	1.651052
C	9.697244	1.897714	-1.628104
F	8.986067	3.047835	-1.656356
F	9.798531	1.474552	-2.912521
F	10.94495	2.207871	-1.219139
F	11.271032	-2.114665	1.128369
F	9.463142	-3.083013	1.855413
F	10.24518	-1.332048	2.874953
F	-10.944941	-2.207446	-1.220413

F	-8.986056	-3.047335	-1.657764
F	-9.798402	-1.473658	-2.913511
F	-11.271087	2.114308	1.128435
F	-10.245191	1.331294	2.874816
F	-9.463218	3.082532	1.855696

8i

Energy = -2104.28054316

Sum of electronic and zero-point Energies = -2103.863829

Imaginary Frequencies = 0

Atom	X	Y	Z
H	-0.320415	-2.504698	0.176519
H	0.320415	2.504698	-0.176519
H	5.237865	-1.471975	0.239717
H	3.010223	2.974461	-0.170063
H	5.464606	2.81302	-0.137711
H	-5.237865	1.471975	-0.239717
H	-3.010224	-2.974461	0.170063
H	-5.464606	-2.81302	0.137711
H	7.54755	2.509931	1.008395
H	10.063091	1.813985	0.804886
H	-7.54755	-2.50993	-1.008395

H	-10.063092	-1.813985	-0.804886
H	3.073393	-5.055705	0.434357
H	-3.073393	5.055705	-0.434357
H	-10.768449	1.722064	-0.245056
H	-11.55565	0.157697	-0.006581
H	-10.851439	1.013662	1.36973
H	11.55565	-0.157697	0.006581
H	10.76845	-1.722064	0.245058
H	10.851439	-1.013663	-1.369729
C	-1.099399	0.853542	-0.083154
C	-1.281185	-0.591187	0.019456
C	-0.207232	-1.4286	0.1005
C	1.099399	-0.853542	0.083154
C	0.207232	1.4286	-0.100501
C	1.281185	0.591187	-0.019457
C	2.349348	-1.4616	0.152156
C	3.37505	-0.413984	0.092937
C	2.722821	0.840784	-0.00907
C	4.759025	-0.504965	0.134706
C	5.532509	0.669615	0.06503
C	3.481741	2.001953	-0.079058
C	4.87359	1.909452	-0.049589
C	-2.349348	1.4616	-0.152157

C	-3.37505	0.413984	-0.092938
C	-2.722821	-0.840784	0.00907
C	-4.759025	0.504965	-0.134706
C	-5.532509	-0.669615	-0.06503
C	-4.87359	-1.909452	0.049589
C	-3.481741	-2.001953	0.079057
C	6.996858	0.62053	0.11843
C	7.873228	1.571231	0.57951
C	9.240727	1.188723	0.479256
C	9.429044	-0.055361	-0.057147
C	-6.996858	-0.62053	-0.11843
C	-7.873228	-1.571231	-0.57951
C	-9.240727	-1.188723	-0.479256
C	-9.429044	0.055361	0.057148
C	2.61174	-2.838998	0.259642
C	2.85868	-4.018107	0.352582
C	-2.61174	2.838998	-0.259642
C	-2.85868	4.018107	-0.352582
C	-10.715683	0.77999	0.309261
C	10.715683	-0.77999	-0.30926
S	7.890194	-0.777176	-0.4579
S	-7.890194	0.777176	0.4579

Complete Acknowledgement

We thank the National Science Foundation (CHE-1013032) for support of this research, as well as for instrumentation grant support (CHE-0639170 and CHE-0923589). The electrochemical work was funded by the Division of Chemical Sciences, Geosciences, and Biosciences, Office of Basic Energy Sciences of the U.S. Department of Energy through Grant DE-FG02-07ER15907. C.D.W. and C.E.S. acknowledge the NSF for an IGERT fellowship (DGE-0549503) and REU program stipend (CHE-0755544), respectively. S.N. thanks the Global COE Program at Osaka University ("Global Education and Research Center for Bio-Environmental Chemistry") for the support to his research at Oregon. MS were obtained at the Mass Spectrometry Facilities and Services Core of the Environmental Health Sciences Center, Oregon State University, supported by grant #P30-ES00210, National Institute of Environmental Health Sciences, National Institutes of Health.

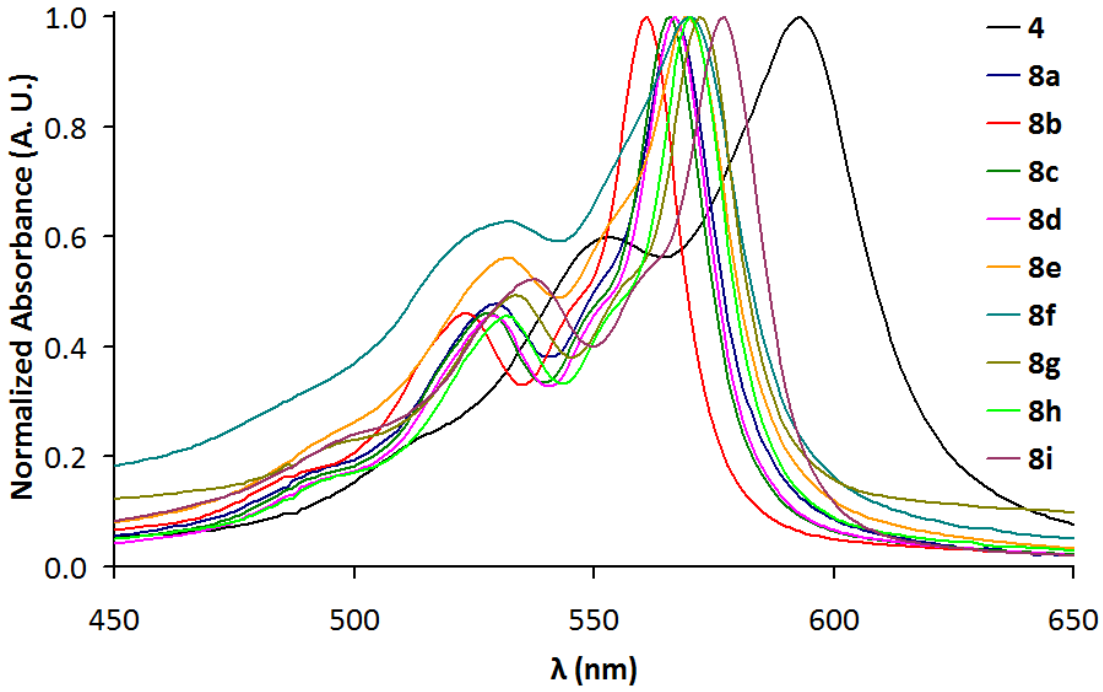

Figure 1. Absorption spectra of IFs **4** and **8a**–**i**.

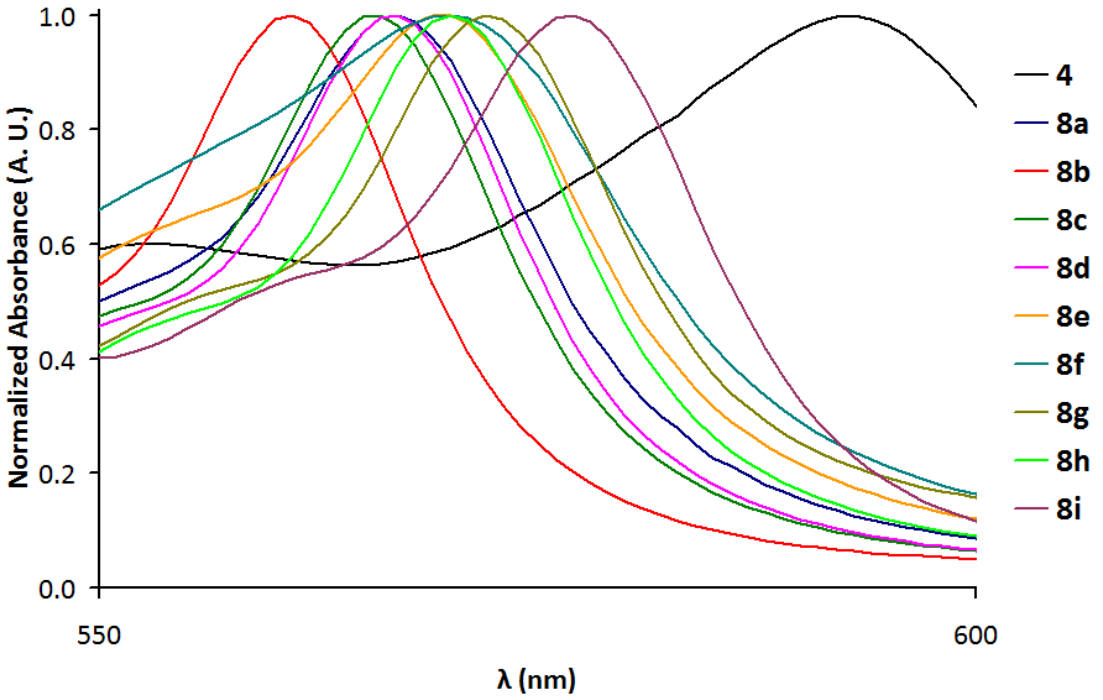

Figure 2. Expansion of absorption spectra of IFs **4** and **8a**–**i**.

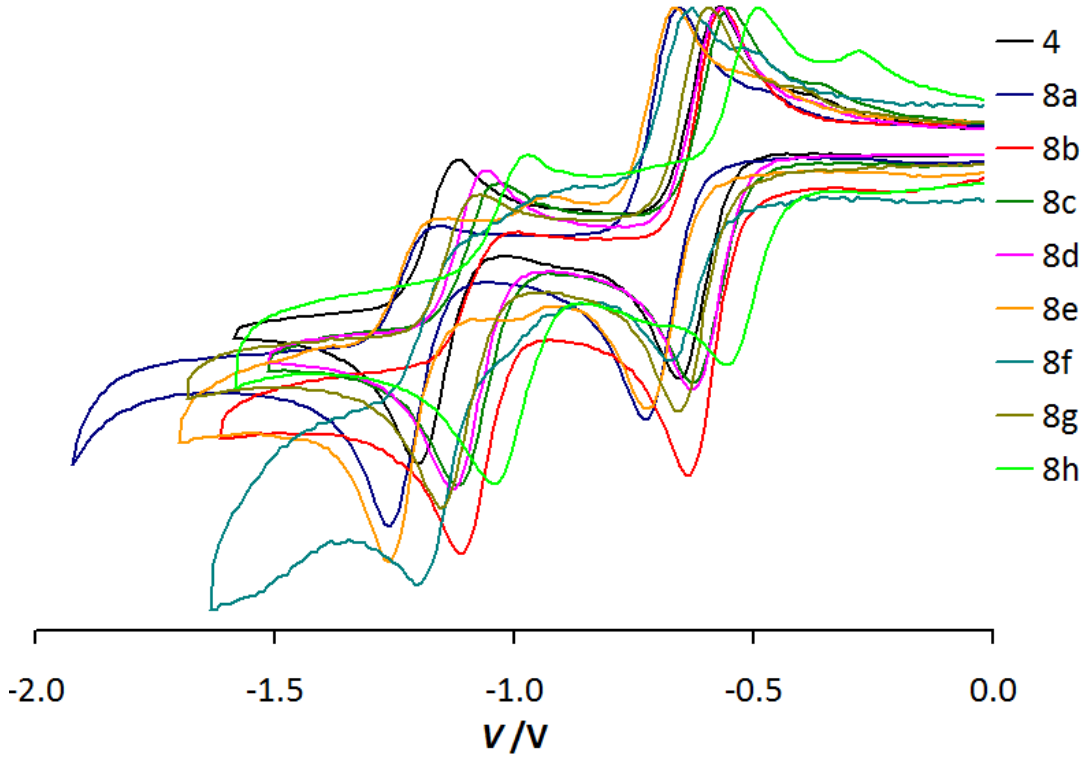

Figure 3. Cyclic voltammetry of IFs **4** and **8a**–**h**; currents normalized to the E_{pa} (A/A^{-}) peak.

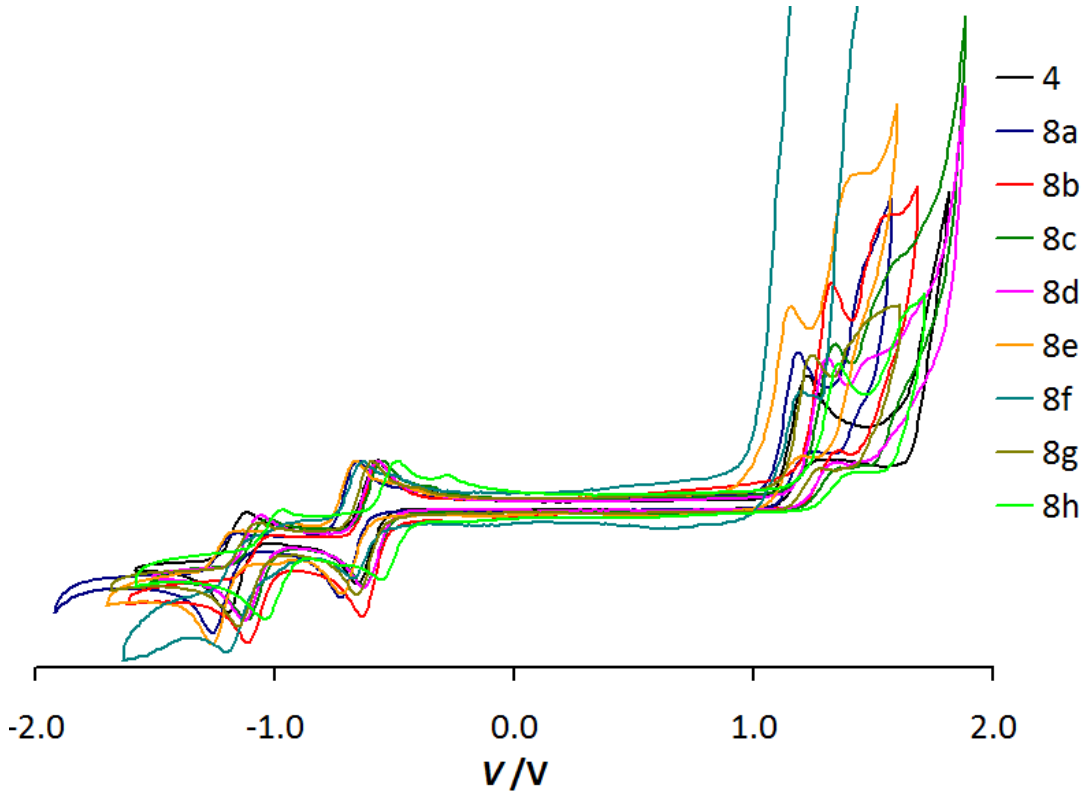

Figure 4. Full CVs of IFs **4** and **8a**–**h**; currents normalized to the E_{pa} (A/A^{-}) peak.

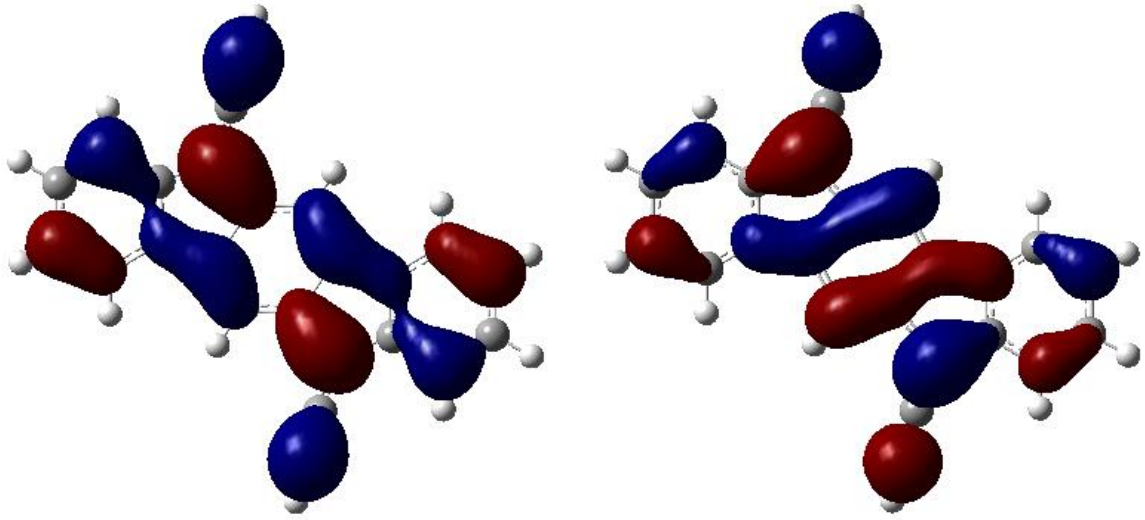

Figure 5. Calculated HOMO (left) and LUMO (right) plots of **8a**.

APPENDIX B

EXPERIMENTAL DETAILS FOR CHAPTER III

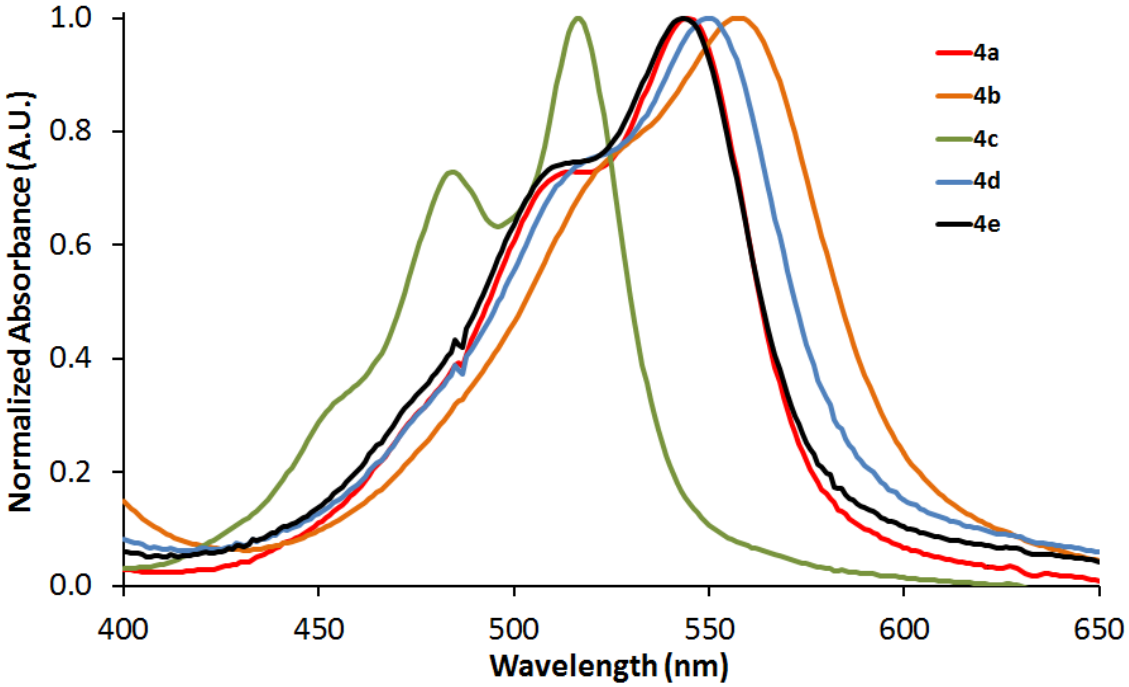

Figure 1. Electronic Absorption Spectra of 6,12-Diarylindeno[1,2-b]fluorenes **4a**–**e**.

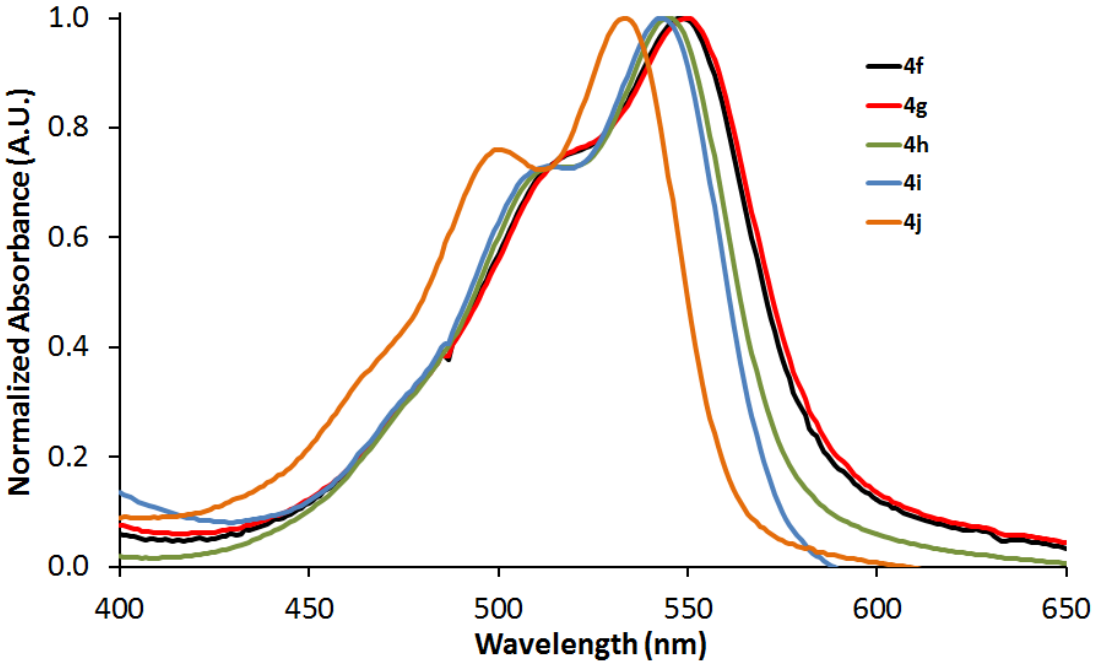

Figure 2. Electronic Absorption Spectra of 6,12-Diarylindeno[1,2-b]fluorenes **4f**–**j**.

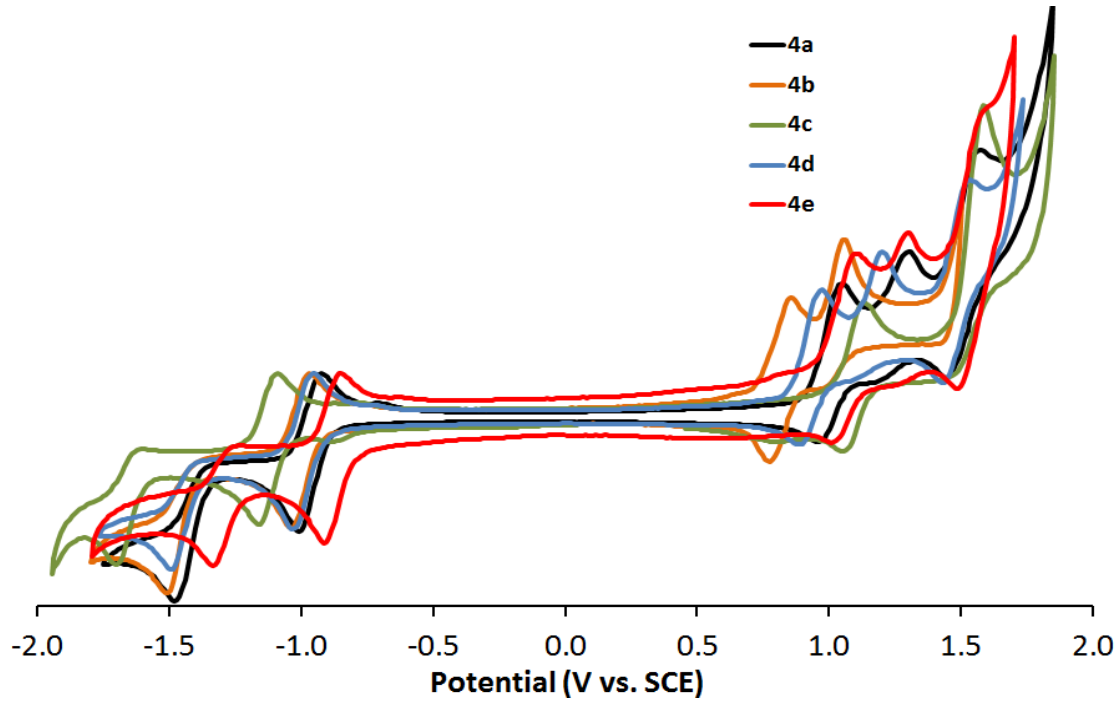

Figure 3. Cyclic Voltammetry of 6,12-Diarylindeno[1,2-b]fluorenes **4a**–**e**.

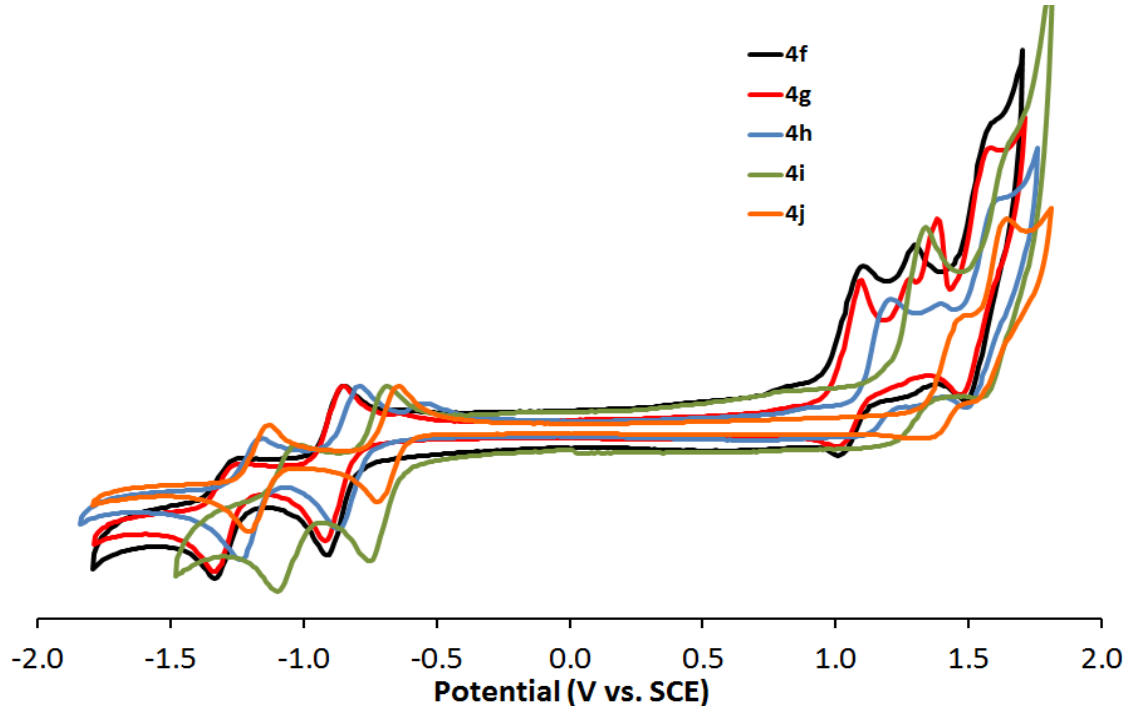

Figure 4. Cyclic Voltammetry of 6,12-Diarylindeno[1,2-b]fluorenes **4f**–**j**.

Calculations

All calculations were performed using Gaussian 09.[4] The structures were minimized using the B3LYP method[5] using the 6-31(d) basis set and minimized structures were verified with frequency analysis. Single point energies were then calculated with B3LYP/6-311+G(d,p)// B3LYP/6-31G(d). All energies are given in Hartrees.

2

B3LYP/6-31G(d)

E_{el} = –921.652619204

E_{ZPE} = 0.270088

Imaginary Frequencies = 0

B3LYP/6-311+G(d,p)//B3LYP/6-31G(d)

E_{el} = –921.872187459

Symbol	X	Y	Z
C	1.255641	-0.646548	0.000000
C	1.255641	0.720105	0.000000
C	-0.003249	1.394921	0.000000
C	-1.255641	0.646548	0.000000
C	-1.255641	-0.720105	0.000000
C	0.003249	-1.394921	0.000000
C	-0.292890	2.759689	0.000000
C	-1.749926	2.921638	0.000000
C	-2.343054	1.630244	0.000000
C	2.343054	-1.630244	0.000000
C	0.292890	-2.759689	0.000000
C	1.749926	-2.921638	0.000000
C	-3.727409	1.499114	0.000000
H	-4.196063	0.518236	0.000000
C	-2.537247	4.071136	0.000000
H	-2.076974	5.055325	0.000000
C	3.727409	-1.499114	0.000000
H	4.196063	-0.518236	0.000000
C	2.537247	-4.071136	0.000000
H	2.076974	-5.055325	0.000000
C	4.516361	-2.657323	0.000000
H	5.599152	-2.566859	0.000000
C	3.928564	-3.927623	0.000000
H	4.560011	-4.811821	0.000000
C	-3.928564	3.927623	0.000000
H	-4.560011	4.811821	0.000000

C	-4.516361	2.657323	0.000000
H	-5.599152	2.566859	0.000000
C	-0.637618	-3.817772	0.000000
C	-1.427451	-4.738868	0.000000
H	-2.124210	-5.546171	0.000000
C	0.637618	3.817772	0.000000
C	1.427451	4.738868	0.000000
H	2.124210	5.546171	0.000000
H	2.175826	1.298837	0.000000
H	-2.175826	-1.298837	0.000000

4a

B3LYP/6-31G(d)

E_{el} = –1231.47016530

E_{ZPE} = 0.414943

Imaginary Frequencies = 0

B3LYP/6-311+G(d,p)//B3LYP/6-31G(d)

E_{el} = –1231.75589385

Symbol	X	Y	Z
C	0.669247	-1.236571	0.001874
C	-0.695847	-1.264982	0.000532
C	-1.409866	-0.023073	0.032921
C	-0.669377	1.236722	0.001820
C	0.695716	1.265134	0.000495
C	1.409745	0.023228	0.032966
C	-2.776888	0.245316	0.011748
C	-2.948605	1.702273	-0.032852
C	-1.661821	2.311482	-0.038534
C	1.661680	-2.311339	-0.038482
C	2.776763	-0.245175	0.011810
C	2.948464	-1.702141	-0.032838
C	-1.534810	3.695998	-0.058073
H	-0.554285	4.165853	-0.061871
C	-4.097655	2.497277	-0.020473
H	-5.085259	2.047648	0.018389
C	1.534664	-3.695856	-0.058020
H	0.554138	-4.165707	-0.061784
C	4.097516	-2.497140	-0.020515
H	5.085123	-2.047512	0.018313
C	2.692891	-4.483089	-0.068384
H	2.606261	-5.566123	-0.086890

C	3.959407	-3.888681	-0.044950
H	4.847313	-4.515169	-0.039762
C	-3.959551	3.888818	-0.044904
H	-4.847458	4.515304	-0.039674
C	-2.693038	4.483230	-0.068391
H	-2.606410	5.566264	-0.086899
H	-1.240932	-2.203989	-0.041955
H	1.240788	2.204142	-0.042059
C	-3.867059	-0.737263	0.027966
C	-4.970664	-0.608138	-0.838378
C	-3.838956	-1.838031	0.906670
C	-5.997609	-1.549556	-0.833302
C	-4.869676	-2.775750	0.912539
C	-5.952767	-2.637018	0.042079
C	3.867043	0.737287	0.027975
C	4.970593	0.607920	-0.838408
C	3.839231	1.838047	0.906701
C	5.997750	1.549107	-0.833374
C	4.870166	2.775529	0.912529
C	5.953185	2.636572	0.042017
H	-6.833340	-1.436491	-1.518903
H	-6.756618	-3.368089	0.048009
H	-4.831334	-3.611888	1.605857
H	-5.000864	0.220012	-1.539840
H	-3.016061	-1.932996	1.608724
H	5.000565	-0.220234	-1.539875
H	3.016429	1.933169	1.608839
H	4.832051	3.611658	1.605871
H	6.757200	3.367463	0.047924
H	6.833429	1.435855	-1.519007

4b

B3LYP/6-31G(d)

E_{el} = –1460.51696269

E_{ZPE} = 0.480495

Imaginary Frequencies = 0

B3LYP/6-311+G(d,p)//B3LYP/6-31G(d)

E_{el} = –1460.86961595

Symbol	X	Y	Z
H	-2.655254	-3.252060	-0.037665
H	1.986809	-5.110608	0.066583

H	2.655254	3.252060	-0.037665
H	-1.986809	5.110608	0.066583
H	2.274826	5.707237	-0.059600
H	-0.024398	6.624072	0.000309
H	0.024398	-6.624072	0.000309
H	-2.274826	-5.707237	-0.059600
H	2.454097	0.607840	-0.012971
H	-2.454097	-0.607840	-0.012971
H	3.291019	-3.842914	-1.441851
H	3.480773	-0.828190	1.615791
H	5.729773	-4.047458	-1.412264
H	5.954143	-1.011527	1.626046
H	-3.291019	3.842914	-1.441851
H	-3.480773	0.828190	1.615791
H	-5.729773	4.047458	-1.412264
H	-5.954143	1.011527	1.626046
H	-7.921675	3.256937	-1.681960
H	-9.139085	3.315185	-0.377131
H	-7.807423	4.504632	-0.403950
H	7.921675	-3.256937	-1.681960
H	9.139085	-3.315185	-0.377131
H	7.807423	-4.504632	-0.403950
C	0.440310	1.333967	0.033631
C	1.397330	0.358966	0.032652
C	0.984084	-1.011698	0.067060
C	-0.440310	-1.333967	0.033631
C	-1.397330	-0.358966	0.032652
C	-0.984084	1.011698	0.067060
C	1.726403	-2.192953	0.048201
C	0.780081	-3.314429	0.000939
C	-0.544751	-2.792430	-0.009252
C	0.544751	2.792430	-0.009252
C	-1.726403	2.192953	0.048201
C	-0.780081	3.314429	0.000939
C	-1.642069	-3.646694	-0.031173
C	0.984084	-4.696978	0.018520
C	1.642069	3.646694	-0.031173
C	-0.984084	4.696978	0.018520
C	1.425226	5.029948	-0.039090
C	0.125459	5.547715	-0.008856
C	-0.125459	-5.547715	-0.008856
C	-1.425226	-5.029948	-0.039090

C	3.185723	-2.315333	0.076079
C	3.861345	-3.228917	-0.751629
C	3.972542	-1.515238	0.934037
C	5.251667	-3.339321	-0.744901
C	5.354576	-1.618876	0.955064
C	6.008761	-2.531051	0.112426
C	-3.185723	2.315333	0.076079
C	-3.861345	3.228917	-0.751629
C	-3.972542	1.515238	0.934037
C	-5.251667	3.339321	-0.744901
C	-5.354576	1.618876	0.955064
C	-6.008761	2.531051	0.112426
C	-8.084537	3.463634	-0.616039
C	8.084537	-3.463634	-0.616039
O	7.368245	-2.555465	0.206579
O	-7.368245	2.555465	0.206579

4c

B3LYP/6-31G(d)

E_{el} = –1467.36725635

E_{ZPE} = 0.580119

Imaginary Frequencies = 0

B3LYP/6-311+G(d,p)//B3LYP/6-31G(d)

E_{el} = –1467.71169861

Symbol	X	Y	Z
H	-0.185155	-4.226814	-0.012399
H	4.638457	-2.884204	0.000225
H	0.185151	4.226828	-0.012492
H	-4.638458	2.884211	0.000317
H	-1.604795	5.947712	-0.012064
H	-3.990112	5.290250	-0.005170
H	3.990107	-5.290242	-0.005190
H	1.604789	-5.947701	-0.011993
H	1.639136	1.935424	-0.017277
H	-1.639137	-1.935410	-0.017172
H	6.386694	1.126460	-2.101959
H	6.017669	1.694937	2.129836
H	-6.386625	-1.126483	-2.101943
H	-6.017678	-1.695006	2.129850
H	4.031039	-1.390176	-2.494952
H	3.137520	0.103457	-2.746638

H	4.802145	-0.036357	-3.338623
H	2.734067	0.879356	2.523117
H	3.496380	-0.695386	2.701704
H	4.289466	0.747657	3.357982
H	8.514816	1.578948	0.215288
H	7.853899	2.750199	-0.928803
H	7.683056	3.015636	0.815523
H	-4.031159	1.390204	-2.494915
H	-3.137376	-0.103295	-2.746447
H	-4.801974	0.036219	-3.338585
H	-2.733788	-0.878519	2.523029
H	-3.497388	0.695532	2.702245
H	-4.289280	-0.748395	3.357978
H	-8.514828	-1.578990	0.214927
H	-7.853672	-2.750510	-0.928746
H	-7.683141	-3.015507	0.815678
C	-0.426028	1.346883	-0.009003
C	0.918328	1.120884	-0.010102
C	1.384348	-0.236717	-0.005008
C	0.426030	-1.346870	-0.008989
C	-0.918327	-1.120871	-0.010048
C	-1.384346	0.236729	-0.004971
C	2.674360	-0.739279	-0.007208
C	2.587934	-2.201753	-0.012477
C	1.215509	-2.581200	-0.013168
C	-1.215510	2.581212	-0.013181
C	-2.674359	0.739290	-0.007138
C	-2.587935	2.201763	-0.012437
C	0.859456	-3.924901	-0.012683
C	3.590597	-3.172867	-0.006922
C	-0.859460	3.924914	-0.012736
C	-3.590598	3.172876	-0.006871
C	-1.871983	4.894394	-0.011641
C	-3.221096	4.522435	-0.008281
C	3.221092	-4.522426	-0.008292
C	1.871978	-4.894383	-0.011601
C	3.939669	0.038436	0.001189
C	4.652478	0.239656	-1.201375
C	4.438464	0.569048	1.211175
C	5.845841	0.967570	-1.170790
C	5.637236	1.288963	1.194235
C	6.358815	1.498249	0.015902

C	-3.939664	-0.038433	0.001275
C	-4.652449	-0.239661	-1.201310
C	-4.438481	-0.569058	1.211244
C	-5.845800	-0.967586	-1.170760
C	-5.637241	-1.289003	1.194264
C	-6.358792	-1.498286	0.015919
C	4.130901	-0.298710	-2.515069
C	3.702427	0.365240	2.517234
C	7.667811	2.253140	0.029279
C	-4.130843	0.298718	-2.514987
C	-3.702560	-0.365196	2.517362
C	-7.667772	-2.253207	0.029248

4d

B3LYP/6-31G(d)

E_{el} = –1310.10689966

E_{ZPE} = 0.469817

Imaginary Frequencies = 0

B3LYP/6-311+G(d,p)//B3LYP/6-31G(d)

E_{el} = –1310.41155206

Symbol	X	Y	Z
H	0.205924	-4.196257	-0.068137
H	-4.632656	-2.931627	0.010771
H	-0.205925	4.196256	-0.068071
H	4.632655	2.931631	0.010860
H	1.558899	5.944290	-0.094529
H	3.953319	5.315575	-0.047994
H	-3.953321	-5.315571	-0.048114
H	-1.558902	-5.944288	-0.094637
H	-1.616380	1.944817	-0.048687
H	1.616381	-1.944816	-0.048715
H	-4.902075	-1.128950	-1.524472
H	-3.310766	1.386233	1.577682
H	-6.992455	0.168055	-1.499980
H	-5.390923	2.702571	1.573374
H	4.902123	1.129028	-1.524357
H	3.310719	-1.386316	1.577618
H	6.992494	-0.167981	-1.499883
H	5.390873	-2.702665	1.573287
H	8.152492	-2.289649	-0.899560
H	8.344615	-1.897854	0.811352

H	7.476534	-3.361162	0.340441
H	-8.153429	2.288089	-0.899017
H	-8.343861	1.899041	0.812723
H	-7.476297	3.361607	0.338610
C	0.436223	1.336160	-0.003892
C	-0.912041	1.118604	-0.005294
C	-1.391658	-0.230879	0.027306
C	-0.436223	-1.336160	-0.003917
C	0.912042	-1.118604	-0.005309
C	1.391659	0.230879	0.027318
C	-2.688848	-0.741044	0.004860
C	-2.593926	-2.205310	-0.040833
C	-1.218278	-2.572077	-0.045823
C	1.218278	2.572079	-0.045772
C	2.688849	0.741044	0.004892
C	2.593927	2.205312	-0.040778
C	-0.843364	-3.911057	-0.065160
C	-3.580117	-3.195317	-0.028648
C	0.843363	3.911058	-0.065090
C	3.580117	3.195320	-0.028566
C	1.839998	4.894744	-0.076039
C	3.193117	4.539037	-0.053024
C	-3.193118	-4.539034	-0.053124
C	-1.840000	-4.894741	-0.076133
C	-3.937822	0.027125	0.023013
C	-5.010893	-0.303984	-0.826980
C	-4.106676	1.127540	0.885676
C	-6.188073	0.438804	-0.819402
C	-5.289140	1.861915	0.890265
C	-6.354038	1.532976	0.040602
C	3.937820	-0.027128	0.023044
C	5.010923	0.304025	-0.826906
C	4.106647	-1.127585	0.885646
C	6.188094	-0.438763	-0.819337
C	5.289114	-1.861969	0.890225
C	6.354032	-1.532988	0.040619
C	7.646706	-2.313084	0.071564
C	-7.646700	2.313091	0.071571

4e

B3LYP/6-31G(d)

E_{el} = –1429.93674059

E_{ZPE} = 0.398341

Imaginary Frequencies = 0

B3LYP/6-311+G(d,p)//B3LYP/6-31G(d)

E_{el} = –1430.29283040

Symbol	X	Y	Z
H	-0.139438	-4.199860	-0.066098
H	4.678754	-2.859480	0.014812
H	0.139420	4.199870	-0.065730
H	-4.678752	2.859481	0.016218
H	-1.652900	5.919171	-0.092008
H	-4.036855	5.252748	-0.044063
H	4.036841	-5.252742	-0.045534
H	1.652875	-5.919159	-0.092968
H	1.584722	1.970936	-0.046384
H	-1.584735	-1.970927	-0.046187
H	7.002770	0.297157	-1.504602
H	4.907666	-1.051065	-1.531952
H	3.291645	1.423094	1.594077
H	5.381795	2.782334	1.586815
H	-3.291241	-1.423247	1.594741
H	-5.381390	-2.782490	1.587875
H	-4.908054	1.051207	-1.530647
H	-7.003147	-0.297021	-1.502898
C	-0.457125	1.329599	-0.000546
C	0.894141	1.133131	-0.002196
C	1.394787	-0.208933	0.030021
C	0.457124	-1.329595	-0.000785
C	-0.894143	-1.133127	-0.002087
C	-1.394781	0.208934	0.030381
C	2.699022	-0.699325	0.007319
C	2.628262	-2.164717	-0.037794
C	1.258691	-2.553076	-0.043054
C	-1.258704	2.553083	-0.042504
C	-2.699022	0.699327	0.008043
C	-2.628273	2.164723	-0.036950
C	0.905028	-3.897677	-0.062857
C	3.630184	-3.138726	-0.025729
C	-0.905046	3.897686	-0.062266
C	-3.630193	3.138731	-0.024551
C	-1.917290	4.865401	-0.073142
C	-3.264498	4.488446	-0.049439

C	3.264483	-4.488438	-0.050654
C	1.917270	-4.865391	-0.074068
C	3.935986	0.089202	0.023748
C	5.008522	-0.225144	-0.835178
C	4.088298	1.185541	0.896162
C	6.179886	0.527331	-0.835768
C	5.255743	1.944625	0.908697
C	6.285214	1.603335	0.038856
C	-3.935980	-0.089204	0.024703
C	-5.008732	0.225220	-0.833924
C	-4.088070	-1.185628	0.897050
C	-6.180094	-0.527256	-0.834292
C	-5.255510	-1.944715	0.909805
C	-6.285201	-1.603344	0.040256
F	-7.419165	-2.333199	0.048086
F	7.419181	2.333187	0.046469

4f

B3LYP/6-31G(d)

E_{el} = –2150.66214850

E_{ZPE} = 0.395604

Imaginary Frequencies = 0

B3LYP/6-311+G(d,p)//B3LYP/6-31G(d)

E_{el} = –2151.00141477

Symbol	X	Y	Z
H	-0.589754	-4.160995	-0.068337
H	4.344905	-3.345154	0.011947
H	0.589736	4.161006	-0.067973
H	-4.344903	3.345155	0.013369
H	-1.008526	6.062844	-0.095234
H	-3.449753	5.655666	-0.047635
H	3.449740	-5.655658	-0.049133
H	1.008502	-6.062830	-0.096209
H	1.787932	1.789247	-0.046105
H	-1.787944	-1.789239	-0.045906
H	6.976858	-0.460218	-1.522137
H	4.762854	-1.564980	-1.541737
H	3.429284	1.056388	1.596715
H	5.635095	2.181655	1.592394
H	-3.428922	-1.056552	1.597420
H	-5.634732	-2.181819	1.593484

H	-4.763203	1.565134	-1.540464
H	-6.977202	0.460369	-1.520475
C	-0.311308	1.371533	-0.001900
C	1.010915	1.030894	-0.003012
C	1.363415	-0.357535	0.029094
C	0.311307	-1.371531	-0.002135
C	-1.010916	-1.030891	-0.002901
C	-1.363409	0.357534	0.029451
C	2.607007	-0.985765	0.005989
C	2.380374	-2.435044	-0.039814
C	0.977159	-2.674247	-0.044502
C	-0.977171	2.674254	-0.043952
C	-2.607006	0.985766	0.006715
C	-2.380384	2.435050	-0.038963
C	0.481068	-3.972925	-0.064974
C	3.272463	-3.510328	-0.028335
C	-0.481085	3.972935	-0.064382
C	-3.272471	3.510333	-0.027143
C	-1.384071	5.043455	-0.075990
C	-2.763847	4.812964	-0.052456
C	2.763833	-4.812955	-0.053689
C	1.384052	-5.043443	-0.076927
C	3.920843	-0.334029	0.020651
C	4.951310	-0.757355	-0.841528
C	4.192734	0.736454	0.894522
C	6.196036	-0.133748	-0.843381
C	5.434960	1.365588	0.906129
C	6.429639	0.925735	0.033293
C	-3.920838	0.334027	0.021608
C	-4.951500	0.757438	-0.840295
C	-4.192530	-0.736544	0.895433
C	-6.196226	0.133830	-0.841929
C	-5.434754	-1.365681	0.907257
C	-6.429630	-0.925742	0.034691
Cl	-8.000618	-1.713218	0.043667
Cl	8.000630	1.713207	0.041997

4g

B3LYP/6-31G(d)

E_{el} = –6373.67954568

E_{ZPE} = 0.394629

Imaginary Frequencies = 0

B3LYP/6-311+G(d,p)//B3LYP/6-31G(d)

E_{el} = –6378.84070588

Symbol	X	Y	Z
H	-0.976913	-4.086935	-0.077476
H	4.012569	-3.738195	0.001007
H	0.976898	4.086942	-0.077104
H	-4.012567	3.738187	0.002429
H	-0.435464	6.130134	-0.106933
H	-2.904259	5.954260	-0.060159
H	2.904246	-5.954258	-0.061654
H	0.435440	-6.130124	-0.107910
H	1.946787	1.614484	-0.054827
H	-1.946796	-1.614483	-0.054622
H	6.903992	-1.113194	-1.525134
H	4.597493	-2.004911	-1.547172
H	3.512430	0.731588	1.590003
H	5.812736	1.643852	1.587667
H	-3.512093	-0.731778	1.590720
H	-5.812404	-1.644034	1.588770
H	-4.597816	2.005090	-1.545903
H	-6.904313	1.113374	-1.523482
C	-0.181957	1.394440	-0.009348
C	1.102640	0.931786	-0.010443
C	1.324305	-0.483514	0.022156
C	0.181957	-1.394444	-0.009591
C	-1.102640	-0.931791	-0.010330
C	-1.324297	0.483504	0.022522
C	2.503630	-1.225521	-0.001261
C	2.142130	-2.647297	-0.048303
C	0.722727	-2.753703	-0.052949
C	-0.722736	2.753705	-0.052392
C	-2.503627	1.225515	-0.000527
C	-2.142138	2.647297	-0.047446
C	0.106843	-4.000016	-0.074390
C	2.929275	-3.801711	-0.038505
C	-0.106858	4.000021	-0.073791
C	-2.929282	3.801710	-0.037311
C	-0.905239	5.150606	-0.086789
C	-2.300539	5.050858	-0.063696
C	2.300526	-5.050856	-0.064930
C	0.905220	-5.150600	-0.087729

C	3.872652	-0.699827	0.014476
C	4.859689	-1.218303	-0.846664
C	4.242825	0.340786	0.888466
C	6.157521	-0.713868	-0.847038
C	5.538973	0.850117	0.900978
C	6.488200	0.318523	0.029666
C	-3.872648	0.699820	0.015437
C	-4.859865	1.218399	-0.845434
C	-4.242637	-0.340893	0.889384
C	-6.157699	0.713968	-0.845590
C	-5.538784	-0.850220	0.902114
C	-6.488195	-0.318523	0.031065
Br	8.269267	1.009207	0.042163
Br	-8.269262	-1.009201	0.043863

4h

B3LYP/6-31G(d)

E_{el} = –1905.54484637

E_{ZPE} = 0.424353

Imaginary Frequencies = 0

B3LYP/6-311+G(d,p)//B3LYP/6-31G(d)

E_{el} = –1906.05420662

Symbol	X	Y	Z
H	4.083535	-0.995962	-0.043770
H	3.756773	3.995342	0.028934
H	-4.083535	0.995962	-0.043770
H	-3.756773	-3.995342	0.028934
H	-6.132740	-0.407455	-0.071721
H	-5.967929	-2.876874	-0.028485
H	5.967929	2.876874	-0.028485
H	6.132740	0.407455	-0.071721
H	-1.605302	1.954749	-0.025514
H	1.605302	-1.954749	-0.025514
H	2.025314	4.576504	-1.529730
H	-0.707483	3.519278	1.619188
H	1.142355	6.883233	-1.518037
H	-1.613453	5.818979	1.601715
H	-2.025314	-4.576504	-1.529730
H	0.707483	-3.519278	1.619188
H	-1.142355	-6.883233	-1.518037
H	1.613453	-5.818979	1.601715

C	-1.395830	-0.174963	0.018976
C	-0.926978	1.107117	0.017543
C	0.489779	1.321375	0.049884
C	1.395830	0.174963	0.018976
C	0.926978	-1.107117	0.017543
C	-0.489779	-1.321375	0.049884
C	1.237636	2.496512	0.026006
C	2.658009	2.129340	-0.018718
C	2.757865	0.709632	-0.022103
C	-2.757865	-0.709632	-0.022103
C	-1.237636	-2.496512	0.026006
C	-2.658009	-2.129340	-0.018718
C	4.001205	0.088107	-0.041312
C	3.815489	2.911717	-0.008423
C	-4.001205	-0.088107	-0.041312
C	-3.815489	-2.911717	-0.008423
C	-5.155350	-0.881610	-0.053470
C	-5.061893	-2.277235	-0.032277
C	5.061893	2.277235	-0.032277
C	5.155350	0.881610	-0.053470
C	0.715789	3.867666	0.034707
C	1.237636	4.846739	-0.833885
C	-0.321171	4.244655	0.910332
C	0.733171	6.142787	-0.838342
C	-0.824972	5.541458	0.909885
C	-0.300805	6.495442	0.033780
C	-0.715789	-3.867666	0.034707
C	-1.237636	-4.846739	-0.833885
C	0.321171	-4.244655	0.910332
C	-0.733171	-6.142787	-0.838342
C	0.824972	-5.541458	0.909885
C	0.300805	-6.495442	0.033780
C	0.883613	-7.881061	-0.012057
C	-0.883613	7.881061	-0.012057
F	-1.405861	8.248552	1.179181
F	-1.882250	7.972670	-0.922411
F	0.041701	8.805387	-0.354074
F	-0.041701	-8.805387	-0.354074
F	1.405861	-8.248552	1.179181
F	1.882250	-7.972670	-0.922411

4i

B3LYP/6-31G(d)

E_{el} = –2579.61497276

E_{ZPE} = 0.433395

Imaginary Frequencies = 0

B3LYP/6-311+G(d,p)//B3LYP/6-31G(d)

E_{el} = –2580.34684597

Symbol	X	Y	Z
H	-0.726098	4.140634	-0.034252
H	4.233967	3.489739	0.021739
H	0.726090	-4.140700	-0.033861
H	-4.233970	-3.489785	0.022401
H	-0.808975	-6.093282	-0.059403
H	-3.262209	-5.766638	-0.025356
H	3.262197	5.766584	-0.026192
H	0.808959	6.093218	-0.060106
H	1.842758	-1.734006	-0.030044
H	-1.842758	1.733944	-0.030097
H	4.683775	1.728589	-1.555564
H	3.472672	-0.962174	1.571650
H	-4.683889	-1.728765	-1.555071
H	-3.472550	0.962253	1.571833
H	-7.442621	1.199345	-0.051753
H	7.442668	-1.199302	-0.052115
C	-0.266254	-1.381838	0.013515
C	1.043659	-0.998856	0.010361
C	1.350315	0.401311	0.040242
C	0.266257	1.381781	0.013350
C	-1.043655	0.998799	0.010330
C	-1.350309	-0.401364	0.040380
C	2.570211	1.072262	0.013884
C	2.298993	2.513686	-0.025054
C	0.889152	2.706228	-0.024417
C	-0.889155	-2.706288	-0.024068
C	-2.570208	-1.072314	0.014178
C	-2.298997	-2.513743	-0.024628
C	0.350080	3.987268	-0.036952
C	3.156058	3.616833	-0.013221
C	-0.350088	-3.987331	-0.036504
C	-3.156064	-3.616886	-0.012620
C	-1.217942	-5.086928	-0.046863
C	-2.604270	-4.902201	-0.030474

C	2.604260	4.902145	-0.031173
C	1.217930	5.086867	-0.047487
C	3.905567	0.463285	0.011588
C	4.906966	0.925701	-0.861809
C	4.218213	-0.605188	0.869515
C	6.168142	0.332959	-0.878744
C	5.481397	-1.195988	0.844256
C	6.465759	-0.732393	-0.027777
C	-3.905557	-0.463322	0.011904
C	-4.907017	-0.925803	-0.861382
C	-4.218128	0.605238	0.869756
C	-6.168184	-0.333032	-0.878300
C	-5.481293	1.196069	0.844510
C	-6.465718	0.732417	-0.027429
C	5.784860	-2.313044	1.809861
C	7.229255	0.881904	-1.798587
C	-7.229398	-0.882094	-1.797955
C	-5.784702	2.313335	1.809891
F	-4.742760	3.169342	1.915123
F	-6.030684	1.841738	3.052335
F	-6.864049	3.028807	1.431685
F	-8.177715	0.036325	-2.077452
F	-7.855810	-1.946706	-1.246454
F	-6.704305	-1.299635	-2.970159
F	4.743327	-3.169638	1.914472
F	6.029772	-1.841260	3.052443
F	6.864843	-3.027921	1.432363
F	8.177676	-0.036470	-2.077875
F	7.855551	1.946747	-1.247401
F	6.704062	1.299060	-2.970885

4j

B3LYP/6-31G(d)

E_{el} = –2223.72826161

E_{ZPE} = 0.331521

Imaginary Frequencies = 0

B3LYP/6-311+G(d,p)//B3LYP/6-31G(d)

E_{el} = –2224.36026153

Symbol	X	Y	Z
H	-0.422562	-4.185621	0.020352
H	4.475057	-3.167808	-0.021270

H	0.422508	4.185799	0.020667
H	-4.475146	3.168208	-0.020010
H	-1.253224	6.020134	0.012299
H	-3.675441	5.512010	-0.000673
H	3.675434	-5.511686	-0.002137
H	1.253240	-6.019882	0.011345
H	1.714018	1.862512	-0.005118
H	-1.714134	-1.862266	-0.004862
C	-0.363720	1.360664	0.009980
C	0.968908	1.072951	0.007401
C	1.373352	-0.302388	0.018218
C	0.363596	-1.360415	0.009839
C	-0.969031	-1.072702	0.007536
C	-1.373476	0.302641	0.018508
C	2.634303	-0.883761	-0.009101
C	2.473107	-2.341787	-0.025022
C	1.082203	-2.636448	-0.008948
C	-1.082323	2.636694	-0.008573
C	-2.634449	0.884019	-0.008590
C	-2.473239	2.342061	-0.024415
C	0.639286	-3.953568	0.004140
C	3.409986	-3.376022	-0.017499
C	-0.639353	3.953797	0.004627
C	-3.410068	3.376348	-0.016464
C	-1.586379	4.986120	0.003072
C	-2.955160	4.698751	-0.004529
C	2.955130	-4.698446	-0.005677
C	1.586358	-4.985856	0.002210
C	3.923686	-0.176824	-0.007055
C	4.929592	-0.470566	-0.941756
C	4.226458	0.819560	0.935146
C	6.160203	0.178436	-0.943096
C	5.448384	1.485451	0.948921
C	6.421525	1.163247	0.006458
C	-3.923762	0.176973	-0.006264
C	-4.930134	0.470771	-0.940454
C	-4.225954	-0.819816	0.935714
C	-6.160623	-0.178466	-0.941458
C	-5.447743	-1.485941	0.949813
C	-6.421364	-1.163619	0.007893
F	-7.596337	-1.796498	0.013370
F	-5.696338	-2.423539	1.870829

F	-3.331642	-1.151456	1.878717
F	-7.086112	0.126397	-1.857559
F	-4.714794	1.393047	-1.889816
F	3.332600	1.151024	1.878637
F	5.697574	2.422705	1.870126
F	7.596621	1.795903	0.011632
F	7.085268	-0.126335	-1.859656
F	4.713655	-1.392642	-1.891173

APPENDIX C

EXPERIMENTAL DETAILS FOR CHAPTER IV

Cyclic Voltammetry. All electrochemical experiments were conducted in a traditional 3-electrode geometry using a custom made potentiostat. Electrolyte solutions (0.1 M) were prepared from HPLC-grade CH_2Cl_2 and anhydrous Bu_4NOTf, and the solutions were freeze-pump-thaw degassed (3x) prior to analysis. Cyclic voltammetry was conducted under a nitrogen atmosphere. The working electrode was a glassy carbon electrode (3-mm diameter), with a Pt coil counter electrode and Ag wire pseudo reference. The ferrocene/ferrocenium (Fc/Fc^+) couple was used as an internal standard following each experiment. Potential values were re-referenced to SCE using a value of 0.46 (V vs. SCE) for the Fc/Fc^+ couple in CH_2Cl_2. When necessary, potentials were re-referenced to NHE using SCE = –0.24 (V vs. NHE). LUMO and HOMO levels were approximated using SCE = –4.68 eV vs. vacuum.[1] Cyclic voltammetry experiments were conducted at sweep rates of 50 (reported), 75, 100 and 125 mV s^{-1}. All scan rates show quasi-reversible kinetics with no alteration of peak splitting with scan rate. $E_{1,2}$ values were calculated assuming $E_{1/2} \approx E^{o\prime}=(E_{anodic} + E_{cathodic})/2$ based on these observations. The $E_{a,c}$ peak splitting of the Fc/Fc^+ couple was similar to that of the analyte (~90 mV). The anodic peak current increases linearly with the square root of the scan rate in the range 50 to 125 mV s^{-1}, indicating a diffusion-controlled process. Analyte concentrations were ca. 1-5 mM.

X-ray Crystallography. X-ray diffraction intensities were measured on a Bruker Smart Apex diffractometer at 193 K using MoKλ radiation (λ=0.71073Å). Absorption corrections were applied by SADABS.[2] The structure was solved using the direct methods. All non-hydrogen atoms were refined with anisotropic thermal parameters. H atoms were refined in a rigid group model. In the crystal there are two symmetrically independent molecules. ORTEP diagrams of both are given in the Figure 3. All calculations were performed by Bruker SHELXTL package.[3]

Crystal data for **5a**: $C_{38}H_{32}$, M_r=488.64, dark-green block, 0.46 x 0.38 x 0.24 mm. Orthorhombic, space group *Pna*2$_1$, *a*=29.183(3), *b*=9.2281(11), *c*=20.653(2) Å, *V*=5561.8(11) Å^3, *Z*=8, Z'=2, ρ_{calcd}=1.167 g·cm^{-3}, μ= 0.066 mm^{-1}, F(000)=2080, $2\theta_{max}$=57.0°, 57332 reflections collected, 12146 unique [R_{int}=0.0256], *R* indices [$I>2\sigma(I)$]: *R*1=0.0374, *wR*2=0.0985, GOF=1.069.

The non-planarity of the two independent molecules was determined using the following least-squares planes (x,y,z in crystal coordinates) and deviations from them (* indicates atom used to define plane):

4.3196 (0.0187) x + 1.3822 (0.0063) y + 20.1895 (0.0037) z = 7.8349 (0.0116)

* –0.0258 (0.0011) C4
* 0.0200 (0.0011) C5
* 0.0017 (0.0012) C7
* –0.0180 (0.0012) C8
* 0.0120 (0.0012) C9
* 0.0100 (0.0012) C10

Rms deviation of fitted atoms = 0.0165

3.5205 (0.0218) x + 2.0252 (0.0066) y + 19.9945 (0.0045) z = 8.0860 (0.0119)

Angle to previous plane (with approximate esd) = 4.32 (0.05)

* 0.0102 (0.0009) C2
* –0.0189 (0.0009) C3
* 0.0214 (0.0009) C4
* –0.0157 (0.0009) C5
* 0.0031 (0.0009) C6

Rms deviation of fitted atoms = 0.0153

2.9926 (0.0176) x + 2.3434 (0.0053) y + 19.8630 (0.0041) z = 8.1046 (0.0083)

Angle to previous plane (with approximate esd) = 2.26 (0.05)

```
 *  –0.0063 (0.0011)  C1
 *  –0.0076 (0.0010)  C2
 *    0.0213 (0.0010)  C3
 *  –0.0209 (0.0010)  C13
 *    0.0068 (0.0010)  C12
 *    0.0067 (0.0011)  C11

Rms deviation of fitted atoms =    0.0134


3.7821 (0.0226) x + 2.5260 (0.0066) y + 19.6827 (0.0052) z = 8.5374 (0.0095)

Angle to previous plane (with approximate esd) = 1.98 ( 0.05 )

 *  –0.0051 (0.0009)  C12
 *    0.0141 (0.0009)  C13
 *  –0.0184 (0.0009)  C14
 *    0.0158 (0.0009)  C15
 *  –0.0064 (0.0009)  C16

Rms deviation of fitted atoms = 0.0131


4.8233 (0.0242) x + 2.7015 (0.0046) y + 19.4506 (0.0053) z = 9.0197 (0.0094)

Angle to previous plane (with approximate esd) = 2.40 ( 0.06 )

 *    0.0349 (0.0010)  C14
 *    0.0098 (0.0013)  C15
 *  –0.0351 (0.0010)  C16
 *    0.0207 (0.0013)  C17
 *    0.0074 (0.0013)  C18
 *  –0.0378 (0.0011)  C19
    –0.0304 (0.0023)  C20

Rms deviation of fitted atoms =    0.0272


–3.2556 (0.0214) x –1.9088 (0.0069) y + 20.0742 (0.0044) z = 17.1431 (0.0151)

Angle to previous plane (with approximate esd) = 33.24 ( 0.04 )

 *    0.0262 (0.0012)  C4'
 *  –0.0228 (0.0011)  C5'
 *    0.0002 (0.0012)  C7'
```

* 0.0193 (0.0014) C8'
* –0.0158 (0.0014) C9'
* –0.0071 (0.0013) C10'

Rms deviation of fitted atoms = 0.0177

–3.1255 (0.0230) x –2.9084 (0.0071) y + 19.4749 (0.0061) z = 15.6194 (0.0155)

Angle to previous plane (with approximate esd) = 6.43 (0.06)

* –0.0238 (0.0010) C2'
* 0.0313 (0.0010) C3'
* –0.0284 (0.0010) C4'
* 0.0147 (0.0010) C5'
* 0.0061 (0.0010) C6'

Rms deviation of fitted atoms = 0.0228

–1.9125 (0.0198) x - 3.5432 (0.0058) y + 19.0215 (0.0060) z = 15.0547 (0.0123)

Angle to previous plane (with approximate esd) = 4.78 (0.07)

* 0.0157 (0.0013) C1'
* 0.0205 (0.0012) C2'
* –0.0461 (0.0011) C3'
* 0.0354 (0.0011) C13'
* 0.0013 (0.0012) C12'
* –0.0268 (0.0013) C11'

Rms deviation of fitted atoms = 0.0282

–1.1731 (0.0238) x –4.1974 (0.0066) y + 18.3738 (0.0078) z = 14.0602 (0.0150)

Angle to previous plane (with approximate esd) = 4.67 (0.08)

* 0.0190 (0.0010) C12'
* –0.0208 (0.0010) C13'
* 0.0158 (0.0010) C14'
* –0.0047 (0.0010) C15'
* –0.0091 (0.0010) C16'

Rms deviation of fitted atoms = 0.0152

–1.0566 (0.0237) x –4.7133 (0.0040) y + 17.7398 (0.0058) z = 12.9610 (0.0119)

Angle to previous plane (with approximate esd) = 3.66 (0.08)

*	–0.0426 (0.0010)	C14'
*	–0.0327 (0.0013)	C15'
*	0.0562 (0.0010)	C16'
*	–0.0264 (0.0012)	C17'
*	–0.0047 (0.0012)	C18'
*	0.0502 (0.0011)	C19'
	0.0427 (0.0023)	C20'

Rms deviation of fitted atoms = 0.0393

Computational Details. The indeno[2,1-*c*]fluorene scaffold was examined for biradical character. All geometries were minimized in Gaussian 09[4] using DFT B3LYP/6-31+G(d,p)[5] method and verified as stationary points on the potential energy surface as containing no imaginary frequencies. The transition state was characterized as having one imaginary frequency (–51.4021) corresponding to the transition between M and P isomers. The mesityl groups of **5a** were omitted and hydrogen atoms were used in their place (i.e., **5**).

Table S1. Bond lengths (Å) for calculated structure of **5** and X-ray structure of **5a**. There are two columns for the crystallographically independent compounds. The dihedral angle measured is highlighted in blue.

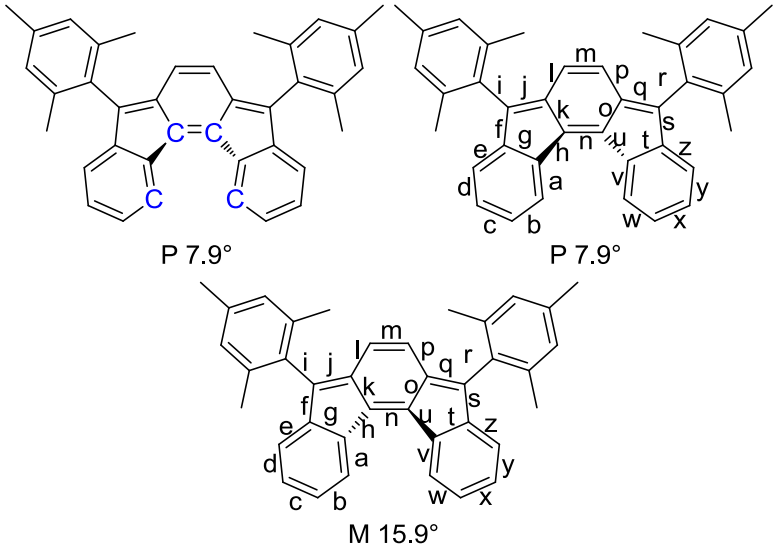

	Calculated Structure of **5**		X-ray Data for **5a**		
bond	B3LYP/6-31+G(d,p), M (10.97° dihedral)	deviation	X-ray average	P (7.9° dihedral)	M (15.9° dihedral)
a	1.392	0.010	1.382	1.380	1.384
b	1.406	0.009	1.397	1.401	1.393
c	1.396	0.011	1.385	1.383	1.387
d	1.403	0.014	1.389	1.396	1.382
e	1.393	0.007	1.387	1.384	1.389
f	1.464	–0.001	1.465	1.467	1.462
g	1.426	0.012	1.414	1.415	1.413
h	1.481	0.003	1.479	1.482	1.475
i	1.486	0.002	1.484	1.484	1.483
j	1.378	0.008	1.370	1.370	1.370
k	1.478	0.005	1.473	1.473	1.473
l	1.438	0.005	1.433	1.429	1.436
m	1.361	0.005	1.356	1.359	1.352
n	1.371	0.006	1.366	1.367	1.364
o	1.478	0.008	1.471	1.471	1.470
p	1.438	0.004	1.434	1.432	1.435
q	1.378	0.005	1.373	1.371	1.375
r	1.486	–0.002	1.488	1.488	1.487
s	1.465	0.002	1.464	1.466	1.461
t	1.426	0.008	1.418	1.414	1.421
u	1.481	0.006	1.476	1.479	1.472
v	1.392	0.008	1.384	1.385	1.383
w	1.406	0.010	1.396	1.395	1.397
x	1.396	0.011	1.386	1.388	1.383
y	1.403	0.014	1.389	1.389	1.389
z	1.393	0.010	1.383	1.382	1.384
	Mean average error	0.007			

Single point energies with a larger basis set reveal that the broken symmetry solution has identical energy to that of the restricted closed shell. Additionally, the square of the spin expectation value is zero for the broken symmetry solution. The broken symmetry

solution was tested for stability and found to be stable. The triplet state is 23.9 kcal mol^{-1} (1.04 eV) above the singlet state.

Table S2. Energies of converged wavefunctions.

Method	energy (hartree)
BS-UB3LYP/6-311+G(2df,2pd)	–769.573507379
RB3LYP/6-311+G(2df,2pd)	–769.573507379
UB3LYP/6-311+G(2df,2pd) triplet	–769.535353266

For determining energies of the states RB3LYP/6-31+G(d,p) minimized structures were used. The open shell (OS) singlet were computed using broken symmetry DFT (BS-UB3LYP/6-311+G(2df,2pd)). Closed shell (CS) and triplet (E_T) energies were calculated using RB3LYP/6-311+G(2df,2pd). OS energies were corrected using the approximate spin projection (AP) method as defined in Equation 1 and 2:[6]

Eq 1. $$J = \frac{E_{OS} - E_T}{\langle S^2 \rangle_T - \langle S^2 \rangle_{OS}}$$

Eq 2. $$E_{AP-OS} = E_{OS} + J \cdot \langle S^2 \rangle_{OS}$$

where J is an effective exchange integral, E_{OS} is the OS singlet energy, E_T is the OS triplet energy, $\langle S^2 \rangle_{OS}$ is the spin expectation value squared for the OS singlet, $\langle S^2 \rangle_T$ is the spin expectation value squared for the triplet, $E_{AP\text{-}OS}$ is the approximate spin projection (AP) energy for the open shell singlet.

Table S3. Calculated energies of states, in hartrees, for M isomer.

E_{CS}	–769.573507379
E_{OS}	–769.573507379
$\langle S^2 \rangle_{OS}$	0.0000
E_T	–769.535353266
$\langle S^2 \rangle_T$	2.0222
J	–0.0188676259

E_{AP-OS}	–769.573507379
E_{CS}-E_{AP-OS}	0.000000000
E_T-E_{CS}	0.038154113

The planar transition state was located and characterized as having one imaginary frequency corresponding to the interconversion between the M and P isomers. The transition state is 0.02 kcal/mol above the ground state.

Figure 2. Energy barrier between M and P [2,1-*c*]IF.

Compound	Electronic energy	Zero point energy	$E_{el} + E_{ZPE}$
TS	–769.384196082	0.251368	–769.132828
M isomer	–769.384504423	0.251651	–769.132853

Table 4. Coordinates for B3LYP/6-31+G(d,p) minimized structures.

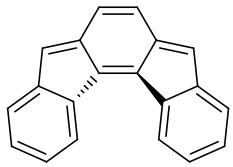

Symbol	X	Y	Z
C	-1.391440	1.882441	0.071051
C	-0.678181	3.132154	0.045797
C	0.678180	3.132156	-0.045690
C	1.391439	1.882444	-0.070986
C	0.684897	0.581311	-0.000297
C	-0.684897	0.581310	0.000320
C	2.740651	1.657153	-0.155321
C	2.994979	0.226873	-0.094417
C	4.199481	-0.473475	-0.096307
C	4.174860	-1.868074	0.051972

C	2.961284	-2.536882	0.217984
C	1.743433	-1.833161	0.212822
C	1.745870	-0.453915	0.028645
C	-2.740652	1.657147	0.155376
C	-2.994979	0.226869	0.094425
C	-1.745870	-0.453915	-0.028657
C	-4.199481	-0.473479	0.096289
C	-1.743433	-1.833154	-0.212883
C	-2.961284	-2.536875	-0.218072
C	-4.174859	-1.868073	-0.052039
H	3.507729	2.419403	-0.236461
H	-1.240137	4.060806	0.085870
H	1.240136	4.060809	-0.085733
H	5.144497	0.053241	-0.197516
H	5.105731	-2.427637	0.053404
H	2.951865	-3.613432	0.359723
H	0.826286	-2.378953	0.384844
H	-3.507730	2.419395	0.236540
H	-5.144498	0.053234	0.197513
H	-0.826285	-2.378939	-0.384923
H	-2.951864	-3.613420	-0.359849
H	-5.105731	-2.427635	-0.053492

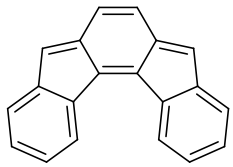

Symbol	X	Y	Z
C	1.389954	1.875456	0.000053
C	0.679013	3.125670	0.000178
C	-0.679067	3.125660	0.000110
C	-1.389986	1.875434	-0.000031
C	-0.686253	0.568095	-0.000029
C	0.686245	0.568100	-0.000045
C	-2.742795	1.663244	-0.000187
C	-3.006147	0.235504	-0.000169
C	-4.219697	-0.448563	-0.000111
C	-4.210519	-1.850605	0.000117
C	-2.999360	-2.542442	0.000254
C	-1.773525	-1.852777	0.000157

C	-1.758885	-0.461283	-0.000073
C	2.742768	1.663304	0.000038
C	3.006150	0.235512	-0.000079
C	1.758891	-0.461282	-0.000178
C	4.219709	-0.448537	0.000062
C	1.773553	-1.852781	-0.000200
C	2.999398	-2.542427	-0.000070
C	4.210547	-1.850577	0.000082
H	-3.505590	2.434013	-0.000272
H	1.244592	4.052953	0.000348
H	-1.244660	4.052934	0.000234
H	-5.159348	0.097100	-0.000210
H	-5.148216	-2.398580	0.000187
H	-2.995590	-3.628294	0.000445
H	-0.862504	-2.431367	0.000162
H	3.505546	2.434091	0.000007
H	5.159354	0.097138	0.000146
H	0.862543	-2.431393	-0.000461
H	2.995644	-3.628278	-0.000075
H	5.148251	-2.398542	0.000213

APPENDIX D

EXPERIMENTAL DETAILS FOR CHAPTER V

Cyclic Voltammetry. All electrochemical experiments were conducted in a traditional 3-electrode geometry using a custom made potentiostat. Electrolyte solutions (0.1 M) were prepared from HPLC-grade CH_2Cl_2 and anhydrous Bu_4NOTf, and the solutions were freeze-pump-thaw degassed (3x) prior to analysis. Cyclic voltammetry was conducted under a nitrogen atmosphere. The working electrode was a glassy carbon electrode (3-mm diameter), with a Pt coil counter electrode and Ag wire pseudo reference. The ferrocene/ferrocenium (Fc/Fc^+) couple was used as an internal standard following each experiment. Potential values were re-referenced to SCE using a value of 0.46 (V vs. SCE) for the Fc/Fc^+ couple in CH_2Cl_2. When necessary, potentials were re-referenced to NHE using SCE = –0.24 (V vs. NHE). LUMO and HOMO levels were approximated using SCE = –4.68 eV vs. vacuum.[1] Cyclic voltammetry experiments were conducted at sweep rates of 50 (reported), 75, 100 and 125 mV s^{-1}. All scan rates show quasi-reversible kinetics with no alteration of peak splitting with scan rate. $E_{1,2}$ values were calculated assuming $E_{1/2} \approx E^{o\prime}=(E_{anodic} + E_{cathodic})/2$ based on these observations. The $E_{a,c}$ peak splitting of the Fc/Fc^+ couple was similar to that of the analyte (~90 mV). The anodic peak current increases linearly with the square root of the scan rate in the range 50 to 125 mV s^{-1}, indicating a diffusion-controlled process. Analyte concentrations were ca. 1-5 mM.

X-ray Crystallography. X-ray diffraction intensities were measured on a Bruker Smart Apex diffractometer at 100 K using MoKλ radiation (λ=0.71073Å). Absorption corrections were applied by SADABS.[2] The structure was solved using the direct methods. All non-hydrogen atoms were refined with anisotropic thermal parameters. H atoms were refined in a rigid group model. In the crystal there are two symmetrically independent molecules. ORTEP diagrams of both are given in the Figure 3. All calculations were performed by Bruker SHELXTL package.[3]

Crystal Data for 2a. $C_{40}H_{50}SSi_2$, M_r = 619.04, 0.25 x 0.12 x 0.02 mm^3, triclinic,

P-1, a = 8.3989(9) Å, b = 12.4017(10) Å, c = 17.7936(19) Å, α= 88.626(6)°, β= 88.890(8)°, γ = 81.912(6)°, V = 1834.2(3) Å^3, Z = 2, ρ_{calcd} = 1.121 Mg/m^3, μ = 1.585 mm^{-1}, θ_{max} = 67.29˚, T = 100(2) K, 22289 measured reflections, 6439 independent reflections [R_{int} = 0.0405], 388 independent refined parameters, $R1$ = 0.0395, $wR2$ = 0.0997 (with $I > 2\sigma(I)$), $R1$ = 0.0511, $wR2$ = 0.1071 (all data), GOF = 1.031, max/min residual electron density 0.383/-0.282 e Å^{-3}.

Crystal Data for 6. $C_{18}H_8O_2S$, M_r = 288.03, 0.16 x 0.12 x 0.08 mm^3, orthorhombic, Pca2(1), a = 15.913(6) Å, b = 11.398(4) Å, c = 6.921(2) Å, α= 90(6)°, β= 90°, γ = 90°, V = 1255.4(8) Å^3, Z = 4, ρ_{calcd} = 1.525 Mg/m^3, μ = 0.258 mm^{-1}, θ_{max} = 26.00˚, T = 100(2) K, 5496 measured reflections, 2112 independent reflections [R_{int} = 0.0608], 191 independent refined parameters, $R1$ = 0.0529, $wR2$ = 0.1001 (with $I > 2\sigma(I)$), $R1$ = 0.0960, $wR2$ = 0.1145 (all data), GOF = 1.038, max/min residual electron density 0.308/-0.434 e Å^{-3}.

Computational Details. Structures were minimized using the B3LYP[4] method and cc-pVTZ basis set. All energies are given in Hartrees.

APPENDIX E

EXPERIMENTAL DETAILS FOR CHAPTER VI

Cyclic Voltammetry. All electrochemical experiments were conducted in a traditional 3-electrode geometry using a custom made potentiostat. Electrolyte solutions (0.1 M) were prepared from HPLC-grade CH_2Cl_2 and anhydrous Bu_4NOTf, and the solutions were freeze-pump-thaw degassed (3x) prior to analysis. Cyclic voltammetry was conducted under a nitrogen atmosphere. The working electrode was a glassy carbon electrode (3-mm diameter), with a Pt coil counter electrode and Ag wire pseudo reference. The ferrocene/ferrocenium (Fc/Fc^+) couple was used as an internal standard following each experiment. Potential values were re-referenced to SCE using a value of 0.46 (V vs. SCE) for the Fc/Fc^+ couple in CH_2Cl_2. When necessary, potentials were re-referenced to NHE using SCE = –0.24 (V vs. NHE). LUMO and HOMO levels were approximated using SCE = –4.68 eV vs. vacuum.[1] Cyclic voltammetry experiments were conducted at sweep rates of 50 (reported), 75, 100 and 125 mV s^{-1}. All scan rates show quasi-reversible kinetics with no alteration of peak splitting with scan rate. $E_{1,2}$ values were calculated assuming $E_{1/2} \approx E^{o\prime}=(E_{anodic} + E_{cathodic})/2$ based on these observations. The $E_{a,c}$ peak splitting of the Fc/Fc^+ couple was similar to that of the analyte (~90 mV). The anodic peak current increases linearly with the square root of the scan rate in the range 50 to 125 mV s^{-1}, indicating a diffusion-controlled process. Analyte concentrations were ca. 1-5 mM.

X-ray Crystallography. X-ray diffraction intensities were measured on a Bruker Smart Apex diffractometer at 100 K using MoKλ radiation (λ=0.71073Å). Absorption

corrections were applied by SADABS.[2] The structure was solved using the direct methods. All non-hydrogen atoms were refined with anisotropic thermal parameters. H atoms were refined in a rigid group model. In the crystal there are two symmetrically independent molecules. ORTEP diagrams of both are given in the Figure 3. All calculations were performed by Bruker SHELXTL package.[3]

Crystal data for 5c. $C_{38}H_{32}$, M_r = 488.64, 0.46 x 0.38 x 0.24 mm, orthorhombic, space group $Pna2_1$, a = 29.183(3), b = 9.2281(11), c = 20.653(2) Å, V = 5561.8(11) Å^3, Z = 8, Z' = 2, ρ_{calcd} = 1.167 g·cm^{-3}, μ = 0.066 mm^{-1}, T = 173(2), F(000) = 2080, $2\theta_{max}$ = 57.0°, 57332 reflections collected, 12146 unique [R_{int}=0.0256], R indices [$I>2\sigma(I)$]: $R1$=0.0374, $wR2$ = 0.0985, GOF = 1.069.

Crystal Data for 6a. $C_{46}H_{54}SSi_2$, M_r = 663.07, 0.19 x 0.16 x 0.02 mm, monoclinic, space group C2/c, a = 32.5578(19) Å, b = 12.0117(7) Å, c = 22.2964(13) Å, α= 90°, β= 116.1810(10)°, γ = 90°, V = 7825.0(8) Å^3, Z = 8, ρ_{calcd} = 1.126 Mg/m^3, μ = 0.121 mm^{-1}, T = 173(2) K, $2\theta_{max}$ = 48.0, 34031 measured reflections, 6142 independent reflections [R_{int} = 0.0475], 433 independent refined parameters, $R1$ = 0.0911, $wR2$ = 0.1892 (with $I > 2\sigma(I)$), $R1$ = 0.0916, $wR2$ = 0.1923 (all data), GOF = 1.250, max/min residual electron density 0.578/-0.300 e Å^{-3}.

Crystal Data for 7a. $C_{40}H_{50}SSi_2$, M_r = 619.04, 0.25 x 0.12 x 0.02 mm, triclinic, space group P-1, a = 8.3989(9) Å, b = 12.4017(10) Å, c = 17.7936(19) Å, α= 88.626(6)°, β= 88.890(8)°, γ = 81.912(6)°, V = 1834.2(3) Å^3, Z = 2, ρ_{calcd} = 1.121 Mg/m^3, μ = 1.585 mm^{-1}, T = 100(2) K, $2\theta_{max}$ = 134.58, 22289 measured reflections, 6439 independent reflections [R_{int} = 0.0405], 388 independent refined parameters, $R1$ = 0.0395, $wR2$ =

0.0997 (with $I > 2\sigma(I)$), $R1$ = 0.0511, $wR2$ = 0.1071 (all data), GOF = 1.031, max/min residual electron density 0.383/-0.282 e $Å^{-3}$.

Crystal Data for 10. $C_{18}H_8O_2S$, M_r = 288.03, 0.16 x 0.12 x 0.08 mm, orthorhombic, space group *Pca*2(1), a = 15.913(6) Å, b = 11.398(4) Å, c = 6.921(2) Å, α= 90(6)°, β= 90°, γ = 90°, V = 1255.4(8) $Å^3$, Z = 4, ρ_{calcd} = 1.525 Mg/m^3, μ = 0.258 mm^{-1}, T = 100(2) K, $2\theta_{max}$ = 52.00°, 5496 measured reflections, 2112 independent reflections [R_{int} = 0.0608], 191 independent refined parameters, $R1$ = 0.0529, $wR2$ = 0.1001 (with $I > 2\sigma(I)$), $R1$ = 0.0960, $wR2$ = 0.1145 (all data), GOF = 1.038, max/min residual electron density 0.308/-0.434 e $Å^{-3}$.

Computational Details. Structures were minimized using the B3LYP[4] method and cc-pVTZ basis set. All energies are given in Hartrees.

APPENDIX F

EXPERIMENTAL DETAILS FOR OTHER UNPUBLISHED COMPOUNDS

This appendix contains information about a small number of unpublished compounds that I envisioned and for which I developed synthetic routes. It also contains limited characterization for these compounds.

5,11-dibromoindeno[1,2-b]fluorene-6,12-dione. The synthetic route for this compound is depicted in Scheme 1. The initial iodination step used a known synthetic method that hadn't yet been tried on this substrate.[1]

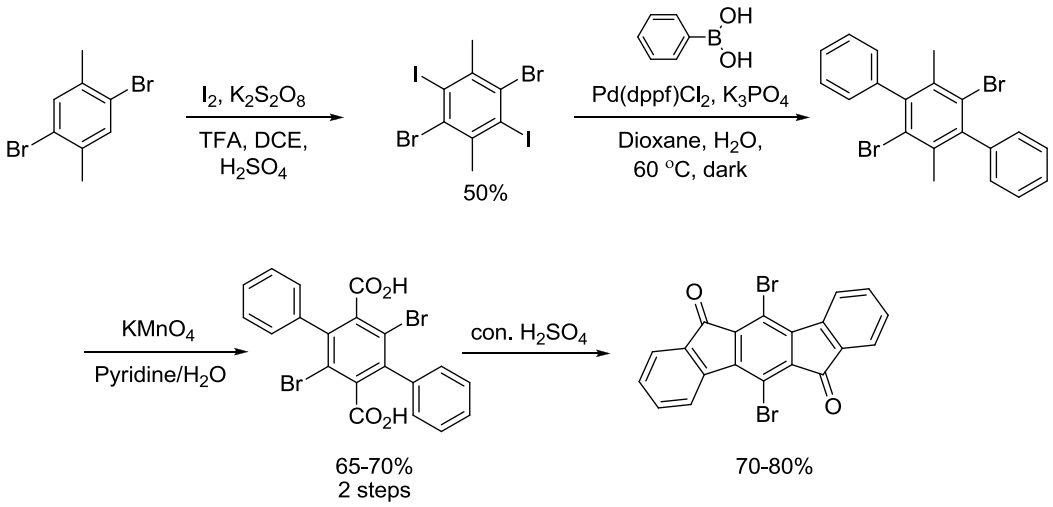

Scheme 1. Synthesis of 5,11-dibromoindeno[1,2-*b*]fluorene-6,12-dione.

2,8-difluoro-5,11-dibromoindeno[1,2-b]fluorene-6,12-dione. The synthetic route for this compound is depicted in Scheme 2.

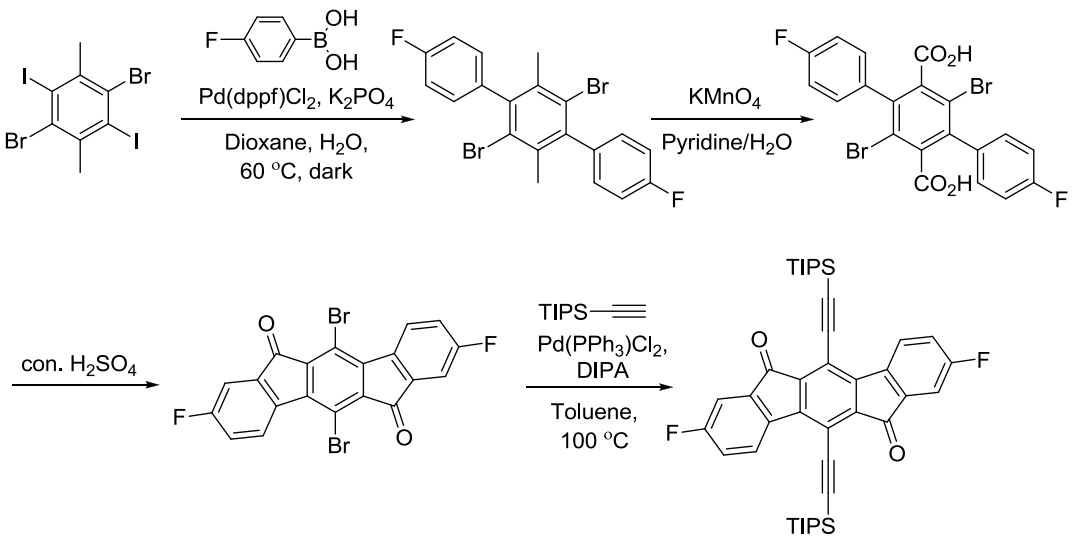

Scheme 2. Synthesis of 2,8-difluoro-5,11-dibromoindeno[1,2-b]fluorene-6,12-dione and 2,8-difluoro-5,11-bis(triisopropylsilylethynyl)-[1,2-b]fluorene-6,12-dione.

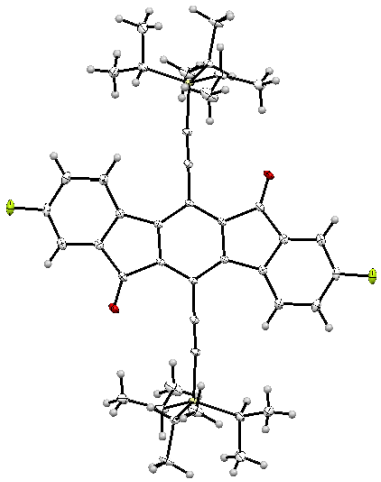

Figure 1. Crystal structure of 2,8-difluoro-5,11-bis(triisopropylsilylethynyl)-[1,2-b]fluorene-6,12-dione with ellipsoids drawn at the 30% probability level..

Crystal Data for 2,8-difluoro-5,11-bis(triisopropylsilylethynyl)-[1,2-b]fluorene-6,12-dione. $C_{21}H_{12}FOSi$, M_r = 339.49, 0.42 x 0.21 x 0.07 mm, triclinic, space group *P*-1, *a* = 7.5322(6) Å, *b* = 7.5937(6) Å, *c* = 16.6082(14) Å, α= 83.400(2)°, β= 88.824(2)°, γ = 81.793(2)°, *V* = 933.98(13) Å^3, *Z* = 2, ρ_{calcd} = 1.207 Mg/m^3, μ = 0.139 mm^{-1}, *T* = 100(2) K, $2\theta_{max}$ = 56°, 14435 measured reflections, 4395 independent reflections [R_{int} = 0.0224], 313 independent refined parameters, *R*1 = 0.0356, *wR*2 = 0.0920 (with $I > 2\sigma(I)$), *R*1 = 0.0383, *wR2* = 0.0945 (all data), GOF = 1.031, max/min residual electron density 0.413/-0.206 e Å^{-3}.

APPENDIX G

EMISSION FROM REGIOISOMERIC BIS(PHENYLETHYNYL)BENZENES DURING PULSE RADIOLYSIS

This appendix contains the first paper that I contributed to in this graduate program. I performed the synthesis for approximately one third of the studied compounds. Torben Ryhding and Brittany M. Armstrong performed synthesis of the other compounds. The pulse radiolysis experiments and the writing of the paper were the contributions of the following authors: Shingo Samori, Sachiko Tojo, Mamoru Fujitsuka, Michael M. Haley, and Tetsuro Majima

Introduction

Electron detachment from and attachment to a solute molecule (M) generates a radical cation ($M^{\bullet+}$) and anion ($M^{\bullet-}$), respectively. $M^{\bullet+}$ and $M^{\bullet-}$ are known as important ionic intermediates in photochemistry, electrochemistry, and radiation chemistry.[1] It is well-known that M in the excited states (M* = ^{1}M* (excited singlet state) and ^{3}M* (excited triplet state)) can be formed by charge recombination between $M^{\bullet+}$ and $M^{\bullet-}$ ($M^{\bullet+} + M^{\bullet-} \rightarrow M^* + M$), after which ^{1}M* deactivates to M in the ground state by emitting light ($^1M^* \rightarrow M + h\nu_{fl}$).[2] This process is significant for optoelectronic materials such as OLEDs because electrochemical energies can be converted to photochemical energies.

Recently, we have found that various π-conjugated compounds showed emission during pulse radiolysis in benzene (Bz).[3] In pulse radiolysis of M in Bz, the ionization of Bz to give Bz radical cation ($Bz^{\bullet+}$) and formation of an electron (e^-) occur at the same time, which react with M to give $M^{\bullet+}$ and $M^{\bullet-}$, respectively. In our previous work, we have proposed that the charge recombination of $M^{\bullet+}$ and $M^{\bullet-}$ gives ^{1}M* and/or $^1M_2$* as

the emissive species for the organic electrochemiluminescent molecules such as phenylquinolinylethynes,[3a] phenyl(9-acridinyl)ethynes,[3b] phenyl(9-cyanoanthracenyl)ethynes,[3b,3d] arylethynylpyrenes,[3c] 9-cyano-10-(*p*-substituted phenyl)anthracenes,[3e] and 1,2,4,5-tetrakis(arylethynyl)benzenes (TAEBs).[3f,3g]

For optoelectronic applications, organic compounds possessing a high degree of π-conjugation with donor and/or acceptor groups have been recognized as ideal materials.[4-6] Changes in the substituents and substitution pattern, electronic structure, and conjugation can provide highly variable photophysical properties for such materials. As a class of π-conjugated molecules with remarkable optoelectronic properties, functionalized phenylacetylene structures have received considerable attention because of their characteristic conjugated pathways.[6-8] In particular, 1,4-, 1,3-, and 1,2-bis(phenylethynyl)benzenes (bPEBs = ***n*a**, ***n*b**, and ***n*c**) containing both donor and acceptor functionality are an ideal class of molecules for studying the differences between the linear- (path i), cross- (path ii), and "bent" conjugated (path iii) pathways to gain a better understanding of the geometric aspects of the charge-transfer pathways (Figure 1). By varying the substitution pattern of the donor or acceptor substituted phenylacetylene group at the central benzene ring, each charge-transfer pathway can be modified. Therefore, the donor-acceptor type bPEB structures can avoid the complexity of the charge transfer pathways observed in TAEB structures having two-donor and two-acceptor groups. In addition, the HOMO-LUMO energy gap of neutral **1a** and **1c** have reported to be 7.043 and 6.874 eV, respectively, which are much lower than that of **1b** (7.338 eV).[9] This feature indicates that the emission wavelength of the bPEB structure dramatically changes with the different types of branching. Consequently, we can easily

fine-tune the emission wavelength and intensity by changing the various types of donor and acceptor substituents and the substitution pattern of the central arene. Some of these compounds are expected to be useful for OLED materials because of the sufficiently large fluorescent quantum yield (Φ_{fl}) and excess energy value ($-\Delta H^{o} - E_{S1}$) (details are discussed below). In addition, bPEB structures can rotate freely about their C–C single bonds,[3f,3g] decreasing π-orbital overlap, and thus formation of the face-to-face excimer structure with less luminescence intensity cannot be expected. The time-resolved transient absorption and emission measurements during the pulse radiolysis of various bPEBs are useful to gain a better understanding of the emission mechanism, providing valuable information for molecular design with efficient luminescence character.

In this paper, we report the emission from the charge recombination $bPEB^{\bullet+}$ and $bPEB^{\bullet-}$ of 21 different bPEB derivatives (***n*a**, ***n*b**, and ***n*c**; n = 1-7): non-substituted (**1a-c**), methyl-substituted (**2a-c**), methoxy-substituted (**3a-c**), cyano-substituted (**4a-c**), methyl- and cyano-substituted (**5a-c**), methoxy- and cyano-substituted (**6a-c**), and dimethylamino- and cyano-substituted bPEBs (**7a-c**). When a number (n) is the same, 1,4- (***n*a**), 1,3- (***n*b**), and 1,2-bPEBs (***n*c**) are regioisomers (Figure 1). The detailed study of 21 different kinds of bPEBs potentially leads to customization of optical band gaps and luminescent efficiency for specialized materials applications.

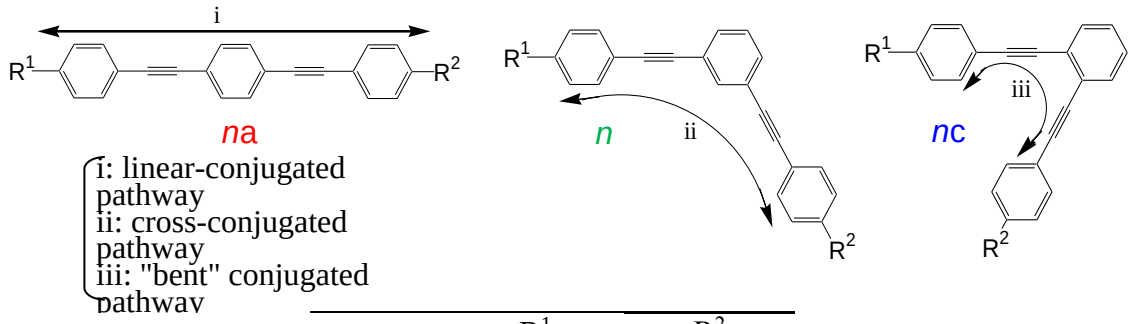

n	R^1	R^2
1	H	H
2	Me	H
3	OMe	H
4	CN	H
5	Me	CN
6	OMe	CN
7	NMe_2	CN

Figure 1. Chemical structures of bis(phenylethynyl)benzene derivatives (bPEBs). Arrows (i-iii) show three type of charge transfer conjugated pathways in bPEBs.

Results and Discussion

Synthesis. Of the 21 bPEBs in this study, compounds **1a-c**,[10] **2a**,[11] **3a-c**,[12] **4a**,[13] **6a**,[14] and **7a**[14] have been previously described in the literature. The other eleven bPEB structures were synthesized by sequential Sonogashira reactions using 1,2-, 1,3-, or 1,4-bromoiodobenzene as the core arene, illustrated for **6c** in Scheme 1. Cross-coupling 4-ethynylanisole to 1-bromo-2-iodobenzene afforded bromoarene **8c**. This was in turn cross-coupled to 4-ethynylbenzonitrile using the more reactive catalytic system ($PdCl_2(PhCN)_2$/*t*-Bu_3P) first reported by Buchwald and Fu,[15] furnishing bPEB **6c** in 36% yield for the two steps. The remaining ten bPEBs were prepared analogously in ca. 20-40% unoptimized yield (see Supporting Information).

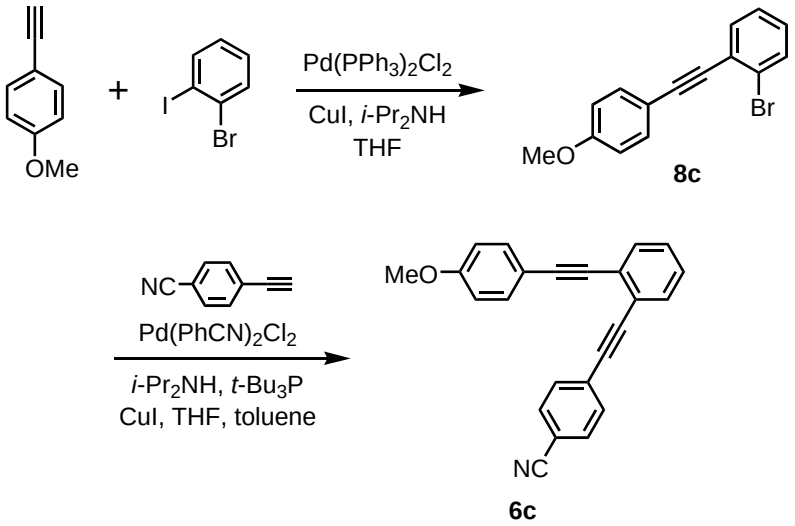

Scheme 1. Synthesis of bPEB **6c**.

Steady-state Spectral Properties of bPEB. Normalized steady-state absorption and fluorescence spectra of bPEB in Bz are shown in Figure 2. It seems that the electronic structures of bPEB strongly depend on the substitution pattern of the phenylacetylene group because the regioisomers (*ortho*-, *meta*-, and *para*-substituted isomers) have similar spectral shapes. It is well-known that the *meta* branching type **1b** disrupts the π-conjugation; thus, the absorption spectra of **1b** is predicted to resemble the absorption spectrum of diphenylacetylene (DPA).[16] A comparison of the absorption spectra of DPA and **1b** show that, indeed, this is the case: the spectrum of **1b** reproduces the spectral width and vibronic structure displayed by DPA. In contrast, when substitution occurs at the *para* position (**1a**), the absorption band edge is red-shifted by 30 nm with respect the band edge of **1b** and appears at 355 nm. The relatively large red shift and loss of the sharp vibronic structure reflect the π-electron delocalization over the linear three-ring chain. The *ortho* branching type **1c** exhibits an absorption band edge at 350 nm, which confirms that π-electron delocalization occurs over the bent three-ring chain, although the red shift is somewhat smaller than **1a**. Compared to neutral **1**, donor

type **2** and **3**, and acceptor type **4**, the corresponding absorption bands of donor-acceptor-substituted bPEBs **5-7** are broadened and show further bathochromic shifts, indicating the intramolecular charge transfer (ICT) from the donor to the acceptor for the HOMO-LUMO transition.[7]

Fluorescence was observed for all bPEBs (Figure 2). Compared to neutral **1**, donor-acceptor type **5-7** showed a large red-shift in the fluorescence maxima in Bz. This again indicates ICT character for donor-acceptor-substituted bPEB in the S_1 state (Table 1). **5-7** showed strong fluorescence solvatochromism, experiencing bathcromic shifts in switching to the more polar solvent such as CH_3CN. This also indicates the ICT character for the donor-acceptor substituted bPEBs in the S_1 state. It should be noted that the fluorescence maxima of neutral **1** increase in the following order, **1b** (331 nm) < **1c** (346 nm) < **1a** (351 nm), while those of donor-acceptor-type **7** increase in the following order, **7b** (452 nm) < **7a** (462 nm) < **7c** (490 nm). This result clearly indicates that the bent-conjugated charge transfer pathway (path iii) leads the fluorescence band to longer wavelength than the linear-conjugated charge transfer pathway (path i). Compared to cross- (path ii) and bent-conjugated (path iii) charge transfer pathways, it seems that the linear conjugated charge transfer pathway (path i) leads a slight red-shift when bPEB has both donor and acceptor substituents. Consequently, it is clearly evident that the difference in the charge transfer conjugated pathways between donor and acceptor substituents strongly influences the HOMO-LUMO energy gap, although we cannot clearly investigate this due to the complexity of the charge transfer pathways observed in TAEB structures in our previous reports.[3f,g,7,8]

The fluorescence quantum yield (Φ_{fl}) values of the bPEBs range from 0.065 to 0.99, and showed the tendency for *para* (0.39-0.99), *ortho* (0.34-0.63), and *meta* isomers (0.065-0.63), in decreasing order. Recently, it was reported that there was a correlation between the Φ_{fl} and the magnitude (A_π) of the π-conjugation length in the excited singlet state for various π-conjugated hydrocarbons including **1a**, **1b**, and non-substituted TAEB.[17] The relationship between Φ_{fl} and A_π is expressed by the following simple equation,

$$\Phi_{fl} = 1 / \exp(-A_\pi) + 1 \qquad (1).$$

As mentioned above, the *meta* branching disrupts the π-electron conjugation; thus, the A_π value of ***n*b** should be smaller than those of ***n*a** and ***n*c**. The lower Φ_{fl} value of ***n*b** can be reasonably explained by eq 1. On the other hand, for the *para* type ***n*a**, the π-electrons are delocalized over the whole molecule, indicating the A_π value of ***n*a** should be larger than those of the others. Although the π-electron delocalization also occurs in *ortho* type ***n*c**, the degree of the π-conjugation is assumed to be smaller than ***n*a**. As a result, the Φ_{fl} value of ***n*c** is midway between those of ***n*a** and ***n*b**. The lower Φ_{fl} value of **7** than the others can be explained by the energy-gap law.[18] From the intersection point of the absorption and fluorescence spectra, the excitation energies of **7a**, **7b**, and **7c** (E_{S1} = 2.94, 3.18, and 2.88 eV, respectively) are estimated to be smaller than those of other bPEBs (3.33-3.97 eV). The increase of internal conversion rate is expected and responsible for the low Φ_{fl} values of **7**. The Φ_{fl} value of **3b** is exceptionally-low (0.065). Methoxy groups are not known to quench fluorescence in fluorescent molecules, such as

in stilbenes,[19a] coumarins,[19b,c] quinolinones,[19c] and fluoranthenes.[19d] The reason for the strong fluorescence quenching of **3b** is still unclear.

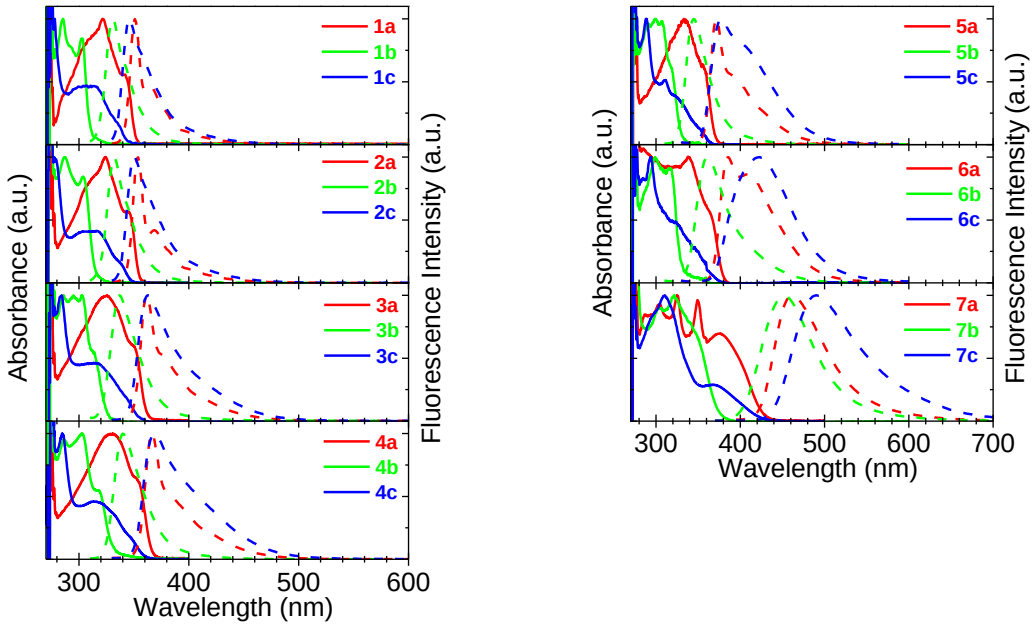

Figure 2. Absorption (solid line) and fluorescence (broken line) spectra observed by the steady-state measurement of bPEB in Ar-saturated Bz. All solutions were prepared at a dilute concentration (10^{-5} M).

Table 1. Emission properties of bPEB in Ar-saturated Bz.

bPEB	a		b		c	
	λ^{Fl} (nm)	Φ_{fl}	λ^{Fl} (nm)	Φ_{fl}	λ^{Fl} (nm)	Φ_{fl}
1	351	0.90	331	0.25	346	0.34
2	354	0.93	332	0.22	350	0.44
3	362	0.82	337	0.065	363	0.63
4	367	0.93	340	0.54	369	0.61
5	372	0.99	345	0.63	377	0.60
6	386	0.85	361	0.63	422	0.50
7	462	0.39	452	0.29	490	0.34

Emission Generated from Charge Recombination between bPEB$^{\bullet+}$ and bPEB$^{\bullet-}$. Emission spectra were observed after an electron pulse during the pulse radiolysis of bPEB in Ar-saturated Bz (1.0 mM) (Figure 3). According to previous reports,[3] the emission of M indicates the generation of ^{1}M* by charge recombination of M$^{\bullet+}$ and M$^{\bullet-}$ during pulse radiolysis in Bz. When N_2O gas was added to the solution as the electron scavenger, the emission intensity observed during the pulse radiolysis of bPEB in Bz was reduced. This result clearly indicates that bPEB$^{\bullet+}$ and bPEB$^{\bullet-}$ are responsible to the emission during the pulse radiolysis. The same emission mechanism was assumed for bPEB as shown the following (Scheme 2).

$$Bz \rightarrow e^- + Bz^{\bullet+}$$

$$Bz^{\bullet+} + e^- \rightarrow Bz^*$$

$$Bz^{\bullet+} + bPEB \rightarrow bPEB^{\bullet+}$$

$$e^- + bPEB \rightarrow bPEB^{\bullet-}$$

$$bPEB^{\bullet+} + bPEB^{\bullet-} \rightarrow {}^1bPEB^* + bPEB \text{ and } {}^3bPEB^* + bPEB \text{ (within pulse duration (8 ns))}$$

$$^1bPEB^* \rightarrow bPEB + h\nu_{fl} \; (\tau_{fl} < 8 \text{ ns})$$

Scheme 2. Proposed mechanism of the emission during the pulse radiolysis of bPEB in Bz. For donor-acceptor-substituted bPEBs (**5-7**), ^{1}bPEB* = ^{1}(A$^{\bullet-}$-D$^{\bullet+}$)* (ICT state).

Little or no emission was observed during the pulse radiolysis of bPEB in 1,2-dichloroethane (DCE) or *N,N*-dimethylformamide (DMF), indicating that bPEB$^{\bullet+}$ and bPEB$^{\bullet-}$ do not emit light. In other words, both bPEB$^{\bullet+}$ and bPEB$^{\bullet-}$ must be formed at the same time in order to emit light. In Bz, no transient absorption band of bPEB$^{\bullet+}$ and bPEB$^{\bullet-}$ was observed immediately after an 8 ns electron pulse. Therefore, it is assumed that bPEB$^{\bullet+}$ and bPEB$^{\bullet-}$ immediately recombine to give ^{1}bPEB* and ^{3}bPEB*, and

^{1}bPEB* emits light within a pulse duration. The transient absorption spectra observed during the pulse radiolysis of bPEB in Ar-saturated Bz can be assigned to ^{3}bPEB* (triplet-triplet absorption).

Because of the considerable repulsion between the substituents induced by the rotation around C–C single bonds, a π-stacked structure cannot be formed for the interaction between bPEB$^{\bullet+}$ and bPEB$^{\bullet-}$. Therefore, bPEB showed only monomer emission, although some electrochemiluminescent molecules showed both monomer and excimer emissions with less luminescence intensity during pulse radiolysis as mentioned in previous reports.[3]

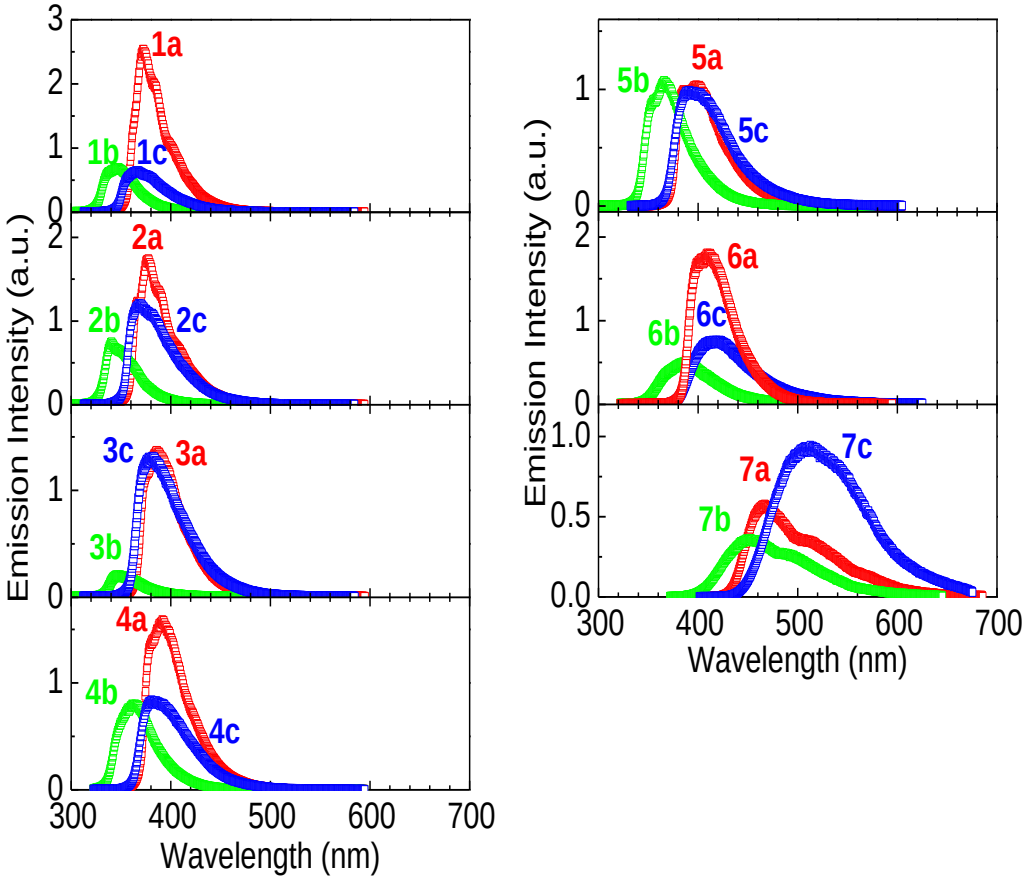

Figure 3. Emission spectra observed in the time range of 0-100 ns during pulse radiolysis of bPEB in Ar-saturated Bz (10^{-3} M).

Compounds **1-7** showed emission peaks at 373-513 nm during the pulse radiolysis (Figures 2). The shape of the emission spectra of bPEB was similar to those observed in the steady-state measurements, although the emission spectra of bPEB were observed at the slightly longer wavelength due to the self absorption as a result of the high concentrations.[3] Therefore, the formation of ^{1}bPEB* with ICT character can be assumed for **5-7** during pulse radiolysis. The intensity (*I*) of the radiolysis induced emission spectra of **1-7** were determined from the total amount of the emission observed during pulse radiolysis and summarized in Tables 2.

Table 2. Emission maxima (λ_{max}^{Em}) and relative emission intensities (*I*) during pulse radiolysis of bPEB in Ar-saturated Bz (1.0 mM).

	a		**b**		**c**	
bPEB	λ_{max}^{Em} (nm)	I [a]	λ_{max}^{Em} (nm)	I	λ_{max}^{Em} (nm)	I
1	373	100	348	35.2	365	35.0
2	378	73.5	341	34.0	368	64.3
3	386	64.6	348	9.92	382	71.0
4	392	74.1	361	42.5	381	46.5
5	398	53.1	366	57.7	391	59.0
6	409	85.0	386	31.1	421	45.6
7	467	30.4	453	23.9	513	56.4

[a] *I* values of bPEB were determined from the total amount of the emission spectra observed during pulse radiolysis. Relative to *I* value of **1a** in Ar-saturated Bz.

Table 3. Electrochemical properties of bPEBs in CH_3CN, and annihilation enthalpy changes ($-\Delta H°$), E_{S1}, and ($-\Delta H° - E_{S1}$) of bPEBs in Bz.

bPEB	E_{ox} (V)	E_{red} (V)	$-\Delta H°$ (eV)	E_{S1} (eV)	$-\Delta H°-E_{S1}$ (eV)
	in CH_3CN		in Bz		
1a	1.38 [a]	–2.35 [a]	3.92	3.54	+0.38
1b	1.65	–2.52	4.36	3.97	+0.39
1c	1.69	–2.38	4.26	3.68	+0.58
2a	1.45	–2.30	3.94	3.54	+0.40
2b	1.62	–2.52	4.33	3.97	+0.36
2c	1.56	–2.37	4.10	3.67	+0.43
3a	1.25	–2.35	3.79	3.46	+0.33
3b	1.32	–2.48	3.99	3.88	+0.11
3c	1.33	–2.39	3.91	3.56	+0.35
4a	1.57	–2.17	3.93	3.44	+0.49
4b	1.74	–2.36	4.29	3.82	+0.47
4c	1.69	–2.22	4.10	3.54	+0.56
5a	*b*	*b*	-	3.37	-
5b	1.63	–2.39	4.21	3.82	+0.39
5c	1.60	–2.28	4.07	3.46	+0.61
6a	1.27	–2.24	3.70	3.33	+0.37
6b	1.32	–2.39	3.90	3.76	+0.14
6c	1.34	–2.28	3.81	3.36	+0.45
7a	0.60	–2.26	3.05	2.94	+0.11
7b	0.60	–2.36	3.15	3.14	+0.01
7c	0.59	–2.28	3.06	2.88	+0.18

To elucidate the emission mechanism of the bPEBs, we estimated the annihilation enthalpy change ($-\Delta H°$) value for the charge recombination between $M^{\bullet+}$ and $M^{\bullet-}$. This $-\Delta H°$ value is a criterion for whether $^1M^*$ can be formed by the charge recombination or not.[2] $-\Delta H°$ is calculated by equation (2),[20]

$$-\Delta H° = [(E_{ox} - E_{red})]^{\varepsilon_s} - \Delta G_{sol}{}^{\varepsilon_s} - w_{a,\mu} + T\Delta S°, \qquad (2)$$

where E_{ox} and E_{red} are the oxidation and reduction potentials of M**,** respectively. ε_s, ΔG_{sol}, and $w_{a,\mu}$ represent the static dielectric constant of solvent, the free energy change of solvation, and the work required to bring $M^{\bullet+}$ and $M^{\bullet-}$ within a likely separation distance, respectively. For bPEB in Bz, $-\Delta H°$ can be expressed using E_{ox} and E_{red} measured in CH_3CN by simplified equation (3),[3]

$$-\Delta H° = E_{ox} - E_{red} + 0.19 \text{ eV} \quad (3).$$

The calculated $-\Delta H°$ values for bPEB are listed in Table 3, together with their oxidation and reduction potentials, and E_{S1} values. $-\Delta H^o$ values for all bPEBs (3.05-4.36 eV) are consistently larger than their E_{S1} values (2.88-3.97 eV), indicating that the energy available in the charge recombination is sufficient to populate all bPEBs in the S_1 states.

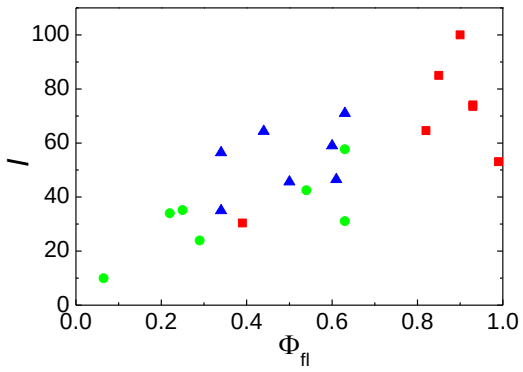

Figure 4. Plots of *I* value vs. Φ_{fl} for ***n*a** (red square), ***n*b** (green circle), and ***n*c** (blue triangle) in Bz.

As shown in Figure 4, the *I* value seems proportional to Φ_{fl}. However, the *I* value of some bPEBs deviates from the fitted line. The decrease of the *I* value were explained by the self-absorption. In our previous paper,[3] the energy differences between $-\Delta H^o$ and E_{S1} ($-\Delta H^o - E_{S1}$ (= +0.01-0.61 eV)) were also assumed as one of the key factors for the *I*

value of Ms. Therefore, these deviated plots are assumed to depend on not only Φ_{fl} and the amount of the self absorption but also the $(-\Delta H^{o} - E_{S1})$ value.

Fine-tuning of the Emission Color and Intensity by Changing the Substitution Pattern of Donor-acceptor-subsituted bPEB. Donor-acceptor-substituted bPEBs ***n*a**, ***n*b**, and ***n*c** (*n* = 5-7) can contain the conjugated pathways: linear- (path i), cross- (path ii), and "bent" conjugated (path iii) pathways, respectively, as shown in Figure 1. The emission spectra of ^{1}bPEB* with ICT character depends on the substitution pattern by the steady-state measurement and during the pulse radiolysis as shown in Figures 2 and 3, respectively. The radiolysis induced emission spectra of all bPEBs showed emission bands in the region of wavelength where the fluorescence bands were observed by the steady-state measurements. For **5-7**, therefore, the charge recombination between bPEB$^{\bullet+}$ and bPEB$^{\bullet-}$ generates ^{1}bPEB* with ICT character as shown in Scheme 3. The results also indicate that the difference in the charge transfer conjugated pathways strongly influences the HOMO-LUMO energy gap: the bent-conjugated charge transfer pathway (path iii) leads the fluorescence band to longer wavelength than the linear- (path i) and cross conjugated (path ii) charge transfer pathways when bPEB has both donor and acceptor substituents. Consequently, it is evident that judicious choice of the donor/acceptor unit permits control of the HOMO-LUMO energy gap, and thus the emission wavelengths can be fine-tuned at around 450-650 nm in the visible region.

As shown in Table 2, the *I* values of ***n*b** are lower than those of ***n*a** and ***n*c**. This difference can be explained by the degree of the π-conjugation in S_1 states; the A_π value of ***n*b** is assumed to be smaller than those of ***n*a** and ***n*c**. Therefore, it is suggested that the

molecular design which extends the π-conjugation length is desirable in order to achieve the efficient charge recombination emission.

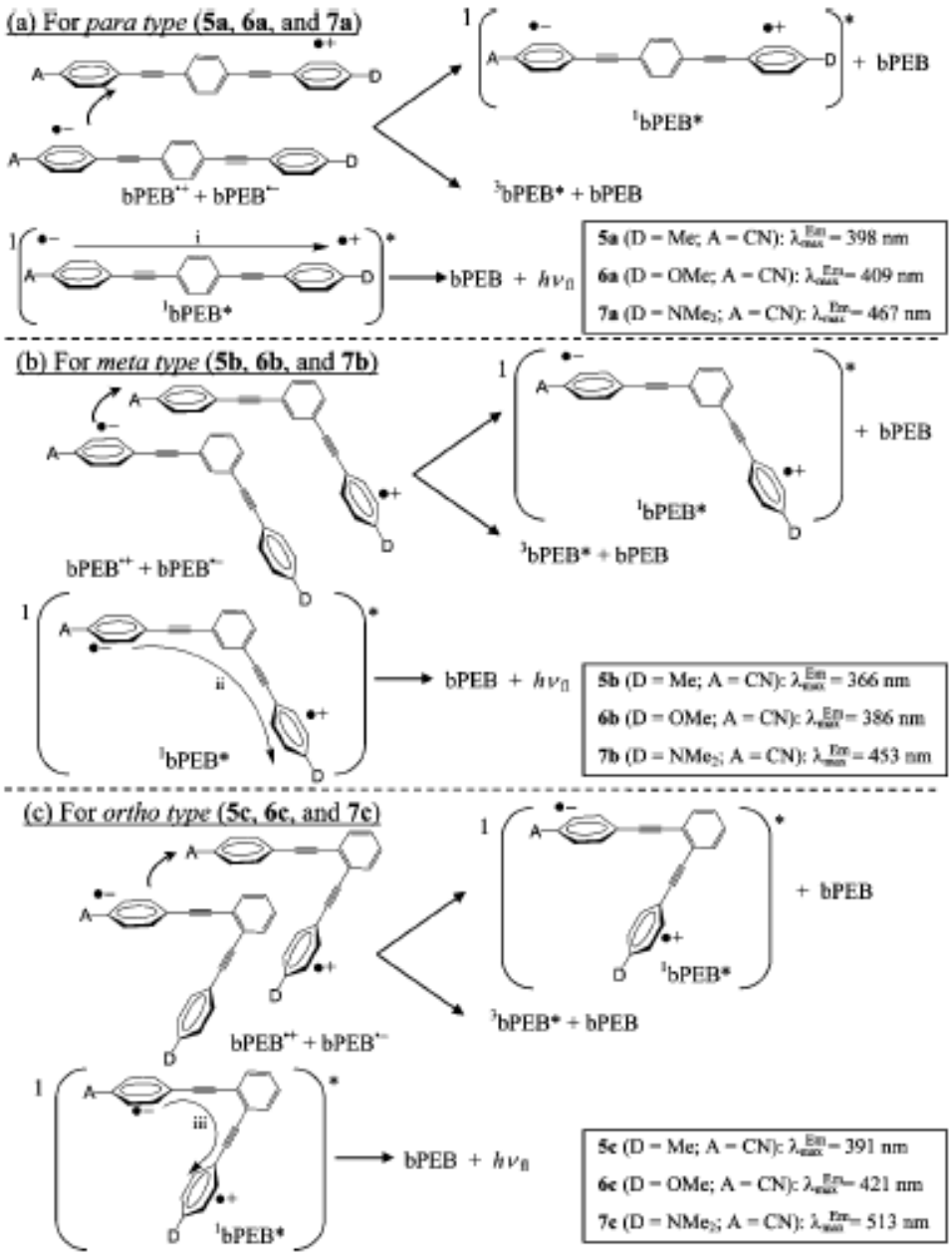

Scheme 3. Proposed Structure for the Formation of Donor-Acceptor-Type bPEBs in the S1 and T1 States during Pulse Radiolysis in Bz

Conclusions

Through control of the substitution pattern, the regioisomeric electron donor and/or acceptor substituted bPEBs **1-7**, the fine-tuning of radiolysis induced emission color and intensity can be achieved. Using pulse radiolysis technique, the charge recombination between $bPEB^{\bullet+}$ and $bPEB^{\bullet-}$ gives $^{1}bPEB^{*}$ as the emissive species, which has the emission wavelengths 350-650 nm in the visible region. It is clearly indicated that the difference in the charge transfer conjugated pathways between donor and acceptor substituents: the linear- (path i), cross- (path ii), and "bent" conjugated (path iii) pathways strongly influence the HOMO-LUMO energy gap. In addition, our results show that the degree of the π-conjugation influences the luminescence intensity during pulse radiolysis. These specific emission properties of donor-acceptor-substituted bPEB may lead to customization of optical band gaps and luminescent efficiency for specialized materials applications.

Experimental Section

Solution Preparation. Bz was purchased from Nacalai Tesque (Spectral grade) and used as a solvent without further purification. All the sample solutions were freshly prepared in 1 mM concentration in Bz in a rectangular quartz cell (1.0 × 1.0 × 4.0 cm, path length of 1.0 cm). These solutions were saturated with Ar-gas by bubbling for 10 min at room temperature before irradiation. All experiments were carried out at room temperature.

Measurements of Steady-state Spectral Properties. UV Spectra were recorded in Bz with a Shimadzu UV-3100PC UV/visible spectrometer. Fluorescence spectra were

measured by a Hitachi 850 spectrofluorometer. The fluorescence quantum yields (Φ_{fl}) were determined by using **1a** (Φ_{fl} = 0.90 in cyclohexane, λ_{ex}= 360 nm)[22] standard.

Pulse Radiolysis. Pulse radiolysis experiments were performed using an electron pulse (28 MeV, 8 ns, 0.87 kGy per pulse) from a linear accelerator at Osaka University. The kinetic measurements were performed using a nanosecond photoreaction analyzer system (Unisoku, TSP-1000). The monitor light was obtained from a pulsed 450-W Xe arc lamp (Ushio, UXL-451-0), which was operated by a large current pulsed-power supply that was synchronized with the electron pulse. The monitor light was passed through an iris with a diameter of 0.2 cm and sent into the sample solution at a perpendicular intersection to the electron pulse. The monitor light passing through the sample was focused on the entrance slit of a monochromator (Unisoku, MD200) and detected with a photomultiplier tube (Hamamatsu Photonics, R2949). The transient absorption and emission spectra were measured using a photodiode array (Hamamatsu Photonics, S3904-1024F) with a gated image intensifier (Hamamatsu Photonics, C2925-01) as a detector. All emission spectra were corrected for the spectral sensitivity of the apparatus. To avoid pyrolysis of the sample solution by the monitor light, a suitable cutoff filter was used.

Measurements of Electrochemical Properties. Oxidation (E_{ox}) and reduction potentials (E_{red}) were measured by cyclic voltammetry (BAS, CV-50W) with platinum working and auxiliary electrodes and an Ag/Ag^+ reference electrode at a scan rate of 100 mV s^{-1}. Measurements were performed in dry AN containing approximately 1 mM of AHs and 0.1 M tetraethylammonium perchlorate.

Acknowledgements. We thank the members of the Radiation Laboratory of ISIR, Osaka Univ. for running the linear accelerator. This work has been partly supported by a Grant-in-Aid for Scientific Research (Project 17105005, 19350069, Priority Research (477), and others) from the Ministry of Education, Culture, Sports, Science and Technology (MEXT) of Japanese Government and the US National Science Foundation (CHE-0718242). One of the authors (S.S.) expresses his thanks for JSPS Research Fellowship for Young Scientists and the Global COE Program "Global Education and Research Center for Bio-Environmental Chemistry" of Osaka University.

APPENDIX H

SYNTHESIS AND PHOTOPHYSICAL PROPERTIES OF EXPANDED DEHYDROBENZOANNULENOANNULENE TREFOILS

This appendix encompasses the project that I worked on prior to joining the indenofluorene project. Takashi T. Takeda synthesized half of the finished compounds and wrote the text of the paper with the assistance of Michael M. Haley.

Highly conjugated carbon-rich compounds[1] continue to receive considerable attention not only because of the fundamental science aspects[2] (e.g., aromaticity/ antiaromaticity) of these aesthetically appealing compounds but also due to the interesting chemical and physical properties that these π-electron-rich species possess.[3]

Our studies have focused on the synthesis and optoelectronic attributes of a particular subset of carbon-rich compounds named dehydrobenzoannulenes (DBAs).[4] We and others have shown that DBAs exhibit a myriad of technologically relevant properties including nonlinear optical activity,[5] two-photon absorption,[6] and liquid crystalline behavior,[7] among many others.[8] More recent work has turned to the investigation of increasingly larger and synthetically more complex systems (e.g., trefoils) containing multiple fused DBAs.[9] In a vast majority of these molecules, the annulene rings have been the same size, typically 12-membered[9b,d-f] or 18-membered rings.[9a,c] We were curious to learn what effect, if any, that variation of the ring size of the central arene in a series of expanded molecular trefoils might have. To that end, we report herein

the synthesis and optoelectronic properties of trefoil-shaped DBAs **1**-**3** possessing [6]-, [12]-, and [18]annulenes, respectively, as the central fused ring (Figure 1). In addition, we also present trefoil **4**, a structural isomer of **1**, prepared from a common intermediate via an alternative homocoupling procedure.

Given prior problems of expanded DBAs with poor molecule solubility,[4a,9] we designed our syntheses such that **1**-**4** incorporated 12 decyl units. Starting from **5**,[9e] Sonogashira cross-coupling of (triisopropylsilyl)acetylene (TIPSA) afforded differentially protected diyne **6** (Scheme 1). Protiodesilylation and a second Sonogashira reaction with hexabromotriphenylene[10] gave dodecayne **8** in a reasonable ca. 50% yield for the two steps. Molecular modeling suggested that once desilylated, the terminal alkynes were sufficiently close to one another that either trefoil **1**, possessing three 14-membered DBA rings, or **4**, containing three 18-membered rings, could form during the homocoupling reaction. We recently reported reaction conditions that made it possible to discriminate between annulene ring size, depending upon ring strain in the organometallic intermediate prior to reductive elimination.[11] Gratifyingly, desilylation of **8** with TBAF and subsequent treatment with catalytic $PdCl_2$(dppe) and stoichiometric I_2 as oxidant furnished a single product. Conversely, use of excess $Cu(OAc)_2$ in the homocoupling step afforded a sole yet different compound. We have provisionally assigned these as trefoils **1** and **4**, respectively, based on the upfield NMR chemical shift of the triphenylene protons of **4** (*δ* 9.20 for **1** vs 8.29 for **4**, starting from 8.72 for **8**) which lie in the shielding cone of the aromatic 18-membered *π*-system,[12] as well as based on the aforementioned "organometallic intermediate" argument. Simply put, the *cis*-oriented Pd(dppe) intermediate that could possibly lead to the 18-membered ring is too

highly strained to form, whereas the analogous "*trans*-like" dimeric Cu species leading to **4** is relatively strain-free. The reverse argument applies for **1**: the *cis*-oriented Pd(dppe) intermediate that leads to the 14-membered ring is relatively strainfree, whereas a "*trans*-like" dimeric Cu-species leading to **1** is highly strained.[11]

Preparation of trefoil **2** began with known triazene **9** (Scheme 2).[9c] Sequential Sonogashira reactions with 2 equiv of **7** and then excess TMSA provided triazene **10**, which was followed by triazene conversion to iodoarene **11** using HI/I_2 at rt.[13] Protiodesilylation and subsequent cyclotrimerization using the conditions of Iyoda[14] furnished precursor **12** in 39% yield. Removal of the six TIPS groups by TBAF followed by Pd-mediated homocoupling under pseudohigh dilution conditions gave **2** in a respectable 69% yield.

Starting again with triazene **9**, sequential Sonogashira reactions with 2 equiv of **7** and then excess TIPSA provided **13** (Scheme 3). Triazene conversion as before and then cross-coupling with (trimethylsilyl)butadiyne gave heptyne **14**. Selective protiodesilylation with K_2CO_3 in MeOH/THF followed by Sonogashira reaction with another 1 equiv of **9** afforded **15**. While triazene iodide conversion with HI/I_2 occurred in similar fashion, subsequent cross-coupling with excess **7** proceeded poorly such that the overall yield of the two steps furnished precursor **16** in no more than 12%. Nonetheless, a final desilylation with TBAF and subsequent Pd-mediated homocoupling gave **3**.

As desired, all four trefoils possessed sufficient solubility such that they could be easily purified by column chromatography and their complete spectral data secured. Other than the aforementioned triphenylene proton shifts, NMR analysis of **1**-**4** did not provide sufficient detail about core size differences. The periphery arene protons of the

trefoils did exhibit lower field shifts compared with the corresponding precursors ($\Delta\delta$ 0.05-0.15 ppm), typical of the weak aromatic character of the fused 14 and/or 18 π-electron systems.[15] Similar to our previous results of purely hydrocarbon expanded DBAs, no evidence for self-association in solution was observed.

More instructive are the electronic absorption and emission spectra of trefoils **1**-**4**. As shown in Figure 2 (top), **2**-**4** red-shift ca. 30 nm to lower energy compared to their acyclic precursors, whereas the shift of **1** is more modest (ca. 10 nm). Interestingly, trefoils **2** and **3** appear to have the same low energy band at 436 nm. Closer inspection of **2** (as well as precursor **12**) reveals the characteristic vibronic spectral pattern of the antiaromatic [12]DBA core,[9e,16] with discernible shoulders at 450 and 470 nm, a spectral feature lacking in **3**.

The most notable differences arising from variation of core size are depicted in the emission spectra in Figure 2 (bottom) and Table 1. Trefoils **1**, **3**, and **4** possess maxima roughly 20 nm red-shifted compared to their precusor molecules, emitting in the general range of 400-550 nm. In contrast, trefoil **2** and precursor **12** emit at lower energy (475-625 nm), with the spectra exhibiting the vibrational splitting often observed for [12]DBA derivatives.[9d,e] While the additional alkyne units in **3** afford a slightly longer linear conjugation pathway compared to **2**, the ca. 90 nm lower energy λ_{em} maximum of **2** suggests that the longest conjugation length does not dictate the fluoresence properties of these trefoilshaped hydrocarbons; instead, it is the intrinsic spectral features of the particular core unit that predominate.

In summary, we have synthesized a series of expanded annulene derivatives that possess different sizes of the central ring system. Optoelectronic measurements clearly

show that the absorption and emission properties of the trefoil-shaped molecules can vary significantly depending on use of an aromatic (**1**, **3**, **4**) or antiaromatic (**2**) annulene core. Further studies on additional expanded annulene derivatives will be reported in due course.

Experimental Details

General Methods. ^{1}H and ^{13}C NMR spectra were recorded in $CDCl_3$ using a Varian INOVA-300 (^{1}H: 299.94 MHz, ^{13}C: 75.43 MHz) or Varian INOVA-500 (^{1}H: 500.11 MHz, ^{13}C: 125.75 MHz) NMR spectrometer. Chemical shifts (δ) are expressed in ppm relative to the residual $CHCl_3$ (^{1}H: 7.28 ppm, ^{13}C: 77.3 ppm) or CD_2Cl_2 (^{1}H: 5.32 ppm, ^{13}C: 54.0 ppm). IR spectra were recorded using an FTIR spectrometer. Mass spectra were recorded on an MALDI-TOF mass spectrometer using trans-2-[3-(4-*tert*-butylphenyl)-2-methyl-2-propenylidene]malononitrile as matrix. THF and Et_2O were purified by distillation from Na/benzophenone under N_2. All other chemicals were reagent grade quality and used as obtained from manufacturers. Column flash chromatography was performed using air pressure on silica gel (230-450 mesh) and reagent quality solvents. Reactions were carried out in an inert atmosphere (dry Ar or N_2) when necessary. All deprotected terminal alkynes were used directly without further purification. UV-Vis and fluorescence spectra were taken using spectrum grade CH_2Cl_2. Quantum yields were determined by comparing with 9,10-diphenylanthracene as reference.[1]

General TMS Deprotection Procedure A. To a solution of TMS protected alkyne in Et_2O/MeOH (1:1, ~0.01 M) was added an excess amount of K_2CO_3. The suspension was stirred at room temperature overnight. After dilution with Et_2O and water, the aqueous layer was extracted twice with Et_2O. The combined organic layer was washed with water,

brine and dried over $MgSO_4$. After evaporation of the solvent, the crude material was used directly in the next reaction.

General Sonogashira Cross-coupling Procedure B. Haloarene (1 equiv) and terminal alkyne (1.1 equiv. per transformation) were dissolved in 1:1 *i*-Pr_2NH/THF or *i*-Pr_2NH (0.01-0.02 M) and the solution was purged for ca. 30 min by bubbling Ar. This was followed by addition of $Pd(PPh_3)_4$ (0.05 equiv per transformation) and CuI (0.1 equiv per transformation). When either trimethylsilylacetylene or triisopropylsilylacetylene was used, it was added after addition of the $Pd(PPh_3)_4$ and CuI. The reaction mixture then stirred overnight at 50 °C (for iodide) or 80 °C (for bromide) under an inert atmosphere. Upon completion, the solvent was removed in vacuo and the crude material was purified by column chromatography or preparative TLC.

General Pd-mediated Macrocyclization Procedure C. To a solution of triisopropylsilyl-protected alkyne (1 equiv) in THF (~0.01 M) was added TBAF (1.0 M in THF, 5 equiv per silyl group). The reaction mixture was stirred for 1 h at room temperature. The mixture was diluted with Et_2O and water and the aqueous layer was extracted twice with Et_2O. The combined organic layer was washed with water and brine, dried over $MgSO_4$, and concentrated in vacuo. The resultant terminal alkyne was then redissolved in THF (30 mL) and added via syringe pump over 12 h to a solution of $Pd(dppe)Cl_2$ (1.25-1.5 equiv), CuI (2.5-3.0 equiv) and I_2 (3.1-3.8 equiv) in *i*-Pr_2NH/THF (1:1, 0.1-0.4 mM) at 50 °C open to air. Upon completion of addition, the reaction mixture was stirred for 2 h further. After removal of solvent in vacuo, the crude mixture was purified by preparative TLC.

Orthogonally-protected Diyne 6. Iodide **5**[2] (1.72 g, 2.97 mmol) was reacted with triisopropylsilylacetylene (870 μL, 4.45 mmol) at 50 °C in *i*-Pr_2NH using general

procedure B. The crude material was purified by column chromatography (hexane) to give **6** (1.59 g, 84%) as a yellow oil. ^{1}H NMR (300 MHz) δ 7.26 (s, 1H), 7.23 (s, 1H), 2.59-2.48 (m, 4H), 1.60-1.44 (m, 4H), 1.40-1.22 (m, 28H), 1.16 (s, 18H), 0.96-0.84 (m, 6H), 0.25 (s, 9H); ^{13}C NMR (75 MHz) δ 141.50, 141.40, 138.81, 133.64, 123.38, 123.15, 105.96, 104.19, 96.85, 93.41, 32.75, 32.69, 32.22, 31.38, 29.93, 29.81, 29.65, 23.00, 19.09, 14.40, 11.61, 0.30; IR (neat) 2956, 2925, 2855, 2155, 1464, 1249, 867, 843, 759, 676, 660 cm^{-1}; HRMS (ESI) for $C_{42}H_{74}Si_2$ [M^+]: calcd 634.5329, found 634.5298.

Triphenylene 8. Diyne **6** (1.15 g, 1.8 mmol) was deprotected according to general procedure A to afford terminal acetylene **7** which was used directly in the next step. Alkyne **7** (954 mg, 1.69 mmol) was reacted with hexabromotriphenylene (132 mg, 0.188 mol) at 80 °C in THF/*i*-Pr_2NH in a sealed pressure vessel using general procedure B. The crude material was purified by column chromatography (hexanes) to give **8** (358 mg, 53%) as a viscous orange oil. ^{1}H NMR (300 MHz, $CDCl_3$) δ 8.73 (s, 6H), 7.38 (s, 6H), 7.28 (s, 6H), 2.56 (t, *J* = 6.9 Hz, 12H), 2.47 (t, *J* = 7.0 Hz, 12H), 1.73-1.58 (m, 24H), 1.55-1.20 (m, 168H), 1.06 (s, 126H), 0.94-0.82 (m, 36H); ^{13}C NMR (125 MHz, $CDCl_3$) δ 141.08, 141.00, 133.49, 133.08, 128.46, 126.84, 125.61, 123.32, 123.09, 105.64, 93.97, 93.73, 90.98, 32.60, 32.44, 31.94, 31.16, 31.02, 29.83, 29.78, 29.72, 29.68, 29.56, 29.40, 29.38; IR (neat) 2955, 2924, 2853, 2192, 1539, 1507, 1466, 1437, 888, 722, 671 cm^{-1}; HRMS (MALDI) for $C_{252}H_{396}Si_6$ [M^+]: calcd 3590.960, found 3590.955.

Trefoil 1. Triphenylene **8** (150 mg, 41.7 μmol) was deprotected and cyclized using general procedure C. The crude product was purified by preparative TLC (9:1 hexanes:CH_2Cl_2) to give **1** (50 mg, 43%) as a viscous orange oil. ^{1}H NMR (300 MHz, $CDCl_3$) δ 9.20 (s, 6H), 7.87 (s, 6H), 7.41 (s, 6H), 2.56 (t, *J* = 6.9 Hz, 12H), 2.47 (t, *J* = 6.9 Hz, 12H), 1.76-1.58 (m, 24H), 1.55-1.18 (m, 168H), 0.98-0.82 (m, 36H); ^{13}C NMR

(500 MHz, $CDCl_3$) δ 142.09, 141.67, 134.12, 131.65, 129.65, 128.40, 126.62, 122.97, 120.64, 94.23, 92.91, 86.24, 79.67, 33.40, 32.54, 31.94, 31.42, 30.90, 29.67, 29.38, 22.70, 14.12; IR (neat) 2923, 2852, 1559, 1539, 1457, 668 cm^{-1}; HRMS (MALDI) for $C_{198}H_{270}$ [M^+]: calcd 2648.113, found 2648.118.

Trefoil 4. Triphenylene **8** (299 mg, 83.2 μmol) in THF (100 mL) was deprotected using general procedure C. The resulting terminal alkyne was dissolved in THF (35 mL) and injected over 24 h into a slurry of $Cu(OAc)_2•H_2O$ (332 mg, 1.66 mmol) in pyridine (125 mL) at 45 °C. Upon completion, the reaction mixture was concentrated in vacuo and purified by column chromatography (9:1 hexanes:CH_2Cl_2) to give **4** (81 mg, 37%) as a viscous orange oil. ^{1}H NMR (300 MHz, $CDCl_3$) δ 8.28 (s, 6H), 7.37 (s, 6H), 7.12 (s, 6H), 2.62 (t, *J* = 6.8 Hz, 12H), 2.45 (t, *J* = 6.9 Hz, 12H), 1.72-1.60 (m, 24H), 1.44-1.08 (m, 168H), 0.98-0.78 (m, 36H); ^{13}C NMR (125 MHz, $CDCl_3$) δ 141.23, 140.77, 134.70, 131.35, 130.04, 127.64, 122.87, 122.15, 122.07, 92.91, 92.85, 82.85, 77.49, 32.61, 32.43, 32.02, 30.52, 30.23, 30.09, 30.02, 29.90, 29.85, 29.80, 29.76, 29.59, 29.51, 22.76, 14.14, 14.12; IR (neat) 3021, 2923, 2855, 2210, 2152, 2063, 1599, 1533, 1486, 1464, 883, 678 cm^{-1}; HRMS (MALDI) for $C_{198}H_{270}$ [M^+]: calcd 2648.113, found 2648.110.

Triazene 10. Diyne **6** (3.55 g, 5.59 mmol) was subjected to general procedure A to obtain terminal alkyne **7** (3.13 g), which was reacted with bromodiiodotriazene **9**[3] (1.27 g, 2.65 mmol) at 50 °C in THF/*i*-Pr_2NH using general procedure B. The crude material was purified by column chromatography (10:1 hexanes/CH_2Cl_2) to give the tetrayne precursor to **10** (3.01 g, 84%) as yellow oil. This material (2.39 g, 1.77 mmol) was then reacted with TMSA (800 μL, 4.12 mmol) at 80 °C in THF/*i*-Pr_2NH in a sealed pressure vessel using general procedure B. The crude material was purified by column chromatography (7:1 hexanes/CH_2Cl_2) to give **10** (1.51 g, 60%) as a yellow oil. ^{1}H NMR

(300 MHz) δ 7.70 (s, 1H), 7.65 (s, 1H), 7.34 (s, 1H), 7.29 (s, 1H), 7.28 (s, 2H), 3.58 (br s, 3H), 3.30 (br s, 3H), 2.60-2.42 (m, 8H), 1.60-1.50 (m, 4H), 1.50-1.18 (m, 60H) 1.15 (s, 21H), 1.12 (s, 21H), 0.94-0.86 (m, 12H), 0.28 (s, 9H); ^{13}C NMR (75 MHz) δ 151.22, 141.39, 141.34, 141.26, 141.19, 136.86, 133.65, 133.38, 133.31, 133.26, 126.85, 123.74, 123.64, 123.23, 123.04, 122.96, 119.85, 117.93, 105.94, 102.54, 100.15, 94.10, 93.81, 93.76, 93.03, 91.49, 91.04, 32.82, 32.73, 32.02, 31.42, 31.23, 30.09, 29.93, 29.80, 29.65, 22.98, 19.01, 14.40, 11.69, 11.62, 0.30; IR (neat) 2955, 2924, 2855, 2153, 1498, 1466, 1401, 1341, 1324, 1248, 1087, 900, 883, 861, 842, 759, 673 cm^{-1}; HRMS (ESI) for $C_{91}H_{147}N_3Si_3$ [M^+]: calcd 1366.0903, found 1366.0878.

Iodoarene 11. To a solution of aqueous HI (57 wt%, 1.044 g, 4.65 mmol) and I_2 (1.19 g, 4.65 mmol) in MeCN (20 mL) was added a solution of triazene **10** (1.27 g, 0.93 mmol) in MeCN (10 mL) and CCl_4 (20 mL) slowly at room temperature. The mixture was stirred at room temperature for 30 min. After dilution with Et_2O and water, the aqueous layer was extracted with Et_2O. The combined organics were washed successively with saturated aqueous solutions of $NaHCO_3$, $Na_2S_2O_3$ and NaCl. The organic layer was dried over $MgSO_4$ and concentrated in vacuo. The crude material was purified by column chromatography (hexane) to give **11** (1.03 g, 78%) as a yellow oil. ^{1}H NMR (300 MHz) δ 8.01 (s, 1H), 7.62 (s, 1H), 7.31 (s, 1H), 7.30 (s, 1H), 7.29 (s, 2H), 2.62-2.42 (m, 8H), 1.64-1.52 (m, 4H), 1.48-1.20 (m, 60H), 1.14 (s, 42H), 0.95-0.84 (m, 12H), 0.32 (s, 9H); ^{13}C NMR (75 MHz) δ 141.94, 141.81, 141.41(3C), 135.45, 133.50, 133.45, 133.42, 133.31, 129.09, 127.22, 126.45, 123.39, 123.07, 122.98, 105.87, 105.72, 105.64, 100.83, 99.27, 95.95, 94.70, 94.20, 94.08, 89.83, 89.56, 32.83, 32.73, 32.15, 31.39, 31.23, 30.07, 29.93, 29.78, 29.64, 22.96, 18.97, 14.39, 11.66, -0.01; IR (neat) 2956, 2924, 2864, 2854,

2212, 2151, 1492, 1465, 1250, 897, 883, 860, 844, 761, 677 cm^{-1}; HRMS (ESI) for $C_{89}H_{141}ISi_3$ [M^+]: calcd 1420.9386, found 1420.9393.

[12]DBA 12. Iodoarene **11** (553 mg, 0.389 mmol) was subjected to general procedure A to obtain the terminal alkyne. The resultant material was dissolved in DMF (1 mL) and 1,2-$Cl_2C_6H_4$ (1 mL) and purged with bubbling Ar for 30 min. CuI (22 mg, 0.117 mmol), PPh_3 (31 mg, 0.117 mmol), and K_2CO_3 (161 mg, 1.17 mmol) were then added. The mixture was stirred at 160 °C under Ar for 17 h. After cooling, the mixture was diluted with CH_2Cl_2 and water and the aqueous layer extracted with CH_2Cl_2. The combined organics were washed successively with saturated aqueous solutions of $NaHCO_3$ and NaCl and then dried over $MgSO_4$. The solution was concentrated in vacuo and the crude material was purified by column chromatography (25:1 hexanes/CH_2Cl_2) to give **12** (187 mg, 39%) as yellow oil. ^{1}H NMR (300 MHz) δ 7.51 (s, 6H), 7.29 (s, 12H), 2.62-2.40 (m, 24H), 1.64-1.20 (m, 192H), 1.13 (s, 126H), 0.96-0.84 (m, 36H); ^{13}C NMR (75 MHz) δ 141.75, 141.37, 135.13, 133.46, 133.31, 127.18, 125.57, 123.38, 123.19, 105.65, 95.84, 94,22, 93.94, 90.15, 32.85, 32.66, 32.19, 31.40, 31.24, 30.08, 29.96, 29.92, 29.80, 29.64, 22.98, 18.96, 14.39, 11.63; IR (neat) 2955, 2924, 2854, 2209, 2152, 1501, 1464, 1072, 996, 900, 883, 677 cm^{-1}; HRMS (MALDI) for $C_{258}H_{396}Si_6$ [M^+]: calcd 3662.960, found 3662.956.

Trefoil 2. [12]DBA **12** (102 mg, 27.8 μmol) was subjected to general procedure C. The crude material was purified by preparative TLC (4:1 hexanes/CH_2Cl_2) to give **2** (52 mg, 69%) as a yellow solid. ^{1}H NMR (300 MHz) δ 7.69 (s, 6H), 7.56 (s, 6H), 7.28 (s, 6H), 2.66-2.44 (m, 24H), 1.70-1.42 (m, 16H), 1.40-1.00 (m, 176H), 0.98-0.78 (m, 36H); ^{13}C NMR (75 MHz) δ 142.27, 141.70, 139.28, 133.62, 129.20, 126.85, 125.49, 123.44, 120.44, 95.43, 94.41, 92.91, 86.26, 80.05, 33.10, 32.59, 32.24, 31.10, 30.62, 30.25, 30.16,

30.07, 29.90, 29.85, 29.74, 23.02, 14.40; IR (neat) 2955, 2924, 2853, 1515, 1495, 1466, 893 cm^{-1}; HRMS (MALDI) for $C_{204}H_{270}$ [M^+]: calcd 2720.113, found 2720.116.

Triazene 13. Diacetylene **6** (3.55 g, 5.59 mmol) was subjected to general procedure A to obtain terminal alkyne **7** (3.13 g), which was reacted with bromodiiodotriazene **9**[3] (1.27 g, 2.65 mmol) at 50 °C in THF/*i*-Pr_2NH using general procedure B. The crude material was purified by column chromatography (10:1 pentane/CH_2Cl_2) to give the tetrayne precursor to **13** (3.01 g, 84%) as yellow oil. This material (2.23 g, 1.65 mmol) was reacted with triisopropylacetylene (800 μL, 4.12 mmol) at 80 °C in THF/*i*-Pr_2NH in a sealed pressure vessel using general procedure B. The crude material was purified by column chromatography (10:1 hexanes/CH_2Cl_2) to give **13** (2.08 g, 87%) as yellow oil. ^1H NMR (300 MHz) δ 7.70 (s, 1H), 7.68 (s, 1H), 7.35 (s, 1H), 7.33 (s, 1H), 7.29 (br s, 2H), 3.58 (s, 3H), 3.28 (s, 3H), 2.60-2.40 (m, 8H), 1.65-1.52 (m, 4H), 1.48-1.22 (m, 60H), 1.19 (s, 21H), 1.16 (s, 21H), 1.14 (s, 21H), 0.96-0.85 (m, 12H); ^{13}C NMR (125 MHz) δ 151.31, 141.34 (2C), 141.28, 141.30, 136.90, 133.73, 133.61, 133.34, 126.92, 123.86, 123.73, 123.02(2C), 122.97, 119.92, 118.56, 106.20, 106.04, 106.02, 104.66, 96.30, 93.99, 93.75, 93.14, 91.68, 91.15, 32.82, 32.71, 31.40, 31.20, 30.10, 29.94, 29.81, 29.65, 22.97, 19.02, 14.38, 11.67; IR (neat) 2957, 2924, 2863, 2854, 2151, 1498, 1464, 1401, 1342, 1087, 996, 900, 883, 677 cm^{-1}; HRMS (ESI) for $C_{97}H_{159}N_3Si_3$ [M^+]: calcd 1450.1842, found 1450.1866.

Heptayne 14. To a solution of aqueous HI (57 wt%, 615 mg, 2.74 mmol) and I_2 (695 mg, 2.74 mmol) in MeCN (15 mL) was added a solution of triazene **13** (795 mg, 0.548 mmol) in MeCN (10mL) and CCl_4 (20 mL) slowly at 35 °C. After stirring at 35 °C for 30 min, the mixture was diluted with Et_2O and water and the aqueous layer extracted with Et_2O. The combined organics were washed successively with saturated aqueous solutions of

$NaHCO_3$, $Na_2S_2O_3$ and NaCl. The organic layer was dried over $MgSO_4$ and concentrated in vacuo. The crude material was purified by column chromatography (pentane) to give the iodide precursor to **14** (621 mg, 75%) as yellow oil. This material (1.40 g, 931 μmol) was reacted with trimethylsilyl-1,3-butadiyne[4] (285 mg, 2.33 mmol) at 50 °C in THF/*i*-Pr_2NH using general procedure B. The crude material was purified by column chromatography (hexanes) to give **14** (1.24 g, 88%) as a yellow oil. ^{1}H NMR (300 MHz) δ 7.63 (s, 1H), 7.62 (s, 1H), 7.33 (s, 1H), 7.31 (s, 1H), 7.30 (s, 1H), 7.28 (s, 1H), 2.62-2.38 (m, 8H), 1.64-1.52 (m, 4H), 1.48-1.23 (m, 60H), 1.21 (s, 21H), 1.16 (s, 21H), 1.13 (s, 21H), 0.96-0.84 (m, 12H), 0.26 (s, 9H); ^{13}C NMR (125 MHz) δ 141.87, 141.84, 141.40(2C), 135.84, 135.20, 133.75, 133.47 (2C), 133.31, 126.91, 126.72, 126.28, 123.77, 123.50, 123.25, 123.09, 123.06, 105.77, 105.66, 103.98, 98.15, 96.14, 95.40, 94.30, 94.07, 92.66, 90.33, 90.12, 88.25, 79.69, 74.65, 32.83, 32.73, 32.69, 32.20, 31.38, 31.24, 31.20, 30.09, 30.06, 29.95, 29.92, 29.78, 29.64, 22.97, 18.95, 14.37, 11.66, 11.59, -0.18; IR (neat) 2956, 2925, 2864, 2855, 2206, 2152, 2103, 1498, 1465, 1251, 1186, 1072, 996, 901, 883, 846, 761, 678 cm^{-1}; HRMS (MALDI) for $C_{102}H_{162}Si_4$ [M^+]: calcd 1499.1754, found 1499.1734.

Bromotriazene 15. Heptayne **14** (555 mg, 0.366 mmol) and triazene **9** (84 mg, 0.174 mmol) were dissolved in *i*-Pr_2NH (10 mL) and THF (10 mL). To this solution was added KOH (207 mg, 3.66 mmol) dissolved in a minimal amount of water. The mixture was stirred and purged for ca. 30 min by bubbling Ar. $Pd(PPh_3)_4$ (42 mg, 0.0366 mmol) and CuI (14 mg, 0.0732 mmol) were then added and the mixture was stirred overnight at 50 °C under inert atmosphere. After removal of solvent in vacuo, the crude material was purified by column chromatography (9:1 hexanes/CH_2Cl_2) to give **15** (274 mg, 51%) as yellow oil. ^{1}H NMR (300 MHz) δ 7.78 (s, 1H), 7.70 (s, 1H), 7.69 (s, 1H), 7.65 (s, 1H),

7.65 (s, 1H), 7.33 (s, 2H), 7.31 (s, 2H), 7.30 (s, 2H), 7.29 (s, 2H), 3.62 (s, 3H), 3.33 (s, 3H), 2.63-2.40 (m, 16H), 1.64-1.23 (m, 128H), 1.19 (s, 21H), 1.19 (s, 21H), 1.16 (s, 42H), 1.12 (s, 21H), 1.11 (21H), 0.95-0.86 (m, 24H); ^{13}C NMR (125 MHz) δ 148.68, 141.84, 141.82, 141.77, 141.75, 141.40, 141.32, 141.31 138.20, 135.94, 135.90, 135.31, 133.80, 133.48, 133.31, 126.86, 126.81, 126.51, 126.50, 126.29, 126.28, 124.78, 124.07, 124.03, 123.57,123.24, 123.17, 123.15, 123.12, 123.11, 123.00, 122.06, 120.61, 105.79, 105.60, 103.98, 98.46, 98.43, 96.10, 96.06, 95.38, 95.37, 94.40, 94.37, 94.07, 90.46, 90.43, 90.16, 90.14, 81.62, 81.28, 81.17, 80.64, 79.61, 79.58, 79.00, 78.46, 43.68, 36.84, 32.86, 32.83, 32.75, 32.71, 32.20, 31.25, 31.22, 29.92, 29.79, 29.64, 22.97, 19.00, 14.38, 11.71, 11.66, 11.62; IR (neat) 2958, 2924, 2865, 2863, 2210, 2151, 1467, 1350, 1094, 966, 883, 677 cm^{-1}; HRMS (MALDI) for $C_{206}H_{314}BrN_3Si_6$ [M^+]: calcd 3077.246, found 3077.239.

Octadecayne 16. To a solution of aqueous HI (57 wt%, 105 mg, 0.467 μmol) and I_2 (1.19 mg, 4.67 μmol) in MeCN (3 mL) was added a solution of triazene **15** (289 mg, 93.4 μmol) in MeCN (2 mL) and CCl_4 (6 mL) slowly at room temperature. After stirring at 35 °C for 30 min, the mixture was diluted with Et_2O and water and the aqueous layer extracted with Et_2O. The combined organics were washed successively with saturated aqueous solutions of $NaHCO_3$, $Na_2S_2O_3$ and NaCl. The organic layer was dried over $MgSO_4$ and concentrated in vacuo. The crude material was purified by column chromatography (hexanes) to give the bromoiodoarene precursor to **16** (200 mg, 68%) as yellow oil. This material (197.2 mg, 62.6 μmol) and terminal alkyne **7** (200 mg, 0.315 mmol), obtained as before from diacetylene **6** via deprotection procedure A, were reacted at 80 °C in THF/*i*-Pr_2NH in a sealed pressure vessel using general procedure B. The crude material was purified by preparative TLC (50:1 hexanes/CH_2Cl_2) to give **16** (45

mg, 18%) as a viscous yellow oil. ^{1}H NMR (300 MHz, CD_2Cl_2) δ 7.69 (s, 4H), 7.63 (s, 2H), 7.30 (s, 6H), 7.29 (s, 2H), 7.28 (s, 4H), 2.64-2.40 (m, 24H), 1.60-1.20 (m, 192H), 1.16 (s, 42H), 1.12 (s, 84H), 1.09 (s, 42H), 0.94-0.82 (m, 36H); ^{13}C NMR (125 MHz, CD_2Cl_2) δ 142.80, 142.70, 142.60, 142.17, 142.13, 142.07, 136.32, 135.66, 134.01, 133.78, 127.62, 127.52, 127.29, 126.89, 126.56, 124.58, 124.16, 123.73, 123.65, 123.45, 123.08, 122.97, 106.06, 105.96, 104.10, 99.18, 96.86, 96.54, 95.84, 94.70, 94.51, 90.53, 90.22, 82.27, 80.82, 80.10, 79.57, 32.52, 30.27, 30.23, 30.09, 29.95, 23.29, 19.08, 14.47, 12.03, 11.98, 11.92; IR (neat) 2977, 2925, 2863, 2855, 2207, 2152, 1498, 1464, 1072, 1018, 996, 900, 893, 764, 677 cm^{-1}; HRMS (MALDI) for $C_{282}H_{438}Si_8$ [M^+]: calcd 4049.243, found 4049.237.

Trefoil 3. Octadecayne **16** (56 mg, 13.8 μmol) was subjected to general cyclization procedure C. The crude material was purified by preparative TLC (4:1 hexanes/CH_2Cl_2) to give **3** (20.1 mg, 52%) as a viscous yellow oil. ^{1}H NMR (300 MHz) δ 7.89 (s, 6H), 7.53 (s, 6H), 7.33 (s, 6H), 2.70-2.45 (m, 24 H) 1.70-0.75 (m, 228H); ^{13}C NMR (125 MHz) δ 142.26, 142.08, 139.90, 133.56, 129.22, 126.66, 123.96, 123.56, 120.69, 96.46, 92.41, 86.20, 81.06, 80.21, 80.08, 33.00, 32.73, 32.25, 3.026, 30.12, 30.03, 29.97, 29.86, 29.79, 29.70, 29.62, 23.03, 23.00, 14.41; IR (neat) 2954, 2924, 2853, 1486, 1466, 895 cm^{-1}; HRMS (MALDI) for $C_{210}H_{270}$ [M^+]: calcd 2792.113, found 2792.116.

REFERENCES CITED

Chapter I

1. Harvey RG (1997) Polycyclic Aromatic Hydrocarbons. Wiley-VCH, New York
2. Clar E (1964) Polycyclic Hydrocarbons. Academic Press, London
3. Wise SA, Campbell RM, West WR, Lee ML, Bartle KD (1986) Chem Geol 54:339
4. Müller TJJ, Bunz UHF (eds) (2007) Functional Organic Materials. Wiley-VCH, Weinheim
5. Müllen K, Scherf U (eds) (2006) Organic Light Emitting Devices: Synthesis, Properties, and Applications. Wiley-VCH, Weinheim
6. Haley MM, Tykwinski RR (eds) (2006) Carbon-Rich Compounds: From Molecules to Materials. Wiley-VCH, Weinheim
7. Anthony JE, Facchetti A, Heeney M, Marder SR, Zhan X (2010) Adv Mater 22:3876
8. Bendikov M, Wudl F, Perepichka DF (2004) Chem Rev 104:4891
9. Anthony JE (2006) Chem Rev 106:5028
10. Anthony JE (2008) Angew Chem Int Ed 47:452
11. Herwig P, Kayser CW, Müllen K, Spiess HW (1996) Adv Mater 8:510
12. Wu J, Pisula W, Müllen K (2007) Chem Rev 107:718
13. Kastler M, Pisula W, Wasserfallen D, Pakula T, Müllen K (2005) J Am Chem Soc 127:4286
14. Langa F, Nierengarten JF (eds) (2011) Fullerenes: Principles and Applications. Royal Society of Chemistry, Cambridge
15. Scott LT (2010) Polycyclic Aromat Cmpd 30:247
16. Gabriel S (1884) Ber Dt Chem Ges 17:1389
17. Errera G (1907) Gazz Chim Ital 37:II:624
18. Errera G (1908) Gazz Chim Ital 38:II:588

19. Errera G, Vaccarino G (1909) Gazz Chim Ital 39:I:1

20. Marotta D (1911) Gazz Chim Ital 41:II:59

21. Radulescu D, Georgescu V (1925) Bull Soc Chim Fr 37:1187

22. Strauss F, Kühnel R, Hansel R (1933) Ber Dt Chem Ges 66:1847

23. Weizmann Ch, Bergmann E, Haskelberg L (1939) J Chem Soc 391

24. Radulescu D, Alexa M (1943) Chem Zentralbl I:622.

25. Deuschel W (1951) Helv Chim Acta 35:168

26. Deuschel W (1951) Helv Chim Acta 35:2403

27. Chardonnens L, Ritter R (1955) Helv Chim Acta 38:393

28. Poriel C, Liang J-J, Rault-Berthelot J, Barrière F, Cocherel N, Slawin AMZ, Horhant D, Virboul M, Alcaraz G, Audebrand N, Vignau L, Huby N, Wantz G, Hirsch L (2007) Chem Eur J 13:10055

29. Cocherel N, Poriel C, Rault-Berthelot J, Barrière F, Audbrand N, Slawin AMZ, Vignau L. (2008) Chem Eur J 14:11328

30. Poriel C, Barrière F, Thirion D, Rault-Berthelot J (2009) Chem Eur J 15:13304

31. Thirion D, Poriel C, Barrière F, Métivier R, Jeannin O, Rault-Berthelot J (2009) Org Lett 11:4794

32. Cocherel N, Poriel C, Vignau L, Bergamini J-F, Rault-Berthelot J (2010) Org Lett 12:452

33. Thirion D, Poriel C, Rault-Berthelot J, Barrière F, Jeannin O (2010) Chem Eur J 16:13646

34. Cocherel N, Poriel C, Vignau L, Bergamini J-F, Rault-Berthelot J (2011) Org Lett 12:452

35. Usta H, Facchetti A, Marks TJ (2008) Org Lett 10:1385

36. Usta H, Facchetti A, Marks TJ (2008) J Am Chem Soc 130:8580

37. Usta H, Risko C, Wang Z, Huang H, Deliomeroglu MK, Zhukhovitskiy A, Facchetti A, Marks TJ (2009) J Am Chem Soc 131:5586

38. Chardonnens L, Laroche B, Sieber W (1974) Helv Chim Acta 57:585

39. Chardonnens L, Häger J (1974) Helv Chim Acta 57:1472

40. Chardonnens L, Bitsch S, Häger J (1975) Helv Chim Acta 58:503

41. Behr OM, Eglinton G, Galbraith AR, Raphael RA (1960) J Chem Soc 3614

42. Friedrich E, Deuschel W (1956) Chem Ber 89:2794

43. Chardonnens L, Salamin L (1968) Helv Chim Acta 51:1096

44. Chardonnens L, Rody J (1959) Helv Chim Acta 42:1328

45. Chardonnens L, Häger J (1970) Helv Chim Acta 53:843

46. Shi Y, Liu Q, Wu G, Rong L, Tang J (2011) Tetrahedron 67:1201

47. Minuti L, Taticchi A, Marrocchi A, Gacs-Baitz (2005) E Poly Arom Cmpds 25:13

48. Merlet S, Birau M, Wang ZY (2002) Org Lett 4:2157

49. Zhou Q, Carroll PJ, Swager TM (1994) J Org Chem 59:1294

50. Nishinaga T, Nodera N, Miyata Y, Komtasu K (2002) J Org Chem 67:6091

51. Miyata Y, Minari T, Nemoto T, Isoda S, Komatsu K (2007) Org Biomol Chem 5:2592

52. Nakagawa T, Kumaki D, Nishida J-I, Tokito S, Yamashita Y (2008) Chem Mater 20:2615

53. Rose BD, Chase DT, Weber CD, Zakharov LN, Lonergan, MC, Haley, MM (2011) Org Lett 13:2106

54. Anthony JE, Eaton DL, Parkin SR (2002) Org Lett 4:15

55. Chase DT, Fix AG, Rose BD, Weber CD, Nobusue S, Stockwell CE, Zakharov LN, Lonergan MC, Haley MM (2011) Angew Chem Int Ed 50:11103

56. Hellwinkel D, Kistenmacher T (1989) Liebigs Ann Chem 10:945

57. Scherf U (1993) Macromol Rapid Commun 14:575

58. Liu T-P, Liao Y-X, Xing C-H, Hu Q-S (2011) Org Lett 13:2452

59. Wolfgang F, Gompper R (1987) Tetrahedron Lett 28:3083

60. Chase DT, Rose BD, McClintock SP, Zakharov LN, Haley MM (2011) Angew Chem Int Ed 50:1127

61. Reisch H, Wiesler U, Scherf U, Tuytuylkov N (1996) Macromolecules 29:8204

62. Reisch H. (1995) Ph.D. Thesis, University of Mainz

63. Brunetti F, Gong X, Tong M, Heeger AJ, Wudl F (2010) Angew Chem Int Ed 49:532

64. Anthony JE, Brooks JS, Eaton DL, Parkin SR (2001) J Am Chem Soc 123:9482

65. Payne MM, Parkin SR, Anthony JE (2005) J Am Chem Soc 127:8028

66. Purushothaman B, Parkin SR, Anthony JE (2010) Org Lett 12:2060

67. Purushothaman B, Bruzek M, Parkin SR, Miller A-F, Anthony JE (2011) Angew Chem Int Ed 50:7013

68. Kaur I, Jia W, Kopreski RP, Selvarasah S, Dokmeci MR, Pramanik C, McGreur NE, Miller GP (2008) J Am Chem Soc 130:16274

69. Kaur I, Stein NN, Kopreski RP, Miller GP (2009) J Am Chem Soc 131:3424

70. Tverskoy O, Rominger F, Peters A, Himmel H-J, Bunz UHF (2011) Angew Chem Int Ed 50:3557

71. Bunz UHF (2009) Chem Eur J 15:6780

72. Bunz UHF (2010) Pure Appl Chem 82:953

73. Miao Q (2012) Synlett 326

74. Montgomery LK, Huffman JC, Jurczak EA, Grendze MP (1986) J Am Chem Soc 108:6004

75. Holmes D, Kumaraswamy S, Matzger AJ, Vollhardt KPC (1999) Chem Eur J 5:3399

76. Dong H, Wang C, Hu W (2010) Chem Commun 46:5211

77. Chase DT, Fix AG, Kang SJ, Rose BD, Weber CD, Zhong Y, Zakharov LN, Lonergan MC, Nuckolls C, Haley MM (2012) J Am Chem Soc 134:10349

78. Nishida JI, Tsukaguchi S, Yamashita Y (2012) Chem Eur J 18:8964

79. Hsiao C-C, Lin Y-K, Liu C-J, Wu T-C, Wu Y-T (2010) Adv Synth Catal 352:3267

80. Setayesh S, Marsitzky D, Müllen K (2000) Macromolecules 33:2016

81. Horhant D, Liang J-J, Virboul M, Poriel C, Alcaraz G, Rault-Berthelot J (2006) Org Lett 8:257

82. Poriel C, Rault-Berthelot J, Thirion D, Barrière F, Vignau L (2011) Chem Eur J 17:14031

83. Poriel C, Cocherel N, Rault-Berthelot J, Vignau L, Jeannin O (2011) Chem Eur J 17:12631

84. Chi L-C, Hung W-Y, Chiu H-C, Wong K-T (2009) Chem Comm 3892

85. Lee KH, Kim SO, You JN, Kang S, Lee JY, Yook KS, Jeon SO, Lee JY, Yoon SS (2012) J Mater Chem 22:5145

86. Lee KH, Kim SO, Kang S, Lee JY, Yook KS, Lee JY, Yoon SS (2012) Eur J Org Chem 18:2748

87. Ie Y, Nitani M, Aso Y (2007) Chem Lett 36:1326

88. LeBerre A (1957) Ann Chim 2:371

89. Shimizu A, Tobe Y (2011) Angew Chem Int Ed 50:6906

90. Shimizu A, Tobe Y (2011) Private communication

91. Poriel C, Métivier R, Rault-Berthelot J, Thirion D, Barrière F, Jeannin O (2011) Chem Commun 47:11703

92. Altman Y, Ginsburg DJ (1961) Chem Soc 1498

93. Chardonnens L, Chardonnens H (1966) Helv Chim Acta 49:1931

94. Wang X-M, Hou X-L, Zhou Z-Y, Mak TCW, Wong HNC (1993) J Org Chem 58:7498

95. Yang Y, Peterson JL, Wang KK (2003) J Org Chem 68:5832

96. Hilt G, Paul A, Harms K (2008) J Org Chem 73:5187

97. Fix AG, Deal PE, Haley MM (2012) Unpublished work

98. Youngs WJ, Djebli A, Tessier CA (1991) Organometallics 10:2089

Chapter II

[1] a) *Functional Organic Materials* (Eds.: T. J. J. Müller, U. H. F. Bunz), Wiley-VCH, Weinheim, **2007**; b) *Organic Light Emitting Devices: Synthesis, Properties and Applications* (Eds.: K. Mullen, U. Scherf), Wiley-VCH, Weinheim, **2006**; c) *Carbon-Rich Compounds* (Eds.: M. M. Haley, R. R. Tykwinski), Wiley-VCH, Weinheim, **2006**.

[2] a) J. E. Anthony, *Chem. Rev.* **2006**, *106*, 5028–5048; b) J. E. Anthony, *Angew. Chem.* **2008**, *120*, 460–492; *Angew. Chem. Int. Ed.* **2008**, *47*, 452–483.

[3] a) J. E. Anthony, J. S. Brooks, D. L. Eaton, S. R. Parkin, *J. Am. Chem. Soc.* **2001**, *123*, 9482–9483; b) J. E. Anthony, D. L. Eaton, S. R Parkin, *Org. Lett.* **2002**, *4*, 15–18.

[4] Inter alia: a) M. Saito, M. Nakamura, T. Tajima, T. *Chem. Eur. J.* **2008**, *14*, 6062–6068; b) T. Kawase, A. Konishi, Y. Hirao, K. Matsumoto, H. Kurata, T. Kubo, *Chem. Eur. J.* **2009**, *15*, 2653–2661; c) U. L. Zerubba, T. D. Tilley, *J. Am. Chem. Soc.* **2009**, *131*, 2796–2797; d) H. Zhang, T. Karasawa, H. Yamada, A. Wakamiya, S. Yamaguchi, S. *Org. Lett.* **2009**, *11*, 3076–3079; e) M. Saito, *Symmetry* **2010**, *2*, 950–969; f) U. L. Zerubba, T. D. Tilley, *J. Am. Chem. Soc.* **2010**, *132*, 11012–11014; g) T. Kawase, T. Fujiwara, C. Kitamura, A. Konishi, Y. Hirao, K. Matsumoto, H. Kurata, T. Kubo, S. Shinamura, H. Mori, E. Miyazaki, K. Takimiya, *Angew. Chem.* **2010**, *122*, 7894–7898; *Angew. Chem. Int. Ed.* **2010**, *49*, 7728–7732.

[5] a) H. Usta, A. Facchetti, T. J. Marks, *J. Am. Chem. Soc.* **2008**, *130*, 8580–8581; b) H. Usta, C. Risko, Z. Wang, H. Huang, M. K. Deliomergolu, A. Zhukhovitskiy, A. Facchetti, T. J. Marks, *J. Am. Chem. Soc.* **2009**, *131*, 5586–5608.

[6] *Inter alia*: a) C.-P. Chen, S.-H. Chan, T.-C. Chao, C. Ting, B.-T. Ko, *J. Am. Chem. Soc.* **2008**, *130*, 12828–12833; b) N. Cocherel, C. Poriel, J. Rault-Berthelot, F. Barrière, N. Audebrand, A. M. Z. Slawin, L. Vignau, L. *Chem. Eur. J.* **2008**, *14*, 11328–11342; c) W. Zhang, J. Smith, R. Hamilton, M. Heeney, J. Kirkpatrick, K. Song, S. E. Watkins, T. Anthopoulos, I. McCulloch, *J. Am. Chem. Soc.* **2009**, *131*, 10814–10815; d) W. Zhang, J. Smith, S. E. Watkins, R. Gysel, M. McGehee, A. Salleo, J. Kirkpatrick, S. Ashraf, T. Anthopoulos, M. Heeney, I. McCulloch, *J. Am. Chem. Soc.* **2010**, *132*, 11437–11439.

[7] Q. Zhou, P. J. Carroll, T. M. Swager, *J. Org. Chem.* **1994**, *59*, 1294–1301.

[8] H. Reisch, U. Wiesler, U. Scherf, N. Tuytuylkov, *Macromolecules* **1996**, *29*, 8204–8210.

[9] D. T. Chase, B. D. Rose, S. P. McClintock, L. N. Zakharov, M. M. Haley, *Angew. Chem.* **2011**, *50*, 1127–1130; *Angew. Chem. Int. Ed.* **2011**, *50*, 1127–1130.

[10] M. J. Frisch, G. W. Trucks, H. B. Schlegel, G. E. Scuseria, M. A. Robb, J. R. Cheeseman, G. Scalmani, V. Barone, B. Mennucci, G. A. Petersson, H. Nakatsuji, M. Caricato, X. Li, H. P. Hratchian, A. F. Izmaylov, J. Bloino, G. Zheng, J. L. Sonnenberg, M. Hada, M. Ehara, K. Toyota, R. Fukuda, J. Hasegawa, M. Ishida, T. Nakajima, Y. Honda, O. Kitao, H. Nakai, T. Vreven, J. A. Montgomery, Jr., J. E. Peralta, F. Ogliaro, M. Bearpark, J. J. Heyd, E. Brothers, K. N. Kudin, V. N. Staroverov, R. Kobayashi, J. Normand, K. Raghavachari, A. Rendell, J. C. Burant, S. S. Iyengar, J. Tomasi, M. Cossi, N. Rega, J. M. Millam, M. Klene, J. E. Knox, J. B. Cross, V. Bakken, C. Adamo, J. Jaramillo, R. Gomperts, R. E. Stratmann, O. Yazyev, A. J. Austin, R. Cammi, C. Pomelli, J. W. Ochterski, R. L. Martin, K. Morokuma, V. G. Zakrzewski, G. A. Voth, P. Salvador, J. J. Dannenberg, S. Dapprich, A. D. Daniels, O. Farkas, J. B. Foresman, J. V. Ortiz, J. Cioslowski, and D. J. Fox, *Gaussian 09*, Revision A.02, Gaussian, Inc., Wallingford, CT, 2009.

[11] a) J. E. Anthony, A. Facchetti, M. Heeney, S. R. Marder, X. Zhan, *Adv. Mater.* **2010**, *22*, 3876–3892; (b) H. Dong, C. Wang, W. Hu, *Chem. Commun.* **2010**, *46*, 5211–5222.

[12] J. A. Mikroyannidis, A. N. Kabanakis, S. S. Sharma, G. D. Sharma, *Adv. Funct. Mater.* **2011**, *21*, 746–755.

[13] B. D. Rose, D. T. Chase, C. D. Weber, L. N. Zakharov, M. C. Lonergan, M. M. Haley, *Org. Lett.* **2011**, *13*, 2106–2109.

[14] S. Merlet, M. Birau, Z. Y. Wang, *Org. Lett.* **2002**, *4*, 2157–2159.

[15] T. Nakagawa, D. Kumaki, J.-i. Nishida, S. Tokito, Y. Yamashita, *Chem. Mater.* **2008**, *20*, 2615–2617.

[16] A. Almenningen, O. Bastiansen, L. Fernholt, B. N. Cyvin, S. J. Cyvin, S. Samdal, *J. Mol. Struct.* **1985**, *128*, 59–76.

Chapter III

1) (a) *Functional Organic Materials*, Müller, T. J. J.; Bunz, U. H. F., Eds.; Wiley-VCH: Weinheim, Germany, 2007. (b) *Organic Light Emitting Devices: Synthesis, Properties and Applications*, Mullen, K.; Scherf, U., Eds.; Wiley-VCH: Weinheim, Germany, 2006. (c) *Carbon-Rich Compounds*, Haley, M. M.; Tykwinski, R. R., Eds.; Wiley-VCH: Weinheim, Germany, 2006.

2) (a) Anthony, J. E. *Chem. Rev.* **2006**, *106*, 5028–5048. (b) Anthony, J. E. *Angew. Chem. Int. Ed.* **2008**, *47*, 452–483.

3) Chase, D. T.; Rose, B. D.; Zakharov, L. N.; Haley, M. M. *Angew. Chem. Int. Ed.* **2011**, *50*, 1227–1230.

4) Inter alia: (a) Saito, M.; Nakamura, M.; Tajima, T. *Chem.–Eur. J.* **2008**, *14*, 6062–6068. (b) Kawase, T.; Konishi, A.; Hirao, Y.; Matsumoto, K.; Kurata, H.; Kubo, T. *Chem.–Eur. J.* **2009**, *15*, 2653–2661. (c) Zerubba, U. L.; Tilley, T. D. *J. Am. Chem. Soc.* **2009**, *131*, 2796–2797. (d) Zhang, H.; Karasawa, T.; Yamada, H.; Wakamiya, A.; Yamaguchi, S. *Org. Lett.* **2009**, *11*, 3076–3079. (e) Saito, M. *Symmetry* **2010**, *2*, 950–969. (f) Zerubba, U. L.; Tilley, T. D. *J. Am. Chem. Soc.* **2010**, *132*, 11012–11014. (g) Kawase, T.; Fujiwara, T.; Kitamura, C.; Konishi, A.; Hirao, Y.; Matsumoto, K.; Kurata, H.; Kubo, T.; Shinamura, S.; Mori, H.; Miyazaki, E.; Takimiya, K. *Angew. Chem. Int. Ed.* **2010**, *49*, 7728–7732.

5) Chase, D. T.; Fix, A. G.; Rose, B. D.; Weber, C. D.; Nobusue, S.; Stockwell, C. E.; Zakharov, L. N.; Lonergan, M. C.; Haley, M. M. *Angew. Chem. Int. Ed.* **2011**, *50*, 1103–1106.

6) Rose, B. D.; Chase, D. T.; Weber, C. D.; Zakharov, L. N.; Lonergan, M. C.; Haley, M. M. *Org. Lett.* **2011**, *13*, 2106–2109.

7) Anthony, J. E.; Facchetti, A.; Heeney, M.; Marder, S. R.; Zhan, X. *Adv. Mater.* **2010**, *22*, 3876–3892. (b) Dong, H.; Wang, C.; Hu, W. *Chem. Commun.* **2010**, *46*, 5211–5222. (c) Mikroyannidis, J. A.; Kabanakis, A. N.; Sharma, S. S., Sharma, G. D. *Adv. Funct. Mater.* **2011**, *21*, 746–755.

8) Shimizu, A.; Tobe, Y. *Angew. Chem. Int. Ed.* **2011**, *50*, 6906–6910.

9) Reisch, H.; Wiesler, U.; Scherf, U.; Tuytuylkov, N. *Macromolecules* **1996**, *29*, 8204–8210.

10) Merlet, S.; Birau, M.; Wang, Z. Y. *Org. Lett.* **2002**, *4*, 2157–2159.

11) Kaur, I.; Jia, W.; Kopreski, R. P.; Selvarasah, S.; Dokmeci, M. R.; Pramanik, C.; McGruer, N. E.; Miller, G. P. *J. Am. Chem. Soc.* **2008**, *130*, 16274–16286.

12) Almenningen, A.; Bastiansen, O.; Fernholt, L.; Cyvin, B. N.; Cyvin, S. J.; Samdal, S. *J. Mol. Struct.* **1985**, *128*, 59-76.

13) Reiss, H.; Heller, A. *J. Phys. Chem.* **1985**, *89*, 4207-4213.

14) Balakrishnan, K.; Datar, A.; Oitker, R.; Chen, H.; Zuo, J. M.; Zang, L. *J. Am. Chem. Soc.* **2005**, *127*, 10496–10497.

15) Kang, S. J.; Bae, I.; Park, Y. J.; Park, T. H.; Sung, J.; Yoon, S. C.; Kim, K. H.; Choi, D. H.; Park, C. *Adv. Funct. Mater.* **2009**, *19*, 1609–1616.

16) Chua, L. L.; Zaumseil, J.; Chang, J. F.; Ou, E. C. W.; Ho, P. K. H.; Sirringhaus, H.; Friend, R. H. *Naπture* **2005**, *434*, 194–197.

17) (a) Chen, Z. Y.; Lee, M. J.; Ashraf, R. S.; Gu, Y.; Albert-Seifried, S.; Nielsen, M. M.; Schroeder, B.; Anthopoulos, T. D.; Heeney, M.; McCulloch, I.; Sirringhaus, H. *Adv. Mater.* **2012**, *24*, 647–652. (b) Zaumseil, J.; Sirringhaus, H. *Chem. Rev.* **2007**, *107*, 1296–1323.

18) (a) de Boer, R. W. I.; Stassen, A. F.; Craciun, M. F.; Mulder, C. L.; Molinari, A.; Rogge, S.; Morpurgo, A. F. *Appl. Phys. Lett.* **2005**, *86*. 262109-1–262109-3. (b) Takahashi, T.; Takenobu, T.; Takeya, J.; Iwasa, Y. *Appl. Phys. Lett.* **2006**, *88*. 033505-1–033505-3.

Chapter IV

1) Li, F. M.; Nathan, A.; Wu, Y.; Ong, B. S. *Organic Thin Film Transistor Integration: AHybrid Approach*;Wiley-VCH:Weinheim, 2011.

2) (a) Katz, H. E.; Huang, J. *Annu. Rev. Mater. Res.* **2009**, *39*, 71–92. (b) Zhou, Y.; Fuentes-Hernandez, C.; Shim, J.;Meyer, J.; Giordano, A. J.; Li, H.;Winget, P.; Papadopoulos, T.; Cheun,H.; Kim, J.; Fenoll, M.;Dindar, A.; Haske, W.; Najafabadi, E.; Khan, T. M.; Sojoudi, H.; Barlow, S.; Graham, S.; Brédas, J.-L.; Marder, S.R.; Khan, A.; Kippelen, B. *Science* **2012**, *336*, 327–332. (c) Lambrecht, J.; Saragi, T. P. I.; Salbeck, J. *J. Mater. Chem.* **2011**, *21*, 18266–18270. (d) Sekitani, T.; Yokota, T.; Zschieschang, U.; Klauk, H.; Bauer, S.; Takeuchi, K.; Takamiya, M.; Sakurai, T.; Someya, T. *Science* **2009**, *326*, 1516–1519. (e) Irimia-Vladu, M.; Sariciftci, N. S.; Bauer, S. *J. Mater. Chem.* **2011**, *21*, 1350–1361.

3) Anthony, J. E.; Facchetti, A.; Heeney, M.; Marder, S. R.; Zhan, X. *Adv. Mater.* **2010**, *22*, 3876–3892.

4) *Fullerenes: Principles and Applications*; Langa, F., Nierengarten, J.-F., Eds.; Royal Society of Chemistry: Cambridge, U.K., 2011.

5) (a) Scott, L. T. *Polycyclic Aromat. Cmpd.* **2010**, *30*, 247–259. (b) *Fragments of Fullerenes and Carbon Nanotubes. Designed Synthesis, Unusual Reactions, and Coordination Chemistry*; Petrukhina, M. A., Scott, L. T., Eds.; John Wiley & Sons: Hoboken, NJ, 2011.

6) Other recent CP-PAH examples, inter alia: (a) Saito, M.; Nakamura, M.; Tajima, T. *Chem.-Eur. J.* **2008**, *14*, 6062–6068. (b) Levi, Z. U.; Tilley, T. D. *J. Am. Chem. Soc.* **2009**, *131*, 2796–2797. (c) Kawase, T.; Konishi, A.; Hirao, Y.; Matsumoto, K.; Kurata, H.; Kubo, T. *Chem.-Eur. J.* **2009**, *15*, 2653–2661. (d) Mohebbi, A. R.; Wudl, F. *Chem.-Eur. J.* **2011**, *17*, 2642–2646. (e) Mohebbi, A. R.; Yuen, J.; Fan, J.; Munoz, C.; Wang, M. F.; Shirazi, R. S.; Seifter, J.; Wudl, F. *Adv. Mater.* **2011**, *23*, 4644–4648. (f) Lütke-Eversloh, C.; Avlasevich, Y.; Li, C.; Müllen, K. *Chem.-Eur. J.* **2011**, *17*, 12756–12762. (g) Wood, J. D.; Jellison, J. L.; Finke, A. D.; Wang, L.; Plunkett, K. N. *J. Am. Chem. Soc.* **2012**, *134*, 15783–15789.

7) Fix, A. G.; Chase, D. T.; Haley, M. M. In *Topics in Current Chemistry*; Siegel, J. S.,Wu,Y.-T., Eds.; Springer: Berlin, Germany, 2013, in press (DOI: 10.1007/128_2012_376).

8) (a) Chase, D. T.;Rose, B. D.;McClintock, S. P.; Zakharov, L. N.; Haley, M. M. *Angew. Chem., Int. Ed.* **2011**, *50*, 1127–1130. (b) Chase,D.T.; Fix, A. G.; Rose, B. D.; Weber, C. D.; Nobusue, S.; Stockwell, C. E.; Zakharov, L. N.; Lonergan, M. C.; Haley, M. M. *Angew. Chem., Int. Ed.* **2011**, *50*, 11103–11106. (c) Chase, D. T.; Fix, A. G.; Kang, S. J.; Rose, B. D.; Weber,C. D.; Zhong, Y.; Zakharov, L. N.; Lonergan, M. C.; Nuckolls, C.; Haley, M. M. *J. Am. Chem. Soc.* **2012**, *134*, 10349–10352.

9) (a) Zhou, Q.; Carroll, P. J.; Swager, T. M. *J. Org. Chem.* **1994**, *59*, 1294–1301. (b) Reisch, H.; Wiesler, U.; Scherf, U.; Tuytuylkov, N. *Macromolecules* **1996**, *29*, 8204–8210. (c) Nishida, J.; Tsukaguchi, S.; Yamashita, Y. *Chem.-Eur. J.* **2012**, *18*, 8964–8970.

10) (a) LeBerre, A. *Ann. Chim.* **1957**, *2*, 371–423. (b) Shimizu, A.; Tobe, Y. *Angew. Chem., Int. Ed.* **2011**, *50*, 6906–6910.

11) Scanlon, L. G.; Balbuena, P. B.; Zhang, Y.; Sandi, G.; Back, C. K.; Feld, W. A.; Mack, J.; Rottmayer, M. A.; Riepenhoff, J. L. *J. Phys. Chem. B* **2006**, *110*, 7688–7694.

12) All calculations were performed with Gaussian 09, revision C.01. Frisch, M. J. et al. Gaussian, Inc., Wallingford, CT, 2009. See Supporting Information for full citation.

13) Density functional theory [B3LYP/6-31*G(d,p)] was used for minimization of all molecular geometries: (a) Becke, A. D. J. *Chem. Phys.* **1993**, *98*, 5648–5652. (b) Lee, C.; Yang, W.; Parr, R. G. *Phys. Rev. B: Condens. Matter* **1988**, *37*, 785–789. (c) Stephens, P. J.; Devlin, F. J.; Chabalowski, C. F.; Frisch, M. J. *J. Phys. Chem.* **1994**, *98*, 11623–11627.

14) (a) Anthony, J. E. *Chem. Mater.* **2011**, *23*, 583–590. (b) Lin, Y.; Li, Y.; Zhan, X. *Chem. Soc. Rev.* **2012**, *41*, 4245–4272.

15) For comparison, the potential references were changed from Fc/Fc^+ to SCE, as described in: Connelly, N. G.; Geiger, W. E. *Chem. Rev.* **1996**, *96*, 877–910.

16) Reiss, H.; Heller, A. *J. Phys. Chem.* **1985**, *89*, 4207–4213.

17) Scanlon, L. G.; Balbuena, P. B.; Zhang, Y.; Sandi, G.; Back, C. K.; Feld, W. A.; Mack, J.; Rottmayer, M. A. Riepenhoff, J. L. *J. Phys. Chem.B* **2006**, *110*, 7688–7694.

Chapter V

1) (a) Anthony, J. E.; Facchetti, A.; Heeney, M.; Marder, S. R.; Zhan, X. *Adv. Mater.* **2010**, *22*, 3876-3892. (b) Li, F. M.; Nathan, A.; Wu, Y.; Ong, B. S. *Organic Thin Film Transistor Integration: AHybrid Approach*; Wiley-VCH: Weinheim, 2011. (c) Zhou, Y.; Fuentes-Hernandez, C.; Shim, J.; Meyer, J.; Giordano, A. J.; Li, H.;Winget, P.; Papadopoulos, T.; Cheun, H.; Kim, J.; Fenoll, M.; Dindar, A.; Haske, W.; Najafabadi, E.; Khan, T. M.; Sojoudi, H.; Barlow, S.; Graham, S.; Brédas, J.-L.; Marder, S. R.; Khan, A.; Kippelen, B. *Science* **2012**, *336*, 327–332.

2) (a) *Semiconductor Nanomaterials for Flexible Technologies: From Photovoltaics and Electronics to Sensors and Energy Storage*; Sun, Y.; Rogers, J. A., Eds.; William Andrew Publishing: Oxford, 2010. (b) Mei, J.; Diao, Y.; Appleton, A. L.; Fang, L.; Bao, Z. *J. Am. Chem. Soc.* **2013**, *135*, 6724-6746.

3) (a) Zhang, L.; Colella, N. S.; Feng, L.; Trahan, S.; Baral, J. K.; Winter, H. H.; Mannsfeld, S. C. B.; Briseno, A. L. *J. Am. Chem. Soc.* **2013**, *135*, 844-854. (b) Perepichka, I. F.; Prepichka, D. F. *Handbook of Thiophene-bassed Materials: Applications in Organic Electronics and Photonics*; John Wiley and Sons Ltd: Chichester, 2009.

4) (a) Chesterfield, R. J.; Newman, C. R.; Pappenfus, T. M.; Ewbank, P. C.; Haukaas, M. H.; Mann, K. R.; Miller, L. L., Frisbie, C. D. *Adv. Mater.* **2003**, *15*, 1278-1282. (b) Takahashi, K.; Suzuki, T.; Akiyama, K.; Ikegami, Y.; Fukazawa, Y. *J. Am. Chem. Soc.* **1991**, *12*, 4576-4583. (c) Ribierre, J. C.; Fujihara, T.; Muto, T.; Aoyama, T. *Org. Electron.* **2010**, *11*, 1469-1475. (d) Ribierre, J. C.; Watanabe, S.; Matsumoto, M.; Muto, T.; Aoyama, T. *Appl. Phys. Lett.* **2010**, *96*, 83303(1)-83303(3). (e) Suzuki, Y.; Miyazaki, E.; Takimiya, K. *J. Am. Chem. Soc.* **2010**, *132*, 10453-10466. (f) Qiao, Y.; Guo, Y.; Yu, C; Zhang, F.; Xu, W.; Liu, Y.; Zhu, D. *J. Am. Chem. Soc.* **2012**, *134*, 4084-4087. (g) Li, J.; Qiao, X.; Xiong, Y.; Hong, W.; Gao, X.; Li, H. *J. Mater. Chem.*

C **2013**, *1*, 5128-5132. (h) Kubo, T.; Sakamoto, M.; Akanabe, M.; Fujiwara, Y.; Yamamoto, K.; Akita, M.; Inoue, K.; Takui, T.; Nakasuji, K. *Angew. Chem., Int. Ed.* **2004**, *43*, 6474-6479.

5) (a) Chase, D. T.; Rose, B. D.; McClintock, S. P.; Zakharov, L. N.; Haley, M. M. *Angew. Chem., Int. Ed.* **2011**, *50*, 1127–1130. (b) Chase, D. T.; Fix, A. G.; Rose, B. D.; Weber, C. D.; Nobusue, S.; Stockwell, C. E.; Zakharov, L. N.; Lonergan, M. C.; Haley, M. M. *Angew. Chem., Int. Ed.* **2011**, *50*, 11103–11106. (c) Chase, D. T.; Fix, A. G.; Kang, S. J.; Rose, B. D.; Weber, C. D.; Zhong, Y.; Zakharov, L. N.; Lonergan, M. C.; Nuckolls, C.; Haley, M. M. *J. Am. Chem. Soc.* **2012**, *134*, 10349–10352.

6) Other recent CP-PAH examples, inter alia: (a) Saito, M.; Nakamura, M.; Tajima, T. *Chem.-Eur. J.* **2008**, *14*, 6062–6068. (b) Levi, Z. U.; Tilley, T. D. *J. Am. Chem. Soc.* **2009**, *131*, 2796–2797. (c) Kawase, T.; Konishi, A.; Hirao, Y.; Matsumoto, K.; Kurata, H.; Kubo, T. *Chem.-Eur. J.* **2009**, *15*, 2653–2661. (d) Mohebbi, A. R.; Wudl, F. *Chem.-Eur. J.* **2011**, *17*, 2642–2646. (e) Mohebbi, A. R.; Yuen, J.; Fan, J.; Munoz, C.; Wang, M. F.; Shirazi, R. S.; Seifter, J.; Wudl, F. *Adv. Mater.* **2011**, *23*, 4644–4648. (f) Lütke-Eversloh, C.; Avlasevich, Y.; Li, C.; Müllen, K. *Chem.-Eur. J.* **2011**, *17*, 12756–12762. (g) Wood, J. D.; Jellison, J. L.; Finke, A. D.; Wang, L.; Plunkett, K. N. *J. Am. Chem. Soc.* **2012**, *134*, 15783–15789.

7) Fix, A. G.; Deal, P. E.; Vonnegut, C. L.; Rose, B. D.; Zakharov, L. N.; Haley, M. M. *Org. Lett.*, **2013**, *15*, 1362–1365.

8) Li, R.; Dong, H.; Zhan X.; He, Y.; Li, H.; Hu, W. *J. Mater. Chem.*, **2010**, *20*, 6014–6018.

9) All calculations were performed with Gaussian 09, revision C.01. Frisch, M. J. et al. Gaussian, Inc., Wallingford, CT, 2009. See Supporting Information for full citation.

10) MacDowell, D. W. H.; Patrick T. B. *J. Heterocycl. Chem.* **1967**, *4*, 425-6.

11) a) H. Usta, A. Facchetti, T. J. Marks, *J. Am. Chem. Soc.* **2008**, *130*, 8580–8581; b) H. Usta, C. Risko, Z. Wang, H. Huang, M. K. Deliomergolu, A. Zhukhovitskiy, A. Facchetti, T. J. Marks, *J. Am. Chem. Soc.* **2009**, *131*, 5586–5608.

12) Anthony, J. E. *Chem. Mater.* **2011**, *23*, 583–590.

13) For comparison, the potential references were changed from Fc/Fc^+ to SCE, as described in: Connelly, N. G.; Geiger, W. E. *Chem. Rev.* **1996**, *96*, 877–910.

14) Reiss, H.; Heller, A. *J. Phys. Chem.* **1985**, *89*, 4207–4213.

Chapter VI

1) (a) Anthony, J. E.; Facchetti, A.; Heeney, M.; Marder, S. R.; Zhan, X. *Adv. Mater.* **2010**, *22*, 3876-3892. (b) Li, F. M.; Nathan, A.; Wu, Y.; Ong, B. S. *Organic Thin Film Transistor Integration:AHybrid Approach*; Wiley-VCH: Weinheim, 2011. (c) *Semiconductor Nanomaterials for Flexible Technologies: From Photovoltaics and Electronics to Sensors and Energy Storage*; Sun, Y.; Rogers, J. A., Eds.; William Andrew Publishing: Oxford, 2010.

2) (a) Katz, H. E.; Huang, J. *Annu. Rev. Mater. Res.* **2009**, *39*, 71–92. (b) Zhou, Y.; Fuentes-Hernandez, C.; Shim, J.;Meyer, J.; Giordano, A. J.; Li, H.;Winget, P.; Papadopoulos, T.; Cheun,H.; Kim, J.; Fenoll, M.;Dindar, A.; Haske, W.; Najafabadi, E.; Khan, T. M.; Sojoudi, H.; Barlow, S.; Graham, S.; Brédas, J.-L.; Marder, S.R.; Khan, A.; Kippelen, B. *Science* **2012**, *336*, 327–332. (c) Lambrecht, J.; Saragi, T. P. I.; Salbeck, J. *J. Mater. Chem.* **2011**, *21*, 18266–18270. (d) Sekitani, T.; Yokota, T.; Zschieschang, U.; Klauk, H.; Bauer, S.; Takeuchi, K.; Takamiya, M.; Sakurai, T.; Someya, T. *Science* **2009**, *326*, 1516–1519. (e) Irimia-Vladu, M.; Sariciftci, N. S.; Bauer, S. *J. Mater. Chem.* **2011**, *21*, 1350–1361.

3) (a) Mei, J.; Diao, Y.; Appleton, A. L.; Fang, L.; Bao, Z. *J. Am. Chem. Soc.* **2013**, *135*, 6724. (b) Anthony, J. E.; Facchetti, A.; Heeney, M.; Marder, S. R.; Zhan, X. *Adv. Mater.* **2010**, *22*, 3876–3892.

4) *Fullerenes: Principles and Applications*; Langa, F., Nierengarten, J.-F., Eds.; Royal Society of Chemistry: Cambridge, U.K., 2011.

5) (a) Scott, L. T. *Polycyclic Aromat. Cmpd.* **2010**, *30*, 247–259. (b) *Fragments of Fullerenes and Carbon Nanotubes. Designed Synthesis, Unusual Reactions, and Coordination Chemistry*; Petrukhina, M. A., Scott, L. T., Eds.; John Wiley & Sons: Hoboken, NJ, 2011.

6) Other recent CP-PAH examples, inter alia: (a) Saito, M.; Nakamura, M.; Tajima, T. *Chem.-Eur. J.* **2008**, *14*, 6062–6068. (b) Levi, Z. U.; Tilley, T. D. *J. Am. Chem. Soc.* **2009**, *131*, 2796–2797. (c) Kawase, T.; Konishi, A.; Hirao, Y.; Matsumoto, K.; Kurata, H.; Kubo, T. *Chem.-Eur. J.* **2009**, *15*, 2653–2661. (d) Mohebbi, A. R.; Wudl, F. *Chem.-Eur. J.* **2011**, *17*, 2642–2646. (e) Mohebbi, A. R.; Yuen, J.; Fan, J.; Munoz, C.; Wang, M. F.; Shirazi, R. S.; Seifter, J.; Wudl, F. *Adv. Mater.* **2011**, *23*, 4644–4648. (f) Lütke-Eversloh, C.; Avlasevich, Y.; Li, C.; Müllen, K. *Chem.-Eur. J.* **2011**, *17*, 12756–12762. (g) Wood, J. D.; Jellison, J. L.; Finke, A. D.; Wang, L.; Plunkett, K. N. *J. Am. Chem. Soc.* **2012**, *134*, 15783–15789.

7) Fix, A. G.; Chase, D. T.; Haley, M. M. In *Topics in Current Chemistry*; Siegel, J. S.,Wu,Y.-T., Eds.; Springer: Berlin, Germany, 2013, in press (DOI: 10.1007/128_2012_376).

8) (a) Chase, D. T.;Rose, B. D.;McClintock, S. P.; Zakharov, L. N.; Haley, M. M. *Angew. Chem., Int. Ed.* **2011**, *50*, 1127–1130. (b) Chase,D.T.; Fix, A. G.; Rose, B. D.; Weber, C. D.; Nobusue, S.; Stockwell, C. E.; Zakharov, L. N.; Lonergan, M. C.; Haley, M. M. *Angew. Chem., Int. Ed.* **2011**, *50*, 11103–11106. (c) Chase, D. T.; Fix, A. G.; Kang, S. J.; Rose, B. D.; Weber,C. D.; Zhong, Y.; Zakharov, L. N.; Lonergan, M. C.; Nuckolls, C.; Haley, M. M. *J. Am. Chem. Soc.* **2012**, *134*, 10349–10352.

9) (a) Zhou, Q.; Carroll, P. J.; Swager, T. M. *J. Org. Chem.* **1994**, *59*, 1294–1301. (b) Reisch, H.; Wiesler, U.; Scherf, U.; Tuytuylkov, N. *Macromolecules* **1996**, *29*, 8204–8210. (c) Nishida, J.; Tsukaguchi, S.; Yamashita, Y. *Chem.-Eur. J.* **2012**, *18*, 8964–8970.

10) (a) LeBerre, A. *Ann. Chim.* **1957**, *2*, 371–423. (b) Shimizu, A.; Tobe, Y. *Angew. Chem., Int. Ed.* **2011**, *50*, 6906–6910.

11) Shimizu, A.; Kishi, R.; Nakano, M.; Shiomi, D.; Sato, K.; Takui, T.; Hisaki, I.; Miyata, M.; Tobe, Y. *Angew. Chem., Int. Ed.* **2013**, *52*, 6076 –6079

12) Scanlon, L. G.; Balbuena, P. B.; Zhang, Y.; Sandi, G.; Back, C. K.; Feld, W. A.; Mack, J.; Rottmayer, M. A.; Riepenhoff, J. L. *J. Phys. Chem. B* **2006**, *110*, 7688–7694.

13) Fix, A. G.; Deal, P. E.; Vonnegut, C. L.; Rose, B. D.; Zakharov, L. N.; and Haley, M. M. *Org. Lett.*, **2013**, *15* (6), pp 1362–1365.

14) Yang, Yonghong; Petersen, Jeffrey L.; Wang, Kung K. *J. Org. Chem.* **2003**, *68*, 5832-5837.

15) (a) Anthony, J. E. *Chem. Mater.* **2011**, *23*, 583–590; b) H. Usta, C. Risko, Z. Wang, H. Huang, M. K. Deliomergolu, A. Zhukhovitskiy, A. Facchetti, T. J. Marks, *J. Am. Chem. Soc.* **2009**, *131*, 5586–5608.

16) All calculations were performed with Gaussian 09, revision C.01. Frisch, M. J. et al. Gaussian, Inc., Wallingford, CT, 2009. See Supporting Information for full citation.

17) Density functional theory [B3LYP/6-31*G(d,p)] was used for minimization of these molecular geometries: (a) Becke, A. D. J. *Chem. Phys.* **1993**, *98*, 5648–5652. (b) Lee, C.; Yang, W.; Parr, R. G. *Phys. Rev. B: Condens. Matter* **1988**, *37*, 785–789. (c)

Stephens, P. J.; Devlin, F. J.; Chabalowski, C. F.; Frisch, M. J. *J. Phys. Chem.* **1994**, *98*, 11623–11627.

18) For comparison, the potential references were changed from Fc/Fc^+ to SCE, as described in: Connelly, N. G.; Geiger, W. E. *Chem. Rev.* **1996**, *96*, 877–910.

19) Reiss, H.; Heller, A. *J. Phys. Chem.* **1985**, *89*, 4207–4213.

Appendix A

[1] S. Merlet, M. Birau, Z. Y. Wang, *Org. Lett.* **2002**, *4*, 2157–2159.

[2] T. Nakagawa, D. Kumaki, J.-i. Nishida, S. Tokito, Y. Yamashita, *Chem. Mater*. **2008**, *20*, 2615–2617.

[3] G. M. Sheldrick, *Bruker/Siemens Area Detector Absorption Correction Program*, Bruker AXS, Madison, WI, 1998.

[4] SHELXTL-6.10 "Program for Structure Solution, Refinement and Presentation" BRUKER AXS Inc., 5465 East Cheryl Parkway, Madison, WI 53711-5373 USA.

[5] (a) A. D. Becke, *J. Chem. Phys.* **1993**, *98*, 5648-5652. (b) C. Lee, W. Yang, R. G. Parr, *Phys. Rev. B* **1988**, *37*, 785-789. (c) P. J. Stephens, F. J. Devlin, C. F. Chabalowski, M. J. Frisch, *J. Phys. Chem.* **1994**, *98*, 11623-11627.

Appendix B

1. Merlet, S.; Birau, M.; Wang, Z. Y. *Org. Lett*. **2002**, *4*, 2157–2159.

2. Sheldrick, G. M. Bruker/Siemens Area Detector Absorption Correction Program, Bruker AXS, Madison, WI, 1998.

3. SHELXTL-6.10 "Program for Structure Solution, Refinement and Presentation", BRUKER AXS Inc., 5465 East Cheryl Parkway, Madison, WI 53711-5373 USA

4. Gaussian 09, Revision A.02, Frisch, M. J.; Trucks, G. W.; Schlegel, H. B.; Scuseria, G. E.; Robb, M. A.; Cheeseman, J. R.; Scalmani, G.; Barone, V.; Mennucci, B.; Petersson, G. A.; Nakatsuji, H.; Caricato, M.; Li, X.; Hratchian, H. P.; Izmaylov, A. F.; Bloino, J.; Zheng, G.; Sonnenberg, J. L.; Hada, M.; Ehara, M.; Toyota, K.; Fukuda, R.; Hasegawa, J.; Ishida, M.; Nakajima, T.; Honda, Y.; Kitao, O.; Nakai, H.; Vreven, T.; Montgomery, Jr., J. A.; Peralta, J. E.; Ogliaro, F.; Bearpark, M.;. Heyd, J. J; Brothers, E.; Kudin, K. N.; Staroverov, V. N.; Kobayashi, R.; Normand, J.; Raghavachari, K.; Rendell, A.; Burant, J. C.; Iyengar, S. S.; Tomasi, J.; Cossi, M.; Rega, N.; Millam, J. M.; Klene, M.; Knox, J. E.; Cross, J. B.; Bakken, V.; Adamo, C.; Jaramillo, J.; Gomperts, R.; Stratmann, R. E.; Yazyev, O.; Austin, A. J.; Cammi, R.; Pomelli, C.; Ochterski, J. W.; Martin, R. L.; Morokuma, K.; Zakrzewski, V. G.; Voth,

G. A.; Salvador, P.; Dannenberg, J. J.; Dapprich, S.; Daniels, A. D.; Farkas, O.; Foresman, J. B.; Ortiz, J. V.; Cioslowski, J.; Fox, D. J.; Gaussian, Inc., Wallingford CT, 2009.

5. (a) Becke, A. D. *J. Chem. Phys.* **1993**, *98*, 5648–5652; (b) Lee, C.; Yang, W.; Parr, R. G. *Phys. Rev. B* **1988**, *37*, 785–789; (c) Stephens, P. J.; Devlin, F. J.; Chabalowski, C. F.; Frisch, M. J. *J. Phys. Chem*. **1994**, *98*, 11623–11627.

Appendix C

(1) Reiss, H.; Heller, A. *J. Phys. Chem.* **1985**, *89*, 4207–4213.

(2) G. M. Sheldrick, SADABS, University of Göttingen, Germany (1995).

(3) Bruker (2000). SMART, SAINT and SHELXTL. Bruker AXS Inc., Madison, Wisconsin, USA.

(4) Frisch, M. J.; Trucks, G. W.; Schlegel, H. B.; Scuseria, G. E.; Robb, M. A.; Cheeseman, J. R.; Scalmani, G.; Barone, V.; Mennucci, B.; Petersson, G. A.; Nakatsuji, H.; Caricato, M.; Li, X.; Hratchian, H. P.; Izmaylov, A. F.; Bloino, J.; Zheng, G.; Sonnenberg, J. L.; Hada, M.; Ehara, M.; Toyota, K.; Fukuda, R.; Hasegawa, J.; Ishida, M.; Nakajima, T.; Honda, Y.; Kitao, O.; Nakai, H.; Vreven, T.; Montgomery, Jr., J. A.; Peralta, J. E.; Ogliaro, F.; Bearpark, M.; Heyd, J. J.; Brothers, E.; Kudin, K. N.; Staroverov, V. N.; Kobayashi, R.; Normand, J.; Raghavachari, K.; Rendell, A.; Burant, J. C.; Iyengar, S. S.; Tomasi, J.; Cossi, M.; Rega, N.; Millam, N. J.; Klene, M.; Knox, J. E.; Cross, J. B.; Bakken, V.; Adamo, C.; Jaramillo, J.; Gomperts, R.; Stratmann, R. E.; Yazyev, O.; Austin, A. J.; Cammi, R.; Pomelli, C.; Ochterski, J. W.; Martin, R. L.; Morokuma, K.; Zakrzewski, V. G.; Voth, G. A.; Salvador, P.; Dannenberg, J. J.; Dapprich, S.; Daniels, A. D.; Farkas, Ö.; Foresman, J. B.; Ortiz, J. V.; Cioslowski, J.; Fox, D. J. Gaussian 09, Revision C.01; 2009.

(5) (a) Becke, A. D. *J. Chem. Phys.* **1993**, *98*, 5648–5652. (b) Lee, C.; Yang, W.; Parr, R. G. Phys. Rev. B: Condens. Matter **1988**, *37*, 785–789. (c) Stephens, P. J.; Devlin, F. J.; Chabalowski, C. F.; Frisch, M. J. J. Phys. Chem. **1994**, *98*, 11623–11627.

(6) (a) Gao, X.; Hodgson, J. L.; Jiang, D.; Zhang, S. B.; Nagase, S.; Miller, G. P.; Chen, Z. Org. Lett. **2011**, *13*, 3316–3319. (b) Takano, Y.; Taniguchi, T.; Isobe, H.; Kubo, T.; Morita, Y.; Yamamoto, K.; Nakasuji, K.; Takui, T.; Yamaguchi, K. J. Am. Chem. Soc. **2002**, *124*, 11122–11130.

Appendix D

(1) Reiss, H.; Heller, A. *J. Phys. Chem.* **1985**, *89*, 4207–4213.

(2) G. M. Sheldrick, SADABS, University of Göttingen, Germany (1995).

(3) Bruker (2000). SMART, SAINT and SHELXTL. Bruker AXS Inc., Madison, Wisconsin, USA.

(4) Frisch, M. J.; Trucks, G. W.; Schlegel, H. B.; Scuseria, G. E.; Robb, M. A.; Cheeseman, J. R.; Scalmani, G.; Barone, V.; Mennucci, B.; Petersson, G. A.; Nakatsuji, H.; Caricato, M.; Li, X.; Hratchian, H. P.; Izmaylov, A. F.; Bloino, J.; Zheng, G.; Sonnenberg, J. L.; Hada, M.; Ehara, M.; Toyota, K.; Fukuda, R.; Hasegawa, J.; Ishida, M.; Nakajima, T.; Honda, Y.; Kitao, O.; Nakai, H.; Vreven, T.; Montgomery, Jr., J. A.; Peralta, J. E.; Ogliaro, F.; Bearpark, M.; Heyd, J. J.; Brothers, E.; Kudin, K. N.; Staroverov, V. N.; Kobayashi, R.; Normand, J.; Raghavachari, K.; Rendell, A.; Burant, J. C.; Iyengar, S. S.; Tomasi, J.; Cossi, M.; Rega, N.; Millam, N. J.; Klene, M.; Knox, J. E.; Cross, J. B.; Bakken, V.; Adamo, C.; Jaramillo, J.; Gomperts, R.; Stratmann, R. E.; Yazyev, O.; Austin, A. J.; Cammi, R.; Pomelli, C.; Ochterski, J. W.; Martin, R. L.; Morokuma, K.; Zakrzewski, V. G.; Voth, G. A.; Salvador, P.; Dannenberg, J. J.; Dapprich, S.; Daniels, A. D.; Farkas, Ö.; Foresman, J. B.; Ortiz, J. V.; Cioslowski, J.; Fox, D. J. Gaussian 09, Revision C.01; 2009.

Appendix E

(1) Reiss, H.; Heller, A. *J. Phys. Chem.* **1985**, *89*, 4207–4213.

(2) G. M. Sheldrick, SADABS, University of Göttingen, Germany (1995).

(3) Bruker (2000). SMART, SAINT and SHELXTL. Bruker AXS Inc., Madison, Wisconsin, USA.

(4) Frisch, M. J.; Trucks, G. W.; Schlegel, H. B.; Scuseria, G. E.; Robb, M. A.; Cheeseman, J. R.; Scalmani, G.; Barone, V.; Mennucci, B.; Petersson, G. A.; Nakatsuji, H.; Caricato, M.; Li, X.; Hratchian, H. P.; Izmaylov, A. F.; Bloino, J.; Zheng, G.; Sonnenberg, J. L.; Hada, M.; Ehara, M.; Toyota, K.; Fukuda, R.; Hasegawa, J.; Ishida, M.; Nakajima, T.; Honda, Y.; Kitao, O.; Nakai, H.; Vreven, T.; Montgomery, Jr., J. A.; Peralta, J. E.; Ogliaro, F.; Bearpark, M.; Heyd, J. J.; Brothers, E.; Kudin, K. N.; Staroverov, V. N.; Kobayashi, R.; Normand, J.; Raghavachari, K.; Rendell, A.; Burant, J. C.; Iyengar, S. S.; Tomasi, J.; Cossi, M.; Rega, N.; Millam, N. J.; Klene, M.; Knox, J. E.; Cross, J. B.; Bakken, V.; Adamo, C.; Jaramillo, J.; Gomperts, R.; Stratmann, R. E.; Yazyev, O.; Austin, A. J.; Cammi, R.; Pomelli, C.; Ochterski, J. W.; Martin, R. L.; Morokuma, K.; Zakrzewski, V. G.; Voth, G. A.; Salvador, P.; Dannenberg, J. J.; Dapprich, S.; Daniels, A. D.; Farkas, Ö.; Foresman, J. B.; Ortiz, J. V.; Cioslowski, J.; Fox, D. J. Gaussian 09, Revision C.01; 2009.

Appendix F

1. Rahman, M.A.; Shito, F; Kitamura, T. *Synthesis* **2010**, 27-29.

Appendix G

1. (a) Fox, M. A.; Chanon, M. *Photoinduced Electron Transfer*; Elsevier: Amsterdam, 1988. (b) G. J. Kavarnos, N. J. Turro, *Chem. Rev.* **1986**, *86*, 401.

2. (a) Faulkner, L. R.; Bard, A. J. *Electroanalytical Chemistry*; Marcel Dekker: New York, 1977, Vol. 10, pp 1-95. (b) Bard, A. J.; Faulkner, L. R. *Electrochemical Methods Fundamentals and Applications Second Edition*; John Wiley and Sons: New York, 2001, pp. 736-745. (c) Richter, M. M. *Chem. Rev.* **2004**, *104*, 3003.

3. (a) Samori, S.; Hara, M.; Tojo, S.; Fujitsuka, M.; Yang, S.-W.; Elangovan, A.; Ho, T.-I.; Majima, T. *J. Phys. Chem. B.* **2005**, *109*, 11735. (b) Samori, S.; Tojo, S.; Fujitsuka, M.; Yang, S.-W.; Elangovan, A.; Ho, T.-I.; Majima, T. *J. Org. Chem.* **2005**, *70*, 6661. (c) Samori, S.; Tojo, S.; Fujitsuka, M.; Yang, S.-W.; Ho, T.-I.; Yang, J.-S.; Majima, T. *J. Phys. Chem. B.* **2006**, *110*, 13296. (d) Samori, S.; Tojo, S.; Fujitsuka, M.; Liang, H.-J.; Ho, T.-I.; Yang, J.-S.; Yang, S.-W.; Majima, T. *J. Org. Chem.* **2006**, *71*, 8732. (e) Samori, S.; Tojo, S.; Fujitsuka, M.; Lin, J.-H.; Ho, T.-I.; Yang, J.-S.; Majima, T. *J. Chin. Chem. Soc.*, **2006**, *53*, 1225. (f) Samori, S.; Tojo, S.; Fujitsuka, M.; Splitler E. L.; Haley, M. M.; Majima, T. *J. Org. Chem.* **2007**, *72*, 2785. (g) Samori, S.; Tojo, S.; Fujitsuka, M.; Splitler E. L.; Haley, M. M.; Majima, T. *J. Org. Chem.* **2008**, *73*, 3551.

4. (a) Goes, M.; Verhoeven, J. W.; Hofstraat, H.; Brunner, K. *ChemPhysChem* **2003**, *4*, 349. (b) Thomas, K. R. J.; Lin, J. T.; Tao, Y.-T.; Chuen, C.-H. *Chem. Mater.* **2002**, *14*, 3852. (c) Zhu, W.; Hu, M.; Yao, R.; Tian, H. *J. Photochem. Photobiol., A* **2003**, *154*, 169. (d) Thomas, K. R. J.; Lin, J. T.; Velusamy, M.; Tao, Y.-T.; Chuen, C.-H. *Adv. Funct. Mater.* **2004**, *14*, 83. (e) Chiang, C.-L.; Wu, M.-F.; Dai, D.-C.; Wen, Y.-S.; Wang, J.-K.; Chen, C.-T. *Adv. Funct. Mater.* **2005**, *15*, 231.

5. (a) Elangovan, A.; Chen, T.-Y.; Chen, C.-Y.; Ho, T.-I. *Chem. Commun.* **2003**, 2146. (b) Elangovan, A.; Yang, S.-W.; Lin, J.-H.; Kao, K.-M.; Ho, T.-I. *Org. Biomol. Chem.* **2004**, *2*, 1597. (c) Elangovan, A.; Chiu, H.-H.; Yang, S.-W.; Ho, T.-I. *Org. Biomol. Chem.* **2004**, *2*, 3113. (d) Elangovan, A.; Kao, K.-M.; Yang, S.-W.; Chen, Y.-L.; Ho, T.-I.; Su, Y. O. *J. Org. Chem.* **2005**, *70*, 4460. (e) Yang, S.-W.; Elangovan, A.; Hwang, K.-C.; Ho, T.-I. *J. Phys. Chem. B.* **2005**, *109*, 16628. (f) Lin, J.-H.; Elangovan, A.; Ho, T.-I. *J. Org. Chem.* **2005**, *70*, 7397.

6. (a) Jayakannan, M.; Van Hal, P. A.; Janssen, R. A. J. *J. Polym. Sci., Part A*: *Polym. Chem.* **2001**, *40*, 251. (b) Tykwinski, R. R.; Schreiber, M.; Carlon, R. P.; Diederich, F.; Gramlich, V.; *Helv. Chim. Acta* **1996**, *79*, 2249. (c) Tykwinski, R. R.; Schreiber, M.; Gramlich, V.; Seiler, P.; Diederich, F. *Adv. Mater.* **1996**, *8*, 226. (d) Wilson, J. N.; Hardcastle, K. I.; Josowicz, M.; Bunz, U. H. F. *Tetrahedron* **2004**, *60*, 7157. (e) Wilson, J. N.; Smith, M. D.; Enkelmann, V.; Bunz, U. H. F. *Chem. Commun.* **2004**, 1700. (f) Wilson, J. N.; Josowicz, M.; Wang, Y.; Bunz, U. H. F. *Chem. Commun.* **2003**, 2962. (g) Miteva, T.; Palmer, L.; Kloppenburg, L.; Neher, D.; Bunz, U. H. F. *Macromolecules* **2000**, *33*, 652. (h) J. Zucchero, A.; Wilson, J. N.; Bunz, U. H. F. *J.*

Am. Chem. Soc. **2006**, *128*, 11872. (i) Ojima, J.; Kakumi, H.; Kitatani, K.; Wada, K.; Ejiri, E.; Nakada, T. *Can. J. Chem.* **1984**, *63*, 2885. (j) Ojima, J.; Enkaku, M.; Uwai, C. *Bull. Chem. Soc. Jpn.* **1977**, *50*, 933.

7. (a) Miller, J. J.; Marsden, J. A.; Haley, M. M. *Synlett* **2004**, 165. (b) Marsden, J. A.; Miller, J. J.; Shirtcliff, L. D.; Haley, M. M. *J. Am. Chem. Soc.* **2005**, *127*, 2464. (c) Spitler, E. L.; Shirtcliff, L. D.; Haley, M. M. *J. Org. Chem.* **2007**, *72*, 86. (d) Spitler, E. L.; Monson, J. M.; Haley, M. M. *J. Org. Chem.* **2008**, *73*, 2211.

8. (a) Marsden, J. A.; Palmer, G. J.; Haley, M. M. *Eur. J. Org. Chem.* **2003**, 2355. (b) Jones, C. S.; O'Connor, M. J.; Haley, M. M. In *Acetylene Chemistry: Chemistry, Biology, and Materials Science*; Diederich, F.; Tykwinski, R. R.; Stang, P. J. Eds.; Wiley-VCH: Weinheim, Germany, 2004; pp 303-385. (c) Marsden, J. A.; Haley, M. M. *J. Org. Chem.* **2005**, *70*, 10213. (d) Anand, S.; Varnavski, O.; Marsden, J. A.; Haley, M. M.; Schlegel, H. B.; Goodson III, T. *J. Phys. Chem. A* **2006**, *110*, 1305. (e) Bhaskar, A.; Guda, R.; Haley, M. M.; Goodson III, T. *J. Am. Chem. Soc.* **2006**, *128*, 13972. (f) Slepkov, A. D.; Hegmann, F. A.; Tykwinski, R. R.; Kamada, K.; Ohta, K.; Marsden, J. A.; Spitler, E. L.; Miller, J. J.; Haley, M. M. *Opt. Lett.* **2006**, *31*, 3315. (g) Spitler, E. L.; McClintock, S. P.; Haley, M. M. *J. Org. Chem.* **2007**, *72*, 6692.

9. Zhang, W.; Huang, C. *Mat. Chem. Phys.* **2006**, *96*, 283.

10. (a) Nguyen, P.; Yuan, Z.; Agocs, L.; Lesley, G.; Marder, T. B. *Inorg. Chem. Acta* **1994**, *220*, 289. (b) Songkram, C.; Takaishi, K.; Yamaguchi, K.; Kagechika, H.; Endo, Y. *Tetrahedron Lett.* **2001**, *42*, 6365. (c) Kovalenko, S. V.; Peabody, S.; Manoharan, M.; Clark, R. J.; Alabugin, I. V. *Org. Lett.* **2004**, *6*, 2457.

11. Drefahl, G.; Plotner, G. *Chem. Ber*. **1958**, *91*, 1280. This compound was originally prepared by stilbene bromination/dehydrobromination. An improved preparation via Sonogashira reactions as well as NMR spectroscopic data are given in the Supporting Information.

12. Ye, F.; Orita, A.; Doumoto, A.; Otera, J. *Tetrahedron* **2003**, *59*, 5635.

13. Dirk, S. M.; Tour, J. M. *Tetrahedron* **2003**, *59*, 287.

14. Nguyen, P.; Lesley, G.; Marder, T. B.; Ledoux, I.; Zyss, J. Chem. Mater. **1997**, *9*, 406.

15. Hundertmark, T.; Littke, A. F.; Buchwald, S. L.; Fu, G. C. *Org. Lett.* **2000**, *2*, 1729.

16. Melinger, J. S.; Pan, Y.; Kleiman, V. D.; Peng, Z.; Davis, B. L.; McMorrow, D.; Lu, M *J. Am. Chem. Soc.* **2002**, *124*, 12002.

17. Yamaguchi, Y.; Matsubara, Y.; Ochi, T.; Wakamiya, T.; Yoshida, Z. *J. Am. Chem. Soc.* **2008**, *130*, 13867.

18. Kasha, M. *Chem. Rev.* **1947**, *41*, 401.

19. (a) Roberts, J. C.; Pincock, J. A. *J. Org. Chem.* **2006**, *71*, 1480. (b) Mateera, N. N.; Kode, R. A.; Redda, K. K. *J. Heterocyclic Chem.* **2002**, *39*,1251. (c) Charitos, C.; Tzougraki, C.; Kokotos, G.; *J. Peptide Res.* **2000**, *56*, 373. (d) Tucker, S. A.; Griffin, J. M.; Acree, W. E. Jr.; Tanga, M. J.; Bupp, J. E.; Tochimoto, T.K.; Lugtenburg, J. A.; Van Haeringen, K.; Cornelisse, J. *Polycyclic Aromatic Compounds* **1994**, *4*, 161.

20. Gross, E. M.; Anderson, J. D.; Slaterbeck, A. F.; Thayumanavan, S.; Barlow, S.; Zhang, S. R. Marder, H. K. Hall, M. F. Nabor, J.-F. Wang, E. A. Mash, N. R. Armstrong, R. M. Wightman, Y. *J. Am. Chem. Soc.* **2000**, *122*, 4972.

21. Kilsa, K.; Kajanus, J.; Macpherson, A. N.; Martensson, J.; Albinsson, B. *J. Am. Chem. Soc.* **2001**, *123*, 3069.

22. Sciano, J. C. *Handbook of Organic Photochemistry*; CRC Press: Boca Raton, FL, 1989; Vol. l, p 231.

Appendix H

1. (a) Morris, J. V.; Mahaney, M. A.; Huber, J. R. *J. Phys. Chem.* **1976**, *80*, 969. (b) Ono, K.; Yoshikawa, K.; Tsuji, Y.; Yamaguchi, H.; Uozumi, R.; Tomura, M.; Taga, K.; Saito, K. *Tetrahedron* **2007**, *63*, 9354.

2. Johnson, C. A.; Lu, Y.; Haley, M. M. *Org. Lett.* **2007**, *9*, 3725.

3. Marsden, J. A.; Haley, M. M. *J. Org. Chem.* **2005**, *70*, 10213.

4. (a) Zweifel, G.; Rajagopalan, S. *J. Am. Chem. Soc.* **1985**, *107*, 700. (b) Bruce, M. I.; Low, P. J.; Werth, A.; Skeleton, B. W.; White, A. H. *J. Chem. Soc. Dalton Trans.* **1996**, 1551. (c) Vito, F.; Fiandanese, V.; Bottalico, D.; Marchese, G.; Punzi, A. *Tetrahedron* **2006**, *62*, 512.